

Aspects of open quantum field theories

A Thesis

Submitted to the
Tata Institute of Fundamental Research, Mumbai
for the degree of Doctor of Philosophy
in Physics

by
Chandan Kumar Jana

International Centre for Theoretical Sciences
Tata Institute of Fundamental Research
Mumbai

(October, 2020)
(final version submitted in September, 2021)

DECLARATION

This thesis is a presentation of my original research work. Whenever contributions of others are involved, every effort is made to indicate this clearly, with due reference to the literature, and acknowledgement of collaborative research and discussions.

The work was done under the guidance of Professor R. Loganayagam, at the Tata Institute of Fundamental Research, Mumbai.

Chandan K. Jana
15/09/2021
Chandan Kumar Jana

In my capacity as supervisor of the candidate's thesis, I certify that the above statements are true to the best of my knowledge.

R. Loganayagam
R. Loganayagam (ICTS - TIFR)
Date: 16/09/2021

List of publications

Relevant to Ph. D. thesis:

1. **'Open quantum systems and Schwinger-Keldysh holograms'**

Chandan Jana, R. Loganayagam, Mukund Rangamani

arXiv:2004.02888 [hep-th]

JHEP07(2020)242

2. **'Renormalisation in Open Quantum Field theory II: Yukawa theory and PV reduction'**

Avinash, Chandan Jana, Arnab Rudra

arXiv:1906.10180 [hep-th]

3. **'Renormalization in Open Quantum Field Theory I: Scalar Field Theory'**

Avinash, Chandan Jana, R. Loganayagam, Arnab Rudra

arXiv:1704.08335 [hep-th]

JHEP 1711, 204 (2017)

Not relevant to Ph. D. thesis:

1. **'Nonlinear Langevin dynamics via holography'**

Bidisha Chakrabarty, Joydeep Chakravarty, Soumyadeep Chaudhuri, Chandan Jana, R. Loganayagam, Akhil Sivakumar

arXiv:1906.07762 [hep-th]

JHEP01(2020)165

Acknowledgement

I would like to express my deepest gratitude to my advisor R. Loganayagam. He has always insisted on critical thinking in both academic and non-academic subjects. He would often come with unconventional ideas to solve problems and eventually would get an alternate picture of the solution. This approach of his has motivated me to look at every problem from many different perspectives. Apart from these, I got lots of encouragement from him to attend seminars on diverse topics. There were many long nights solving problems together, in particular, calculating quantum field theory loops. A memorable instance is a whole night spent on solving a paradox in special relativity. Besides, he has helped me improve my computational and writing skills. I am fortunate to receive his sincere guidance.

I would like to extend my deepest gratitude to Arnab Rudra. His continuous encouragement and mental support have helped me to overcome the difficult times during my PhD. I have learnt many subtle aspects of quantum field theory from him. He is a person whom I could bother at any time on academic/non-academic discussions. I am grateful to him for patiently being at the dispensing end. I also had the pleasure to work with Jagannath Sutradhar. We studied and solved problems together in almost all PhD courses. There were multiple discussions on basic superconductivity, Berry phase, BKT phase transition etc. which have helped me improve my understanding in condensed matter physics. I am privileged to have him as a friend.

I am deeply indebted to Avinash, Bidisha Chakrabarty, Joydeep Chakravarty, Subhabrata Chatterjee, Soumyadeep Chaudhuri, Mukund Rangamani, Akhil Sivakumar for collaborating in various projects. I would especially like to thank Joydeep Chakravarty, Soumyadeep Chaudhuri, Sudip Ghosh, Ajit Mehta, Animesh Nanda, Akhil Sivakumar and Pushkal Srivastava for numerous valuable discussions on quantum field theory and general theory of relativity. I would also like to thank Pinaki Banerjee, Subhro Bhattacharjee, Shiuli Chatterjee, Abhijit Das, Arghya Das, Abhishek Dhar, Sarthak Duary, Shouvik Dutta, Jewel Ghosh, Rajesh Gopakumar, Diksha Jain,

Jaswin Kasi, Anupam Kundu, Aritra Kundu, Aswin P M, Archak Purkayastha, Shiraz Minwalla, Prithvi Narayan, Siddharth Prabhu, Krishnendu Ray, Suvrat Raju, Victor Ivan Giraldo Rivera, Prasant Singh, Vishal Vijayan, Junggi Yoon for their inputs in various projects. I have learnt many things in conversations with them.

I am privileged to have Ganga Prasath, Mukesh Raghav, Sumith Reddy, Rahul Singh and Pushkal Srivastava as friends. Apart from plentiful academic conversation on basics of quantum mechanics, astrophysics, differential geometry, linear algebra etc., I had the pleasure of spending many hours in badminton court with them. Numerous aimless discussions with Mukesh and Rahul, Sumith and Pushkal's instant jokes, badminton wisdom from Ganga, our trekking and hiking tours are the gifts from them. They also taught me a good deal of practical knowledge useful in everyday life. I am extremely grateful to them for being by my side all this time.

I appreciate the assistance and hard work by the academic office, IT and account section at ICTS. In particular, I would like to thank Jenny Burtan, Arshitha Thomas C, Abhijit De, Naveen Kumar L C, Hemanta Kumar G, Mohammad Irshad, Jeeva M, Basavaraj Patil, Suresh R, Srinivasa R, Madhulika Singh and Prashanth Kumar V for their prompt response in all administrative/IT matters.

Finally I would like to thank my parents, my brother Anjan and my wife Avaya for their unconditional and undemanding support. They have always insisted on the importance of being disciplined and being mentally strong throughout this journey. I acknowledge various suggestions from my wife which have improved this thesis.

Contents

| | |
|---|-----------|
| Acknowledgement | IV |
| 1 Introduction | 1 |
| 2 Introduction to SK formalism and open field theories | 5 |
| 2.1 A brief discussion on Schwinger-Keldysh formalism | 6 |
| 2.2 Introduction to open quantum field theories | 9 |
| 3 Renormalisation of open $\phi^3 + \phi^4$ theory | 13 |
| 3.1 Lindblad conditions and Feynman rules | 14 |
| 3.1.1 Lindblad condition | 14 |
| 3.1.2 Exact propagators | 16 |
| 3.1.3 Feynman rules | 18 |
| 3.1.4 Lindblad condition from tree level correlators | 20 |
| 3.2 One loop beta function | 20 |
| 3.2.1 One loop beta function for m^2 | 21 |
| 3.2.2 One loop beta function for m_Δ^2 | 23 |
| 3.2.3 Checking Lindblad condition for mass renormalization | 25 |
| 3.2.4 One loop beta function for λ_3 | 25 |
| 3.2.5 One loop beta function for σ_3 | 27 |
| 3.2.6 Checking Lindblad condition at the level of cubic couplings | 31 |
| 3.2.7 One loop beta function for λ_4 | 31 |
| 3.2.8 One loop beta function for σ_4 | 34 |
| 3.2.9 One loop beta function for λ_Δ | 34 |
| 3.2.10 Checking Lindblad condition for quartic couplings | 37 |

| | | |
|----------|---|-----------|
| 3.2.11 | Summary of the results | 39 |
| 3.3 | Computation in the average-difference basis | 40 |
| 3.3.1 | Action in the average-difference basis | 40 |
| 3.3.2 | One loop computations | 42 |
| 3.3.3 | Lindblad condition is never violated by perturbative corrections | 44 |
| 3.4 | Running of the coupling constants and physical meaning | 47 |
| 3.4.1 | Linearized analysis around the fixed point | 49 |
| 3.4.2 | Numerical analysis of RG equations | 51 |
| 3.5 | Conclusion | 53 |
| 4 | Open Yukawa theory | 58 |
| 4.1 | Action for open Yukawa theory and Feynman rules | 58 |
| 4.1.1 | Propagators | 60 |
| 4.1.2 | Feynman rules | 61 |
| 4.2 | Loop correction | 62 |
| 4.2.1 | Scalar tadpoles | 62 |
| 4.2.2 | Mass renormalization of the scalar field | 63 |
| 4.2.3 | Mass renormalization of fermionic field | 65 |
| 4.3 | Conclusion | 68 |
| 5 | Non-local divergence in scalar loops: a generic discussion | 69 |
| 5.1 | Non-local divergences in generic scalar loop diagrams | 69 |
| 5.1.1 | A simple example | 69 |
| 5.1.2 | Enhancement of divergence | 72 |
| 5.1.3 | Non-locality of divergences | 74 |
| 5.2 | Non-local divergences : open $\phi^3 + \phi^4$ theory | 78 |
| 5.2.1 | C -type SK integrals in four dimensions | 78 |
| 5.2.2 | Correction to σ_3 vertex due to triangle diagrams | 80 |
| 5.3 | Geometry of leading one-loop divergences in open QFTs | 84 |
| 5.3.1 | The parallelotope of cut momenta and its relativistic kinematics | 87 |
| 5.3.2 | The transverse null fluctuations and their contribution to the divergence | 91 |
| 5.4 | Conclusion and discussion | 93 |

| | | |
|----------|---|------------|
| 6 | Derivation of open effective action via holography | 95 |
| 6.1 | grSK: the gravitational Schwinger-Keldysh saddle | 101 |
| 6.2 | Open scalar field theory and holographic baths | 104 |
| 6.2.1 | General set-up | 105 |
| 6.2.2 | Deriving an open EFT from holography | 109 |
| 6.3 | Scalar propagation in grSK geometries | 111 |
| 6.3.1 | Scalar boundary to bulk propagators in grSK geometry | 111 |
| 6.3.2 | Propagators in $d = 2$ | 114 |
| 6.3.3 | Propagators in $d > 2$: gradient expansion | 115 |
| 6.4 | Influence functionals | 117 |
| 6.4.1 | Quadratic effective action | 117 |
| 6.4.2 | Interactions: contact self-interaction | 121 |
| 6.5 | Stochastic description of the open effective field theory | 128 |
| 6.6 | Discussion | 129 |
| 7 | Discussion and Conclusion | 134 |
| A | Loop integrals in open scalar field theory | 139 |
| A.1 | Notations and Conventions | 139 |
| A.2 | Evaluating Passarino-Veltman Loop Integrals for open $\phi^3 + \phi^4$ theory | 141 |
| A.2.1 | Passarino-Veltman A type integrals | 142 |
| A.2.2 | Integrals $B_{PM}(k)$ and $B_{MP}(k)$ | 142 |
| A.2.3 | Integrals $B_{PP}(k)$ and $B_{MM}(k)$ | 144 |
| A.2.4 | Reduction of divergent integrals to $B_{RP}(k)$ | 148 |
| A.2.5 | Evaluation of $B_{RP}(k)$ | 155 |
| A.2.6 | UV divergences and symmetry factors | 158 |
| A.3 | Passarino-Veltman diagrams in the average-difference basis | 159 |
| A.3.1 | Passarino-Veltman A type integral in the average-difference basis | 160 |
| A.3.2 | Passarino-Veltman B type integral in the average-difference basis | 160 |
| A.4 | Computations in the average-difference basis | 161 |
| A.4.1 | Beta functions for the mass terms | 161 |
| A.4.2 | Beta functions for the cubic couplings | 163 |

| | | |
|----------|---|------------|
| A.4.3 | Beta functions for the quartic couplings | 165 |
| A.5 | Tadpoles | 168 |
| B | PV reduction in open Yukawa theory | 178 |
| C | Non-local divergences in scalar loops | 180 |
| C.1 | Leading divergence in open QFTs | 180 |
| C.2 | Feynman parameterisation of $\Xi_{uc\perp}$ | 182 |
| C.2.1 | Leading log divergence | 183 |
| C.2.2 | Leading power divergence | 184 |
| C.3 | Evaluation of C -type triangle diagrams | 185 |
| C.3.1 | Single-cut C -type diagram | 185 |
| C.3.2 | Double-cut C -type diagram | 186 |
| C.3.3 | Triple cut C -type diagram | 188 |
| C.3.4 | Summary of divergences of C -type integrals | 191 |
| D | Open effective field theory via holography: detailed computation | 193 |
| D.1 | Gradient expansion on the grSK contour | 193 |
| D.2 | Gradient expansion of the Green's functions | 195 |
| D.3 | Witten diagrams on the grSK contour | 200 |
| D.4 | Cubic influence functionals in 2d CFTs | 201 |
| D.5 | Counterterm analysis for influence functionals | 206 |
| D.5.1 | Divergence structure for a marginal operator | 208 |
| D.5.2 | Divergence structure for relevant operators | 210 |
| | References | 212 |

Chapter 1

Introduction

Effective field theory (EFT) has been a fundamental tool in our understanding of various physical systems - starting from standard model of elementary particles, study of critical and near critical phenomena, fluid dynamics, to our current understanding of cosmology etc. But, there are other areas of physics involving dissipation and decoherence[1, 2, 3] which we do not have good understanding of from an EFT point of view [4, 5, 6, 7, 8, 9, 10, 11, 12, 13, 14, 15, 16, 17, 18, 19].

Study of most physical systems assumes the fundamental processes to be closed (unitary). But a real system is not closed; it interacts with its surrounding at each instant of time. Real systems that appear in cold atom physics, fluid dynamics, plasma physics, heavy ion collision etc. do not possess an equilibrated and unitary description. Quantum information in these systems is exchanged with the environment and we see decoherence and dissipation while coarse graining. It may seem that the openness, if small, can be neglected, but physicists often are interested in late time behaviour of a system. Thus the effect of the environment should be taken into account to understand certain aspects of physical systems.

Open systems, due to their non-unitary nature, are described by mixed states which are characterised by the density matrix. A quantum mechanical treatment of time evolution for a density matrix was started by Schwinger [20] and formalised by Keldysh [21], commonly called Schwinger-Keldysh (SK) prescription or closed-time-path or in-in prescription. Feynman and Vernon in [22] carried out a systematic study of an open system, interacting with a harmonic bath via bilinear coupling. They constructed an open effective action which they call *influence phase* of the system, by integrating out the bath. This paradigm is well understood for Gaussian dynamics in quantum mechanics, as illustrated by the Caldeira-Leggett description of quantum Brownian motion

[23]. The next major advancement in this direction is the seminal works by Gorini-Kossakowski-Sudarshan [24] and Lindblad [25]. They came up with a master equation to describe Markovian (memoryless) open systems. The master equation can be promoted to path-integral to get the Feynman-Vernon *influence phase* of an open system. A textbook treatment of open systems can be found in [26, 27].

The broad motivation for studying open field theory is to understand decoherence and emergence of dissipation from an EFT point of view. Open EFTs are obtained by integrating light degrees of freedom which are also called the bath degrees of freedom. In this sense it is different from the unitary EFTs which are usually obtained by integrating out heavy degrees of freedom. The physics at different energy scales, in unitary EFTs, are well understood by the notion of Wilsonian renormalisation. A similar understanding for open EFTs at different energy scales is absent in literature. A Wilsonian renormalisation for open systems would help us understand the emergence of dissipation in a coarse-grained description. As a first step we ask rather a simpler question: Can we find UV-complete open field theories by computing the renormalisation flow equation of coupling constants? Is there a systematic procedure to find open EFTs by explicitly integrating out the bath? There are some works regarding UV completion in the non-relativistic context [28]. However, a relativistic treatment is absent in the literature, which will be a check for non-relativistic models and vice-versa.

Apart from decoherence, there are other motivations to construct and make sense of open QFTs. We would like to know how to correct the classical description systematically due to quantum/statistical fluctuations in dissipative field theories (e.g., fluid dynamics, gravity/field theories in black hole backgrounds, field theories in the cosmological context, field theories that emerge around critical points). Another question is whether a particular dissipative effect is relevant or marginal or irrelevant in the Wilsonian sense. Recent progresses in experiment with non-equilibrium quantum many body systems show new dynamical phase transitions [29, 30], dynamical scaling[31, 32], universality in driven systems[33, 34] etc. Understanding these phenomena in non-equilibrium field theory [35] is of acute physical importance.

A consistent model for relativistic open field theory can also be implemented in the study of the following.

- The visible universe can be thought of as an open system in a bath of the unobserved universe. During the inflationary period, quantum fluctuation went outside the horizon.

It decoheres once it exits the horizon and re-enters as classical fluctuation after the end of inflation [36, 37, 38, 39, 40, 41, 42, 43, 44, 45, 46, 47, 48, 49, 50, 51]. An open field theoretic treatment using SK prescription has also been initiated to understand cosmological correlation functions in [52, 53, 54, 55].

- A gravitational SK construction in the context of AdS/CFT (§§6) might help us understand better the physics of disordered non-Fermi liquids [56, 57] (and references there in) and various non-equilibrium steady state processes [58, 59, 60, 61, 62].
- A model for relativistic open QFT can be used in study of heavy ion collision, black hole information paradox etc.

The central theme of this thesis is to study interacting open field theories in a systematic way. We use two different tools for that: Feynman diagrammatic way and holography. In the first approach, we start with a local, Lorentz invariant EFT of an open system and study its one loop renormalisability. We write an ansatz for open scalar field theory using some consistency conditions, then study renormalisation flow equations of coupling constants present in the theory. We find that certain one loop diagrams are non-local divergent - thus can not be cancelled by local counter-terms. We assure that these divergences are not cancelled among different diagrams and channels while computing correction to coupling constants. This observation might be an indication that low frequency and high frequency modes do not decouple in open field theory; although we do not have a clear understanding or resolution to these divergences. We show that open field theories with Fermionic d.o.f. (open Yukawa theory) also possess non-local divergences - the divergences are even severe.

The rest of the thesis deals with derivation of an open SK EFT for a probe field by integrating out a thermal CFT bath. We implement holographic tools to do that. The EFT has various notable features. We find that the noise appearing in stochastic description of the EFT has non-Gaussianity. This originates from the non-linear bath-bath correlation. We also find some fluctuation-dissipation relations at the non-linear level. The relations seem generic, since these appear for non-identical baths.

The organisation of the thesis is the following. We start with a brief discussion on SK formalism followed by an application to open QFT in §§2. In §§3, we explore open $\phi^3 + \phi^4$ theory - an EFT model of open scalar field. We compute one loop correction to various coupling constants

using perturbation theory. We find these models to possess non-local divergences appearing from triangle and higher order loop diagrams. In §§4, we show that these divergences appear even in the bubble diagrams. §§5 deals with the new type of divergence (non-local) at generic one scalar loop diagrams. Then we use a holographic prescription to study open ϕ^n theory in §§6. We derive various fluctuation-dissipation relations at the non-linear level obeyed by a probe scalar field. We end with few concluding remarks and open problems in §§7. In appendix A, we evaluate all one loop integrals explicitly that appear in open $\phi^3 + \phi^4$ theory. We also compute β function of respective couplings in a SK basis called *average-difference* basis. Appendix B deals with Passarino-Veltman reduction of open loop integrals that appear in Fermion self-energy correction. These loop integrals are used in open Yukawa theory discussed in §§4. A detailed computation of non-local divergences in scalar loop integrals (including triangle diagrams) is done in appendix C. In the final appendix D, we evaluate integrals appearing in §§6. These integrals emerge in the process of integrating out thermal bath along the gravitational SK contour (discussed later).

Chapter 2

Introduction to SK formalism and open field theories

A quantum system is described by its state and observables (e.g. correlation functions) are computed w.r.t. that state. As an observable people are often interested in real-time correlation functions which can be computed by solving first the Euclidean problem and then analytically continue to real time. The analytic continuation is difficult to perform at finite temperature because of the following reason. The temperature can be thought of as a compactified Euclidean time. So the Fourier modes (Matsubara modes) corresponding to Euclidean time are discrete. This makes thermal correlations discrete infinite sum over the Matsubara modes. These infinite sums followed by analytic continuation to real time are often difficult to perform. The complication associated to the Euclidean technique can be avoided by switching to SK prescription to compute real-time correlation functions. The SK prescription is designed to compute real-time correlation functions and has the potential to capture fluctuation dynamics[28, 63] in an apparent way.

SK prescription is a path integral prescription for the time evolution of density matrix. It can be used to study both closed and open systems. In that sense, this is a unified approach to study real-time correlation functions. In this chapter we introduce SK formalism for closed systems and then generalise it to open systems. A detailed discussion of SK path-integral and its application to non-equilibrium systems can be found in [63, 28, 55, 64].

2.1 A brief discussion on Schwinger-Keldysh formalism

The SK prescription, as we have emphasised, is designed to compute real-time correlation function. To compute the generating function for correlations let us first consider the density matrix of a unitary system $\rho(\phi, \phi') = \sum_k \lambda_k \psi_k(\phi) \psi_k^*(\phi')$. The time evolution of ψ_k is given as

$$\psi_k(\phi_2) = \int d\phi_1 \int \mathcal{D}\phi \exp\{iS[\phi]\} \psi_k(\phi_1), \quad (2.1.1)$$

where $S[\phi]$ is the action and $\psi_k(\phi_1)$ & $\psi_k(\phi_2)$ are initial and final states at times t_1 and t_2 respectively. Multiplying (2.1.1) to its complex conjugate we get

$$\psi_k(\phi_2) \psi_k^*(\phi'_2) = \int d\phi_1 d\phi'_1 \psi_k(\phi_1) \psi_k^*(\phi_1) \int \mathcal{D}\phi \mathcal{D}\phi' \exp\{iS[\phi] - iS[\phi']\}. \quad (2.1.2)$$

Thus for a general density matrix we can write

$$\rho(\phi_2, \phi'_2) = \int d\phi_1 d\phi'_1 \rho(\phi_1, \phi'_1) \int \mathcal{D}\phi \mathcal{D}\phi' \exp\{iS[\phi] - iS[\phi']\}. \quad (2.1.3)$$

Taking a trace over the out states we get

$$\begin{aligned} 1 &= \int d\phi_2 d\phi'_2 \rho(\phi_2, \phi'_2) \delta(\phi_2 - \phi'_2) \\ &= \int d\phi_1 d\phi'_1 \rho(\phi_1, \phi'_1) \delta(\phi_2 - \phi'_2) \int \mathcal{D}\phi \mathcal{D}\phi' \exp\{iS[\phi] - iS[\phi']\} \\ &\equiv \int_{\rho_i}^{\phi_2=\phi'_2} \mathcal{D}\phi \mathcal{D}\phi' \exp\{iS[\phi] - iS[\phi']\}. \end{aligned} \quad (2.1.4)$$

We call the final expression as the SK generating function in the absence of any source.

The partition function in presence of source is given by

$$\mathcal{Z}_{SK}[J_R, J_L] = \int_{\rho_i}^{\phi_R=\phi_L|_{t=\infty}} \mathcal{D}\phi_R \mathcal{D}\phi_L e^{iS_{SK}[\phi_R, \phi_L] + i \int dt (J_R \phi_R - J_L \phi_L)}. \quad (2.1.5)$$

Here we have relabelled ϕ, ϕ' as ϕ_R, ϕ_L representing the ket and bra d.o.f. respectively (R, L label will be extensively used onwards.) and we have pushed the final time to infinite future. ρ_i is the initial density matrix and J_R, J_L are the sources for ϕ_R, ϕ_L respectively. S_{SK} is the SK action which for unitary system is given by

$$S_{SK}[\phi_R, \phi_L] = S[\phi_R] - S[\phi_L]. \quad (2.1.6)$$

A diagrammatic interpretation of the SK path-integral is shown in figure 1. At future infinity, the R and L d.o.f. are identified, which is known as the SK boundary condition.

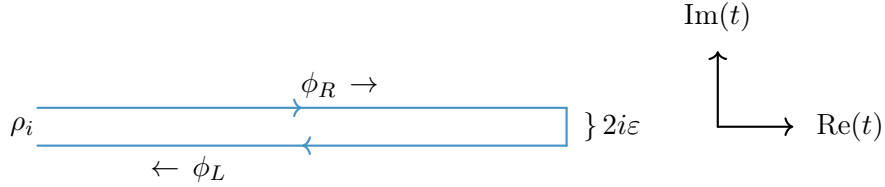


Figure 1: The Schwinger-Keldysh contour - R, L d.o.f. evolve along the forward and backward time respectively. The initial state is described by the density matrix ρ_i .

A consequence of the SK boundary condition is that the generating functional is unity in absence of the sources J_R, J_L . This property of the SK path-integral makes the generating functional a good candidate to compute real-time correlation functions.¹

If a unitary QFT is in perturbative regime, the path integral (2.1.5) can be used to set up the Feynman rules [28, 63]. The Feynman rules, in SK formalism, have the following defining properties for a unitary system.

1. In a unitary QFT, the action does not have any R, L -mixing term. Thus there are no vertices coupling the bra and ket fields. The bra vertices are complex conjugate of ket vertices.
2. The ket propagator is time-ordered while the bra propagator is anti-time ordered. In addition to these, SK boundary condition also induce a bra-ket propagator which is the on-shell propagator (obtained by putting the exchange particle on-shell). We will term these propagators as *cut propagators*. The terminology here is borrowed from the discussion of Cutkosky cutting rules where one thinks of the dividing lines between bra and ket parts of a Feynman diagram as a 'cut' of the diagram where particles go on-shell.

We will call these rules as Veltman rules after Veltman who re-derived these rules in his study of unitarity [65, 66]. To reiterate, a fundamental feature of Veltman rules is the fact that in a unitary theory, bra and ket fields talk only via cut propagators - not via cut vertices. As we will see in the following, Feynman and Vernon [22, 67] showed, there are novel cut vertices which signal non-unitarity.

¹The out states in SK prescription are identified. Thus the generating function does not refer to the out state unlike Feynman path integral. In Feynman path integral, the scattering processes are assumed to be adiabatic. Consequently, the in and out states only differ by a phase which is sum over the vacuum bubbles. Conversely, the SK prescription does not have any vacuum bubbles since it refers only to the in state. A discussion on this can be found in [28]

Now we describe the procedure to relate SK correlators to real-time correlators. The SK correlators are obtained by inserting operators on the SK contour in figure 1. An n -point SK correlation function of operator \mathcal{O} (R and L type) can be written as

$$\langle \mathcal{O}_L(t_n) \dots \mathcal{O}_L(t_{k+1}) \mathcal{O}_R(t_k) \dots \mathcal{O}_R(t_1) \rangle = \text{tr} [U_c(-\infty, -\infty) \mathcal{O}(t_n) \dots \mathcal{O}(t_1) \rho_i(-\infty)] . \quad (2.1.7)$$

Here ρ_i is the initial density matrix defined at past infinity and U_c is the contour ordered time evolution operator. Since the operators are contour ordered, operators on R and L branch should be time ordered and anti-time ordered respectively. Thus (2.1.7) can be written as

$$\begin{aligned} & \langle \mathcal{O}_L(t_n) \dots \mathcal{O}_L(t_{k+1}) \mathcal{O}_R(t_k) \dots \mathcal{O}_R(t_1) \rangle \\ &= \text{tr} \left[\bar{\mathcal{T}} \left(U(-\infty, \infty) \mathcal{O}(t_n) \dots \mathcal{O}(t_{k+1}) \right) \mathcal{T} \left(U(\infty, -\infty) \mathcal{O}(t_k) \dots \mathcal{O}(t_1) \right) \rho_i(-\infty) \right] . \end{aligned} \quad (2.1.8)$$

Note that SK correlators violate the time ordering at most once. However one can in principle consider a generating function of correlators with arbitrary number of time-ordering violation [68, 69, 70] (for example, the correlator used to obtain the Lyapunov exponent involves two time-ordering violations [71]).

We end this section with a short discussion of SK two point functions. Since the d.o.f.s are doubled, we expect to get at most four SK two-point correlators:

$$\begin{aligned} \langle \mathcal{O}_R(t_2) \mathcal{O}_R(t_1) \rangle &= \langle \mathcal{T} \mathcal{O}(t_2) \mathcal{O}(t_1) \rangle, & \langle \mathcal{O}_L(t_2) \mathcal{O}_R(t_1) \rangle &= \langle \mathcal{O}(t_2) \mathcal{O}(t_1) \rangle, \\ \langle \mathcal{O}_L(t_2) \mathcal{O}_L(t_1) \rangle &= \langle \bar{\mathcal{T}} \mathcal{O}(t_2) \mathcal{O}(t_1) \rangle, & \langle \mathcal{O}_R(t_2) \mathcal{O}_L(t_1) \rangle &= \langle \mathcal{O}(t_1) \mathcal{O}(t_2) \rangle. \end{aligned} \quad (2.1.9)$$

The RR and LL ones are the time-ordered and anti-time-ordered two point correlators. The rest of the correlators do not have any time-ordering, thus are the Wightman correlators.

It is often convenient to adopt a basis called the *average-difference* (a - d)/Keldysh basis, defined as

$$\mathcal{O}_a = \frac{1}{2}(\mathcal{O}_R + \mathcal{O}_L) \quad \mathcal{O}_d = \mathcal{O}_R - \mathcal{O}_L . \quad (2.1.10)$$

\mathcal{O}_a can be interpreted as classical d.o.f. and \mathcal{O}_d as fluctuation d.o.f. of a system. In a unitary system, \mathcal{O}_d consists of only quantum fluctuation. But, if the system is in a (thermal) bath, then the fluctuations have bath contribution which is related to noise in the system. The leading order bath contribution is often classical with sub-leading quantum corrections. We can distinguish the classical and quantum components in \mathcal{O}_d in a cleaner way by restoring \hbar and proper scaling of parameters & d.o.f. as shown in [28](chapter 4). Then the classical limit is obtained by taking $\hbar \rightarrow 0$.

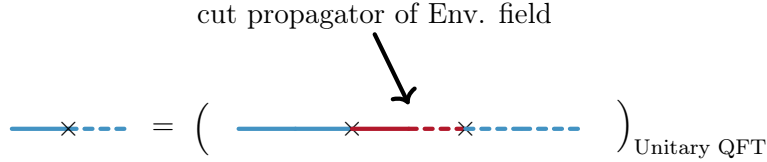


Figure 2: Blue solid, dashed lines represent the system ket, bra d.o.f. respectively. The red line represents the environment. Here we see that non-unitary bilinear coupling (ket-bra mixing coupling) is generated via onshell environment d.o.f.

One advantage of using a - d basis is that the number of correlators is less than that of R - L basis. The two-point correlators in this basis are given as

$$\begin{aligned} \langle \mathcal{O}_a(t_2) \mathcal{O}_d(t_1) \rangle &= \Theta(t_2 - t_1) \langle [\mathcal{O}(t_2), \mathcal{O}(t_1)] \rangle, & \langle \mathcal{O}_a(t_2) \mathcal{O}_a(t_1) \rangle &= \langle \{ \mathcal{O}(t_2), \mathcal{O}(t_1) \} \rangle, \\ \langle \mathcal{O}_d(t_2) \mathcal{O}_a(t_1) \rangle &= -\Theta(t_2 - t_1) \langle [\mathcal{O}(t_2), \mathcal{O}(t_1)] \rangle, & \langle \mathcal{O}_d(t_2) \mathcal{O}_d(t_1) \rangle &= 0. \end{aligned} \quad (2.1.11)$$

We see that dd correlator is identically zero². Later we will argue that correlators with only d -type operator are always zero (A proof can be found in [73]). Another advantage of a - d basis is that the SK path-integral in this basis has a dual classical stochastic description which we will discuss in the holographic context (see §6.2.2).

2.2 Introduction to open quantum field theories

An open system is an effective description of a system, obtained by integrating out the bath. Feynman and Vernon in [22, 67] found an effective path integral for a system interacting linearly with a harmonic bath. They showed that a coupling between bra and ket d.o.f. is induced as shown schematically in figure 2.

The existence of a Markovian limit was proved by Caldeira-Leggett by considering a spectral function for the bath at high temperature. However, an extension of this to field theory is a difficult problem due to the following reasons. First of all, engineering bath spectral function in field theory is hard unlike Caldeira-Leggett model. Moreover, even at high temperature there are long lived hydrodynamic modes which need to be separated out to get a local description. Challenges to derive open EFTs (even for non-field theoretic systems) also appear from non-linear baths. So far

²The d - d correlator being zero is a manifestation of the *largest-time equation*, which is used to prove unitarity in QFTs. A discussion on this can be found in [72]

we have only talked about the linear baths. However a bath need not always be linear and to have a complete description of open systems, we should involve non-linear baths.

Non-linear baths, unlike linear baths, are hard to integrate out in practice; one relies on perturbation theory provided the bath-bath interaction is weak. But, weakly coupled bath is not a good candidate to obtain local (Markovian) description for a system. One has to wait for a non-perturbatively long time for a local description to be valid. On the contrary, strongly coupled baths thermalise fast - thermalisation time scale being roughly proportional to the inverse coupling constant[74]. This means that derivation of local open QFTs inevitably involves the non-perturbative regime of bath. This explains to some extent why there are no simple microscopic models from which a local non-unitary interacting quantum EFT has been systematically derived ³.

We circumvent the above problem by following two alternate procedures: 1. take an ansatz for a local open EFT action and study its dynamics 2. integrate out strongly coupled bath using holography (§§6). We will discuss the first procedure below.

To write an ansatz for an open system, we follow the following steps. First we take the SK action for a closed, unitary system (2.1.6):

$$S_{SK}[\phi_R, \phi_L] = S[\phi_R] - S[\phi_L]. \quad (2.2.1)$$

Here, R and L d.o.f. do not mix. The naive expectation is that R - L mixing terms in the above SK action break unitarity and lead to openness. This is indeed true. However, along with R - L mixing terms, one should also add imaginary pure R and pure L terms. These terms which lead to non-unitarity, are conventionally called the *Feynman-Vernon influence phase*. The phase should be in the following form, called the *Lindblad form*[79, 76].

$$S_{FV} = i \int \sum_k \gamma_k \left(L_k^\dagger(\phi_R) L_k(\phi_L) - \frac{1}{2} L_k^\dagger(\phi_R) L_k(\phi_R) - \frac{1}{2} L_k^\dagger(\phi_L) L_k(\phi_L) \right). \quad (2.2.2)$$

Here L_k are function of fields. The *Lindblad form* can be derived from the master equation of Markovian open quantum systems, known as Gorini-Kossakowski-Sudarshan-Lindblad (GKSL) equation[25, 24].

The GKSL equation is a differential equation for non-unitary time evolution of density matrix,

³See [75] for early work on the subject and [5] for recent attempts in this direction, in addition to [76, 4, 77, 78] for technical issues regarding renormalization.

given by

$$\frac{d\rho}{dt} = -i[H, \rho] + \sum_k \gamma_k \left[L_k \rho L_k^\dagger - \frac{1}{2} \left\{ L_k^\dagger L_k, \rho \right\} \right]. \quad (2.2.3)$$

Here, H is the Hamiltonian of the system leading to unitary part of evolution, whereas non-unitary (Feynman-Vernon) part of the evolution comes from rest of the terms on RHS. The non-unitarity is captured by a set of operators L_k and a set of couplings γ_k of the system. A textbook treatment of GKSL equation can be found in [26, 80, 81, 82, 83]

It is easily checked that (2.2.3) implies

$$\frac{d}{dt} \text{tr} \rho = 0, \quad (2.2.4)$$

i.e., it is trace-preserving. The trace preserving nature is a manifestation of the fact that the system has an underlying microscopic unitary description. We can understand this by the following argument. The density matrix ρ with a unitary microscopic description is obtained by tracing over the bath d.o.f. as $\rho = \text{tr}_b \rho_{sb}$. Taking a further trace over the system d.o.f. we get

$$\text{tr} \rho = \text{tr}_s \text{tr}_b \rho_{sb} = \text{tr}_{sb} \rho_{sb} = 1. \quad (2.2.5)$$

Thus, trace of ρ for a system with a microscopic unitary description, is always preserved as also asserted by GKSL equation. As a result the Feynman-Vernon influence phase in Lindblad form (2.2.2) ensures microscopic unitarity. If γ_k is positive, one can show that (2.2.3) describes a dissipative system. Further, positive γ_k keeps eigenvalues of ρ non-negative. The trace-preserving and positivity condition (along with the linearity of ρ) qualify Lindblad form of evolution as a physically sensible dynamics describing an open quantum system. The GKSL equation in Schrödinger picture has an equivalent Heisenberg picture description via an evolution equation for operators:

$$i\hbar \frac{d\mathcal{A}}{dt} = [\mathcal{A}, H] + i \sum_k \gamma_k \left(L_k^\dagger \mathcal{A} L_k - \frac{1}{2} L_k^\dagger L_k \mathcal{A} - \frac{1}{2} \mathcal{A} L_k^\dagger L_k \right). \quad (2.2.6)$$

Equivalently, one can obtain a path-integral description as

$$\int \mathcal{D}\phi_R \mathcal{D}\phi_L e^{iS_{FV}} \quad (2.2.7)$$

We note that Lindblad form of the influence phase (2.2.2) has a particular structure which relates the ϕ_R - ϕ_L cross-terms with the imaginary parts of both ϕ_R action and ϕ_L action.

Let us note some important features of (2.2.2). If we set $\phi_R = \phi_L$, the influence phase vanishes. It is clear that this is exactly the calculation done few lines ago in the Schrödinger picture to show

that Lindblad evolution is trace-preserving. Thus, trace preserving property in the Schrödinger picture becomes ϕ_R, ϕ_L identification condition at the level of SK path integral for the EFT.

We also note that if we take one of the Lindblad operators as identity operator, the Lindblad form becomes a difference operator, i.e., it can be written as a difference between an operator made of ket fields and the same operator evaluated over the bra fields. This is the form of SK action for a unitary QFT and it merely shifts the system action. But when both Lindblad operators are not identity, one gets various cross terms and associated imaginary contributions to pure ϕ_R and pure ϕ_L action. Thus, once the cross couplings are determined, one can use the Lindblad form to find all imaginary couplings. This is the route we will take to study a toy model of open EFT ($\phi^3 + \phi^4$ theory).

Having finished a brief review of the necessary ideas, let us turn to study renormalisation of open $\phi^3 + \phi^4$ theory. We will begin by describing in detail the effective action and the associated Feynman rules in the next section.

Chapter 3

Renormalisation of open $\phi^3 + \phi^4$ theory

Scalar field theory has been extensively used as toy model for various purposes. The commonly used models are the scalar ϕ^3 and ϕ^4 theory. In our understanding of relativistic open QFTs, we consider $\phi^3 + \phi^4$ theory in $d = 4$ space-time dimensions. We begin by writing an ansatz for the open EFT as the following.

$$\begin{aligned}
 S_\phi = & - \int d^d x \left[\frac{1}{2} z (\partial\phi_R)^2 + \frac{1}{2} m^2 \phi_R^2 + \frac{\lambda_3}{3!} \phi_R^3 + \frac{\lambda_4}{4!} \phi_R^4 + \frac{\sigma_3}{2!} \phi_R^2 \phi_L + \frac{\sigma_4}{3!} \phi_R^3 \phi_L \right] \\
 & + \int d^d x \left[\frac{1}{2} z^* (\partial\phi_L)^2 + \frac{1}{2} m^{2*} \phi_L^2 + \frac{\lambda_3^*}{3!} \phi_L^3 + \frac{\lambda_4^*}{4!} \phi_L^4 + \frac{\sigma_3^*}{2!} \phi_L^2 \phi_R + \frac{\sigma_4^*}{3!} \phi_L^3 \phi_R \right] \\
 & + i \int d^d x \left[z_\Delta (\partial\phi_R) \cdot (\partial\phi_L) + m_\Delta^2 \phi_R \phi_L + \frac{\lambda_\Delta}{2!2!} \phi_R^2 \phi_L^2 \right].
 \end{aligned} \tag{3.0.1}$$

This is the most general local, power-counting renormalisable, Lorentz invariant and CPT invariant action that could be written down involving ϕ_R and ϕ_L . Note that CPT acts as an anti-linear, anti-unitary symmetry exchanging ϕ_R and ϕ_L and taking $i \mapsto (-i)$. It can be easily checked that, under this anti-linear, anti-unitary flip e^{iS} remains invariant provided the couplings appearing in the last line of action $\{z_\Delta, m_\Delta^2, \lambda_\Delta\}$ are real. This action along with a future boundary condition identifying ϕ_R and ϕ_L at future infinity defines the SK effective theory which we will study in this chapter.

There are two features of the above action which makes it distinct from the SK effective action of the unitary $\phi^3 + \phi^4$ theory. First, there are interaction terms which couple ket field ϕ_R with the bra field ϕ_L . Such cross couplings necessarily violate unitarity and the breakdown of the usual Cutkosky cutting rules. They are also necessarily a part of 'influence functionals' as defined by Feynman and Vernon and are generated only when a part of the system is traced out [22, 67]. A more obvious way the above action violates unitarity is due to the fact that S is not purely real.

If we turn off all cross couplings between ϕ_R and ϕ_L and set to zero all imaginary couplings in S , we recover the SK effective action of the unitary ϕ^4 theory :

$$S_{\phi, \text{Unitary}} = - \int d^d x \left[\frac{1}{2} \text{Re}[z] (\partial\phi_R)^2 + \frac{1}{2} \text{Re}[m^2] \phi_R^2 + \frac{\text{Re}[\lambda_3]}{3!} \phi_R^3 + \frac{\text{Re}[\lambda_4]}{4!} \phi_R^4 \right] \\ + \int d^d x \left[\frac{1}{2} \text{Re}[z] (\partial\phi_L)^2 + \frac{1}{2} \text{Re}[m^2] \phi_L^2 + \frac{\text{Re}[\lambda_3]}{3!} \phi_L^3 + \frac{\text{Re}[\lambda_4]}{4!} \phi_L^4 \right]. \quad (3.0.2)$$

Our aim is to deform ϕ^4 theory away from this familiar unitary limit and study the theory defined in (3.0.1) via perturbation theory.

The first question one could ask is whether this theory is renormalisable in perturbation theory, i.e., whether, away from unitary limit, the one-loop divergences in this theory can be absorbed into counter terms of the same form. We show in this chapter that the action is one loop renormalisable due to tadpole and bubble diagrams. It is worthwhile to note at this point that loops in open scalar field theories are not always well behaved. Loop diagrams other than tadpole and bubble diagrams are non-local divergent. These divergences can not be regulated by adapting usual renormalisation prescription. We will elaborate these in §§4 and §§5.

One might ask why are we interested in Lorentz invariance of the EFTs. This is because, if the field theory describes an open system, it most likely dissipates. Thus one should break Lorentz invariance by adding all possible single derivative terms. But, one can show that the Lorentz violating terms have different divergence structures of loop integrals and it does not remove the non-local divergences. Thus to keep the theory simple, we drop all non-Lorentz invariant terms.

3.1 Lindblad conditions and Feynman rules

3.1.1 Lindblad condition

Imposing CPT and demanding that the action (3.0.1) should be of the Lindblad form, we get four constraints among the coupling constants - one for field renormalisation, one for the mass, one for the cubic coupling and one for quartic coupling terms. We call these constraints as the Lindblad conditions. The Lindblad form as discussed in 2.2 ensures the presence of a microscopic unitary description of the system. So, we expect the Lindblad conditions bear the same physical significance. We tabulate all the power counting renormalisable Lindblad terms in the $\phi^3 + \phi^4$ theory in Table. 3.1. We will now consider various parts of the action in turn and rewrite them in a way that Lindblad conditions become manifest.

| Lindblad couplings $\Gamma_{\alpha\beta}$ | $L_\alpha^\dagger[\phi]$ | $L_\beta[\phi]$ | Imaginary coupling of $L_\alpha^\dagger L_\beta$ | Lindblad condition |
|--|--------------------------|---------------------|---|--|
| z_Δ | $\partial_\mu \phi$ | $\partial_\mu \phi$ | $\text{Im } z$ | $\text{Im } z = z_\Delta$ |
| m_Δ^2 | ϕ | ϕ | $\text{Im } m^2$ | $\text{Im } m^2 = m_\Delta^2$ |
| $\frac{\lambda_\Delta}{2!2!}$ | ϕ^2 | ϕ^2 | $\text{Im } \lambda_4$ | $\text{Im } \lambda_4 = 3\lambda_\Delta - 4 \text{Im } \sigma_4$ |
| $i\frac{\sigma_4}{3!}$ | ϕ^3 | ϕ | $\text{Im } \lambda_4$ | |
| $-i\frac{\sigma_4^*}{3!}$ | ϕ | ϕ^3 | $\text{Im } \lambda_4$ | $\text{Im } \lambda_3 = -3 \text{Im } \sigma_3$ |
| $i\frac{\sigma_3}{2!}$ | ϕ^2 | ϕ | $\text{Im } \lambda_3$ | |
| $-i\frac{\sigma_3^*}{2!}$ | ϕ | ϕ^2 | $\text{Im } \lambda_3$ | |

Table 3.1: Renormalisable Lindblad operators for $\phi^3 + \phi^4$ theory

Real terms of the action

The real part of the action is given by

$$\begin{aligned}
\text{Re}[S] = & - \int d^d x \left[\frac{1}{2} \text{Re}[z] [(\partial\phi_R)^2 - (\partial\phi_L)^2] + \frac{1}{2} \text{Re}[m^2](\phi_R^2 - \phi_L^2) \right] \\
& - \int d^d x \left[\frac{\text{Re } \lambda_4}{4!} (\phi_R^4 - \phi_L^4) + \frac{\text{Re } \sigma_4}{3!} \phi_R \phi_L (\phi_R^2 - \phi_L^2) \right] \\
& - \int d^d x \left[\frac{\text{Re } \lambda_3}{3!} (\phi_R^3 - \phi_L^3) + \frac{\text{Re } \sigma_3}{2!} \phi_R \phi_L (\phi_R - \phi_L) \right]
\end{aligned} \tag{3.1.1}$$

We note that CPT constrains this action to vanish when $\phi_R = \phi_L$. As a result, there are no condition on these real coupling from the Lindblad structure.

Imaginary Quadratic terms of the action

The imaginary part of the quadratic terms is given by

$$\begin{aligned}
\text{Im}[S_2] = & - \int d^d x \left[\frac{1}{2} \text{Im}[z] ((\partial\phi_R)^2 + (\partial\phi_L)^2) - z_\Delta (\partial\phi_R) \cdot (\partial\phi_L) \right] \\
& - \int d^d x \left[\frac{1}{2} \text{Im}[m^2](\phi_R^2 + \phi_L^2) - m_\Delta^2 \phi_R \phi_L \right] \\
= & - \int d^d x \left[\frac{1}{2} \text{Im}[z] (\partial\phi_R - \partial\phi_L)^2 + \frac{1}{2} \text{Im}[m^2](\phi_R - \phi_L)^2 \right] \\
& + \int d^d x \left[(z_\Delta - \text{Im}[z]) (\partial\phi_R) \cdot (\partial\phi_L) + (m_\Delta^2 - \text{Im}[m^2]) \phi_R \phi_L \right]
\end{aligned} \tag{3.1.2}$$

The Lindblad condition is given by

$$z_{\Delta} = \text{Im} [z] , \quad m_{\Delta}^2 = \text{Im} [m^2] , \quad (3.1.3)$$

Imaginary Cubic coupling

Now we compute the imaginary part of the cubic terms in the action

$$\begin{aligned} -\text{Im} [S_3] &= \int d^d x \left[\frac{\text{Im} \lambda_3}{3!} \phi_R^3 + \frac{\text{Im} \lambda_3}{3!} \phi_L^3 + \frac{\text{Im} \sigma_3}{2!} \phi_R^2 \phi_L + \frac{\text{Im} \sigma_3}{2!} \phi_L^2 \phi_R \right] \\ &= \int d^d x \left[\frac{\text{Im} \lambda_3}{3!} (\phi_R - \phi_L)(\phi_R^2 - \phi_L^2) + \left(\frac{\text{Im} \lambda_3}{3!} + \frac{\text{Im} \sigma_3}{2!} \right) (\phi_R^2 \phi_L + \phi_L^2 \phi_R) \right] \end{aligned} \quad (3.1.4)$$

The Lindblad condition is given by

$$\begin{aligned} \frac{\text{Im} \lambda_3}{3!} + \frac{\text{Im} \sigma_3}{2!} &= 0 \\ \Rightarrow \text{Im} \lambda_3 + 3\text{Im} \sigma_3 &= 0 \end{aligned} \quad (3.1.5)$$

Imaginary Quartic coupling

The imaginary part of action at the level quartic coupling is given by

$$\begin{aligned} \text{Im}[S_4] &= - \int d^d x \left[\frac{1}{4!} \text{Im}[\lambda_4] (\phi_R^4 + \phi_L^4) + \frac{1}{3!} \text{Im}[\sigma_4] (\phi_R^3 \phi_L + \phi_R \phi_L^3) - \frac{\lambda_{\Delta}}{2!2!} \phi_R^2 \phi_L^2 \right] \\ &= - \int d^d x \left[\left(\frac{1}{4!} \text{Im}[\lambda_4] + \frac{1}{3!} \text{Im}[\sigma_4] \right) (\phi_R^2 - \phi_L^2)^2 + \frac{1}{3!} \text{Im}[\sigma_4] (\phi_R - \phi_L) (\phi_R^3 - \phi_L^3) \right] \\ &\quad + \int d^d x \left[\frac{\lambda_{\Delta}}{2!2!} - 2 \text{Im} \left(\frac{\lambda_4}{4!} + \frac{\sigma_4}{3!} \right) \right] \phi_R^2 \phi_L^2 \end{aligned} \quad (3.1.6)$$

The Lindblad condition at for the quartic couplings is given by

$$\begin{aligned} \frac{\lambda_{\Delta}}{2!2!} &= 2 \text{Im} \left(\frac{\lambda_4}{4!} + \frac{\sigma_4}{3!} \right) \\ \Rightarrow \text{Im} \lambda_4 + 4\text{Im} \sigma_4 - 3\lambda_{\Delta} &= 0 \end{aligned} \quad (3.1.7)$$

Since the Lindblad conditions indicate the presence of a microscopic unitary theory, we expect these conditions are preserved under renormalisation.

3.1.2 Exact propagators

The ket field ϕ_R and the bra field ϕ_L in SK path-integral satisfy the following boundary condition

$$\phi_R(t = \infty) = \phi_L(t = \infty) \quad (3.1.8)$$

Owing to this boundary condition and the mixing term between ϕ_R and ϕ_L fields, the kinetic matrix derived from the action (3.0.1) is given by

$$\mathcal{K} = \begin{pmatrix} i(z k^2 + m^2 - i\varepsilon) & z_\Delta k^2 + m_\Delta^2 - 2\varepsilon \Theta(-k^0) \\ z_\Delta k^2 + m_\Delta^2 - 2\varepsilon \Theta(k^0) & -i(z^* k^2 + (m^2)^* + i\varepsilon) \end{pmatrix} \quad (3.1.9)$$

where the ε prescription implements Schwinger-Keldysh boundary conditions. We define the kinetic matrix \mathcal{K} by

$$iS \ni -\frac{1}{2} \left(\phi_R(-k) \phi_L(-k) \right) \mathcal{K} \begin{pmatrix} \phi_R(k) \\ \phi_L(k) \end{pmatrix} \quad (3.1.10)$$

Its inverse (viz., the propagator) can be written as

$$\begin{aligned} \mathcal{K}^{-1} &\equiv \begin{pmatrix} \langle \phi_R(-k) \phi_R(k) \rangle & \langle \phi_R(-k) \phi_L(k) \rangle \\ \langle \phi_L(-k) \phi_R(k) \rangle & \langle \phi_L(-k) \phi_L(k) \rangle \end{pmatrix} \\ &= \mathfrak{z}^{-1} \begin{pmatrix} \frac{-i}{\text{Re}[zk^2 + m^2] - i\varepsilon} & 2\pi\delta(\text{Re}[zk^2 + m^2])\Theta(-k^0) \\ 2\pi\delta(\text{Re}[zk^2 + m^2])\Theta(k^0) & \frac{i}{\text{Re}[zk^2 + m^2] + i\varepsilon} \end{pmatrix} \\ &\quad + \mathfrak{z}^{-1} \frac{(-i)}{\text{Re}[zk^2 + m^2] - i\varepsilon} \times \frac{i}{\text{Re}[zk^2 + m^2] + i\varepsilon} \times \begin{pmatrix} \text{Im}[zk^2 + m^2] & z_\Delta k^2 + m_\Delta^2 \\ z_\Delta k^2 + m_\Delta^2 & \text{Im}[zk^2 + m^2] \end{pmatrix} \end{aligned} \quad (3.1.11)$$

where,

$$\mathfrak{z} \equiv 1 + \frac{(-i)}{\text{Re}[zk^2 + m^2] - i\varepsilon} \times \frac{i}{\text{Re}[zk^2 + m^2] + i\varepsilon} \times \left((\text{Im}[zk^2 + m^2] - \varepsilon)^2 - (z_\Delta k^2 + m_\Delta^2 - \varepsilon)^2 \right) \quad (3.1.12)$$

Please note that when the Lindblad conditions (3.1.3) are satisfied, we have

$$\mathfrak{z} = 1 . \quad (3.1.13)$$

Further, it can be easily checked that in this limit, the sum of diagonal entries in the propagator matrix equal to the sum of off-diagonal entries, i.e.,

$$(\mathcal{K}^{-1})_{RR} + (\mathcal{K}^{-1})_{LL} = (\mathcal{K}^{-1})_{RL} + (\mathcal{K}^{-1})_{LR} . \quad (3.1.14)$$

The corresponding property in the unitary quantum field theory is the well-known relation between the various correlators in the Keldysh formalism [28]. This can equivalently be reformulated as the vanishing of two point function of two difference correlators :

$$(\mathcal{K}^{-1})_{R-L, R-L} = 0. \quad (3.1.15)$$

In this work, we will work in the limit where the non-unitary couplings $\text{Im}[m^2]$ and m_Δ^2 are considered as perturbations to $\text{Re}[m^2]$, and similarly, $\text{Im}[z^2]$ and z_Δ^2 are considered small compared to $\text{Re}[z^2]$. Further, since 1-loop correction to the propagators do not generate field renormalisation we can also set $z = 1$. In this limit, the propagators in equation (3.1.11) reduced to those given by figure 1.

3.1.3 Feynman rules

In this paper henceforth, we will set $z = z_\Delta = 1$ (which is not renormalised at one-loop in $d=4$ dimensions). We will treat all other parameters in our action except the real part of m^2 (i.e., $\text{Re}(m^2)$) perturbatively. This includes $\lambda_3, \sigma_3, \lambda_4, \sigma_4$ and λ_Δ , as well as $\text{Im} m^2$ and m_Δ^2 .

The propagators of ϕ fields are given below. We have used solid blue and dotted blue lines for ϕ_R (ket fields) and ϕ_L (bra fields) fields respectively. Note that in the cut propagators P and M the energy is restricted to flow from the ket field to the bra field.

| | | |
|--------------|------------------|--------------------------------|
| Propagator R | p ————— | $\frac{-i}{p^2+m^2-i\epsilon}$ |
| Propagator P | p ——— ——— | $2\pi\delta_+(p^2 + m^2)$ |
| Propagator M | p ————— ——— | $2\pi\delta_-(p^2 + m^2)$ |
| Propagator L | p ————— | $\frac{i}{p^2+m^2+i\epsilon}$ |

Figure 1: SK propagator for ϕ fields

We will now set up the Veltman rules for the vertices to compute SK correlators in the open $\phi^3 + \phi^4$ theory:

| Vertex | Factor |
|---------------------|--|
| ϕ_R^3 | $(-i\lambda_3)(2\pi)^d \delta(\sum p)$ |
| ϕ_L^3 | $(i\lambda_3^*)(2\pi)^d \delta(\sum p)$ |
| $\phi_R^2 \phi_L$ | $(-i\sigma_3)(2\pi)^d \delta(\sum p)$ |
| $\phi_R \phi_L^2$ | $(i\sigma_3^*)(2\pi)^d \delta(\sum p)$ |
| ϕ_R^4 | $(-i\lambda_4)(2\pi)^d \delta(\sum p)$ |
| ϕ_L^4 | $(i\lambda_4^*)(2\pi)^d \delta(\sum p)$ |
| $\phi_R^3 \phi_L$ | $(-i\sigma_4)(2\pi)^d \delta(\sum p)$ |
| $\phi_R \phi_L^3$ | $(i\sigma_4^*)(2\pi)^d \delta(\sum p)$ |
| $\phi_R^2 \phi_L^2$ | $(-\lambda_\Delta)(2\pi)^d \delta(\sum p)$ |

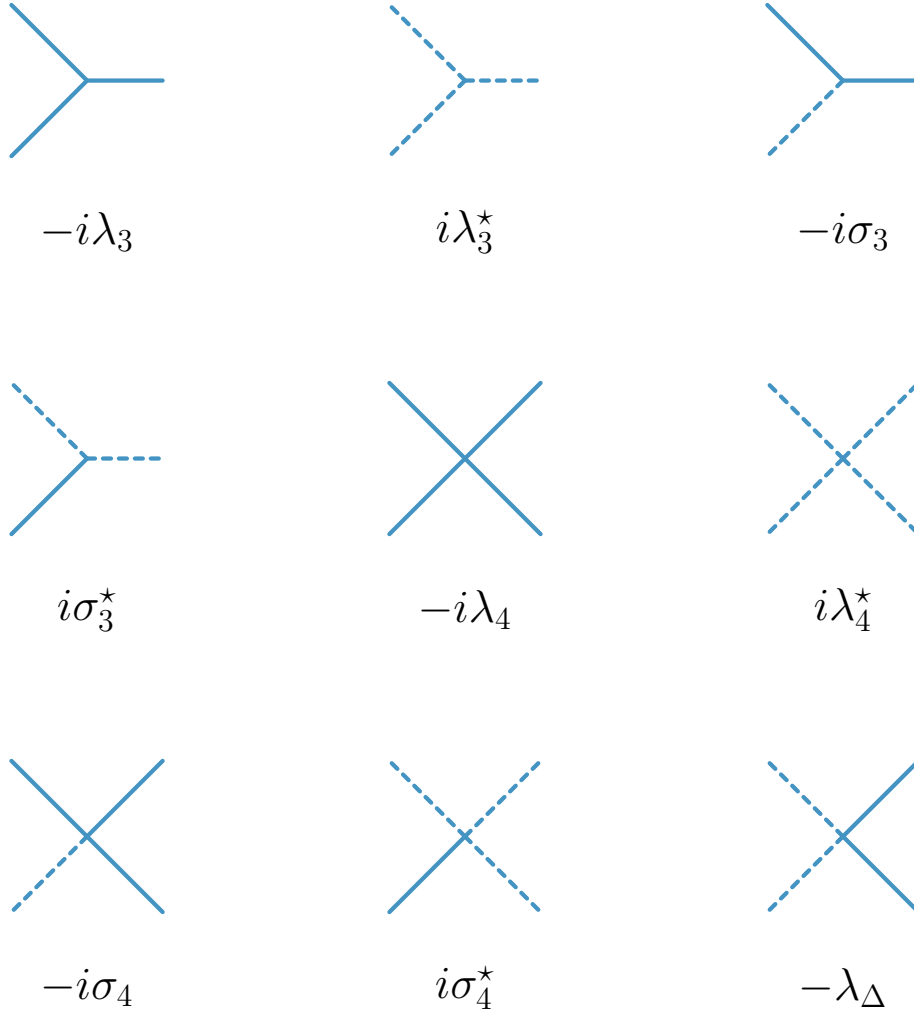


Figure 2: Diagrammatic Representation of all the Tree level processes

3.1.4 Lindblad condition from tree level correlators

In an unitary Schwinger-Keldysh theory, the correlator of difference operators vanishes in all order of perturbation theory and that this is equivalent to Veltman's largest time equation [73]. We want to see whether that statement is valid in our non-unitary theory. We have already remarked during our discussion of propagators around equation (3.1.11) that the quadratic Lindblad conditions are equivalent to the vanishing of difference operator two point functions. We can extend this to higher point functions simply. Consider the tree level correlator of three difference operators

$$\begin{aligned} & \langle (\phi_R(p_1) - \phi_L(p_1))(\phi_R(p_2) - \phi_L(p_2))(\phi_R(p_3) - \phi_L(p_3)) \rangle \\ & = -i(\lambda_3 - \lambda_3^*) - 4i(\sigma_3 - \sigma_3^*) = 2(\text{Im } \lambda_3 + 3 \text{Im } \sigma_3) \end{aligned} \quad (3.1.16)$$

the correlator of four difference operators is given by

$$\begin{aligned} & \langle (\phi_R(p_1) - \phi_L(p_1))(\phi_R(p_2) - \phi_L(p_2))(\phi_R(p_3) - \phi_L(p_3))(\phi_R(p_4) - \phi_L(p_4)) \rangle \\ & = -i(\lambda_4 - \lambda_4^*) - 4i(\sigma_4 - \sigma_4^*) - 3\lambda_\Delta = 2(\text{Im } \lambda_4 + 4 \text{Im } \sigma_4 - 3\lambda_\Delta) \end{aligned} \quad (3.1.17)$$

The correlators of the three and the four difference operators are precisely given by the Lindblad violating couplings. This implies at tree level, Lindblad conditions are same as the vanishing of correlators of the difference operators.

One can, in fact, show the following statement [84]: consider an open EFT, which is obtained by tracing out some subset of fields in an underlying unitary theory. Then, the unitarity of the underlying theory implies that the open EFT satisfies the Lindblad condition.

3.2 One loop beta function

In this section, we compute the beta function for all the mass terms and the coupling constants that appear in the action of the open $\phi^3 + \phi^4$ theory. The main aim in this section would be to demonstrate the following three claims :

1. Despite the novel UV divergences that occur in the open $\phi^3 + \phi^4$ theory, one can use a simple extension of the standard counter term method to deal with the divergences. Thus, the open $\phi^3 + \phi^4$ theory is one-loop renormalisable.
2. Once these UV divergences are countered, the standard derivation of beta functions and RG running also goes through, except for the fact that one has to now also renormalise the non-unitary couplings.

3. We will also demonstrate that the running of a certain combinations of the couplings, the ones which given by the Lindblad conditions (equation (3.1.3), equation (3.1.5) and equation (3.1.7) respectively), under one-loop renormalisation are proportional to the Lindblad conditions.

We shall provide an all-order proof in the next section that the Lindblad conditions are never violated under perturbative corrections. Here we shall use the notations and results presented in appendix A.2.

3.2.1 One loop beta function for m^2

We will now begin a discussion of various loop diagrams. The simplest is perhaps the tadpole diagrams which can be cancelled by a counter term linear in ϕ_R and ϕ_L . It is easily demonstrated that the necessary counter-terms do not violate the Lindblad condition (See appendix A.5).

Let us compute the one loop beta function for m^2 . We shall consider all the one loop Feynman diagrams that contributes to the process $\phi_R \rightarrow \phi_R$. One can verify that there are mainly two types of diagrams - one class of diagrams due to the cubic couplings, as depicted in figure 9, and the other class of diagrams due to quartic couplings, depicted in figure 4.

The sum of the contribution from all the Feynman diagrams is given by

$$\begin{aligned}
& -im^2 \\
& + \frac{(-i\lambda_3)^2}{2} B_{RR}(k) + \frac{(i\sigma_3^*)^2}{2} B_{LL}(k) + (-i\sigma_3)^2 B_{LR}(k) \\
& + \frac{(i\sigma_3^*)(-i\lambda_3)}{2} B_{PM}(k) + \frac{(i\sigma_3^*)(-i\lambda_3)}{2} B_{MP}(k) + (-i\sigma_3)^2 B_{PP}(k) \\
& + (-i\lambda_3)(-i\sigma_3) B_{PR}(k) + (-i\lambda_3)(-i\sigma_3) B_{MR}(k) \\
& + (i\sigma_3^*)(-i\sigma_3) B_{PL}(k) + (i\sigma_3^*)(-i\sigma_3) B_{ML}(k) \\
& + \frac{(-i\lambda_4)}{2} A_R + \frac{(-\lambda_\Delta)}{2} A_L + (-i\sigma_4) A_M
\end{aligned} \tag{3.2.1}$$

Using the results in (A.2.79a)-(A.2.79d), we can see that the contribution is divergent and one needs to add one loop counter-terms δm^2 , in the $\overline{\text{MS}}$ scheme, to absorb the divergences.

$$\begin{aligned}
\delta m^2 \Big|_{\overline{\text{MS}}} &= -\frac{1}{(4\pi)^2} \left[(\lambda_3)^2 - (\sigma_3^*)^2 + 2 \{ \lambda_3 \sigma_3 + |\sigma_3|^2 \} \right] \left[\frac{1}{d-4} + \frac{1}{2} (\gamma_E - 1 - \ln 4\pi) \right] \\
&\quad - \frac{1}{(4\pi)^2} [\lambda_4 - i\lambda_\Delta + 2\sigma_4] \left[\frac{1}{d-4} + \frac{1}{2} (\gamma_E - 1 - \ln 4\pi) \right] (\text{Re } m^2)
\end{aligned} \tag{3.2.2}$$

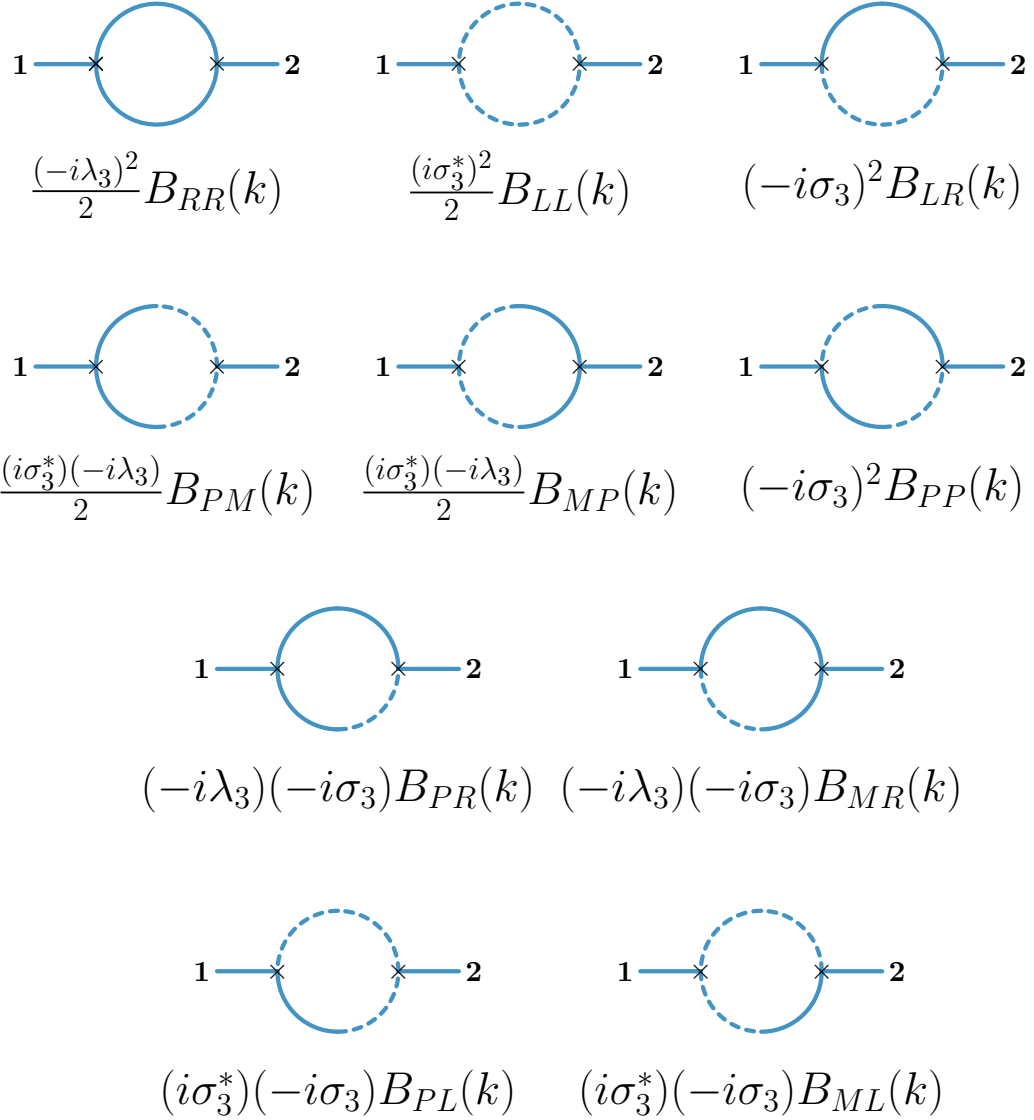


Figure 3: One Loop corrections to m^2 due to cubic couplings

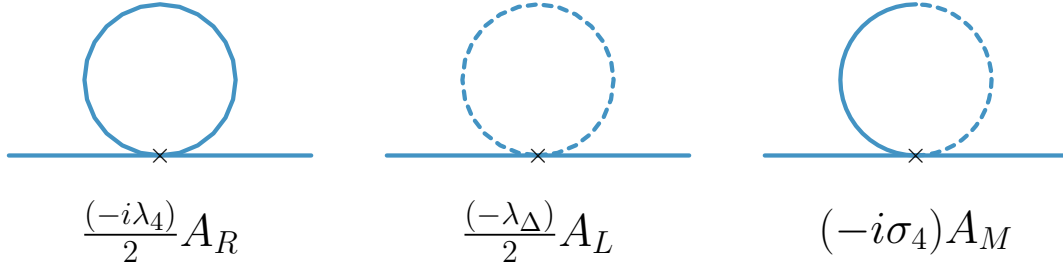


Figure 4: One loop correction to m^2 due to quartic couplings

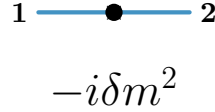


Figure 5: Diagrammatic representation of the one loop counter-term for m^2

Using the standard methods of quantum field theory, one can then compute the one loop beta function as

$$\beta_{m^2} = \frac{1}{(4\pi)^2} \left[(\lambda_3)^2 - (\sigma_3^*)^2 + 2 \{ \lambda_3 \sigma_3 + |\sigma_3|^2 \} + (\lambda_4 - i\lambda_\Delta + 2\sigma_4) (\text{Re } m^2) \right] \quad (3.2.3)$$

If set $\sigma_3 = \sigma_4 = \lambda_\Delta = 0$, then we get back the standard results of $\phi^3 + \phi^4$ theory in $d = 4$ space-time dimensions.

3.2.2 One loop beta function for m_Δ^2

Now, we will compute the one loop beta function for m_Δ^2 . As in the case of m^2 , there will again be two classes of diagrams. The diagrams due to cubic and quartic couplings are as shown in figure 10 and in figure 8 respectively. The sum over all the contributions are given by

$$\begin{aligned} & -m_\Delta^2 \\ & + \frac{(-i\lambda_3)(-i\sigma_3)}{2} B_{RR}(k) + \frac{(i\lambda_3^*)(i\sigma_3^*)}{2} B_{LL}(k) + (-i\sigma_3)(i\sigma_3^*) B_{LR}(k) \\ & + \frac{(-i\lambda_3)(i\lambda_3^*)}{2} B_{PM}(k) + \frac{(-i\sigma_3)(i\sigma_3^*)}{2} B_{MP}(k) + (-i\sigma_3)(i\sigma_3^*) B_{PP}(k) \\ & + (i\sigma_3^*)(-i\lambda_3) B_{PR}(k) + (-i\sigma_3)^2 B_{MR}(k) + (-i\sigma_3)(i\lambda_3^*) B_{PL}(k) + (i\sigma_3^*)^2 B_{ML}(k) \\ & + \frac{(-i\sigma_4)}{2} A_R + \frac{(i\sigma_4^*)}{2} A_L + (-\lambda_\Delta) A_M \end{aligned} \quad (3.2.4)$$

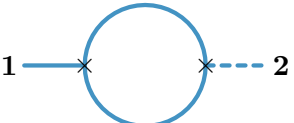

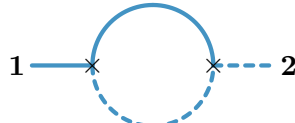
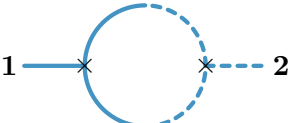
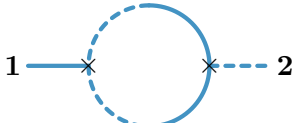
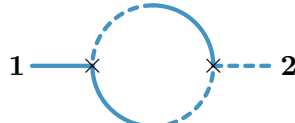
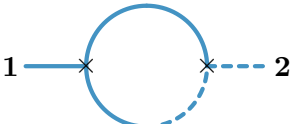
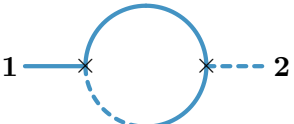
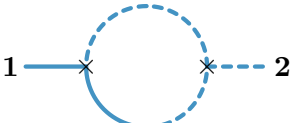
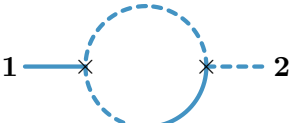
| | | |
|---|--|---|
|  |  |  |
| $\frac{(-i\lambda_3)(-i\sigma_3)}{2} B_{RR}(k)$ | $\frac{(i\lambda_3^*)(i\sigma_3^*)}{2} B_{LL}(k)$ | $(-i\sigma_3)(i\sigma_3^*) B_{LR}(k)$ |
|  |  |  |
| $\frac{(-i\lambda_3)(i\lambda_3^*)}{2} B_{PM}(k)$ | $\frac{(-i\sigma_3)(i\sigma_3^*)}{2} B_{MP}(k)$ | $(-i\sigma_3)(i\sigma_3^*) B_{PP}(k)$ |
|  |  | |
| $(i\sigma_3^*)(-i\lambda_3) B_{PR}(k)$ | $(-i\sigma_3)^2 B_{MR}(k)$ | |
|  |  | |
| $(-i\sigma_3)(i\lambda_3^*) B_{PL}(k)$ | $(i\sigma_3^*)^2 B_{ML}(k)$ | |

Figure 6: One Loop corrections to m_Δ^2 due to cubic couplings

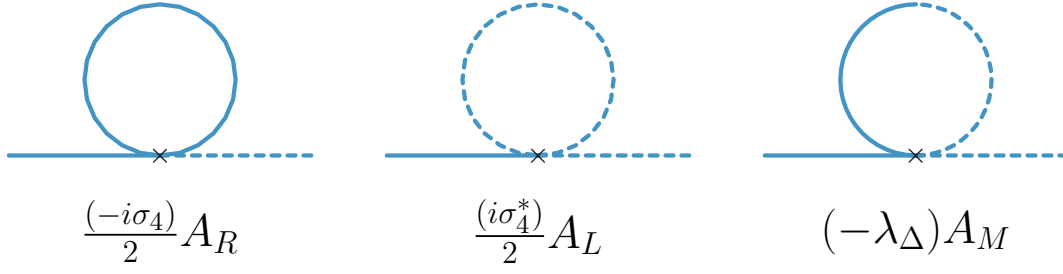


Figure 7: One loop correction to m_Δ^2 due to quartic couplings

Some of these one loop contributions are divergent and one needs to add one loop counter-terms. The m_Δ^2 counter-term in $\overline{\text{MS}}$ scheme is given by

$$\delta m_\Delta^2 \Big|_{\overline{\text{MS}}} = -\frac{1}{(4\pi)^2} \left[-4(\text{Re } \lambda_3 + \text{Re } \sigma_3) \text{Im } \sigma_3 + (2\lambda_\Delta - 2\text{Im } \sigma_4)(\text{Re } m^2) \right] \left[\frac{1}{d-4} + \frac{1}{2}(\gamma_E - 1 - \ln 4\pi) \right] \quad (3.2.5)$$

and the beta function for m_Δ^2 is given by

$$\beta_{m_\Delta^2} = \frac{1}{(4\pi)^2} \left[-4(\text{Re } \lambda_3 + \text{Re } \sigma_3) \text{Im } \sigma_3 + (2\lambda_\Delta - 2\text{Im } \sigma_4)(\text{Re } m^2) \right] \quad (3.2.6)$$

3.2.3 Checking Lindblad condition for mass renormalization

From equation (3.2.3), we find that the beta function for $\text{Im } m^2$ is given by

$$\frac{d(\text{Im } m^2)}{d \ln \mu} = \frac{1}{(4\pi)^2} \left[2(\text{Re } \lambda_3 + \text{Re } \sigma_3)(\text{Im } \lambda_3 + \text{Im } \sigma_3) + (\text{Im } \lambda_4 + 2\text{Im } \sigma_4 - \lambda_\Delta)(\text{Re } m^2) \right] \quad (3.2.7)$$

Now, using equation (3.2.7) and equation (3.2.6), one gets the beta function for $(\text{Im } m^2 - m_\Delta^2)$

$$\beta_{(\text{Im } m^2 - m_\Delta^2)} = \frac{2}{(4\pi)^2} [(\text{Im } \lambda_3 + 3\text{Im } \sigma_3)(\text{Re } \lambda_3 + \text{Re } \sigma_3) + (\text{Im } \lambda_4 + 4\text{Im } \sigma_4 - 3\lambda_\Delta)(\text{Re } m^2)] \quad (3.2.8)$$

equation (3.2.8) shows that the one loop beta function for Lindblad violating mass terms vanish in the absence of Lindblad violating cubic (equation (3.1.5)) and quartic coupling (equation (3.1.7)) at the tree level.

3.2.4 One loop beta function for λ_3

Now we will compute the one loop beta function for various cubic couplings. The Passarino-Veltman C and D integrals will have no contribution to the one loop β function for the cubic

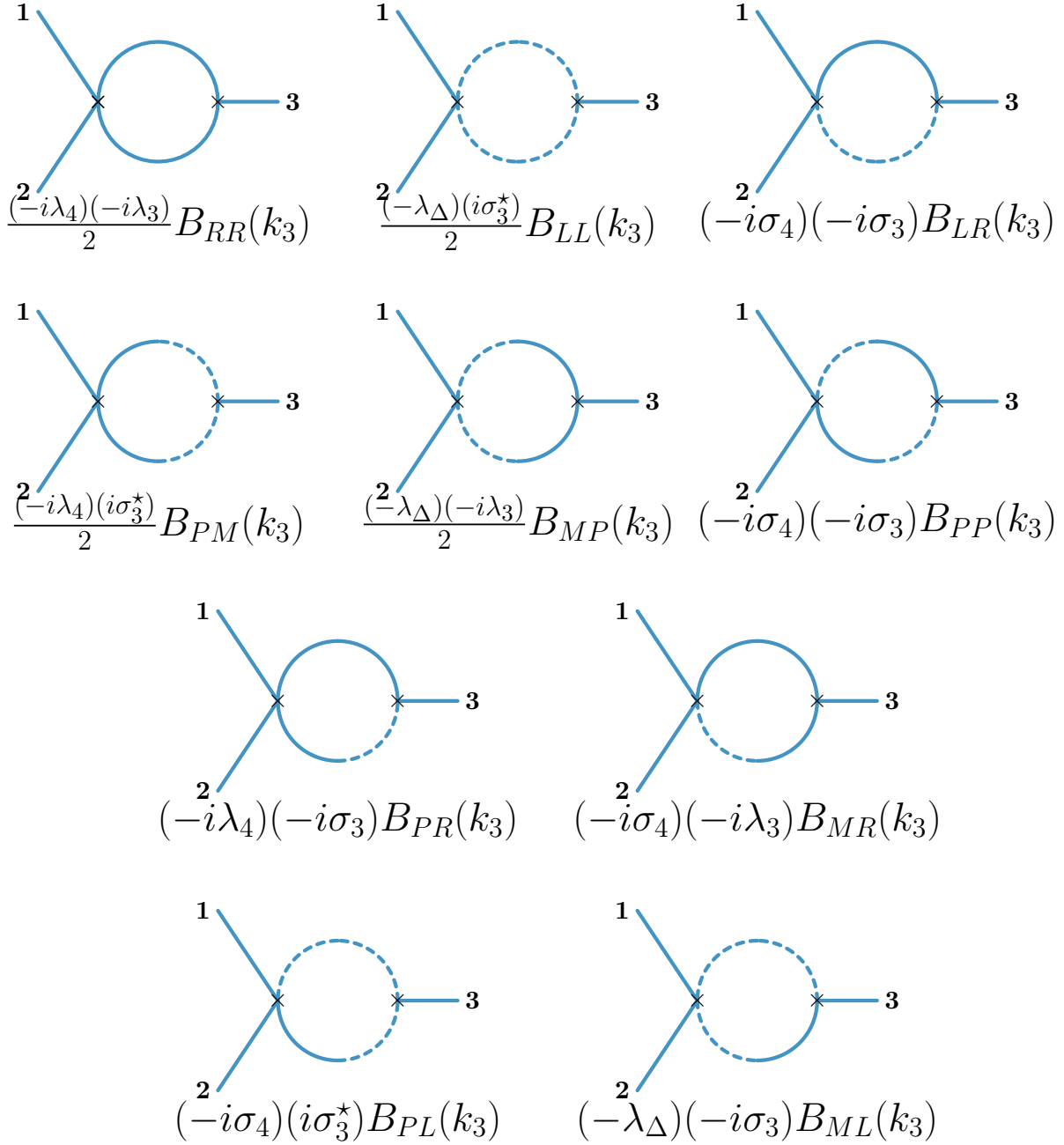


Figure 8: Diagrammatic representation of the Ten 1-Loop Integrals $\phi_R \phi_R \rightarrow \phi_R$

(and quartic) couplings, since they are UV finite ¹. Hence, we shall not consider those Feynman diagrams in our analysis. We begin with the beta function computation of λ_3 . The diagrams for one of the channels are depicted in figure 8. The other two channels are obtained by interchanging $1 \longleftrightarrow 3$ and $2 \longleftrightarrow 3$. The sum over the all the Feynman diagrams is given by

$$\begin{aligned}
& -i\lambda_3 \\
& + \frac{(-i\lambda_4)(-i\lambda_3)}{2} B_{RR}(k_3) + \frac{(-\lambda_\Delta)(i\sigma_3^*)}{2} B_{LL}(k_3) + (-i\sigma_4)(-i\sigma_3) B_{LR}(k_3) \\
& + \frac{(-i\lambda_4)(i\sigma_3^*)}{2} B_{PM}(k_3) + \frac{(-\lambda_\Delta)(-i\lambda_3)}{2} B_{MP}(k_3) + (-i\sigma_4)(-i\sigma_3) B_{PP}(k_3) \\
& + (-i\lambda_4)(-i\sigma_3) B_{PR}(k_3) + (-i\sigma_4)(-i\lambda_3) B_{MR}(k_3) \\
& + (-i\sigma_4)(i\sigma_3^*) B_{PL}(k_3) + (-\lambda_\Delta)(-i\sigma_3) B_{ML}(k_3) \\
& + \text{Two more channels}
\end{aligned} \tag{3.2.9}$$

Using the results in (A.2.79a)-(A.2.79d), we see that the one loop contributions are divergent and we need to add one loop counter-terms $\delta\lambda_3$ to cancel the divergences.

$$\begin{aligned}
\delta\lambda_3 \Big|_{\overline{\text{MS}}} &= -\frac{3}{(4\pi)^2} \left[\lambda_4\lambda_3 - 2\lambda_\Delta \text{Im} \sigma_3 + \lambda_4\sigma_3 + \sigma_4\lambda_3 + \sigma_4\sigma_3^* \right] \\
& \quad \left[\frac{1}{d-4} + \frac{1}{2}(\gamma_E - 1 - \ln 4\pi) \right]
\end{aligned} \tag{3.2.10}$$

Following the standard methods of quantum field theory, we compute the one loop beta function given by

$$\beta_{\lambda_3} = \frac{3}{(4\pi)^2} \left[\lambda_4\lambda_3 - 2\lambda_\Delta \text{Im} \sigma_3 + \lambda_4\sigma_3 + \sigma_4\lambda_3 + \sigma_4\sigma_3^* \right] \tag{3.2.11}$$

3.2.5 One loop beta function for σ_3

As described in previous subsection, we will only consider PV B type diagrams for two of the channels are depicted in figure 9 and in figure 10. The remaining channel is obtained by interchanging $1 \longleftrightarrow 2$ in the diagrams in figure 10. The sum over all the contributions are given by

$$-i\sigma_3 + i\mathcal{M}_1(k_3) + i\mathcal{M}_2(k_2) + i\mathcal{M}_2(k_1) \tag{3.2.12}$$

¹Note that the standard C and D integrals are well-known to be UV finite in the Euclidean theory. Since the SK versions of these integrals are different analytic continuations of these Euclidean integrals, they continue to be UV finite. We will leave the detailed computation including these finite contributions to future work.

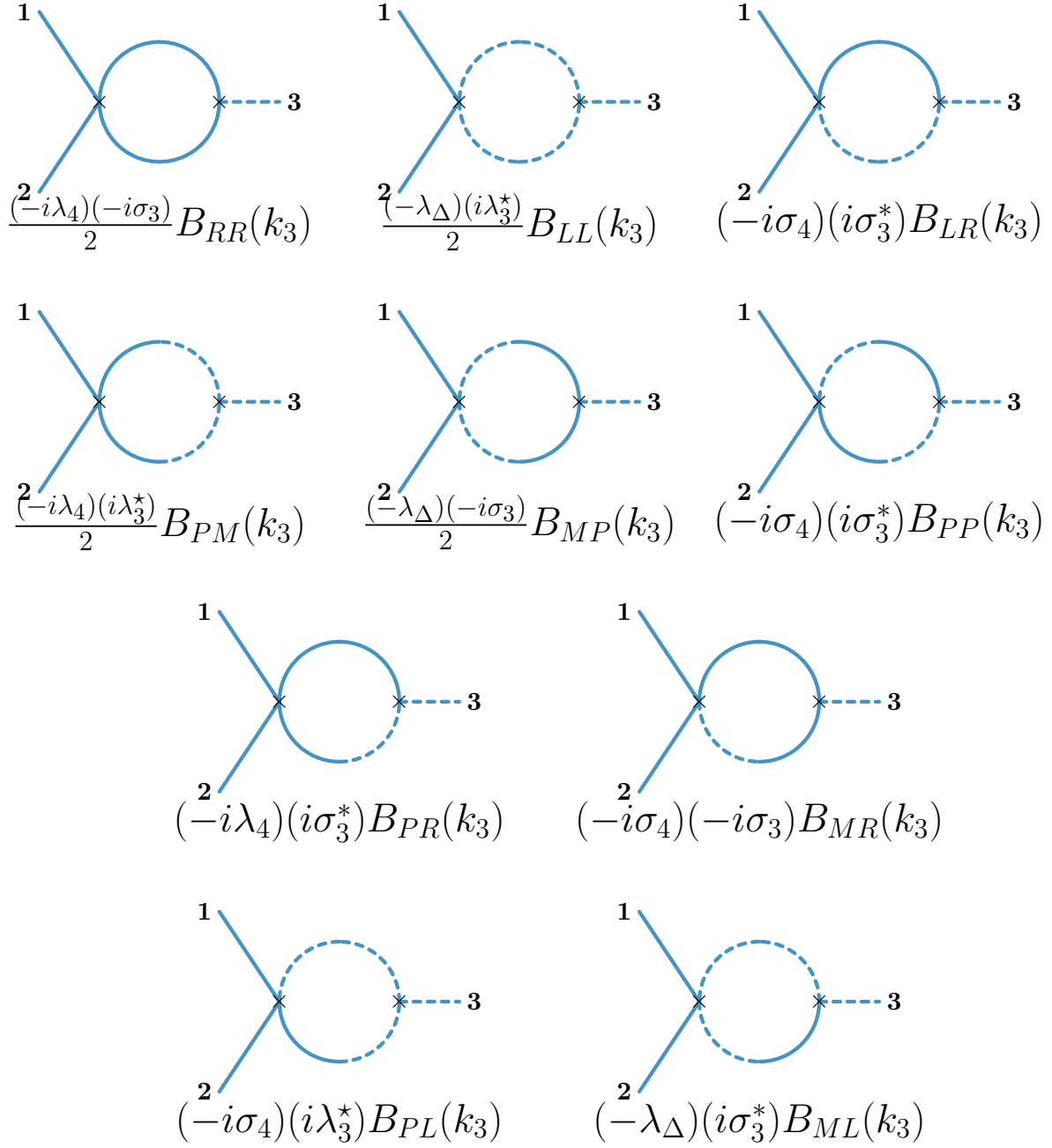


Figure 9: Diagrammatic representation of the Ten 1-Loop Integrals $\phi_R \phi_R \rightarrow \phi_L$

Here $i\sigma_3$ is the tree level contribution. The term $i\mathcal{M}_1(k_3)$ denotes the sum over Feynman diagrams in figure 9 whereas $i\mathcal{M}_2(k_2)$ denotes the sum over Feynman diagrams in figure 10. The contribution $i\mathcal{M}_2(k_1)$ is obtained by interchanging $1 \leftrightarrow 2$ in figure 10. The expression for $i\mathcal{M}_1(k_3)$ is given by

$$\begin{aligned}
i\mathcal{M}_1(k_3) = & \frac{(-i\lambda_4)(-i\sigma_3)}{2} B_{RR}(k_3) + \frac{(-\lambda_\Delta)(i\lambda_3^*)}{2} B_{LL}(k_3) + (-i\sigma_4)(i\sigma_3^*) B_{LR}(k_3) \\
& + \frac{(-i\lambda_4)(i\lambda_3^*)}{2} B_{PM}(k_3) + \frac{(-\lambda_\Delta)(-i\sigma_3)}{2} B_{MP}(k_3) + (-i\sigma_4)(i\sigma_3^*) B_{PP}(k_3) \\
& + (-i\lambda_4)(i\sigma_3^*) B_{PR}(k_3) + (-i\sigma_4)(-i\sigma_3) B_{MR}(k_3) \\
& + (-i\sigma_4)(i\lambda_3^*) B_{PL}(k_3) + (-\lambda_\Delta)(i\sigma_3^*) B_{ML}(k_3)
\end{aligned} \tag{3.2.13}$$

The divergent contributions from $i\mathcal{M}_1(k_3)$ is cancelled by the following counter term

$$\begin{aligned}
\delta\sigma_3 \Big|_{\overline{\text{MS}}}^{(1)} = & -\frac{1}{(4\pi)^2} \left[2i\lambda_4 \text{Im} \sigma_3 - i\lambda_\Delta(\sigma_3^* + \lambda_3^*) + \sigma_4\lambda_3^* + \sigma_4\sigma_3 \right] \\
& \left[\frac{1}{d-4} + \frac{1}{2}(\gamma_E - 1 - \ln 4\pi) \right]
\end{aligned} \tag{3.2.14}$$

The expression for $i\mathcal{M}_2(k_2)$ is given by

$$\begin{aligned}
i\mathcal{M}_2(k_2) = & \frac{(-i\sigma_4)(-i\lambda_3)}{2} B_{RR}(k_2) + \frac{(i\sigma_4^*)(i\sigma_3^*)}{2} B_{LL}(k_2) + (-\lambda_\Delta)(-i\sigma_3) B_{LR}(k_2) \\
& + \frac{(-i\sigma_4)(i\sigma_3^*)}{2} B_{PM}(k_2) + \frac{(i\sigma_4^*)(-i\lambda_3)}{2} B_{MP}(k_2) + (-\lambda_\Delta)(-i\sigma_3) B_{PP}(k_2) \\
& + (-i\sigma_4)(-i\sigma_3) B_{PR}(k_2) + (-\lambda_\Delta)(-i\lambda_3) B_{MR}(k_2) + (i\sigma_4^*)(-i\sigma_3) B_{PL}(k_2) \\
& + (-\lambda_\Delta)(i\sigma_3^*) B_{ML}(k_2)
\end{aligned} \tag{3.2.15}$$

The divergent contributions from $i\mathcal{M}_2(k_2)$ (and from $i\mathcal{M}_2(k_1)$) are cancelled by the following counter term

$$\begin{aligned}
\delta\sigma_3 \Big|_{\overline{\text{MS}}}^{(2)} = & -\frac{2}{(4\pi)^2} \left[\sigma_4\lambda_3 + 2i\text{Im}[\sigma_4\sigma_3] - i\lambda_\Delta(\lambda_3 + \sigma_3^*) + \sigma_4^*\sigma_3 \right] \\
& \left[\frac{1}{d-4} + \frac{1}{2}(\gamma_E - 1 - \ln 4\pi) \right]
\end{aligned} \tag{3.2.16}$$

Hence the total one loop beta function for σ_3 is given by

$$\begin{aligned}
\beta_{\sigma_3} \equiv \frac{d\sigma_3}{d\ln \mu} = & \frac{1}{(4\pi)^2} \left[2i\lambda_4 \text{Im} \sigma_3 - i\lambda_\Delta(\sigma_3^* + \lambda_3^*) + \sigma_4\lambda_3^* + \sigma_4\sigma_3 \right. \\
& \left. + 2\sigma_4\lambda_3 + 4i\text{Im}[\sigma_4\sigma_3] - 2i\lambda_\Delta(\lambda_3 + \sigma_3^*) + 2\sigma_4^*\sigma_3 \right]
\end{aligned} \tag{3.2.17}$$

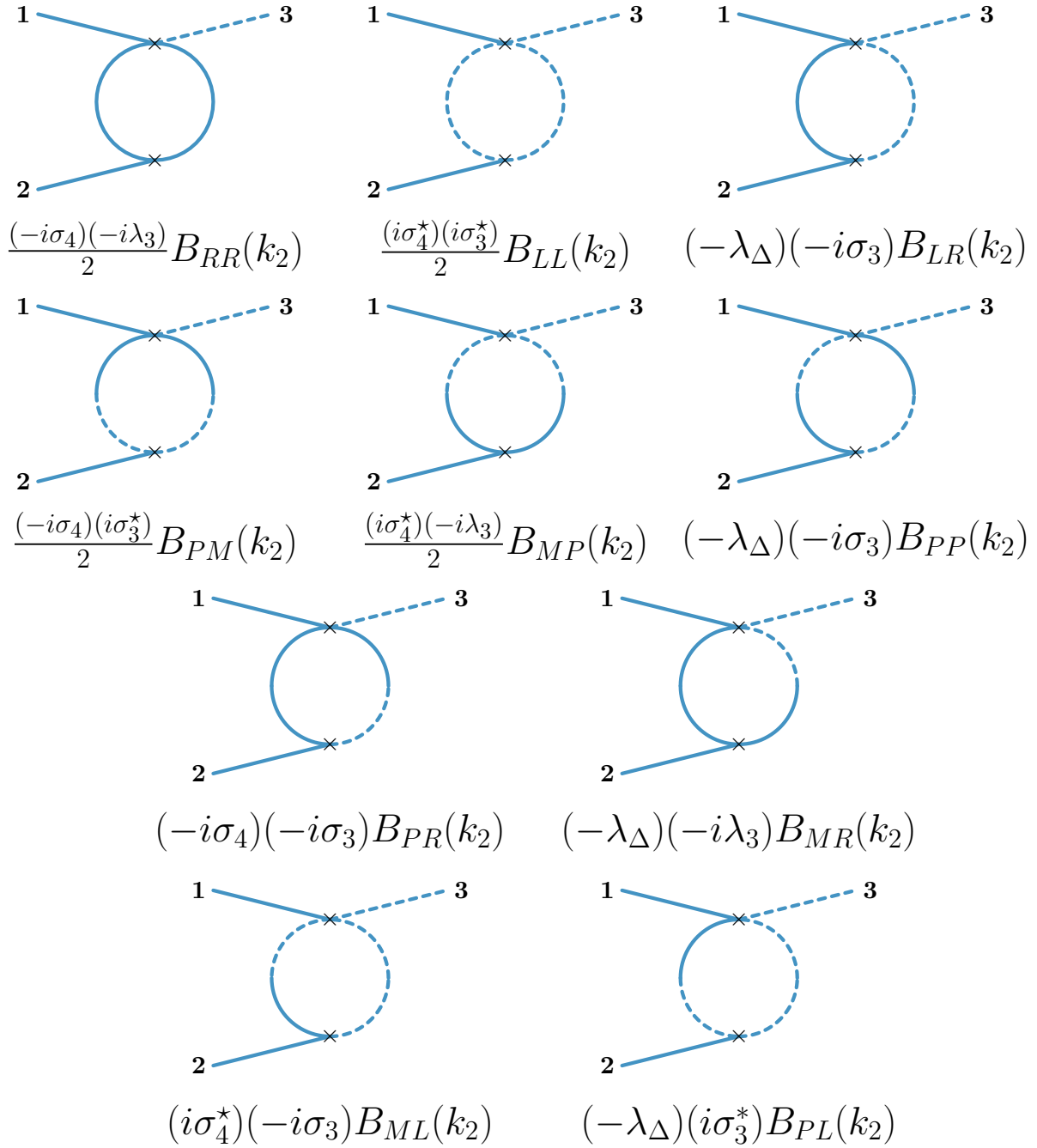


Figure 10: Diagrammatic representation of the Ten 1-Loop Integrals $\phi_R\phi_R \rightarrow \phi_L$

3.2.6 Checking Lindblad condition at the level of cubic couplings

From equation (3.2.11), we obtain the beta function for $\text{Im } \lambda_3$ as

$$\begin{aligned} \frac{d(\text{Im } \lambda_3)}{d \ln \mu} = \frac{3}{(4\pi)^2} & \left[\text{Re } \lambda_4 (\text{Im } \lambda_3 + \text{Im } \sigma_3) + \text{Re } \sigma_4 (\text{Im } \lambda_3 - \text{Im } \sigma_3) \right. \\ & \left. + (\text{Re } \lambda_3 + \text{Re } \sigma_3)(\text{Im } \lambda_4 + \text{Im } \sigma_4) \right] \end{aligned} \quad (3.2.18)$$

and the beta function of $\text{Im } \sigma_3$ can be computed from the imaginary part of equation (3.2.17). We obtain

$$\begin{aligned} \frac{d(\text{Im } \sigma_3)}{d \ln \mu} = \frac{1}{(4\pi)^2} & \left[2\text{Re } \lambda_4 \text{Im } \sigma_3 + \text{Re } \sigma_4 (7 \text{Im } \sigma_3 + \text{Im } \lambda_3) + \right. \\ & \left. 3(\text{Re } \lambda_3 + \text{Re } \sigma_3)(\text{Im } \sigma_4 - \lambda_\Delta) \right] \end{aligned} \quad (3.2.19)$$

Adding these two equations we get

$$\begin{aligned} \frac{d}{d \ln \mu} [\text{Im } \lambda_3 + 3\text{Im } \sigma_3] = \frac{3}{(4\pi)^2} & \left[(\text{Re } \lambda_4 + 2\text{Re } \sigma_4)(\text{Im } \lambda_3 + 3\text{Im } \sigma_3) \right. \\ & \left. + (\text{Re } \lambda_3 + \text{Re } \sigma_3)(\text{Im } \lambda_4 + 4\text{Im } \sigma_4 - 3\lambda_\Delta) \right] \end{aligned} \quad (3.2.20)$$

Again, one can see that the one loop beta function for the Lindblad violating cubic coupling is zero when there is no Lindblad violating coupling in the tree level Lagrangian.

3.2.7 One loop beta function for λ_4

Now we proceed to compute the one loop beta function for the quartic couplings. We will only consider the bubble diagrams since the triangle and box diagrams are finite. Let us consider all the one loop Feynman diagrams that contributes to the process $\phi_R + \phi_R \rightarrow \phi_R + \phi_R$. All the diagrams are depicted in figure 11. The sum over all the Feynman diagrams is given by

$$\begin{aligned} & -i\lambda_4 \\ & + \frac{(-i\lambda_4)^2}{2} B_{RR}(k_s) + \frac{(-\lambda_\Delta)^2}{2} B_{LL}(k_s) + (-i\sigma_4)^2 B_{LR}(k_s) \\ & + \frac{(-\lambda_\Delta)(-i\lambda_4)}{2} B_{PM}(k_s) + \frac{(-\lambda_\Delta)(-i\lambda_4)}{2} B_{MP}(k_s) + (-i\sigma_4)^2 B_{PP}(k_s) \\ & + (-i\lambda_4)(-i\sigma_4) B_{PR}(k_s) + (-i\lambda_4)(-i\sigma_4) B_{MR}(k_s) \\ & + (-\lambda_\Delta)(-i\sigma_4) B_{PL}(k_s) + (-\lambda_\Delta)(-i\sigma_4) B_{ML}(k_s) \\ & + (k_s \longleftrightarrow k_t) + (k_s \longleftrightarrow k_u) \end{aligned} \quad (3.2.21)$$

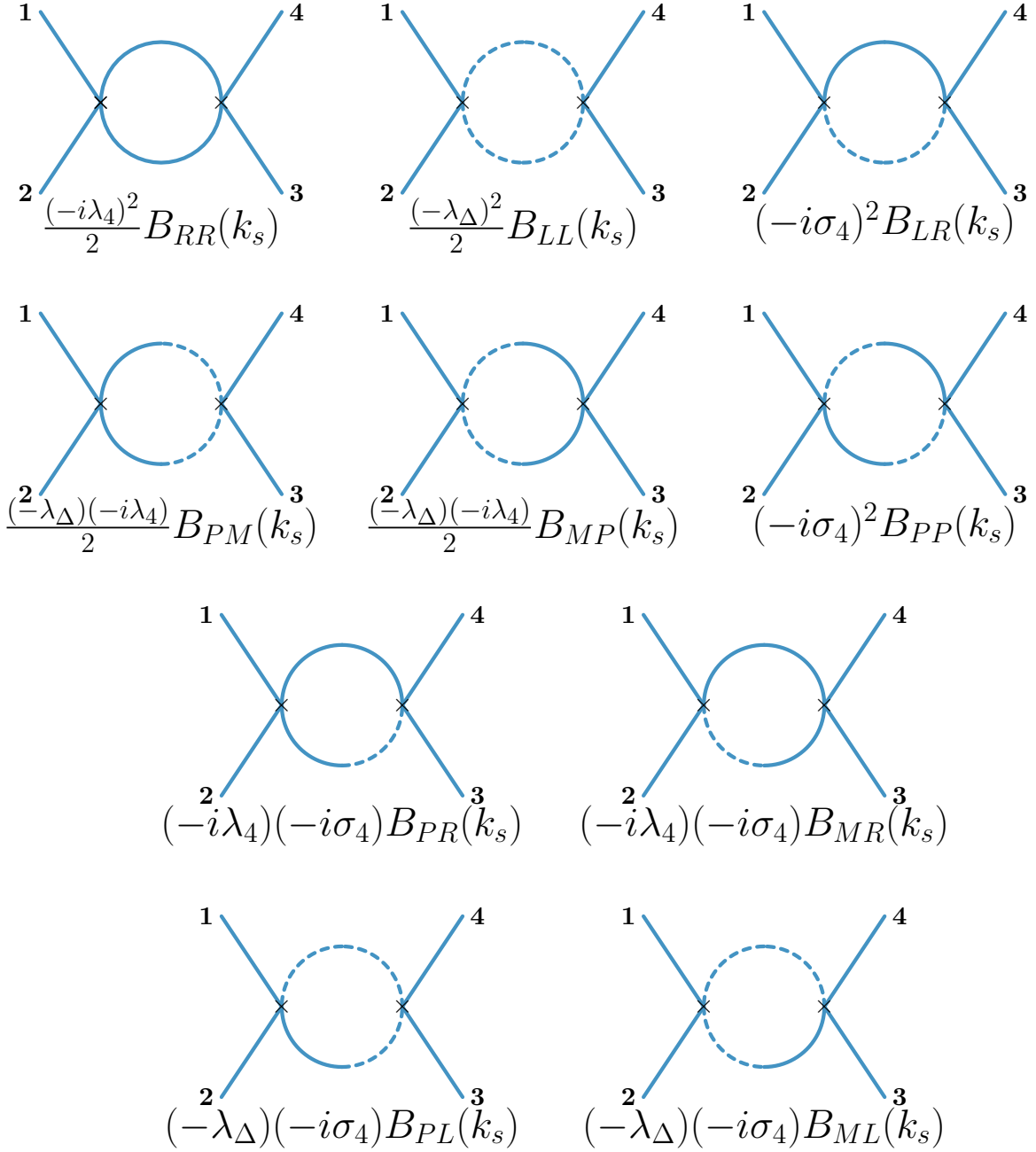


Figure 11: Diagrammatic representation of the Ten 1-Loop Integrals $\phi_R\phi_R \rightarrow \phi_R\phi_R$ (Here $k_s = k_1 + k_2$)

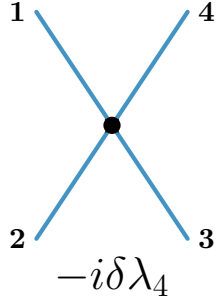


Figure 12: Diagrammatic representation of the one loop counter-term for λ_4

Using the results in (A.2.79a)-(A.2.79d), it's easy to see that the contribution is divergent and we need to add one loop counter-term $\delta\lambda_4$ to cancel the divergences;

$$\delta\lambda_4\Big|_{\overline{\text{MS}}} = -\frac{3}{(4\pi)^2} \left[\lambda_4^2 + 2 \sigma_4(\lambda_4 + i\lambda_\Delta) + \lambda_\Delta^2 \right] \left[\frac{1}{d-4} + \frac{1}{2}(\gamma_E - 1 - \ln 4\pi) \right] \quad (3.2.22)$$

Using the standard methods of quantum field theory, we can compute the one loop beta function as

$$\beta_{\lambda_4} = \frac{3}{(4\pi)^2} \left[\lambda_4^2 + 2 \sigma_4(\lambda_4 + i\lambda_\Delta) + \lambda_\Delta^2 \right] = \frac{3}{(4\pi)^2} (\lambda_4 + 2 \sigma_4 - i\lambda_\Delta)(\lambda_4 + i\lambda_\Delta) \quad (3.2.23)$$

By setting $\sigma_4 = \lambda_\Delta = 0$ we recover the standard result of unitary ϕ^4 theory.

3.2.8 One loop beta function for σ_4

Again, only the Passarino-Veltman B type diagrams contribute to the one loop beta function for σ_4 . All the B type diagrams are depicted in figure 13. The sum over all of them is given by

$$\begin{aligned}
& -i\sigma_4 \\
& + \frac{(-i\lambda_4)(-i\sigma_4)}{2} B_{RR}(k_s) + \frac{(i\sigma_4^*)(-\lambda_\Delta)}{2} B_{LL}(k_s) + (-i\sigma_4)(-\lambda_\Delta) B_{LR}(k_s) \\
& + \frac{(-\lambda_4)(i\sigma_4^*)}{2} B_{PM}(k_s) + \frac{(-\lambda_\Delta)(-i\sigma_4)}{2} B_{MP}(k_s) + (-i\sigma_4)(-\lambda_\Delta) B_{PP}(k_s) \\
& + (-i\lambda_4)(-\lambda_\Delta) B_{PR}(k_s) + (-i\sigma_4)^2 B_{MR}(k_s) \\
& + (-i\sigma_4)(i\sigma_4^*) B_{PL}(k_s) + (-\lambda_\Delta)^2 B_{ML}(k_s) \\
& + (k_s \longleftrightarrow k_t) + (k_s \longleftrightarrow k_u)
\end{aligned} \tag{3.2.24}$$

The one loop counter term for σ_4 is given by

$$\delta\sigma_4 \Big|_{\overline{\text{MS}}} = -\frac{3}{(4\pi)^2} \left[\sigma_4^2 + (\lambda_4 + \sigma_4^*)(\sigma_4 - i\lambda_\Delta) + \lambda_\Delta^2 \right] \left[\frac{1}{d-4} + \frac{1}{2}(\gamma_E - 1 - \ln 4\pi) \right] \tag{3.2.25}$$

and the one loop beta function is found out to be

$$\beta_{\sigma_4} = \frac{3}{(4\pi)^2} \left[\sigma_4^2 + (\lambda_4 + \sigma_4^*)(\sigma_4 - i\lambda_\Delta) + \lambda_\Delta^2 \right] \tag{3.2.26}$$

3.2.9 One loop beta function for λ_Δ

The Passarino-Veltman B type contributions for s -channel and t -channel is being shown in figure 14 and figure 15 respectively. u -channels diagrams are obtained by interchanging $1 \leftrightarrow 2$ in figure 15. The sum over all the contributions is given as

$$\begin{aligned}
& -\lambda_\Delta \\
& + \frac{(-i\lambda_4)(-\lambda_\Delta)}{2} B_{RR}(k_s) + \frac{(i\lambda_4^*)(-\lambda_\Delta)}{2} B_{LL}(k_s) + (-i\sigma_4)(i\sigma_4^*) B_{LR}(k_s) \\
& + \frac{(-i\lambda_4)(i\lambda_4^*)}{2} B_{PM}(k_s) + \frac{(-\lambda_\Delta)^2}{2} B_{MP}(k_s) + (-i\sigma_4)(i\sigma_4^*) B_{PP}(k_s) \\
& + (i\sigma_4^*)(-i\lambda_4) B_{PR}(k_s) + (-i\sigma_4)(-\lambda_\Delta) B_{MR}(k_s) \\
& + (-i\sigma_4)(i\lambda_4^*) B_{PL}(k_s) + (i\sigma_4^*)(-\lambda_\Delta) B_{ML}(k_s) \\
& + \frac{(-i\sigma_4)(-i\sigma_4)}{2} B_{RR}(k_t) + \frac{(i\sigma_4^*)(i\sigma_4^*)}{2} B_{LL}(k_t) + (-\lambda_\Delta)^2 B_{LR}(k_t) \\
& + \frac{(-i\sigma_4)(i\sigma_4^*)}{2} B_{PM}(k_t) + \frac{(i\sigma_4^*)(-i\sigma_4)}{2} B_{MP}(k_t) + (-\lambda_\Delta)^2 B_{PP}(k_t) \\
& + (-i\sigma_4)(-\lambda_\Delta) B_{PR}(k_t) + (-i\sigma_4)(-\lambda_\Delta) B_{MR}(k_t)
\end{aligned} \tag{3.2.27}$$

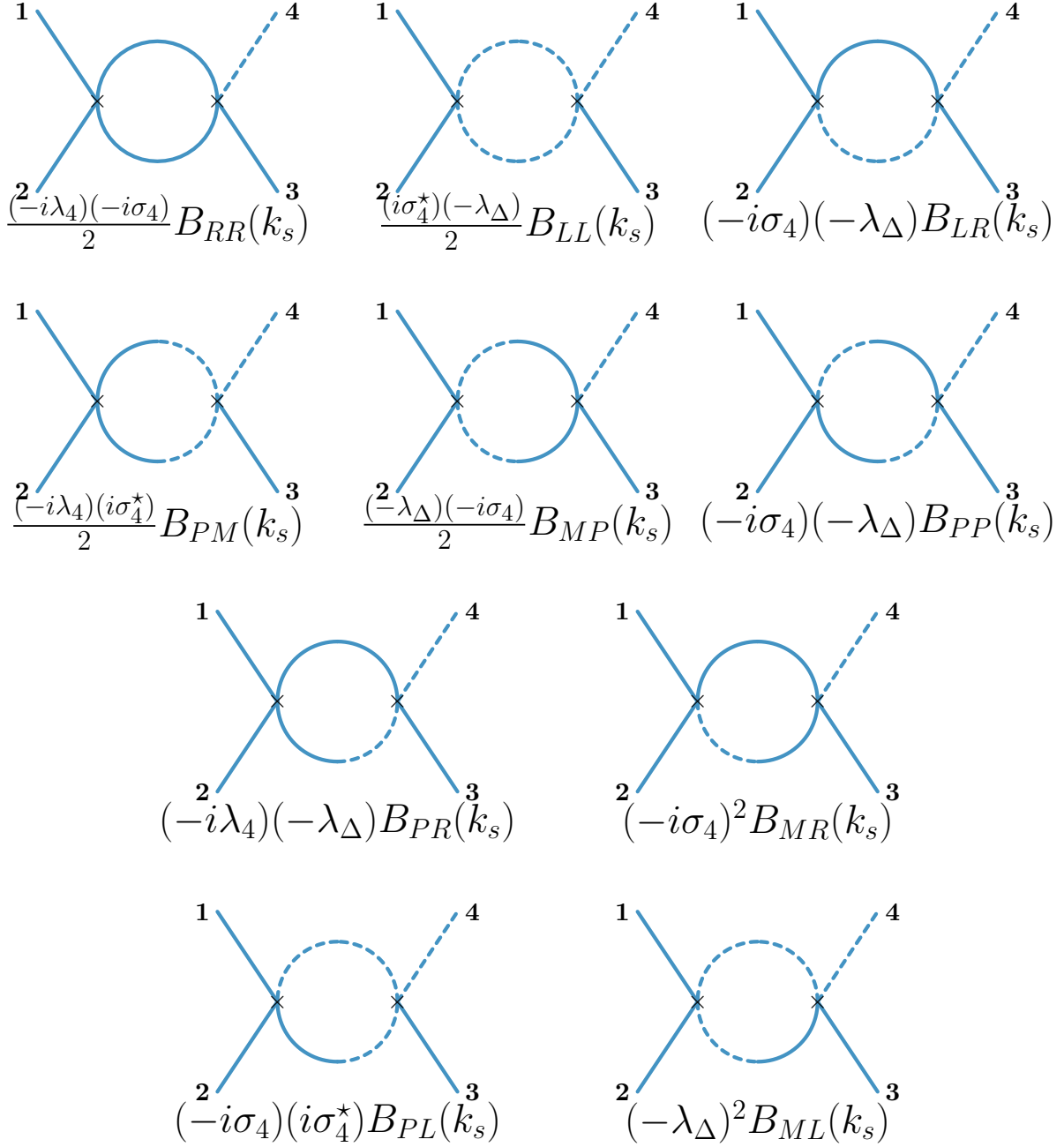


Figure 13: Diagrammatic representation of the Ten 1-Loop Integrals $\phi_R \phi_R \rightarrow \phi_R \phi_L$

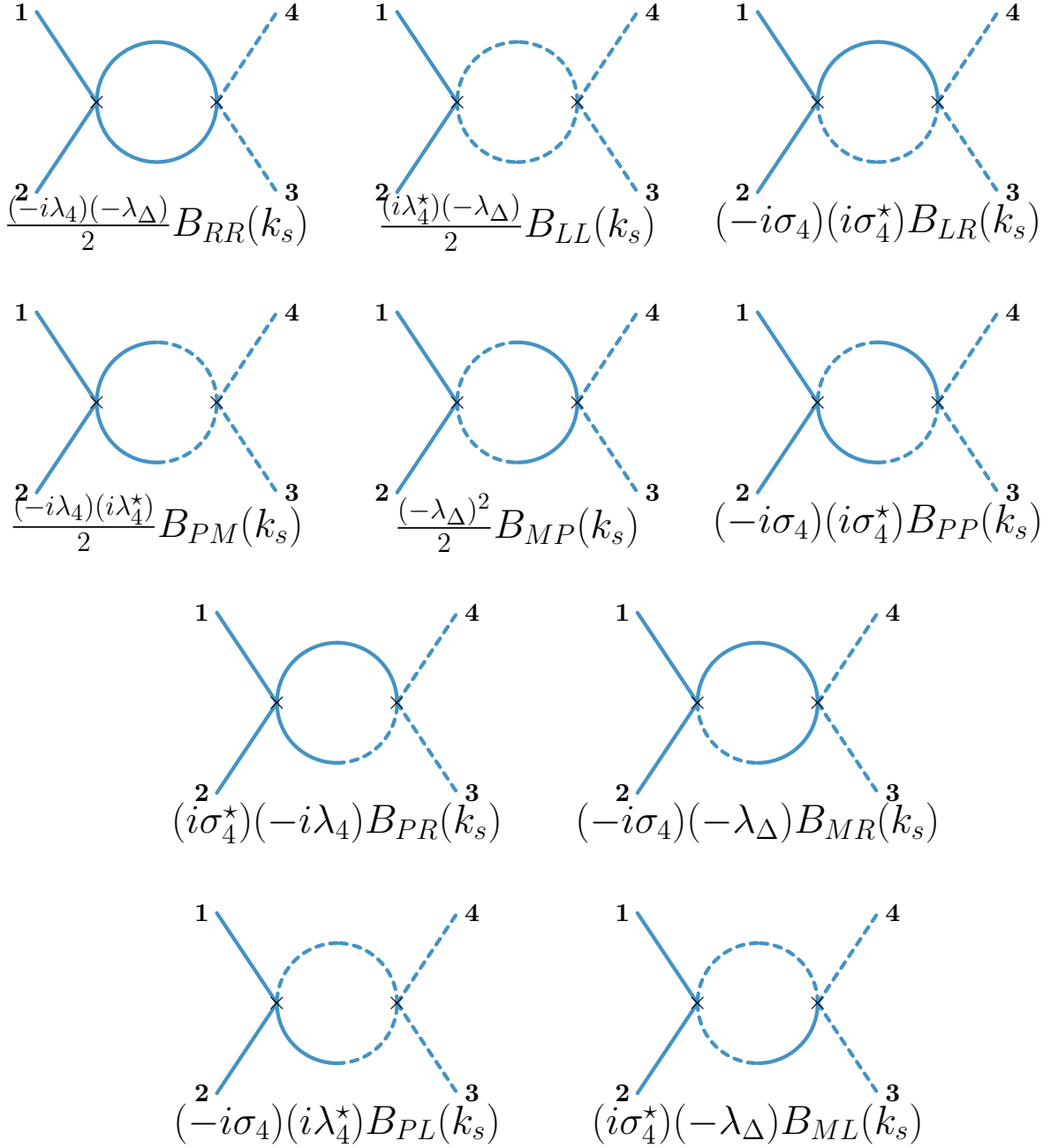


Figure 14: Diagrammatic representation of the Ten 1-Loop Integrals $\phi_R\phi_R \rightarrow \phi_L\phi_L$ (Here $k_t = k_1 + k_2$)

$$\begin{aligned}
&+(i\sigma_4^*)(-\lambda_\Delta)B_{PL}(k_t) + (i\sigma_4^*)(-\lambda_\Delta)B_{ML}(k_t) \\
&+(k_t \longleftrightarrow k_u)
\end{aligned}$$

The one-loop divergence can be removed by adding the following counter term

$$\begin{aligned}
\delta\lambda_\Delta \Big|_{\overline{\text{MS}}} &= -\frac{1}{(4\pi)^2 i} \left[(\lambda_4 + 2\sigma_4^*)(\sigma_4^* + i\lambda_\Delta) + 3i\sigma_4\lambda_\Delta - c.c. \right] \\
&\quad \left[\frac{1}{d-4} + \frac{1}{2}(\gamma_E - 1 - \ln 4\pi) \right]
\end{aligned} \tag{3.2.28}$$

and one loop beta function for λ_Δ is given by

$$\begin{aligned}
\beta_{\lambda_\Delta} &= \frac{1}{(4\pi)^2 i} \left[\lambda_4(\sigma_4^* + i\lambda_\Delta) - 2\sigma_4^2 + 5i\sigma_4\lambda_\Delta - \lambda_4^*(\sigma_4 - i\lambda_\Delta) + 2(\sigma_4^*)^2 + 5i\sigma_4^*\lambda_\Delta \right] \\
&= \frac{1}{(4\pi)^2 i} \left[(\lambda_4 + 2\sigma_4^*)(\sigma_4^* + i\lambda_\Delta) + 3i\sigma_4\lambda_\Delta - c.c. \right]
\end{aligned} \tag{3.2.29}$$

3.2.10 Checking Lindblad condition for quartic couplings

From equation (3.2.23), equation (3.2.26) and equation (3.2.29), we can compute the one loop beta function for the Lindblad combination. We have

$$\beta_{(\text{Im } \lambda_4 + 4 \text{ Im } \sigma_4 - 3\lambda_\Delta)} = \frac{6}{(4\pi)^2} (\text{Im } \lambda_4 + 4 \text{ Im } \sigma_4 - 3\lambda_\Delta) (\text{Re } \lambda_4 + 2\text{Re } \sigma_4) \tag{3.2.30}$$

This equation, along with (3.2.7) and (3.2.8), implies that if one starts with a Lindblad theory then one loop renormalization preserves the Lindblad condition.

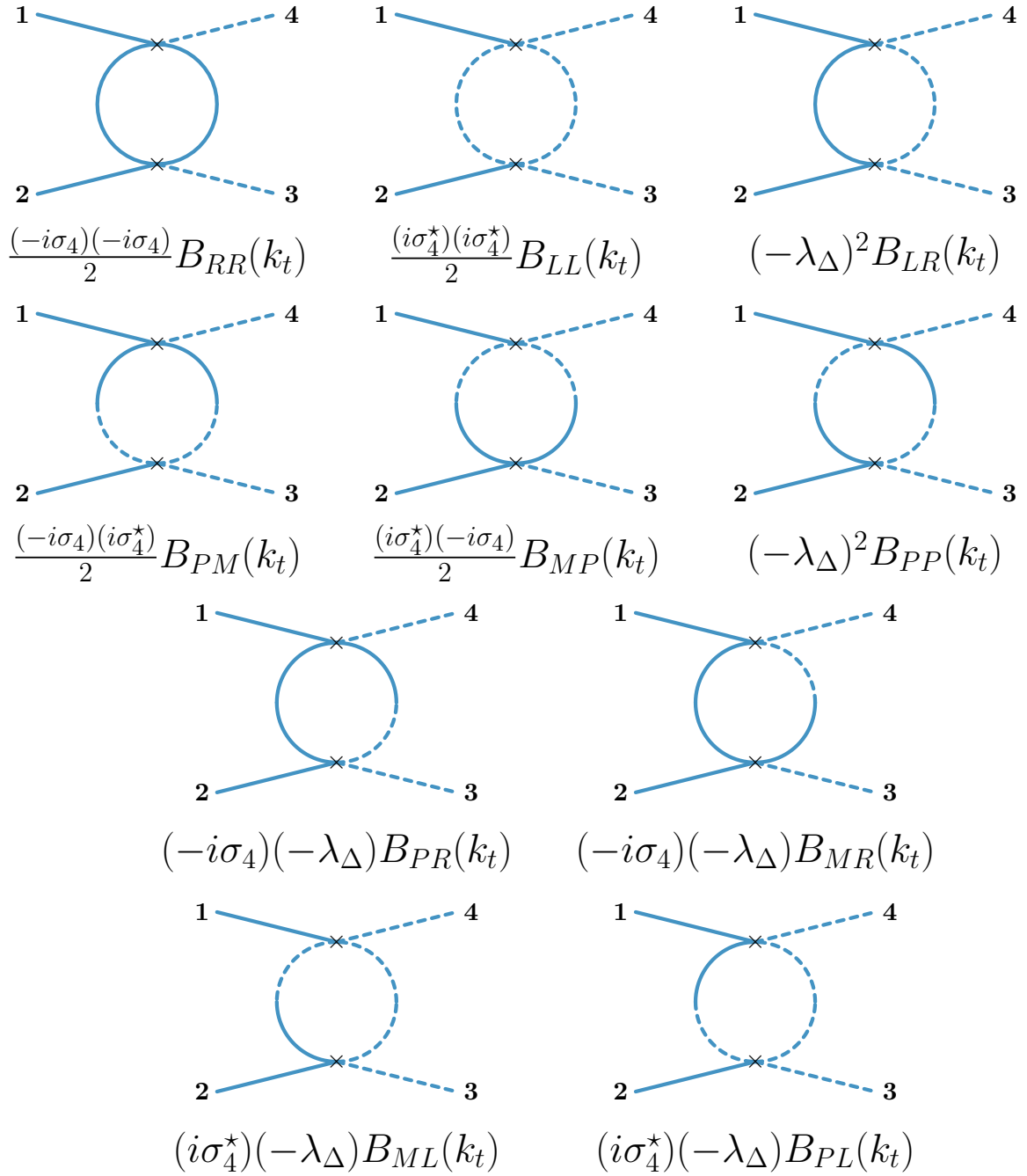


Figure 15: Diagrammatic representation of the Ten 1-Loop Integrals $\phi_R\phi_R \rightarrow \phi_L\phi_L$ (Here $k_t = k_1 + k_4$)

3.2.11 Summary of the results

We started with the most general Lagrangian of a mixed system described by a scalar field with cubic and quartic coupling in (3.0.1). Using this action, we have demonstrated that the standard counter term technique of unitary QFTs can be extended to deal with the one-loop UV divergences of the open EFT. We have then computed the beta functions of this open EFT, summarised as the following.

$$\begin{aligned}
\frac{dm^2}{d\ln \mu} &= \frac{1}{(4\pi)^2} \left[(\lambda_3)^2 - (\sigma_3^*)^2 + 2 \{ \lambda_3 \sigma_3 + |\sigma_3|^2 \} + (\lambda_4 - i\lambda_\Delta + 2\sigma_4) (\text{Re } m^2) \right] \\
\frac{dm_\Delta^2}{d\ln \mu} &= \frac{1}{(4\pi)^2} \left[-4(\text{Re } \lambda_3 + \text{Re } \sigma_3) \text{Im } \sigma_3 + (2\lambda_\Delta - 2\text{Im } \sigma_4) \text{Re } m^2 \right] \\
\frac{d\lambda_3}{d\ln \mu} &= \frac{3}{(4\pi)^2} \left[\lambda_4 \lambda_3 - 2\lambda_\Delta \text{Im } \sigma_3 + \lambda_4 \sigma_3 + \sigma_4 \lambda_3 + \sigma_4 \sigma_3^* \right] \\
\frac{d\sigma_3}{d\ln \mu} &= \frac{1}{(4\pi)^2} \left[2i\lambda_4 \text{Im } \sigma_3 - i\lambda_\Delta (\sigma_3^* + \lambda_3^*) + \sigma_4 \lambda_3^* + \sigma_4 \sigma_3 \right. \\
&\quad \left. + 2\sigma_4 \lambda_3 + 4i\text{Im}[\sigma_4 \sigma_3] - 2i\lambda_\Delta (\lambda_3 + \sigma_3^*) + 2\sigma_4^* \sigma_3 \right] \\
\frac{d\lambda_4}{d\ln \mu} &= \frac{3}{(4\pi)^2} \left[\lambda^2 + 2\sigma(\lambda + i\Delta) + \Delta^2 \right] = \frac{3}{(4\pi)^2} (\lambda + 2\sigma - i\Delta)(\lambda + i\Delta) \\
\frac{d\sigma_4}{d\ln \mu} &= \frac{3}{(4\pi)^2} \left[\sigma^2 + (\lambda + \sigma^*)(\sigma - i\Delta) + \Delta^2 \right] = \frac{3}{(4\pi)^2} (\lambda + \sigma + \sigma^* + i\Delta)(\sigma - i\Delta) \\
\frac{d\lambda_\Delta}{d\ln \mu} &= \frac{1}{(4\pi)^2} i \left[\lambda_4 (\sigma_4^* + i\lambda_\Delta) - 2\sigma_4^2 + 5i\sigma_4 \lambda_\Delta - \lambda_4^* (\sigma_4 - i\lambda_\Delta) + 2(\sigma_4^*)^2 - 5i\sigma_4^* \lambda_\Delta \right].
\end{aligned} \tag{3.2.31}$$

One can then use these beta functions to determine the running of the Lindblad violating combinations $(\text{Im } m^2 - m_\Delta^2)$, $(\text{Im } \lambda_3 + 3\text{Im } \sigma_3)$ and $(\text{Im } \lambda_4 + 4\text{Im } \sigma_4 - 3\lambda_\Delta)$. The following equations shows that the beta function of the Lindblad violating couplings are proportional to the Lindblad violating couplings.

$$\begin{aligned}
\beta_{(\text{Im } m^2 - m_\Delta^2)} &= \frac{2}{(4\pi)^2} \left[(\text{Im } \lambda_3 + 3\text{Im } \sigma_3)(\text{Re } \lambda_3 + \text{Re } \sigma_3) \right. \\
&\quad \left. + (\text{Im } \lambda_4 + 4\text{Im } \sigma_4 - 3\lambda_\Delta)(\text{Re } m^2) \right] \\
\beta_{(\text{Im } \lambda_3 + 3\text{Im } \sigma_3)} &= \frac{3}{(4\pi)^2} \left[(\text{Re } \lambda_4 + 2\text{Re } \sigma_4)(\text{Im } \lambda_3 + 3\text{Im } \sigma_3) \right. \\
&\quad \left. + (\text{Re } \lambda_3 + \text{Re } \sigma_3)(\text{Im } \lambda_4 + 4\text{Im } \sigma_4 - 3\lambda_\Delta) \right] \\
\beta_{(\text{Im } \lambda_4 + 4\text{Im } \sigma_4 - 3\lambda_\Delta)} &= \frac{6}{(4\pi)^2} (\text{Im } \lambda_4 + 4\text{Im } \sigma_4 - 3\lambda_\Delta)(\text{Re } \lambda_4 + 2\text{Re } \sigma_4)
\end{aligned} \tag{3.2.32}$$

In other words, if we set the Lindblad violating coupling to zero at tree level then the Lindblad violating coupling will not be generated under one loop renormalization.

3.3 Computation in the average-difference basis

In section 3.2, we had computed the one loop beta functions for various couplings of an open $\phi^3 + \phi^4$ theory. In particular, by looking at the Lindblad violating couplings, we found that the Lindblad condition is preserved under one loop renormalization. In this section, we will rewrite the perturbation theory in a different basis where this fact is manifest. We would also like to prove that the preservation of Lindblad conditions hold to arbitrary perturbative order. The proof that we present here is very much inspired by a corresponding argument in the context of cutting rules in unitary theory and uses a version of Feynman tree theorem.

The basis we shift to is often termed the Keldysh basis. It is made of the average and difference of bra and ket fields. This basis has an advantage that the difference operator decouplings are more manifest in this basis while it obscures the cutting rule interpretation of various diagrams involved. While the unitary vertices are mixed up with the Feynman-Vernon couplings in this basis, the computations do greatly simplify owing to lesser number of divergent diagrams and vanishing of difference-difference propagator. Our discussion here would necessarily be brief, since the details are straightforward and similar to the computation in the previous section. Reader desiring a more detailed presentation can refer to appendix A.4

3.3.1 Action in the average-difference basis

We define ϕ_d and ϕ_a such that

$$\phi_d = \phi_R - \phi_L \quad \phi_a = \frac{1}{2}(\phi_R + \phi_L) \quad (3.3.1)$$

where the subscripts d and a denote ‘difference’ and ‘average’ respectively.

The Lagrangian in this basis is given by

$$\begin{aligned}
i\mathcal{L} = & +\frac{1}{2 \times 2!}(\text{Im } z + z_\Delta)(\partial\phi_d)^2 + (-i)(\text{Re } z)(\partial\phi_a) \cdot (\partial\phi_d) \\
& + \frac{1}{2 \times 2!}(\text{Im } m^2 + m_\Delta^2)\phi_d^2 + (-i)(\text{Re } m^2)\phi_a\phi_d \\
& + (-i)(\text{Re } \lambda_3 + \text{Re } \sigma_3)\frac{\phi_a^2\phi_d}{2!} + \frac{1}{2}(\text{Im } \lambda_3 - \text{Im } \sigma_3)\frac{\phi_a\phi_d^2}{2!} + \frac{(-i)}{4}(\text{Re } \lambda_3 - 3 \text{Re } \sigma_3)\frac{\phi_d^3}{3!} \\
& + (-i)(\text{Re } \lambda_4 + 2 \text{Re } \sigma_4)\frac{\phi_a^3\phi_d}{3!} + \frac{1}{2}(\text{Im } \lambda_4 + \lambda_\Delta)\frac{\phi_a^2\phi_d^2}{2!2!} + \frac{(-i)}{4}(\text{Re } \lambda_4 - 2 \text{Re } \sigma_4)\frac{\phi_a\phi_d^3}{3!} \quad (3.3.2) \\
& + \frac{1}{8}(\text{Im } \lambda_4 - 4 \text{Im } \sigma_4 - 3\lambda_\Delta)\frac{\phi_d^4}{4!} \\
& + \frac{1}{2!}2(\text{Im } z - z_\Delta)(\partial\phi_a)^2 + \frac{1}{2!}2(\text{Im } m^2 - m_\Delta^2)\phi_a^2 \\
& + 2(\text{Im } \lambda_3 + 3 \text{Im } \sigma_3)\frac{\phi_a^3}{3!} + 2(\text{Im } \lambda_4 + 4 \text{Im } \sigma_4 - 3\lambda_\Delta)\frac{\phi_a^4}{4!}
\end{aligned}$$

The Feynman rules in this basis are given in figure 8. Note that the terms in the last two lines of the Lagrangian involves only the average fields ϕ_a . The coefficients of the purely average couplings are exactly the Lindblad violating couplings. This is expected for the following reason : since ϕ_d vanishes when $\phi_R = \phi_L$, the terms that can contribute to the imaginary part of the action, in that limit, are the pure ϕ_a vertices. Since all Lindblad terms vanish in this limit, it follows that pure ϕ_a vertices should be Lindblad violating. In addition, we observe that in the open $\phi^3 + \phi^4$ theory, all Lindblad violating couplings are of pure average type. This clear separation of the Lindblad violating couplings is the most salient aspect of this basis making it easy to trace their renormalisation.

The propagators in this basis are given by [63, 28, 73]

$$\begin{aligned}
\text{a} : \langle \mathcal{T}_{SK}\phi_a\phi_a \rangle &= \frac{1}{2}\langle \mathcal{T}_{SK}\phi_R\phi_R \rangle + \frac{1}{2}\langle \mathcal{T}_{SK}\phi_L\phi_L \rangle \\
\text{f} : \langle \mathcal{T}_{SK}\phi_a\phi_d \rangle &= \langle \mathcal{T}_{SK}\phi_R\phi_R \rangle - \langle \mathcal{T}_{SK}\phi_R\phi_L \rangle \\
\text{b} : \langle \mathcal{T}_{SK}\phi_d\phi_a \rangle &= \langle \mathcal{T}_{SK}\phi_R\phi_R \rangle - \langle \mathcal{T}_{SK}\phi_L\phi_R \rangle \\
\text{d} : \langle \mathcal{T}_{SK}\phi_d\phi_d \rangle &= 0
\end{aligned} \quad (3.3.3)$$

Please note that we will use a different color for propagators in the average-difference basis. Also, we shall be using results presented in appendix A.3. In this basis, only the tadpole A_a diverges (A.3.1) and its divergence is same as the divergence of usual PV A diagram. All other A integrals, A_f, A_b and A_d , vanish. Similarly, only the bubbles B_{af}, B_{ab} diverge and their divergence is half the divergence of the usual PV B diagram (A.3.3).

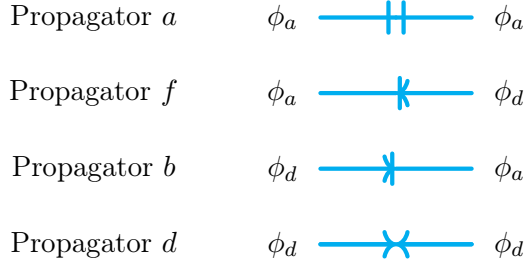


Figure 16: Propagators in the average-difference basis

3.3.2 One loop computations

As mentioned before, the computation greatly simplifies in this basis. All the computations in average-difference basis can be found in appendix A.4. Here we shall demonstrate only a few examples. For instance, let us compute the beta function of one of the Lindblad violating terms, $(\text{Im } m^2 - m_\Delta^2)$. In figure 17, we have considered all the divergent diagrams (i.e., the diagrams involving A_a , B_{af} and B_{ab}) that contributes to the process $\phi_d \rightarrow \phi_d$. The total contribution to the process is given by

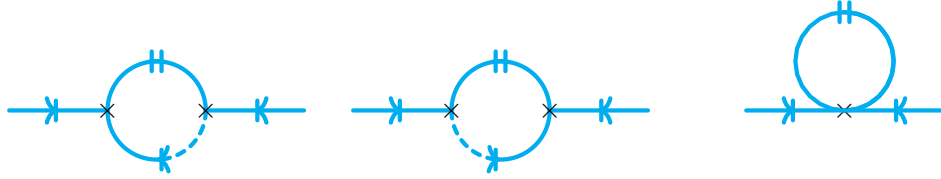


Figure 17: Renormalization of the Lindblad violating mass term in the average-difference basis

$$\begin{aligned}
& 2(\text{Im } m^2 - m_\Delta^2) + 2(\text{Im } \lambda_3 + 3 \text{Im } \sigma_3) \times (-i)(\text{Re } \lambda_3 + \text{Re } \sigma_3)(B_{af} + B_{ab}) \\
& + 2(\text{Im } \lambda_4 + 4 \text{Im } \sigma_4 - 3\lambda_\Delta)(\text{Re } m^2)A_a
\end{aligned} \tag{3.3.4}$$

Hence, the one loop beta function for the Lindblad violating mass term is given by

$$\begin{aligned}
\frac{d}{d\ln \mu}(\text{Im } m^2 - m_\Delta^2) = \frac{1}{(4\pi)^2} & \left[2(\text{Im } \lambda_3 + 3 \text{Im } \sigma_3)(\text{Re } \lambda_3 + \text{Re } \sigma_3) \right. \\
& \left. + (\text{Re } m^2)(\text{Im } \lambda_4 + 4 \text{Im } \sigma_4 - 3\lambda_\Delta) \right]
\end{aligned} \tag{3.3.5}$$

We obtained the same result (equation (3.2.7)) in the other basis. Notice that beta function of the Lindblad violating term can easily be computed just by computing one process in this basis.

Similarly, one can calculate beta function of the Lindblad violating term $(\text{Im } \lambda_3 + 3 \text{ Im } \sigma_3)$. Divergent diagrams for one particular channel is depicted in figure 18. There are two more channels. The total contribution is given as



Figure 18: Renormalization of the Lindblad violating cubic coupling in the average-difference basis

$$\begin{aligned}
& 2(\text{Im } \lambda_3 + 3 \text{ Im } \sigma_3) \\
& + 2(\text{Im } \lambda_3 + 3 \text{ Im } \sigma_3) \times (-i)(\text{Re } \lambda_4 + 2 \text{ Re } \sigma_4)[B_{af}(k_1) + B_{af}(k_2) + B_{af}(k_3)] \\
& + 2(\text{Im } \lambda_4 + 4 \text{ Im } \sigma_4 - 3\lambda_\Delta) \times (-i)(\text{Re } \lambda_3 + \text{Re } \sigma_3)[B_{ab}(k_1) + B_{ab}(k_2) + B_{ab}(k_3)]
\end{aligned} \tag{3.3.6}$$

Following the standard procedures, we can very easily compute the one loop beta function and it is given by

$$\begin{aligned}
\frac{d}{d \ln \mu} (\text{Im } \lambda_3 + 3 \text{ Im } \sigma_3) &= \frac{3}{(4\pi)^2} (\text{Im } \lambda_3 + 3 \text{ Im } \sigma_3) (\text{Re } \lambda_4 + 2 \text{ Re } \sigma_4) \\
&+ \frac{3}{(4\pi)^2} (\text{Im } \lambda_4 + 4 \text{ Im } \sigma_4 - 3\lambda_\Delta) (\text{Re } \lambda_3 + \text{Re } \sigma_3)
\end{aligned} \tag{3.3.7}$$

Now, let us we compute the beta function of Lindblad violating term $(\text{Im } \lambda_4 + 4 \text{ Im } \sigma_4 - 3\lambda_\Delta)$ by computing the process $\phi_d \phi_d \rightarrow \phi_d \phi_d$ via ϕ_a^4 vertex, which is depicted in figure 19. The total contribution is given by



Figure 19: Renormalization of the Lindblad violating quartic coupling in the average-difference basis

$$\begin{aligned}
& 2(\text{Im } \lambda_4 + 4 \text{ Im } \sigma_4 - 3\lambda_\Delta) \\
& + (2 \text{ diagrams})(3 \text{ channels}) \times 2(\text{Im } \lambda_4 + 4 \text{ Im } \sigma_4 - 3\lambda_\Delta) \times (-i)(\text{Re } \lambda_4 + 2 \text{ Re } \sigma_4) \times \frac{i}{32\pi^2} \frac{2}{d-4} \\
& = 2(\text{Im } \lambda_4 + 4 \text{ Im } \sigma_4 - 3\lambda_\Delta) + 2(\text{Im } \lambda_4 + 4 \text{ Im } \sigma_4 - 3\lambda_\Delta) \times (\text{Re } \lambda_4 + 2 \text{ Re } \sigma_4) \times \frac{6}{(4\pi)^2} \frac{1}{d-4}
\end{aligned} \tag{3.3.8}$$

Hence, the one loop beta function is

$$\frac{d}{d \ln \mu} (\text{Im } \lambda_4 + 4 \text{ Im } \sigma_4 - 3\lambda_\Delta) = \frac{6}{(4\pi)^2} (\text{Im } \lambda_4 + 4 \text{ Im } \sigma_4 - 3\lambda_\Delta) (\text{Re } \lambda_4 + 2\text{Re } \sigma_4) \quad (3.3.9)$$

The usefulness of average-difference basis is quite evident from these three calculations. The complete computation in average-difference basis can be found in appendix [A.4](#).

3.3.3 Lindblad condition is never violated by perturbative corrections

In this section, we will give an all order perturbative argument for while Lindblad conditions are not violated to arbitrary order in perturbation theory. Consider the Lagrangian in the average-difference basis given in (3.3.2). From this expression we note that all the Lindblad violating couplings of open $\phi^3 + \phi^4$ theory appear as the coupling constants for the pure average vertices. Our argument below can be easily extended to any open QFT which has this property that all Lindblad violating vertices are pure average vertices. Note that the converse is always true in an open EFT : any pure average vertex is necessarily Lindblad violating (since it contributes to the action even in the $\phi_R = \phi_L$ limit).

Now, we want to show that if we start from the open $\phi^3 + \phi^4$ theory, then Lindblad condition(s) are never violated under perturbative corrections using the fact that they are all of pure average type. In other words, by assuming that there is no pure average vertex at tree level and that there is no difference-difference propagator, we would like to show that such vertex/propagator can never be generated under loop corrections. We will prove it in three steps.

We will begin with an

- **Assumption:** At tree level, one has no pure-average vertex and no pure-difference propagator. All Lindblad violating couplings are assumed to be pure average vertices and hence are taken to vanish at tree level.
- **Statement 1 :** Say we assume that there is no pure-average 1PI 2 point vertex generated at g loop. Then, it implies that there is no pure-difference 1 PI propagator generated at g loop.

Proof : According to our beginning assumption, there is no tree level pure-difference propagator. Such a propagator can then only be generated by a Feynman diagram of type depicted in figure [20](#).

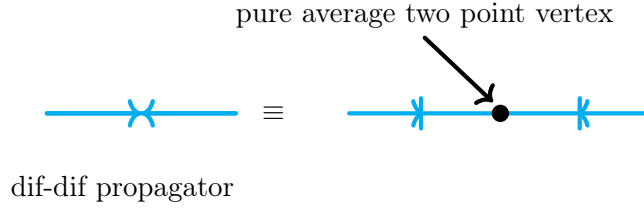


Figure 20: Pure difference propagator from loop correction(s)

So, any contribution to pure-difference 1 PI propagator is of the form

$$(\text{difference to average tree level propagator}) \times (\text{pure-average 1PI 2 point vertex}) \times (\text{average to diff tree level propagator}).$$

Thus, if there are no pure-average 1PI vertices, there are no pure-difference 1PI propagator.(QED)

- **Statement 2** : If there is no pure-average 1PI vertex at g loops, there is no such vertex at $g + 1$ loops. This statement via induction, then implies that pure-average 1PI vertices are never generated at any loop order. By our previous statement, this implies then that pure-difference 1 PI propagators are also never generated at any loop order. In order to prove this, we first prove

- **Statement 2a**: Consider a Feynman diagram contributing to a pure-average 1PI vertex. There must be at least one vertex (internal or external) such that the following is true : there exists a closed path completely made of b -type propagators which begins and ends in that vertex (it may or may not pass through external vertices).

Proof : Since we are considering a diagram contributing to a pure-average 1PI vertex, all the external propagators at every external vertex are of a -type. By our assumption, there is no pure-average 1PI vertex. Thus, there should be at least one d -type line leaving at a given external vertex. Since there is no pure-difference propagator, this d type line necessarily converts itself into an a type line : thus the propagator is of average-difference b type with the arrow leaving the external vertex. This propagator thus ends as an a type line either in the vertex that one began with, or another external vertex or an internal vertex.

In the first case, we have obtained the desired result : there exists a closed path completely made of b -type propagators which begins and ends in that vertex.

In the second case, we note that the external vertex has an external a -type leg, and the b -type propagator which went from the starting vertex also ends with an a -type leg on the second vertex. Since there are no pure-average vertex, there should necessarily be a d -type leg which is going out of the second vertex. The d -type leg can again only be a part of an b -type propagator since there is no pure-difference propagator. A similar argument also applies to the third case of an internal vertex.

We can now follow the b -type propagators and repeat the argument again. This process would terminate (since we are looking at a finite graph) and we would return to some vertex on the path for second time, closing the loop. (QED)

– **Statement 2b:** Any Feynman diagram with a closed path completely made of b -type propagators is zero.

Proof: In position space, b -type propagators are just retarded propagators. The b -type propagator, using equation (3.3.3), in position space is given by,

$$\begin{aligned}
& \int \frac{d^4 p}{(2\pi)^4} \left(\frac{-i}{p^2 + m^2 - i\varepsilon} - 2\pi\delta_-(p^2 + m^2) \right) e^{ip(x-y)} \\
&= \int \frac{d^4 p}{(2\pi)^4} \frac{-i}{p^2 + m^2 - i\varepsilon} e^{ip(x-y)} - \int \frac{d^4 p}{(2\pi)^3} \Theta(-p_0) \delta(p^2 + m^2) e^{ip(x-y)} \\
&= \int \frac{d^3 p}{(2\pi)^3} e^{i\vec{p}\cdot(\vec{x}-\vec{y})} \left(\Theta(x_0 - y_0) \frac{e^{-i\omega_p(x_0-y_0)}}{2\omega_p} + \Theta(y_0 - x_0) \frac{e^{i\omega_p(x_0-y_0)}}{2\omega_p} \right) \\
&- \int \frac{d^3 p}{(2\pi)^3} e^{i\vec{p}\cdot(\vec{x}-\vec{y})} \frac{e^{i\omega_p(x_0-y_0)}}{2\omega_p} (\Theta(x_0 - y_0) + \Theta(y_0 - x_0)) \\
&= \Theta(x_0 - y_0) \int \frac{d^3 p}{(2\pi)^3} e^{i\vec{p}\cdot(\vec{x}-\vec{y})} \left(\frac{e^{-i\omega_p(x_0-y_0)}}{2\omega_p} - \frac{e^{i\omega_p(x_0-y_0)}}{2\omega_p} \right) \\
&= G_R(x - y)
\end{aligned} \tag{3.3.10}$$

where, $\omega_p = (\vec{p}^2 + m^2)^{\frac{1}{2}}$ and $G_R(x - y)$ denotes the retarded propagator.

We will now use the result that a closed loop of retarded propagators is identically zero.

This statement is a part of the Feynman tree theorem [85]. A closed loop of retarded propagators can be written as

$$\int \frac{d^d p}{(2\pi)^d} \prod_i G_R^i(p + k_i) = 0 \tag{3.3.11}$$

where, k_i denotes the external momenta. Since all the poles in a retarded propagator are below the real p_0 axis. So, one can close the contour from above, picking no residues and, as a result, the integral vanishes. (QED)

- Statement 2a and 2b imply that if there is no pure average vertex operator or a pure difference propagator at g loop then there will be no such vertex/propagator at $g + 1$ loop. From this we conclude, via induction, that if there is no Lindblad violating coupling at tree level, such a coupling is never generated by perturbative corrections.(QED)

This then concludes our argument in the average-difference basis that the Lindblad violating couplings are never generated in loops. The readers familiar with cutting rule arguments ala Veltman in unitary theories would recognise the style of the above argument. The proof that difference operators decouple at arbitrary loops in a unitary theory, or equivalently the proof that Keldysh causal structure is preserved under loop corrections for a unitary theory bear a close resemblance to the proof above. The surprise here is that the argument goes through even without assuming unitarity. We also note the perturbative nature of the above argument, since it invokes the fact that the graphs at any given loop order are finite. It would be interesting to try and give a non-perturbative proof of the statement of this section.

With this formal proof in hand, in next section, we will now turn to a preliminary study of what the RG running in our open EFT reveals. The interesting question is to map out behaviour novel to open EFTs which cannot be found in unitary QFTs.

3.4 Running of the coupling constants and physical meaning

In this section, we will perform an analysis of the running of couplings from our 1-loop beta functions. Given the many couplings involved in the the RG equations in (3.2.31), we will begin with a judicious rewriting of our equations. Once the Lindblad conditions are imposed, we obtain the following count for the couplings :

1. 5 quartic couplings + 1 lindblad condition (3.1.7) \implies 4 independent quartic couplings
2. 4 cubic couplings+ 1 lindblad condition (3.1.5) \implies 3 independent cubic couplings
3. 3 mass terms + 1 lindblad condition (3.1.3) \implies 2 independent mass terms

Our RG equations for these 9 independent variables can then be recast into the following convenient form :

$$\begin{aligned}
\beta_{\text{Re } \lambda_4 + 2\text{Re } \sigma_4} &= \frac{3}{(4\pi)^2} (\text{Re } \lambda_4 + 2\text{Re } \sigma_4)^2 \\
\beta_{\text{Im } \lambda_4 + \text{Im } \sigma_4} &= \frac{5}{(4\pi)^2} (\text{Im } \lambda_4 + \text{Im } \sigma_4) (\text{Re } \lambda_4 + 2\text{Re } \sigma_4) \\
\beta_{\text{Re } \lambda_4} &= \frac{1}{3(4\pi)^2} (9\text{Re } \lambda_4 (\text{Re } \lambda_4 + 2\text{Re } \sigma_4) - 8(\text{Im } \lambda_4 + \text{Im } \sigma_4)^2) \\
\beta_{\text{Im } \lambda_4 - 4\text{Im } \sigma_4} &= \frac{10}{(4\pi)^2} \text{Re } \lambda_4 (\text{Im } \lambda_4 + \text{Im } \sigma_4) \\
\beta_{\text{Re } \lambda_3 + \text{Re } \sigma_3} &= \frac{3}{(4\pi)^2} (\text{Re } \lambda_3 + \text{Re } \sigma_3) (\text{Re } \lambda_4 + 2\text{Re } \sigma_4) \\
\beta_{\text{Im } \lambda_3} &= -3\beta_{\text{Im } \sigma_3} = \frac{1}{(4\pi)^2} (3(\text{Im } \lambda_4 + \text{Im } \sigma_4) (\text{Re } \lambda_3 + \text{Re } \sigma_3) + 2\text{Im } \lambda_3 (\text{Re } \lambda_4 + 2\text{Re } \sigma_4)) \\
\beta_{\text{Re } \lambda_3 - \text{Re } \sigma_3} &= \frac{1}{3(4\pi)^2} (9\text{Re } \lambda_4 (\text{Re } \lambda_3 + \text{Re } \sigma_3) - 8\text{Im } \lambda_3 (\text{Im } \lambda_4 + \text{Im } \sigma_4)) \\
\beta_{\text{Re } m^2} &= \frac{1}{(4\pi)^2} ((\text{Re } \lambda_3 + \text{Re } \sigma_3)^2 + \text{Re } m^2 (\text{Re } \lambda_4 + 2\text{Re } \sigma_4)) \\
\beta_{\text{Im } m^2} &= \beta_{m_\Delta^2} = \frac{2}{3(4\pi)^2} (2\text{Im } \lambda_3 (\text{Re } \lambda_3 + \text{Re } \sigma_3) + \text{Re } m^2 (\text{Im } \lambda_4 + \text{Im } \sigma_4))
\end{aligned} \tag{3.4.1}$$

Note the simple structure of the 9 coupled differential equations given above. We have ordered them such that the j th equation depends only on the variables appearing in the first $j-1$ equations. As a result, a step by step method of solution becomes viable : one can start by solving the first equation for a given initial condition and then use the solution of the first equation as an input to solve the second equation and so on, for all the subsequent equations.

The first, the second and the fifth equation imply the existence of the fixed point, given by

$$\text{Re } \lambda_4 = -2\text{Re } \sigma_4, \quad \text{Im } \lambda_4 = -\text{Im } \sigma_4 \tag{3.4.2}$$

$$\text{Re } \lambda_3 = -\text{Re } \sigma_3. \tag{3.4.3}$$

To analyse the nature of this fixed point, we turn to the first equation which drives them all. It can be written as

$$\beta_{|\text{Re } \lambda_4 + 2\text{Re } \sigma_4|} = \text{sign}(\text{Re } \lambda_4 + 2\text{Re } \sigma_4) \frac{3}{(4\pi)^2} |\text{Re } \lambda_4 + 2\text{Re } \sigma_4|^2 \tag{3.4.4}$$

This implies that depending on the sign of the initial value, $\text{Re } \lambda_4 + 2\text{Re } \sigma_4$ either increases or decreases as we go to higher energy scales. As we will see, this sign controls whether theory is UV

free or IR free. We recognise in the RG equation for $\text{Re } \lambda_4 + 2\text{Re } \sigma_4$ the usual ϕ^4 coupling RG equation with $\text{Re } \lambda_4 + 2\text{Re } \sigma_4$ serving as an effective ϕ^4 coupling. The asymptotically free regime and the negative beta function corresponds to this effective ϕ^4 coupling turning negative and is hence akin to the theory studied by Symanzik [86].²

We will begin by performing a linearised analysis around the fixed point mentioned above and follow it up with a more detailed numerical analysis.

3.4.1 Linearized analysis around the fixed point

In this section, we study linearized beta functions around the fixed points and we find the eigenvalues and eigenvectors of the beta function matrix. Consider small deviations around the fixed points

$$\begin{aligned} \text{Re } \lambda_4 + 2\text{Re } \sigma_4 &= \epsilon_1 \\ \text{Im } \lambda_4 + \text{Im } \sigma_4 &= \epsilon_2 \\ \text{Re } \lambda_3 + \text{Re } \sigma_3 &= \epsilon_3 \end{aligned} \tag{3.4.5}$$

where, we have assumed

$$|\epsilon_i| \ll 1 \quad \forall i = 1, 2, 3 \tag{3.4.6}$$

The linearized beta functions for $\text{Re } \lambda_4 + 2\text{Re } \sigma_4$, $\text{Im } \lambda_4 + \text{Im } \sigma_4$ and $\text{Re } \lambda_3 + \text{Re } \sigma_3$ are zero. This suggests that ϵ_1 , ϵ_2 and ϵ_3 remain constant (i.e., they are marginal couplings at the fixed point).

The rest of the linearized beta functions about the fixed point can be written as

$$\frac{d}{dt} \mathcal{G}(t) = \mathcal{B} \mathcal{G}(t) \tag{3.4.7}$$

in terms of the RG time $t \equiv \frac{\ln \mu}{(4\pi)^2}$. Here we have defined the coupling constant matrix \mathcal{G} as

$$\mathcal{G} \equiv \begin{pmatrix} \text{Re } \lambda_4 \\ \text{Im } \lambda_4 - 4\text{Im } \sigma_4 \\ \text{Im } \lambda_3 \\ \text{Re } \lambda_3 - \text{Re } \sigma_3 \\ \text{Re } m^2 \\ \text{Im } m^2 \end{pmatrix} \tag{3.4.8}$$

²We would like to thank Nima Arkani-Hamed for a discussion of this issue and bringing the relevant literature to our attention.

and the beta function matrix \mathcal{B} is given by

$$\mathcal{B} \equiv \begin{pmatrix} 3\epsilon_1 & 0 & 0 & 0 & 0 & 0 \\ 10\epsilon_2 & 0 & 0 & 0 & 0 & 0 \\ 0 & 0 & 2\epsilon_1 & 0 & 0 & 0 \\ 3\epsilon_3 & 0 & -\frac{8\epsilon_2}{3} & 0 & 0 & 0 \\ 0 & 0 & 0 & 0 & \epsilon_1 & 0 \\ 0 & 0 & \frac{4\epsilon_3}{3} & 0 & \frac{2\epsilon_2}{3} & 0 \end{pmatrix} \quad (3.4.9)$$

The six eigenvalues of the matrix \mathcal{B} are $-0, 0, 0, \epsilon_1, 2\epsilon_1, 3\epsilon_1$. The corresponding eigenvectors are given by:

$$\begin{pmatrix} 0 \\ 1 \\ 0 \\ 0 \\ 0 \\ 0 \end{pmatrix}, \begin{pmatrix} 0 \\ 0 \\ 0 \\ 1 \\ 0 \\ 0 \end{pmatrix}, \begin{pmatrix} 0 \\ 0 \\ 0 \\ 0 \\ 0 \\ 1 \end{pmatrix}, \begin{pmatrix} 0 \\ 0 \\ 0 \\ 0 \\ 3\epsilon_1 \\ 2\epsilon_2 \end{pmatrix}, \begin{pmatrix} 0 \\ 0 \\ 3\epsilon_1 \\ -4\epsilon_2 \\ 0 \\ 2\epsilon_3 \end{pmatrix}, \begin{pmatrix} 3\epsilon_1 \\ 10\epsilon_2 \\ 0 \\ 3\epsilon_3 \\ 0 \\ 0 \end{pmatrix} \quad (3.4.10)$$

Eigenvalues of the matrix \mathcal{B} suggest that the first the coupling combinations are also marginal at the fixed point. The asymptotic behavior of rest of the variables depend only on the sign of ϵ_1 or $\text{Re } \lambda_4 + 2\text{Re } \sigma_4$. A positive ϵ_1 would mean that the couplings become relevant in UV, whereas a negative ϵ_1 would mean that the couplings are relevant in IR. This conforms to the intuition we presented in the beginning of this section : the coupling $\text{Re } \lambda_4 + 2\text{Re } \sigma_4$ runs like the quartic coupling of an ordinary ϕ^4 theory : the theory is IR free for positive value of this combination whereas it is UV free (asymptotically free) for negative value of this combination. This coupling then drives all other couplings to be either IR free or asymptotically free.

Let us now extend our analysis beyond the linearised regime around the fixed points, given by

$$\text{Re } \lambda_4 = -2\text{Re } \sigma_4, \quad \text{Im } \lambda_4 = -\text{Im } \sigma_4 \quad (3.4.11)$$

$$\text{Re } \lambda_3 = -\text{Re } \sigma_3. \quad (3.4.12)$$

We will begin by re-examining eqn.(3.4.1) to gain more qualitative insight on the nature of running in this theory:

1. We will begin with the statement that, depending on the sign of the initial value, $\text{Re } \lambda_4 +$

$2\text{Re } \sigma_4$ either increases or decreases as we go to higher energy scales . Thus, we can have two distinct scenarios

(a) $\text{Re } \lambda_4 + 2\text{Re } \sigma_4 > 0$

(b) $\text{Re } \lambda_4 + 2\text{Re } \sigma_4 < 0$.

2. The second equation depends upon the sign of $(\text{Re } \lambda_4 + 2\text{Re } \sigma_4)$ as well as on the sign of the initial value of $\text{Im } \lambda_4 + \text{Im } \sigma_4$. For instance, keeping a positive $\text{Re } \lambda_4 + 2\text{Re } \sigma_4$ and a negative initial value of $\text{Im } \lambda_4 + \text{Im } \sigma_4$ would result in a decreasing behavior as shown in figure 22 and figure 24. Thus, we have two further sub-cases, depending upon the sign of $\text{Im } \lambda_4 + \text{Im } \sigma_4$.
3. The third and fourth equation implies that the evolution of $\text{Re } \lambda_4$ and $\text{Im } \lambda_4 - 4\text{Im } \sigma_4$ depends only on the values of $\text{Re } \lambda_4 + 2\text{Re } \sigma_4$ and $\text{Im } \lambda_4 + \text{Im } \sigma_4$, given the assumption that the imaginary couplings are small compared to the real ones.
4. The fifth equation is similar to the second equation. Hence, there will again be two sub-cases.
5. It's easy to verify that, with the help of similar reasonings, the remaining equations will not provide us with further sub-cases.

We found that the key conclusion remains unchanged for $\text{Re } \lambda_3 + \text{Re } \sigma_3 \gtrless 0$. So we will always be considering the case $\text{Re } \lambda_3 + \text{Re } \sigma_3 \gtrless 0$ together. Thus, we conclude that we can broadly have 8 cases in total and they basically correspond to the two sides of either of these three fixed points: each fixed point will provide two cases and we have 2^3 cases altogether.

With this insight, we will proceed to a more detailed numerical analysis.

3.4.2 Numerical analysis of RG equations

In this subsection, we continue our analysis of the various possible cases in the RG evolution equations. It is useful to have a rough criteria to check the validity of our analysis and as to when the analysis can be interpreted physically. We will perform these analysis only for the Lindblad theory, where the coupling constants obey the Lindblad conditions. We shall always work in a regime where the imaginary couplings are smaller compared to the real ones (since this is the regime where our beta functions were derived). Moreover, we will demand the following bounds

$$\lambda_\Delta < 0, \quad m_\Delta^2 < 0 \tag{3.4.13}$$

which seem to be reasonable from the point of microscopic unitarity[84]. We will deem the couplings which do not satisfy this bound as unphysical in the following. The initial conditions are chosen keeping these physical bounds in consideration and we shall analyse the dynamics corresponding to all the possible behaviors.

I: $\text{Re } \lambda_4 + 2\text{Re } \sigma_4 > 0$, $\text{Im } \lambda_4 + \text{Im } \sigma_4 > 0$ and $\text{Re } \lambda_3 + \text{Re } \sigma_3 \gtrsim 0$

The first equation in (3.4.1) tells us that the sign of $\text{Re } \lambda_4 + 2\text{Re } \sigma_4$ will remain positive in this regime. In particular, $\text{Re } \lambda_4 + 2\text{Re } \sigma_4$ evolves in the same way as λ_{Unitary} ³. Now, from the second equation, one can see that $\text{Im } \lambda_4 + \text{Im } \sigma_4$ will keep increasing if it starts at a positive initial value, but at a slower rate compared to $\text{Re } \lambda_4 + 2\text{Re } \sigma_4$. Similarly, from the third and fourth equation, one can see that, keeping in mind the assumptions, both $\text{Re } \lambda_4$ and $\text{Im } \lambda_4 - 4\text{Im } \sigma_4$ will increase in the way as shown in figure 21. Note here that $\text{Im } \lambda_4 - 4\text{Im } \sigma_4$ rises faster than $\text{Im } \lambda_4 + \text{Im } \sigma_4$ and thus, it results in a continuously increasing $\text{Im } \lambda_4$ and a decreasing $\text{Im } \sigma_4$ as shown in the second diagram in figure 21. Also, the increase of $\text{Im } \lambda_4$ is faster than the decrease of $\text{Im } \sigma_4$ and thus, under the RG flow, λ_Δ becomes positive, which is unphysical. Evolution of the remaining cubic couplings and mass terms variables will not affect the evolution $\text{Im } \lambda_4$ and $\text{Im } \sigma_4$. So, both the sub-cases due to different signs of $\text{Re } \lambda_3 + \text{Re } \sigma_3$ would have a positive λ_Δ and thus, these two cases can be deemed as unphysical.

II: $\text{Re } \lambda_4 + 2\text{Re } \sigma_4 > 0$, $\text{Im } \lambda_4 + \text{Im } \sigma_4 < 0$ and $\text{Re } \lambda_3 + \text{Re } \sigma_3 \gtrsim 0$

The evolution of each variable for this case is depicted in figure 22. We observe that the couplings do not violate the physical conditions throughout. One can see that the couplings become stronger in the UV and attain a Landau pole.

III: $\text{Re } \lambda_4 + 2\text{Re } \sigma_4 < 0$, $\text{Im } \lambda_4 + \text{Im } \sigma_4 > 0$ and $\text{Re } \lambda_3 + \text{Re } \sigma_3 \gtrsim 0$

This is a case where the couplings are relevant in IR and remain within the physical bounds throughout as can be observed in figure 23. In this case, $\text{Re } \lambda_4 + 2\text{Re } \sigma_4$ becomes asymptotically free as can be seen from the first equation in (3.4.1). The second and fifth equation, meanwhile, tells us that $\text{Im } \lambda_4 + \text{Im } \sigma_4$ and $\text{Re } \lambda_3 + \text{Re } \sigma_3$ would go to zero as we go to higher energies. This would also mean that $\text{Im } \lambda_4 - 4\text{Im } \sigma_4$ becomes constant as $\text{Im } \lambda_4 + \text{Im } \sigma_4$ goes to zero. $\text{Im } \lambda_4$ and

³ λ_{Unitary} denotes the coupling constant of an unitary ϕ^4 theory

| $\text{Re } \lambda_4 + 2\text{Re } \sigma_4$ | $\text{Im } \lambda_4 + \text{Im } \sigma_4$ | $\text{Re } \lambda_3 + \text{Re } \sigma_3$ | Conclusion |
|---|--|--|----------------|
| > 0 | > 0 | ≥ 0 | Unphysical |
| > 0 | < 0 | ≥ 0 | Landau pole |
| < 0 | > 0 | ≥ 0 | Relevant in IR |
| < 0 | < 0 | ≥ 0 | Unphysical |

Table 3.2: Running of coupling constants

$\text{Im } \sigma_4$ become constant at higher energies and λ_Δ attains a fixed point. With similar reasonings, one can predict the behavior of other couplings.

IV: $\text{Re } \lambda_4 + 2\text{Re } \sigma_4 < 0$, $\text{Im } \lambda_4 + \text{Im } \sigma_4 < 0$ and $\text{Re } \lambda_3 + \text{Re } \sigma_3 \geq 0$

One can observe from figure 24 that this case can be deemed as unphysical as λ_Δ attains a positive value. It basically comes about due to the sign of $\text{Im } \lambda_4 + \text{Im } \sigma_4$ as can be seen from the second equation in (3.4.1).

3.5 Conclusion

In this chapter, we considered a simple $\phi^3 + \phi^4$ toy model of an open quantum field theory and studied renormalisation of couplings. By enumerating all power-counting renormalisable terms, we demonstrate that the theory is 1-loop renormalisable due to tadpole and bubble diagrams, whereby all UV divergences can be absorbed into appropriate counter-terms. This is in analogy with the standard result for a unitary QFT. The novelty lies in non-unitary Feynman-Vernon couplings and their corresponding β functions. One of the main results of this chapter is that the beta functions surprisingly restrict the Lindblad violating couplings to flow under renormalisation. We end with an all loop argument on why this restriction should extend to any order in perturbation theory.

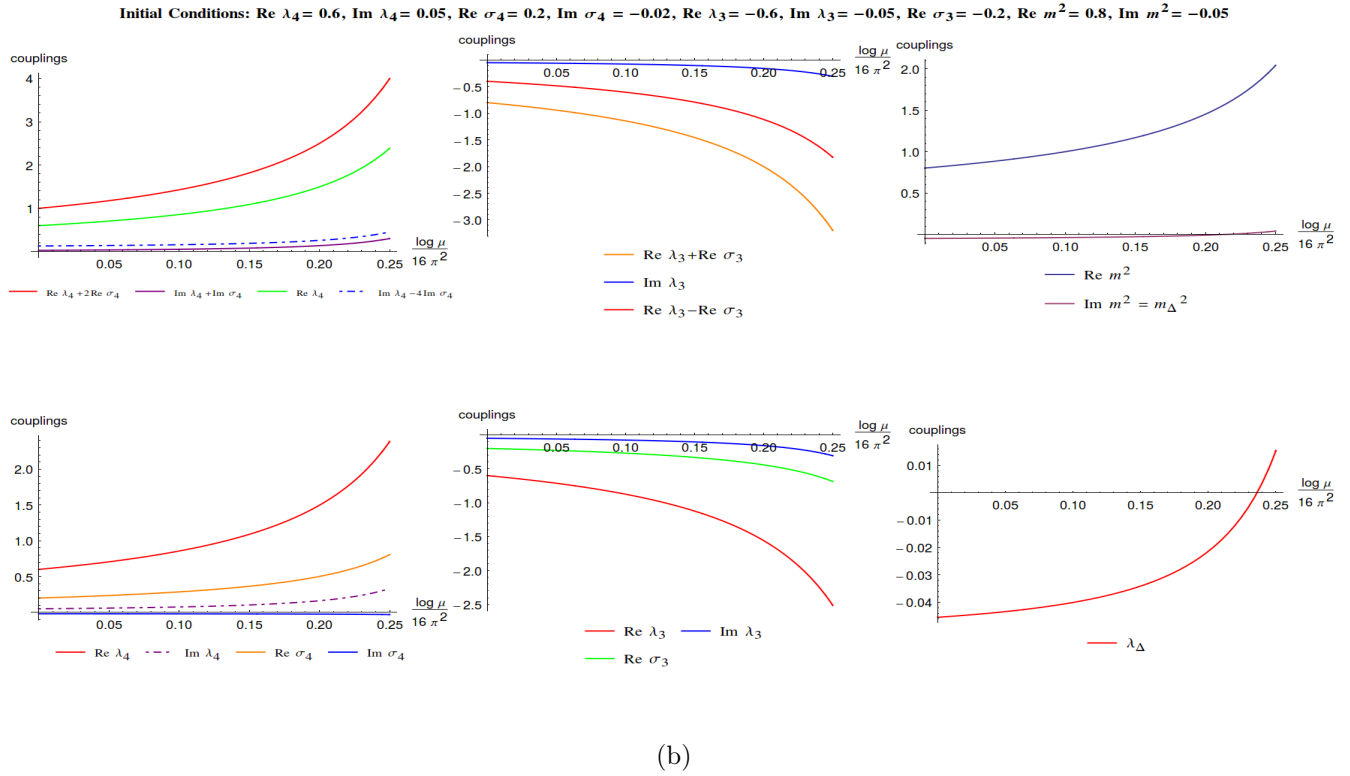
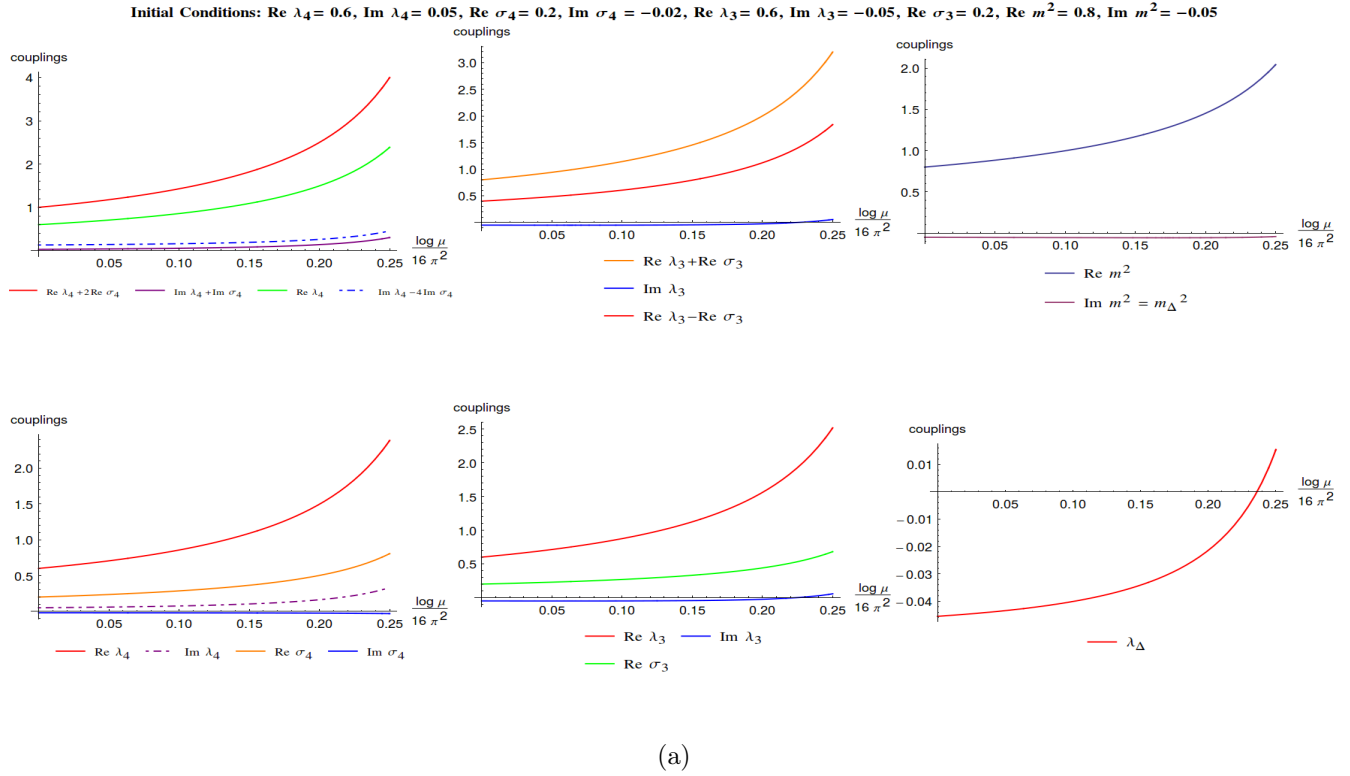
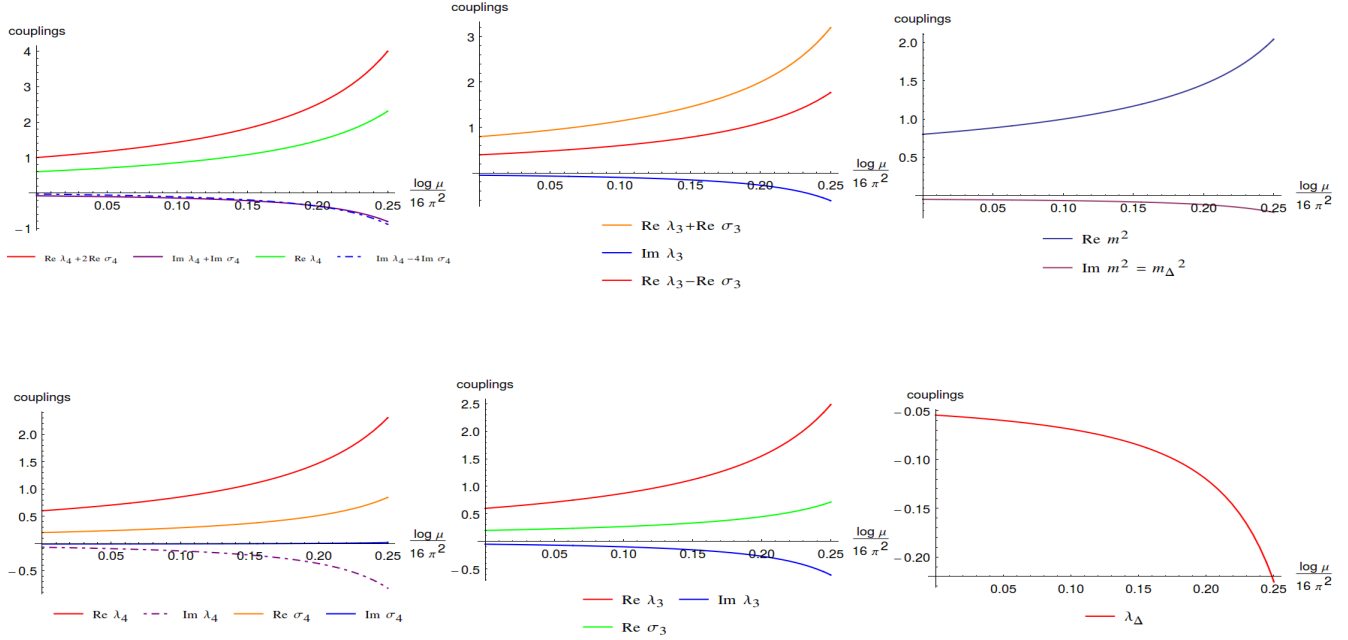


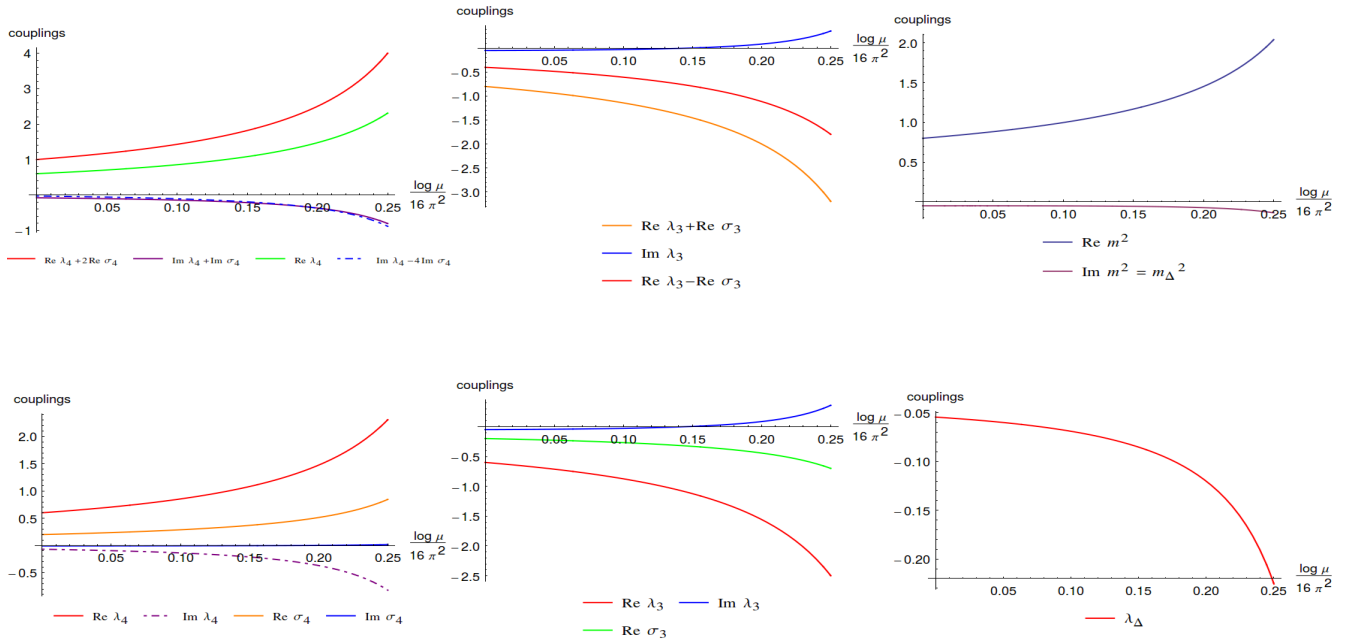
Figure 21: Figures showing the evolution of all the couplings for the case $\text{Re } \lambda_4 + 2\text{Re } \sigma_4 > 0, \text{Im } \lambda_4 + \text{Im } \sigma_4 > 0$ and the two subcases $-\text{Re } \lambda_3 + \text{Re } \sigma_3 > 0$ (figure a) and $\text{Re } \lambda_3 + \text{Re } \sigma_3 < 0$ (figure b)

Initial Conditions: $\text{Re } \lambda_4 = 0.6, \text{Im } \lambda_4 = -0.07, \text{Re } \sigma_4 = 0.2, \text{Im } \sigma_4 = -0.01, \text{Re } \lambda_3 = 0.6, \text{Im } \lambda_3 = -0.05, \text{Re } \sigma_3 = 0.2, \text{Re } m^2 = 0.8, \text{Im } m^2 = -0.05$



(a)

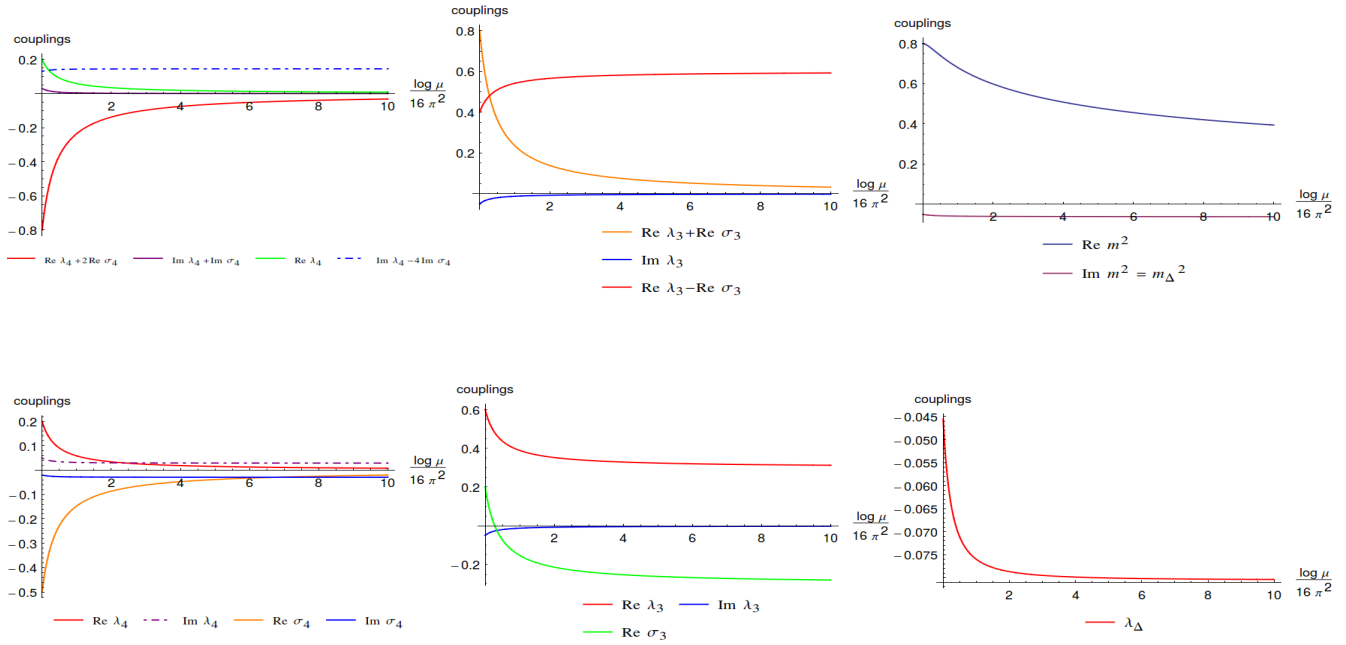
Initial Conditions: $\text{Re } \lambda_4 = 0.6, \text{Im } \lambda_4 = -0.07, \text{Re } \sigma_4 = 0.2, \text{Im } \sigma_4 = -0.01, \text{Re } \lambda_3 = -0.6, \text{Im } \lambda_3 = -0.05, \text{Re } \sigma_3 = -0.2, \text{Re } m^2 = 0.8, \text{Im } m^2 = -0.05$



(b)

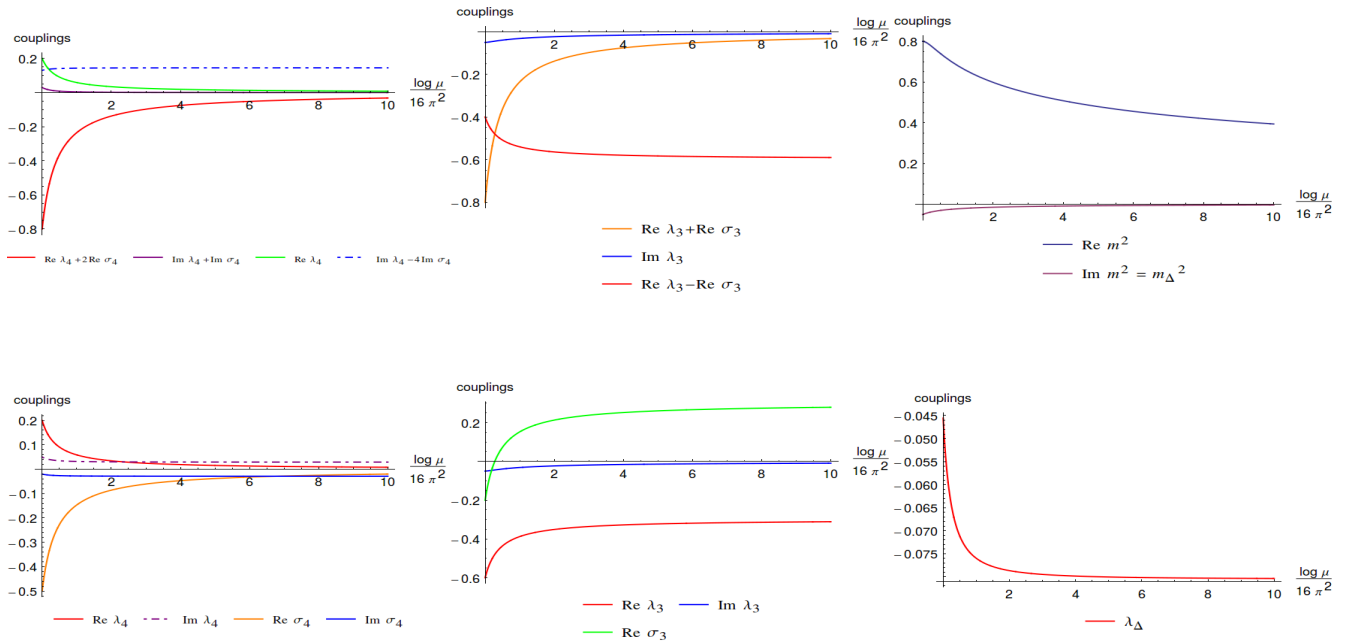
Figure 22: Figures showing the evolution of all the couplings for the case $\text{Re } \lambda_4 + 2\text{Re } \sigma_4 > 0, \text{Im } \lambda_4 + \text{Im } \sigma_4 < 0$ and the two subcases - $\text{Re } \lambda_3 + \text{Re } \sigma_3 > 0$ (figure a) and $\text{Re } \lambda_3 + \text{Re } \sigma_3 < 0$ (figure b)

Initial Conditions: $\text{Re } \lambda_4 = 0.2, \text{Im } \lambda_4 = 0.05, \text{Re } \sigma_4 = -0.5, \text{Im } \sigma_4 = -0.02, \text{Re } \lambda_3 = 0.6, \text{Im } \lambda_3 = -0.05, \text{Re } \sigma_3 = 0.2, \text{Re } m^2 = 0.8, \text{Im } m^2 = -0.05$



(a)

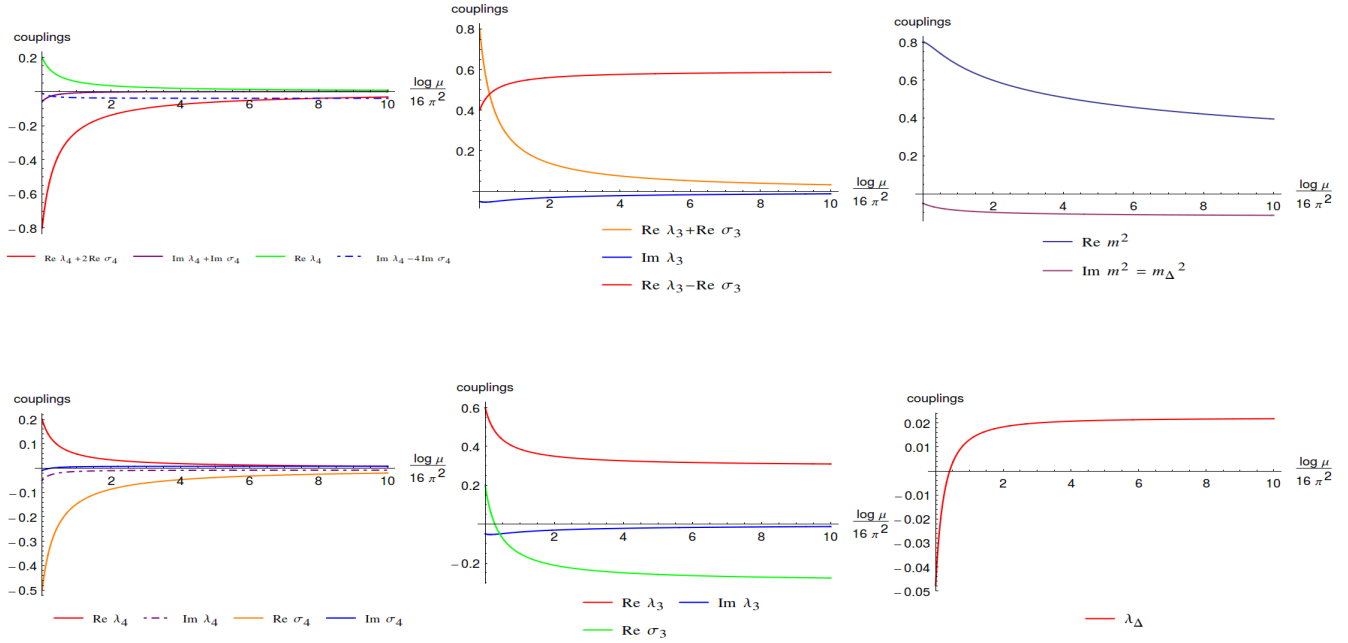
Initial Conditions: $\text{Re } \lambda_4 = 0.2, \text{Im } \lambda_4 = 0.05, \text{Re } \sigma_4 = -0.5, \text{Im } \sigma_4 = -0.02, \text{Re } \lambda_3 = -0.6, \text{Im } \lambda_3 = -0.05, \text{Re } \sigma_3 = -0.2, \text{Re } m^2 = 0.8, \text{Im } m^2 = -0.05$



(b)

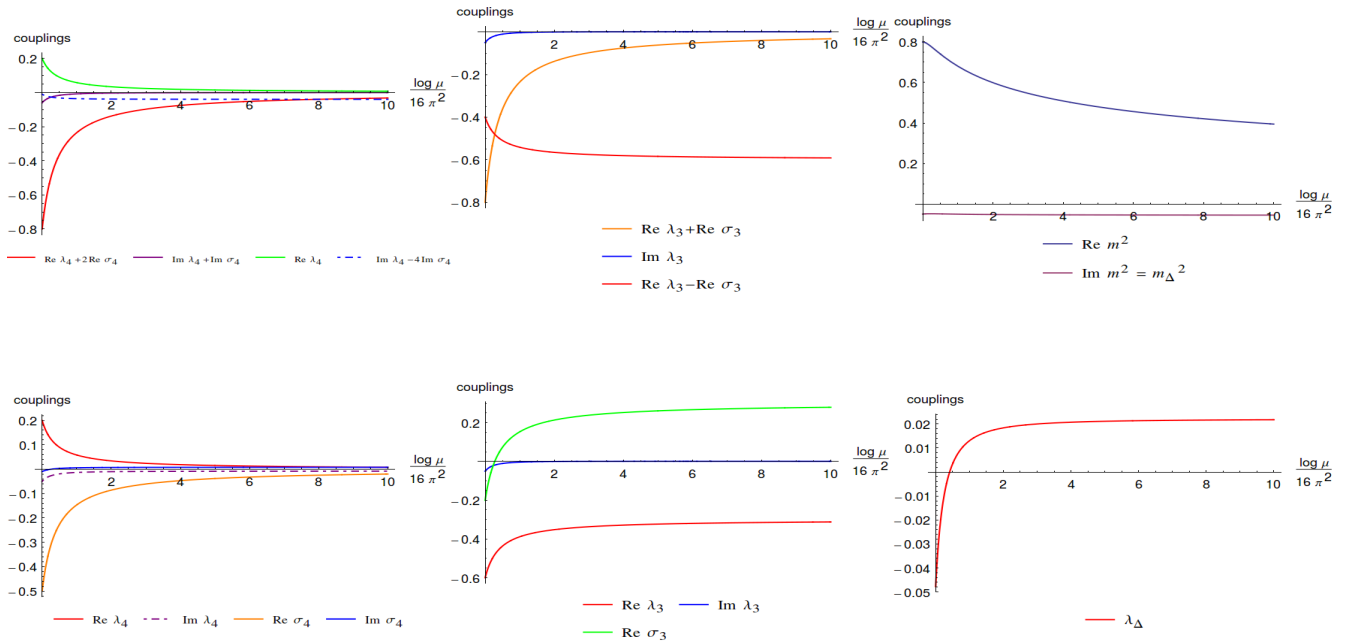
Figure 23: Figures showing the evolution of all the couplings for the case $\text{Re } \lambda_4 + 2\text{Re } \sigma_4 < 0, \text{Im } \lambda_4 + \text{Im } \sigma_4 > 0$ and the two sub-cases - $\text{Re } \lambda_3 + \text{Re } \sigma_3 > 0$ (figure a) and $\text{Re } \lambda_3 + \text{Re } \sigma_3 < 0$ (figure b)

Initial Conditions: $\text{Re } \lambda_4 = 0.2, \text{Im } \lambda_4 = -0.05, \text{Re } \sigma_4 = -0.5, \text{Im } \sigma_4 = -0.01, \text{Re } \lambda_3 = 0.6, \text{Im } \lambda_3 = -0.05, \text{Re } \sigma_3 = 0.2, \text{Re } m^2 = 0.8, \text{Im } m^2 = -0.05$



(a)

Initial Conditions: $\text{Re } \lambda_4 = 0.2, \text{Im } \lambda_4 = -0.05, \text{Re } \sigma_4 = -0.5, \text{Im } \sigma_4 = -0.01, \text{Re } \lambda_3 = -0.6, \text{Im } \lambda_3 = -0.05, \text{Re } \sigma_3 = -0.2, \text{Re } m^2 = 0.8, \text{Im } m^2 = -0.05$



(b)

Figure 24: Figures showing the evolution of all the couplings for the case $\text{Re } \lambda_4 + 2\text{Re } \sigma_4 < 0, \text{Im } \lambda_4 + \text{Im } \sigma_4 < 0$ and the two sub-cases - $\text{Re } \lambda_3 + \text{Re } \sigma_3 > 0$ (figure (a)) and $\text{Re } \lambda_3 + \text{Re } \sigma_3 < 0$ (figure b)

Chapter 4

Open Yukawa theory

We extend our study of open EFTs beyond scalar field theory; we introduce a Fermion in our theory via a Yukawa coupling. We write the most general action for an open Yukawa theory. Then we compute the scalar tadpole and self-energy correction to the Fermion and scalar field. The loop diagrams are evaluated using the PV reduction described in appendix B.

We show that one loop correction to Fermion self energy is non-local divergent. This essentially means that these divergences can not be cancelled by local counter terms. Note that this behaviour is worse than that of a non-renormalisable theory where the UV divergences can be cancelled by local counter terms, albeit an infinity of them in total.

4.1 Action for open Yukawa theory and Feynman rules

The action for unitary Yukawa theory is given by

$$S[\phi, \psi] = \int d^4x \left[-\frac{1}{2}z_\phi(\partial\phi)^2 - \frac{1}{2}m_\phi^2\phi^2 + iZ_\psi\bar{\psi}\not{\partial}\psi - m_\psi\bar{\psi}\psi - \left(\frac{\lambda_3}{3!}\phi^3 + \frac{\lambda_4}{4!}\phi^4 + y\phi\bar{\psi}\psi \right) \right], \quad (4.1.1)$$

where y is the Yukawa coupling. To construct open SK effective action from a unitary one, we follow the procedure described in the last chapter. First we double the degrees of freedom:

$$(\phi, \psi) \longrightarrow (\phi_R, \psi_R), (\phi_L, \psi_L). \quad (4.1.2)$$

R (L) fields evolve along the forward (backward) time on the SK contour. The SK action is given by

$$S_{SK}^{\text{unitary}} = S[\phi_R, \psi_R] - S[\phi_L, \psi_L]. \quad (4.1.3)$$

The above action has no mixed R - L term and the couplings are also real. Thus it describes a unitary system. To get an open action out of (4.1.3), one needs to add all possible Feynman-Vernon influence phases [22, 67] (which include addition of imaginary part to existing couplings). Finally, the action for open Yukawa theory is given by

$$S_{SK} = \int d^4x \left(\mathcal{L}_\phi + \mathcal{L}_\psi + \mathcal{L}_{\text{Yuk}} \right), \quad (4.1.4)$$

where \mathcal{L}_ϕ is the action for open scalar field theory (discussed in the last chapter).

$$\begin{aligned} \mathcal{L}_\phi = & - \left[\frac{1}{2} z_\phi (\partial\phi_R)^2 + \frac{1}{2} m_\phi^2 \phi_R^2 + \frac{\lambda_3}{3!} \phi_R^3 + \frac{\lambda_4}{4!} \phi_R^4 + \frac{\sigma_3}{2!} \phi_R^2 \phi_L + \frac{\sigma_4}{3!} \phi_R^3 \phi_L \right] \\ & + \left[\frac{1}{2} z_\phi^* (\partial\phi_L)^2 + \frac{1}{2} m_\phi^{2*} \phi_L^2 + \frac{\lambda_3^*}{3!} \phi_L^3 + \frac{\lambda_4^*}{4!} \phi_L^4 + \frac{\sigma_3^*}{2!} \phi_L^2 \phi_R + \frac{\sigma_4^*}{3!} \phi_L^3 \phi_R \right] \\ & + i \left[z_\Delta (\partial\phi_R) \cdot (\partial\phi_L) + m_{\phi\Delta}^2 \phi_R \phi_L + \frac{\lambda_\Delta}{2!2!} \phi_R^2 \phi_L^2 \right]. \end{aligned} \quad (4.1.5)$$

where $z_\Delta, m_{\phi\Delta}^2, \sigma_3, \sigma_4, \lambda_\Delta$ are the couplings corresponding to the R, L mixing terms in the action. \mathcal{L}_ψ in (4.1.4) is the open Dirac action with a mass term.

$$\begin{aligned} \mathcal{L}_\psi = & - \left[z_\psi \bar{\psi}_R (-i\cancel{\partial}) \psi_R + m_\psi \bar{\psi}_R \psi_R \right] + \left[z_\psi^* \bar{\psi}_L (-i\cancel{\partial}) \psi_L + m_\psi^* \bar{\psi}_L \psi_L \right] \\ & + i \left[z_{\psi\Delta} \bar{\psi}_R (-i\cancel{\partial}) \psi_L + m_{\psi\Delta} \bar{\psi}_R \psi_L \right] + i \left[\hat{z}_{\psi\Delta} \bar{\psi}_L (-i\cancel{\partial}) \psi_R + \hat{m}_{\psi\Delta} \bar{\psi}_L \psi_R \right]. \end{aligned} \quad (4.1.6)$$

\mathcal{L}_{Yuk} includes all possible open Yukawa action.

$$\begin{aligned} \mathcal{L}_{\text{Yuk}} = & - \left[y_\phi \bar{\psi}_R \psi_R + y_\sigma \bar{\psi}_R \psi_R \right] - \left[y_\kappa \phi_R \bar{\psi}_R \psi_L + y_\rho \phi_R \bar{\psi}_L \psi_R \right] \\ & + \left[y^* \phi_L \bar{\psi}_L \psi_L + y_\sigma^* \phi_R \bar{\psi}_L \psi_L \right] + \left[y_\kappa^* \phi_L \bar{\psi}_R \psi_L + y_\rho^* \phi_L \bar{\psi}_L \psi_R \right], \end{aligned} \quad (4.1.7)$$

where $y_\sigma, y_\kappa, y_\rho$ are R, L mixing terms in the above Yukawa interaction terms.

Note that we have chosen the coupling constants on L branch to be complex conjugate to that of R branch. The couplings corresponding to L, R mixing terms are chosen such that the action respects the SK CPT symmetry [79]. We write the full open Yukawa action in Lindblad form [79] and the corresponding Lindblad conditions are the following.

$$\text{Im } m_\phi^2 = m_{\phi\Delta}^2, \quad 2\text{Im } m_\psi = m_{\psi\Delta} + \hat{m}_{\psi\Delta}, \quad (4.1.8a)$$

$$\text{Im } z_\phi = z_{\phi\Delta}, \quad 2\text{Im } z_\psi = z_{\psi\Delta} + \hat{z}_{\psi\Delta}, \quad (4.1.8b)$$

$$\text{Im}\lambda_3 + 3\text{Im}\lambda_{3\sigma} = 0, \quad \text{Im}\lambda_4 + 4\text{Im}\lambda_{4\sigma} = 3\lambda_{\phi\Delta}, \quad (4.1.8c)$$

$$\text{Im}y + \text{Im}y_\sigma + \text{Im}y_\kappa + \text{Im}y_\rho = 0. \quad (4.1.8d)$$

These conditions ensure that the SK action vanishes if we set $\phi_R = \phi_L$ and $\psi_R = \psi_L$.

To justify perturbation theory, we assume all interaction couplings to be small. We also assume that real part of a coupling is much smaller than its imaginary part. Using perturbation theory we find the Feynman rules for propagators and vertices. Then we study one loop renormalisability of this theory.

4.1.1 Propagators

There are four SK propagators for both scalar ϕ and Fermion ψ in the R - L basis. The explicit derivation of the propagators using $i\varepsilon$ prescription for scalar field is given in (3.1.2). Given the scalar propagators, Fermionic propagators are straightforward to find. The propagators and their diagrammatic representation are shown in figure 1 and 2.





| | | | | |
|-----|----------|---|----------|--|
| R : | ϕ_R | $p \rightarrow$  $p \rightarrow$ | ϕ_R | $\frac{-i}{p^2 + m_\phi^2 - i\varepsilon}$ |
| P : | ϕ_R | $p \rightarrow$  $p \rightarrow$ | ϕ_L | $2\pi\delta_+(p^2 + m_\phi^2)$ |
| M : | ϕ_L | $p \rightarrow$  $p \rightarrow$ | ϕ_R | $2\pi\delta_-(p^2 + m_\phi^2)$ |
| L : | ϕ_L | $p \rightarrow$  $p \rightarrow$ | ϕ_L | $\frac{i}{p^2 + m_\phi^2 + i\varepsilon}$ |

Figure 1: SK propagators for the scalar field





| | | | | |
|---------|----------------|---|----------|---|
| $R^f :$ | $\bar{\psi}_R$ | $p \rightarrow$  $p \rightarrow$ | ψ_R | $\frac{-i(-\not{p} + m_\psi)}{p^2 + m_\psi^2 - i\varepsilon}$ |
| $P^f :$ | $\bar{\psi}_R$ | $p \rightarrow$  $p \rightarrow$ | ψ_L | $(-\not{p} + m_\psi) 2\pi\delta_+(p^2 + m_\psi^2)$ |
| $M^f :$ | $\bar{\psi}_L$ | $p \rightarrow$  $p \rightarrow$ | ψ_R | $(-\not{p} + m_\psi) 2\pi\delta_-(p^2 + m_\psi^2)$ |
| $L^f :$ | $\bar{\psi}_L$ | $p \rightarrow$  $p \rightarrow$ | ψ_L | $\frac{i(-\not{p} + m_\psi)}{p^2 + m_\psi^2 + i\varepsilon}$ |

Figure 2: SK propagators for the Dirac field

4.1.2 Feynman rules

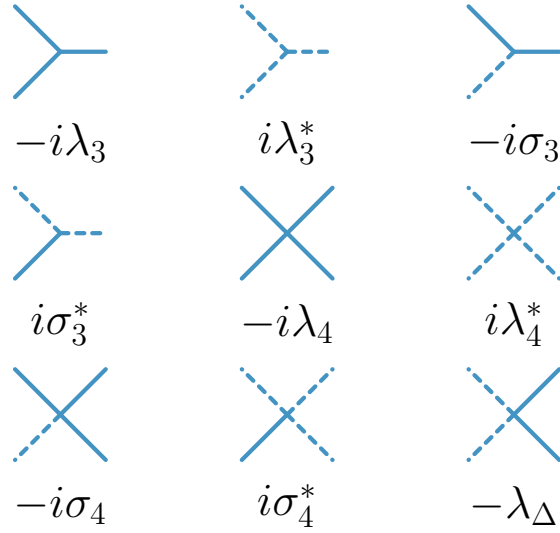


Figure 3: Feynman rules for scalar couplings

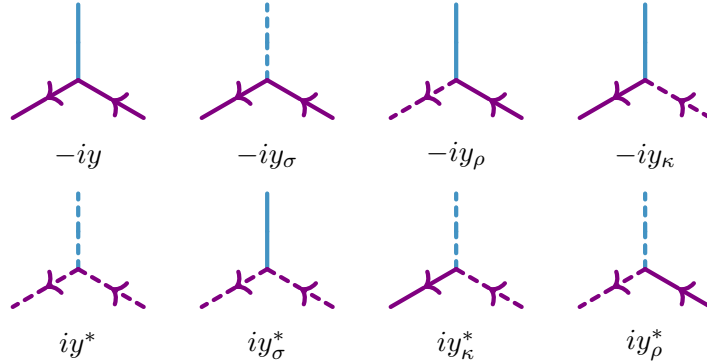


Figure 4: Feynman rules for scalar fermion couplings

The Feynman rules for cubic and quartic vertices are shown in figure 3 and 4. Given the Feynman rules for vertices and propagators, one can compute correction to the self energies for both scalar and fermion. Before proceeding further, let us fix a convention to name the Fermionic loop integrals.

Scalar loop integrals (tadpole, bubble, triangle and square) are named as A , B , C and D type integrals respectively [87, 88]. We will put 'f' in the superscript to refer a Fermionic propagator in that loop. We demonstrate this by an example. Let us consider a bubble diagram with one scalar and one Fermionic propagator as shown in figure 5. In case of bubble diagram, we can always

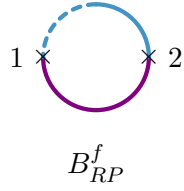


Figure 5: One example of fermionic loop diagram in SK theory

choose the first propagator (from the left) to be Fermionic. Thus we can drop the scalar label from the superscript. We call this diagram as B_{RP}^f .

4.2 Loop correction

4.2.1 Scalar tadpoles

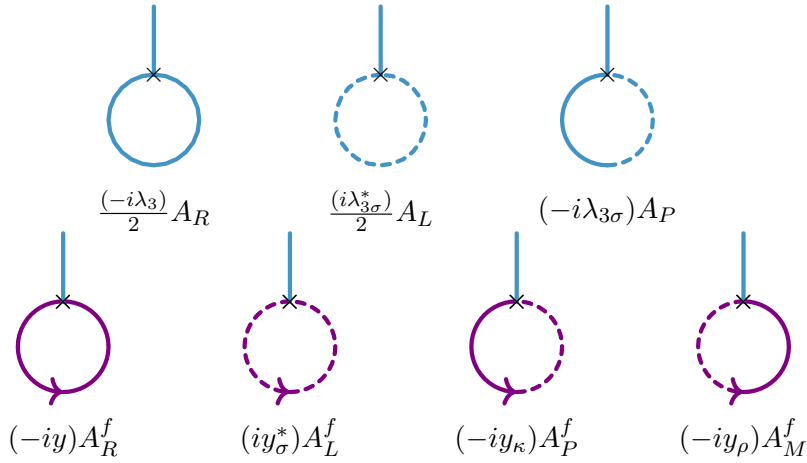


Figure 6: One loop tadpole of ϕ_R

From our elementary understanding of unitary Yukawa theory, there are tadpole diagrams which contribute to one point function of the scalar field. (The tadpole of a Fermionic field vanishes due to underlying Lorentz invariance of QFT.) The contribution from these diagrams are divergent and can be removed from the theory by introducing counter terms in the action. There are two types of tadpole diagrams: scalar and Fermionic. The tadpoles are drawn in figure 6. The contribution

from all of these diagrams are following.

$$\begin{aligned}
& \frac{-i\lambda_3}{2} A_R + \frac{i\lambda_{3\sigma}^*}{2} A_L + (-i\lambda_{3\sigma}) A_P \\
& + (-iy) A_R^f + (iy_\sigma^*) A_L^f + (-iy_\kappa) A_P^f + (-iy_\rho) A_M^f \\
& = \frac{-i}{(4\pi)^2} \frac{1}{d-4} \left[(m_\phi^2)(\lambda_3 - \sigma_3^* + 2\sigma_3) - (8m_\psi^3)(y - y_\sigma^* + y_\kappa + y_\rho) \right] + \dots
\end{aligned} \tag{4.2.1}$$

We see that above divergent piece is local. The scalar tadpole can be removed by a counter-term of the form $\kappa\phi_R$ to the action where κ is given by

$$\frac{i}{(4\pi)^2} \frac{1}{d-4} \left[(m_\phi^2)(\lambda_3 - \sigma_3^* + 2\sigma_3) - (8m_\psi^3)(y - y_\sigma^* + y_\kappa + y_\rho) \right]. \tag{4.2.2}$$

4.2.2 Mass renormalization of the scalar field

Mass renormalisation is associated with the self energy correction of a field. The self energy to the scalar field gets one loop correction from scalar tadpoles and scalar & Fermion bubble diagrams.

The relevant Feynman diagrams are drawn in figure 7, 8, 9 and 10.

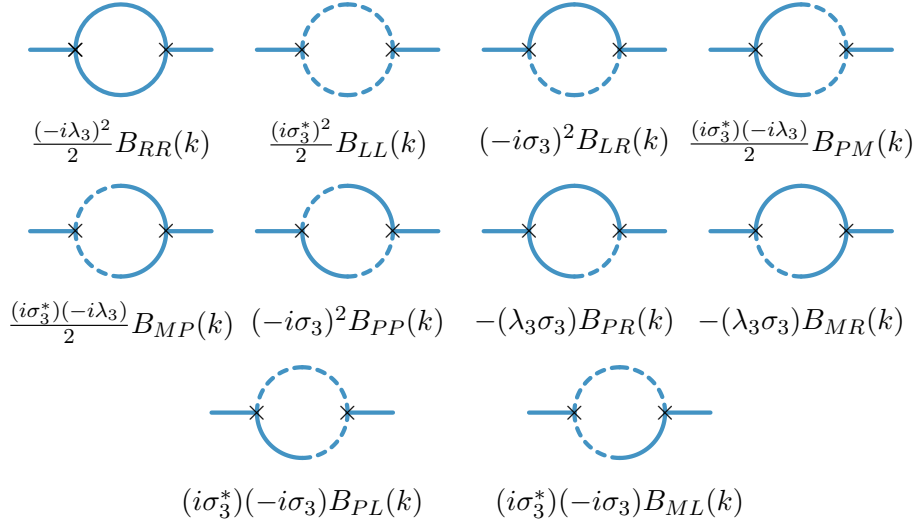


Figure 7: One loop corrections to m_ϕ^2 due to cubic couplings

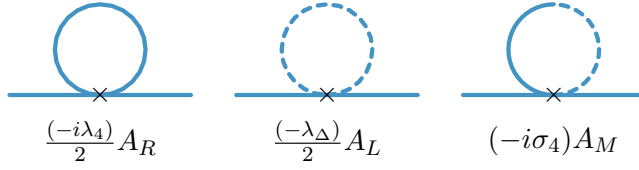


Figure 8: One loop correction to m_ϕ^2 due to quartic couplings

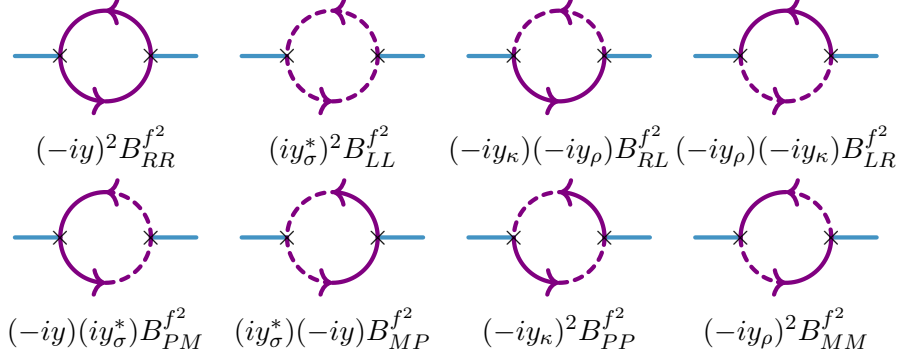


Figure 9: One loop corrections to m_ϕ^2 due to fermionic couplings

The self energy of the scalar field, in dimensional regularisation, is given by

$$\begin{aligned}
& -iz_\phi k^2 - im_\phi^2 \\
& - \frac{i}{(4\pi)^2} \left[\frac{1}{d-4} + \frac{1}{2}(\gamma_E - 1 - \ln(4\pi)) \right] [\lambda_4 - i\lambda_\Delta + 2\sigma_4] (\text{Re } m^2) \\
& - \frac{i}{(4\pi)^2} \left[\frac{1}{d-4} + \frac{1}{2}(\gamma_E - 1 - \ln(4\pi)) \right] \left[(\lambda_3)^2 - (\sigma_3^*)^2 + 2 \{ \lambda_3 \sigma_3 + |\sigma_3|^2 \} \right] \\
& + \frac{4i}{(4\pi)^2} \left[\frac{1}{d-4} + \frac{1}{2}(\gamma_E - 1 - \ln(4\pi)) \right] \left[(k^2 + 6m_\psi^2)(y + y_\sigma^*)(y - y_\sigma^* + y_\kappa + y_\rho) \right].
\end{aligned} \tag{4.2.3}$$

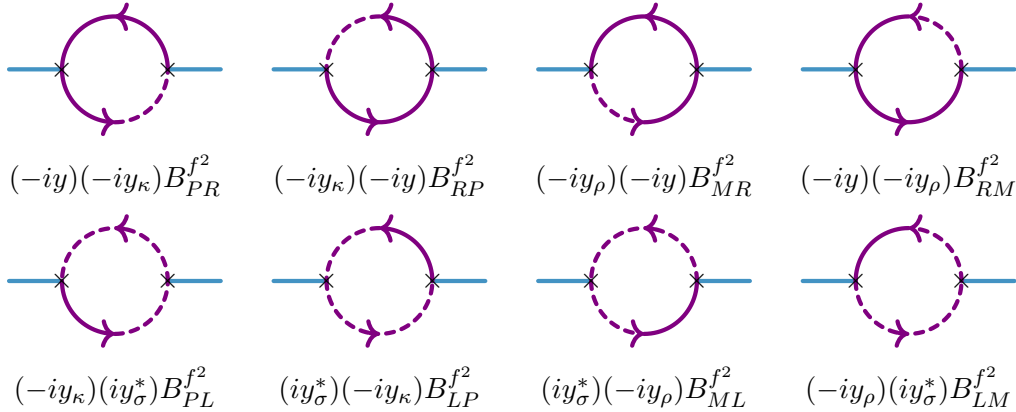


Figure 10: One loop corrections to m_ϕ^2 due to fermionic couplings

The terms in the above expression get contribution from various loop integrals. The second, third and fourth line correspond to scalar A -type, scalar B -type and Fermionic B -type integrals respectively. We find that the divergences to be local and thus can be removed by introducing a local counter term to the action.

The anomalous dimension of the scalar field and its mass renormalisation can be found from the self energy correction of the scalar field. The anomalous dimension is given by

$$\gamma_\phi \equiv \frac{1}{2} \frac{d \ln z_\phi}{d \ln \mu} = -\frac{2}{(4\pi)^2} (y + y_\sigma^*)(y - y_\sigma^* + y_\kappa + y_\rho). \quad (4.2.4)$$

The beta function for m_ϕ^2 is

$$\begin{aligned} \frac{d}{d \ln \mu} (m_\phi^2) &= \frac{4m_\phi^2 - 24m_\psi^2}{(4\pi)^2} (y + y_\sigma^*)(y - y_\sigma^* + y_\rho + y_\kappa) \\ &\quad + \frac{1}{(4\pi)^2} \left[(\lambda_3)^2 - (\sigma_3^*)^2 + 2 \{ \lambda_3 \sigma_3 + |\sigma_3|^2 \} \right] \\ &\quad + \frac{1}{(4\pi)^2} [\lambda_4 - i\lambda_\Delta + 2\sigma_4] (\text{Re } m_\phi^2). \end{aligned} \quad (4.2.5)$$

One can reproduce the well-known anomalous dimension and β function for ϕ in unitary Yukawa theory by setting $y_\sigma = y_\kappa = y_\rho = 0$.

So far we have not noticed any unusual behaviour in open Yukawa theory. We will show that the correction to Fermionic self energy suffers from non-local divergences. As the name 'non-local divergence' indicate, the UV divergent factors are not local in space and time.

4.2.3 Mass renormalization of fermionic field

The one loop self energy correction to Fermion gets contribution from loop integrals consist of one Fermionic propagator and one scalar propagator. The corresponding Feynman diagrams are

drawn in figure 11. The one loop correction is given by

$$\begin{aligned}
& (-iy)^2 B_{RR}^f(k, m_\psi, m_\phi) + (iy_\rho^*)(iy_\kappa^*) B_{LL}^f(k, m_\psi, m_\phi) \\
& + (-iy_\sigma)^2 B_{RL}^f(k, m_\psi, m_\phi) + (-iy_\rho)(-iy_\kappa) B_{LR}^f(k, m_\psi, m_\phi) \\
& + (-iy)(iy_\kappa^*) B_{PM}^f(k, m_\psi, m_\phi) + (iy_\rho^*)(-iy) B_{MP}^f(k, m_\psi, m_\phi) \\
& + (-iy_\rho)(-iy_\kappa) B_{PP}^f(k, m_\psi, m_\phi) + (-iy_\rho)(-iy_\sigma) B_{MM}^f(k, m_\psi, m_\phi) \\
& + (-iy_\sigma)(-iy) B_{RP}^f(k, m_\psi, m_\phi) + (-iy)(-iy_\kappa) B_{PR}^f(k, m_\psi, m_\phi) \\
& + (-iy)(-iy_\sigma) B_{RM}^f(k, m_\psi, m_\phi) + (-iy_\rho)(-iy) B_{MR}^f(k, m_\psi, m_\phi) \\
& + (iy_\rho^*)(-iy_\kappa) B_{LP}^f(k, m_\psi, m_\phi) + (-iy_\sigma)(iy_\kappa^*) B_{PL}^f(k, m_\psi, m_\phi) \\
& + (-iy_\rho)(iy_\kappa^*) B_{LM}^f(k, m_\psi, m_\phi) + (iy_\rho^*)(-iy_\sigma) B_{ML}^f(k, m_\psi, m_\phi) \quad .
\end{aligned} \tag{4.2.6}$$

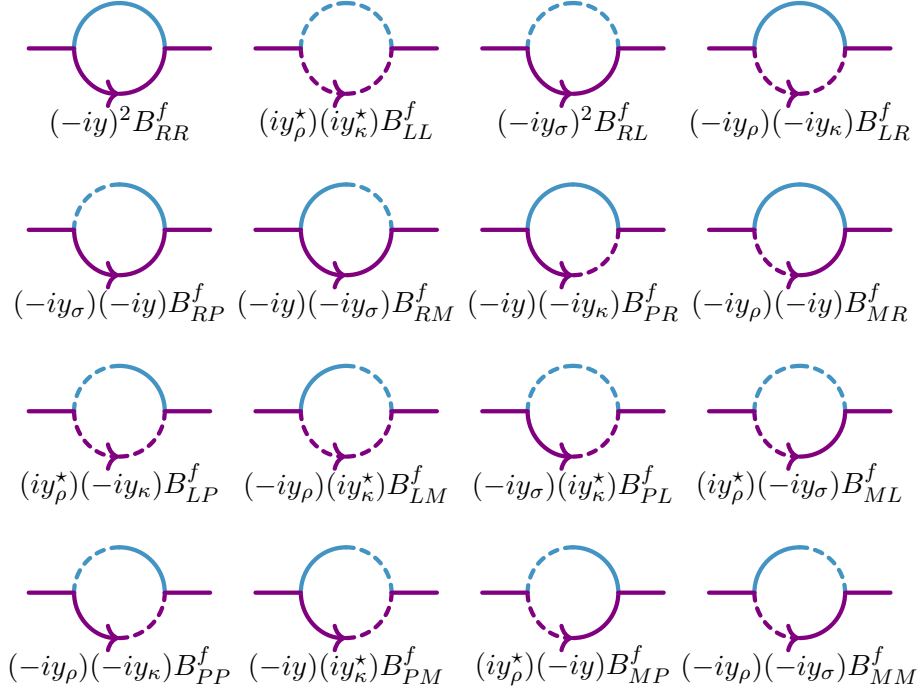


Figure 11: One loop mass renormalization of the fermion

To compute the loop integrals in (4.2.6), we use PV reduction formula summarised in appendix B. The PV reduction formula for each diagram is non-local divergent¹. To see this explicitly we choose an integral $B_{PR}^f(k, m_\psi, m_\phi)$ from the above set of integrals. This integral was chosen, in

¹The PV reduction formula for Fermion self energy correction in unitary Yukawa theory consists of scalar A and B type loop diagrams, which is naively non-local divergent. But, as one substitutes the divergences of A and B type scalar loop integrals, the divergence becomes local.

particular, because the combination of coupling constant that appears with this integral is unique; it does not come with rest of the integrals. So, the divergence of B_{PR}^f does not cancel with the rest. Thus analysing only B_{PR}^f will suffice.

The PV reduction of $B_{PR}^f(k, m_\psi, m_\phi)$ is given by

$$B_{PR}^f(k, m_\psi, m_\phi) = m_\psi B_{PR}(k, m_\psi, m_\phi) - \not{k} \frac{i A_P(m_\psi) - (-k^2 + m_\psi^2 - m_\phi^2) B_{PR}(k, m_\psi, m_\phi)}{2k^2}, \quad (4.2.7)$$

The divergence structure of A_P and B_{PR} are following. (A detailed discussion on these integrals can be found in [A.2](#).)

$$\begin{aligned} A_P(m_\psi) &\sim \frac{m_\psi^2}{(4\pi)^2} \frac{2}{d-4}, \\ B_{PR}(k, m_\psi, m_\phi) &\sim \frac{i}{(4\pi)^2} \frac{k^2 - m_\psi^2 + m_\phi^2}{2k^2} \frac{2}{d-4}. \end{aligned} \quad (4.2.8)$$

Substituting these two back in [\(4.2.7\)](#) we get,

$$B_{PR}^f(k, m_\psi, m_\phi) \sim \frac{i}{(4\pi)^2} \left[m_\psi(k^2 - m_\psi^2 + m_\phi^2) - \not{k} \left(m_\psi^2 + \frac{(k^2 - m_\psi^2 + m_\phi^2)^2}{2k^2} \right) \right] \times \frac{1}{2k^2} \frac{2}{d-4}.$$

The divergent piece is clearly non-local since it has k^2 in the denominator.

Now, since our original action is local, the counter-term action is expected to be local in a renormalisable theory. Thus the one loop non-local divergences can not be cancelled in a renormalisable theory. Note that the divergence in [\(4.2.9\)](#) does not go away in the equal mass limit $m_\phi^2 = m_\psi^2$. We write below the divergent piece of self energy correction for $m_\phi^2 = m_\psi^2$:

$$\begin{aligned} & - (m - \not{k}/2) \left[(y + y_\rho^*)(y + y_\sigma + 2i\text{Im}[y_\kappa]) + (y + y_\kappa^*)(y + y_\sigma + 2i\text{Im}[y_\rho]) \right] \frac{1}{d-4} \frac{i}{(4\pi)^2} \\ & - \frac{\not{k}}{k^2} \left[(y_\sigma - y_\rho)(y + y_\sigma + 2i\text{Im}[y_\kappa]) + (y_\sigma - y_\kappa)(y + y_\sigma + 2i\text{Im}[y_\rho]) \right] \frac{1}{d-4} \frac{i(m^2)}{(4\pi)^2} + \dots \end{aligned} \quad (4.2.9)$$

The non-local divergent piece in the second line seems to go away if we set $y_\sigma = y_\rho = y_\kappa$ which imposes extra constraints on the dynamics. These constraints should not flow under renormalisation. One can show that $(y_\sigma - y_\rho)$ does flow under renormalisation. The non-local divergent piece becomes local in the unitary limit $(y_\sigma, y_\rho, y_\kappa = 0)$.

4.3 Conclusion

In this chapter we write down the action for open Yukawa theory. We show that Fermion self energy correction exhibits non-local divergence in this theory, unlike in open scalar field theory. We do not have a way of resolving these divergences.

The absence of these pathological divergences in scalar field theory does not fit to our intuition, provided Fermionic theory is not free from these. We suspect that either renormalisation prescription for Fermionic theories are different or the scalar theory also possesses non-local divergences. The later suspicion seems reasonable and those divergences might appear in higher order scalar loop diagrams.

In the next chapter we will revisit open scalar field theory and check whether generic scalar loop diagrams are also non-local divergent. We computed tadpole and bubble diagrams in §§3 to self energy and vertex factor corrections. One should also ensure, to show renormalisability, that triangle and box diagrams are finite.

Chapter 5

Non-local divergence in scalar loops: a generic discussion

In this chapter our main focus is on computing and studying the structure of non-local divergences which we pointed out in the last chapter. The structure of these divergences that appear in loop integrals with SK propagators have quite complicated analytic structures where the answer for the UV divergences depends sensitively on external momenta, e.g. whether external momenta are space-like or time-like. The reader should compare this behaviour against usual Feynman perturbation theory where loop integrals have nice analytic properties which allow them to be Wick rotated and studied in Euclidean time. In the standard Feynman perturbation theory, the UV divergences are solely due to high energy virtual particles which are local and insensitive to the detailed structure of the external momenta. On the contrary, the complicated analytic structures in open SK loop integrals preclude us from proposing a clean resolution to the problem of non-local divergences.

5.1 Non-local divergences in generic scalar loop diagrams

5.1.1 A simple example

We move to describing the appearance of non-local divergences in a scalar one loop integral. The Feynman rules (propagators and vertex factors) to write the loop integral, are given in 3.1.3. Using those Feynman rules, let us consider the one loop diagram in figure 1 appearing as a part of the open scalar perturbation theory. It is constructed by a ring of Wightman correlators (i.e., cut P type

propagators). In particular we are interested in a $(D-1)$ -gon diagram in D spacetime dimensions. We will label the external momenta by $p_{j=1,\dots,D-1}$ and call the loop momentum we integrate over as q . The momenta appearing in the loop are then labelled successively as $q + k_1, q + k_2, \dots$ where we have defined the partial sums $k_j \equiv \sum_{i=1}^j p_i$ for future convenience. The partial momentum sums k_i have the same information as the external momenta p_i and we will use it henceforth to encode the external momentum data.

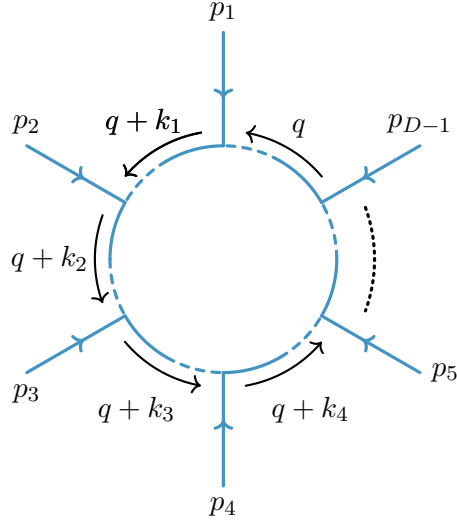


Figure 1: The P^{D-1} diagram made of a ring of Wightman propagators. This illustrates in a simple way, interesting UV divergences that occur in open QFTs.

In the momentum space, the Feynman integral for this diagram then takes the simple form

$$\mathcal{I}[P^{D-1}, \{k_i\}] \equiv \int \frac{d^D q}{(2\pi)^D} \prod_{j=1}^{D-1} 2\pi \delta_+[(q + k_j)^2 + m^2] \quad (5.1.1)$$

Here, P^{D-1} in the argument denotes the fact that there are $(D-1)$ number of P propagators. We are interested in the structure of UV divergences in this integral. To begin with, we proceed naively to estimate by power-counting and dimensional analysis the divergence of this diagram. The naive dimension counting gives a degree of divergence as $D - 2(D-1) = 2 - D$, which is negative for $D > 2$. Thus, a naive expectation would be that, in $D > 2$, this integral would result in a completely convergent expression. As we shall see in a moment, this expectation is entirely wrong and the integral above, in fact, has an interesting UV structure. The crucial subtlety here is that one is integrating over Lorentzian momenta and one cannot analytically continue/Wick

rotate delta functions. To see this, let us begin by re-writing the above integral as

$$\mathcal{I}[P^{D-1}, \{k_i\}] = \int \frac{d^D q}{(2\pi)^D} 2\pi \Theta(q^0) \delta[q^2 + m^2] \prod_{j=1}^{D-2} 2\pi \Theta(q^0 + k_j^0) \delta[2q \cdot k_j + k_j^2] \quad (5.1.2)$$

For simplicity, let us assume that all the k_i^μ are space-like and we will take them to be along the first $(D - 2)$ cartesian axes in the spatial directions, viz., we take $k_i^\mu = |k_i| \hat{e}_i^\mu$ for $i = 1, 2, \dots, (D - 2)$. For example, in $D = 4$, we take $k_1 = |k_1| \hat{e}_x$ and $k_2 = |k_2| \hat{e}_y$. Such a space-like external momenta are appropriate if one is computing SK correlators in an open QFT of space-like separated operators. Since we are taking $k_i^0 = 0$ by construction, all the step functions in the above integrals collapse into just a single step function $\Theta(q^0)$.

Further, we are interested in the contributions from large value of q where we can approximate $\delta[2q \cdot k_j + k_j^2] \approx \delta[2q \cdot k_j]$ and $\delta[q^2 + m^2] \approx \delta[q^2]$. The net effect of the delta/step functions is hence to force the loops momentum q to be future light-like and be transverse to the hyperplane \mathbb{R}^{D-2} defined by the external momenta.

Note that, the hyperplane spanned by $D - 1$ external momenta is indeed \mathbb{R}^{D-2} instead of \mathbb{R}^{D-1} because of momentum conservation constraint $\sum_i p_i = 0$. Thus, the UV contribution in the above integral comes essentially from integrating over future light-like vectors in the (x^0, x^{D-1}) Minkowski plane (see fig. 5). As shown in the figure, we use V_c to denote the space spanned by the external momenta of the open QFT whereas the orthogonal Minkowski plane is denoted by V_\perp . We denote by \mathcal{N}_\perp^+ the space of transverse, future-pointing null vectors.

Putting together the factors, we thus get a logarithmic UV divergence of the form

$$\mathcal{I}[P^{D-1}, \{k_i\}]_{UV} \approx \frac{2}{(2\pi) \prod_{j=1}^{D-2} 2|k_j|} \int_0^\Lambda \frac{dq^0}{2q^0} \approx \frac{1}{2^{D-2} (2\pi) \Sigma_c} \ln \Lambda \quad (5.1.3)$$

Here, in the first expression, the factor of 2 in the numerator comes from summing the contributions from right moving/left-moving future light-like vector contributions. The factors of $2|k_j|$ and $2q^0$ come from the delta functions. In the final expression, we have introduced $\Sigma_c \equiv \prod_{j=1}^{D-2} |k_j|$, which is the volume of the hyper-rectangle formed by k_i^μ . We are done !

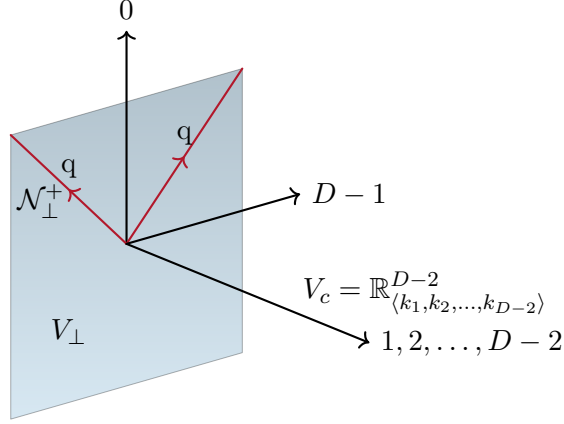


Figure 2: Geometry of P^{D-1} loop : The external momenta form a \mathbb{R}^{D-2} hyperplane denoted here by V_c . The UV part of the loop integral comes from light-like excitations on the transverse Minkowski plane V_\perp . The symbol \mathcal{N}_\perp^+ denotes the space of transverse, future-pointing null vectors, which contribute to the divergence.

5.1.2 Enhancement of divergence

We have learnt in the example above that diagrams expected to converge by naive power counting can, in fact, diverge. To see why, let us revisit the power-counting argument at the beginning of this discussion and try to understand what went wrong.

The crucial step in this regard is the re-writing in Eq.(5.1.2). It is clear from that expression that only one among the $(D-1)$ delta functions actually scale like $\frac{1}{q^2}$. The rest of the delta functions actually scale as $\frac{1}{q}$. We can do power-counting with this new understanding and we do get a degree of divergence to be $D-2-(D-2)=0$ which is consistent with logarithmic divergence in the answer.

As we shall see, this *transmutation of the degree of divergence due to delta functions* is a hallmark of open QFT divergences. As another example of this phenomenon consider the loop integral given by

$$\mathcal{I}[P^{N_c} R^{N-N_c}, \{k_i, \ell_j\}] \equiv \int \frac{d^D q}{(2\pi)^D} 2\pi \delta_+[q^2 + m^2] \frac{\prod_{j=1}^{N_c-1} 2\pi \delta_+[(q+k_j)^2 + m^2]}{\prod_{j=1}^{N-N_c} i[(q+\ell_j)^2 + m^2 - i\varepsilon]}, \quad (5.1.4)$$

which corresponds to the diagram shown in fig.3 with N_c cut Wightman propagators and $N-N_c$ number of un-cut Feynman propagators. $P^{N_c} R^{N-N_c}$ in the argument simply denotes the number of P propagators and R propagators. This has a naive degree of divergence given by $D-2-2(N_c-1)-2(N-N_c)=D-2N$. But, rewriting it as

$$\mathcal{I}[P^{N_c-1} R^{N-N_c}, \{k_i, \ell_j\}] = \int \frac{d^D q}{(2\pi)^D} 2\pi \delta_+[q^2 + m^2] \frac{\prod_{j=1}^{N_c-1} 2\pi \delta_+[2q \cdot k_j + k_j^2]}{\prod_{j=1}^{N-N_c} i[2q \cdot \ell_j + \ell_j^2 - i\varepsilon]}, \quad (5.1.5)$$

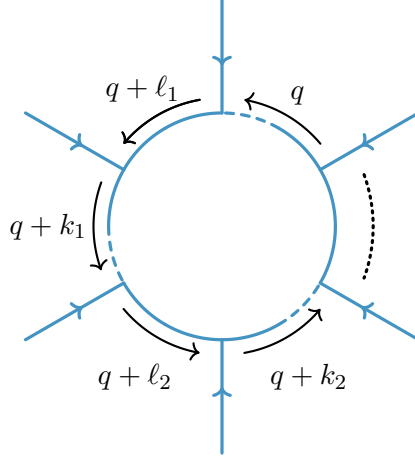


Figure 3: The $P^{N_c} R^{N-N_c}$ diagram : It is naively expected to scale with the UV cutoff as Λ^{D-2N} , but the leading divergence is actually enhanced to $\frac{1}{k^{N_c-1} \ell^{N-N_c}} \Lambda^{D-N-1}$ if even one cut Wightman propagator is present.

shows that the new degree of divergence is actually more and is given instead by

$$D - 2 - (N_c - 1) - (N - N_c) = D - N - 1 .$$

In fact, by looking at the scaling of this integral with k and ℓ momenta, we can guess that the cut-off dependence of divergences change at large ℓ, k into

$$\Lambda^{D-2N} \mapsto \frac{1}{k^{N_c-1} \ell^{N-N_c}} \Lambda^{D-N-1} , \quad (5.1.6)$$

if even one cut Wightman propagator is present. As we shall show later, this new power-counting is indeed the correct guess. As a careful reader might have guessed by now, for dimensional reasons, the enhanced divergence goes hand in hand with momenta appearing in the denominator.

A more subtle example of failure of naive power counting comes about when a single anti-time ordered propagator appears amidst the time-ordered Feynman propagators, viz.,

$$\mathcal{I}[LR^{N-1}, \{\ell_j\}] \equiv \int \frac{d^D q}{(2\pi)^D} \frac{i}{[q^2 + m^2 + i\varepsilon'] \prod_{j=1}^{N-1} i[(q + \ell_j)^2 + m^2 - i\varepsilon]} , \quad (5.1.7)$$

The naive power-counting again gives here a degree of divergence $D - 2N$. This can yet again be proved to be wrong by an explicit calculation. The easiest way to show this is the use of Plemlj formula

$$\frac{i}{[q^2 + m^2 + i\varepsilon']} = -\frac{1}{i[q^2 + m^2 - i\varepsilon']} + 2\pi\delta_+[q^2 + m^2] + 2\pi\delta_-[q^2 + m^2] . \quad (5.1.8)$$

Substituting this into the integral above, the delta functions enhance the degree of divergence to $D - N - 1$ with a non-local divergence of the form $\sim \frac{\Lambda^{D-N-1}}{\ell^{N-1}}$ at large ℓ, k . Going back to the steps

in power counting argument, its failure here can be traced to the fact that poles of the anti-time ordered propagator obstruct Wick-rotation. If one attempts to cross the poles via Plemelj formula, one picks up residues with non-local divergences. The moral here is the failure of power counting when Wick rotation is obstructed.¹

Lest the reader concludes that the delta functions always make the divergence worse, we would like to mention examples where delta functions serve to actually render a divergent diagram finite. The simplest diagrams of this kind are diagrams that appear by cutting the diagrams of the unitary theory which leads to Cutkosky rules [72]. A textbook example is the the cut self-energy diagram in ϕ^3 theory (see fig. 5). This belongs to a class of diagrams with two Wightman correlators driving the loop energy in opposite directions (i.e., diagrams with both P and M type Wightman propagators in the loop). The energy running in loops is bound by the opposite Wightman propagators in this case, thus rendering the diagram UV finite.

To see how this works in general, consider a hexagon diagram with P and M propagators adjacent to each other (see fig. 4 for example). Then the vertex between them is like a unitary (or non Feynman-Vernon) vertex. The step functions of the cut Wightman propagators can be combined into $\Theta(q^0 + \min\{k_i\}_P)\Theta(-(q^0 + \max(\{k_i\}_M))$, which determines the support of the loop integral . Now there are two cases:

- $\max\{k_i\}_M < \min\{k_i\}_P$: Then the integral is over the domain $-\min(\{k_i\}_P) < q^0 < -\max(\{k_i\}_M)$. Since $q^2 + m^2 = 0$ is one of the on-shell conditions, this means that ω_q integral is also over a finite domain. Hence the integral is finite.
- $\max\{k_i\}_M \geq \min\{k_i\}_P$: Then the support of q^0 becomes a measure zero set. Hence the integral is zero.

5.1.3 Non-locality of divergences

Returning back to the P^{D-1} diagram, we note that the diagram is not only UV divergent, but the divergences here are *non-local*. This follows from the fact that the external momenta appear in the *denominator* of the divergence and such a divergence *cannot be cancelled by local counter-terms*. This is in contrast to unitary field theories where UV divergences are always local and cancellable by local counter-terms.

¹We would like to thank Ashoke Sen for a discussion on this issue.

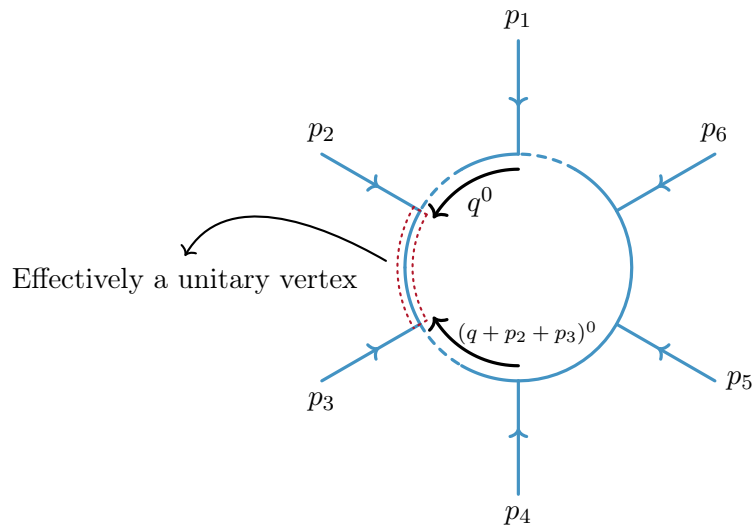


Figure 4: A hexagon one-loop diagram containing a unitary vertex; also shown in arrows the opposing direction of energy flow in the P and M Wightman propagators

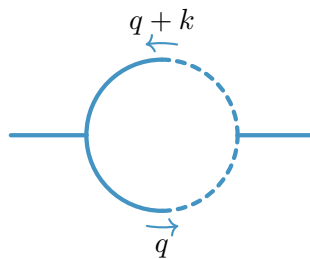


Figure 5: Cut self-energy in ϕ^3 theory in $D = 4$: The delta functions render this diagram finite, though naive power-counting suggests otherwise.

We will begin by briefly reviewing why this is so, followed by an explicit argument for one loop scalar diagrams. Let us first consider any UV-divergent one-loop diagram, of a closed scalar QFT, defined by imposing some regulator. The standard textbook argument for the locality of the divergence is that the diagram can be made “more convergent” by differentiating with respect to the external momenta. If q is the loop momentum and ℓ is some linear combination of external momenta, then differentiating a Feynman propagator with respect to ℓ^μ gives

$$\frac{\partial}{\partial \ell^\mu} \left(\frac{-i}{(q + \ell)^2 + m^2 - i\epsilon} \right) = \frac{2i(q_\mu + \ell_\mu)}{[(q + \ell)^2 + m^2 - i\epsilon]^2} \sim \frac{1}{q^3} \text{ as } q \rightarrow \infty \quad (5.1.9)$$

Thus, differentiating with respect to external momenta always increases the number of powers of q in the denominator. After Wick rotation, this is sufficient to conclude that if we differentiate the diagram sufficiently many times with respect to the external momenta, the diagram will converge. If the divergence can be annihilated by finite number of differentiations, it then follows that the divergences should be polynomial in external momenta, and are hence local. The locality of these UV divergences is what allows us to cancel them via local counter-terms in the Lagrangian.

We can try to extend this argument to loops with cut/Wightman momenta. Consider the integral corresponding to the loop in fig. 3, viz.,

$$\mathcal{I}[P^{N_c-1} R^{N-N_c}, \{k_i, \ell_j\}] = \int \frac{d^D q}{(2\pi)^D} 2\pi \delta_+[q^2 + m^2] \frac{\prod_{j=1}^{N_c-1} 2\pi \delta_+[2q \cdot k_j + k_j^2]}{\prod_{j=1}^{N-N_c} i[2q \cdot \ell_j + \ell_j^2 - i\epsilon]}, \quad (5.1.10)$$

where we have presented the integrand in the linear form. The reader can convince herself/himself that differentiating this integral with respect to ℓ_μ gives no improvement vis a vis power counting at large q . Thus, there is no amelioration of the divergence by differentiation, viz., differentiation with respect to external momenta *does not* decrease the degree of divergence .

For a more explicit argument at one loop level, consider the integral corresponding to the unitary diagram of the form

$$\int \frac{d^D q}{(2\pi)^D} \frac{1}{\prod_{i=1}^N i[(q + \ell_i)^2 + m_i^2 - i\epsilon]}. \quad (5.1.11)$$

The standard estimate of the leading UV divergence goes as follows : combining the denominators via Feynman parameters and shifting the loop momenta, we get

$$\int \prod_{i=1}^N dx_j \delta(1 - \sum x) \int \frac{d^D q}{i^N (2\pi)^D} \frac{\Gamma(N)}{(q^2 + \mathcal{M}^2 - i\epsilon)^N} \quad (5.1.12)$$

where we have defined

$$\mathcal{M}^2 \equiv \sum_{i=1}^N x_i(\ell_i^2 + m_i^2) - \left(\sum_{i=1}^N \ell_i x_i \right)^2 . \quad (5.1.13)$$

We can Wick rotate the integral above and then perform the sphere integrals to obtain

$$\frac{\Gamma(N)|\mathbb{S}^{D-1}|}{i^{N+1}(2\pi)^D} \int \prod_{i=1}^N dx_j \delta(1 - \sum x) \int \frac{q_E^{D-1} dq_E}{(q_E^2 + \mathcal{M}^2)^N} , \quad (5.1.14)$$

whose leading divergence can then be estimated as

$$\frac{\Gamma(N)|\mathbb{S}^{D-1}|}{i^{N+1}(2\pi)^D} \int \prod_{i=1}^N dx_j \delta(1 - \sum x) \int^\Lambda \frac{dq_E}{q_E} q_E^{D-2N} . \quad (5.1.15)$$

This is the standard result that the degree of divergence in this case is $D - 2N$. Note the crucial role played by Feynman parameters and Wick rotation in this argument. Both these techniques fail for open QFT diagrams.

From the above formula, we can note the following points to be contrasted with the open QFT divergences discussed before.

- The leading divergence of cut-free one-loop diagrams is **always** independent of external momenta. This is because of the spherical symmetry of the integral. The leading divergence in open QFTs on the other hand, depend on the external momenta and hence the IR data.
- The sub-leading divergences in general has **at the most** polynomial dependencies in the external momenta. Thus the complete divergence is **local**. This is not true with open QFT diagrams.
- The degree of divergence is $D - 2N$. So whenever $D = 2N$, we have the critical case of logarithmic divergence. In that situation, there are no sub-leading divergences and the expression above gives the full answer. We have already discussed how the degree of divergence need to be estimated with more care in open QFTs.

Finally, a careful reader might note that we have only shown that non-local divergences appear in one of the diagrams in open QFT perturbation theory. There are many instances in unitary QFT where particular diagrams contribute to non-local divergences which cancel out in the eventual answer when the diagrams are summed [89, 90, 91, 92]. In the next section, we will show with a particular example that this seems not to hold in open QFTs.

5.2 Non-local divergences : open $\phi^3 + \phi^4$ theory

We revisit open $\phi^3 + \phi^4$ theory and study loop corrections more carefully. We study, in particular, open triangle diagrams (C -type) which were presumed convergent (from our knowledge of unitary scalar field theory) in §§3. We show that non-local divergences are present in triangle diagrams and do not go away when summing over diagrams in a vertex correction. The action for open $\phi^3 + \phi^4$ theory, as described earlier, is given by

$$\begin{aligned}
S_\phi = & - \int d^d x \left[\frac{1}{2} z (\partial\phi_R)^2 + \frac{1}{2} m^2 \phi_R^2 + \frac{\lambda_3}{3!} \phi_R^3 + \frac{\lambda_4}{4!} \phi_R^4 + \frac{\sigma_3}{2!} \phi_R^2 \phi_L + \frac{\sigma_4}{3!} \phi_R^3 \phi_L \right] \\
& + \int d^d x \left[\frac{1}{2} z^* (\partial\phi_L)^2 + \frac{1}{2} m^{2*} \phi_L^2 + \frac{\lambda_3^*}{3!} \phi_L^3 + \frac{\lambda_4^*}{4!} \phi_L^4 + \frac{\sigma_3^*}{2!} \phi_L^2 \phi_R + \frac{\sigma_4^*}{3!} \phi_L^3 \phi_R \right] \\
& + i \int d^d x \left[z_\Delta (\partial\phi_R) \cdot (\partial\phi_L) + m_\Delta^2 \phi_R \phi_L + \frac{\lambda_\Delta}{2!2!} \phi_R^2 \phi_L^2 \right].
\end{aligned} \tag{5.2.1}$$

To proceed, we briefly summarise the classification of C -type integrals and comment on structures of non-local divergences.

5.2.1 C -type SK integrals in four dimensions

There are 4^3 C -type loop integrals in R - L basis. However we use CPT (described in (3.0.1)) and cutting identity (see (3.1.14)) among all SK propagators to reduce the number of independent loop integrals to four. We choose those to be the following: $C_{RRR}, C_{PRR}, C_{PPR}, C_{PPP}$. We write the leading divergences of these loop integrals in this section. A detailed evaluation is done in C.3.

Single cut C -type: C_{PRR}

The integral expression for C_{PRR} is written below and the corresponding diagram is shown in fig.

6

$$C_{PRR} = (-i)^2 \int \frac{d^4 q}{(2\pi)^4} \frac{2\pi \delta_+(q^2 + m^2)}{[(q + \ell_1)^2 + m^2 - i\varepsilon][(q + \ell_2)^2 + m^2 - i\varepsilon]}. \tag{5.2.2}$$

The above integral is divergent and we regulate it using a hard cutoff regulator Λ . The explicit evaluation of this integral is given in appendix C.3. Here, we will state the divergent piece of the integral, given by

$$C_{PRR} = \frac{1}{(4\pi)^2} \frac{1}{\Sigma_{uc}} \tan^{-1} \left[\frac{\Sigma_{uc}}{\ell_1 \cdot \ell_2} \right] \log \Lambda + \dots \tag{5.2.3}$$

Here $\Sigma_{uc} \equiv \sqrt{\ell_1^2 \ell_2^2 - (\ell_1 \cdot \ell_2)^2}$ is the area of a parallelogram formed by the uncut momenta. Note that the Feynman $i\varepsilon$ prescription translates to shifting ℓ_j^0 's by $i\varepsilon$ in the above formula i.e. $\ell_j^0 \rightarrow \ell_j^0 + i\varepsilon$.

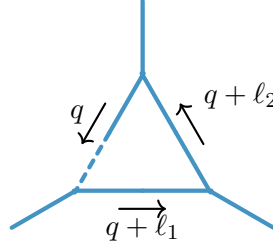


Figure 6: Triangle integral C_{PPR}

Double cut C -type: C_{PPR}

The diagram for C_{PPR} is shown in figure 6 and its integral expression being

$$C_{PPR} = (-i) \int \frac{d^4 q}{(2\pi)^4} \frac{2\pi\delta_+(q^2 + m^2) 2\pi\delta_+((q+k)^2 + m^2)}{(q+l)^2 + m^2 - i\varepsilon}. \quad (5.2.4)$$

This integral vanishes for timelike k but has non-local UV divergence for spacelike k . A detailed computation is done in C.3.2. We list the results below.

$$C_{PPR} = \begin{cases} 0, & \text{if } k \text{ is timelike} \\ \frac{i\pi}{(4\pi)^2} \frac{\text{csgn}(k^2 \ell^0 - (\ell \cdot k) k^0 + i\varepsilon)}{\sqrt{-\Sigma_{c,uc}^2}} \log \Lambda + \dots, & \text{if } k \text{ is spacelike,} \end{cases}$$

where $\Sigma_{c,uc} \equiv \sqrt{k^2 \ell^2 - (k \cdot \ell)^2}$ is the area of a parallelogram formed by the cut momentum k and the uncut momentum ℓ .

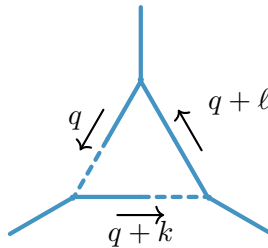


Figure 7: Triangle integral C_{PPR}

Triple cut C -type: C_{PPP}

The diagram for C_{PPP} is shown in fig. 8 and the integral expression for C_{PPP} is the following

$$C_{PPP} = \int \frac{d^4p}{(2\pi)^4} (2\pi)\delta_+(q^2 + m^2)(2\pi)\delta_+((q + k_1)^2 + m^2)(2\pi)\delta_+((q + k_2)^2 + m^2) \quad (5.2.5)$$

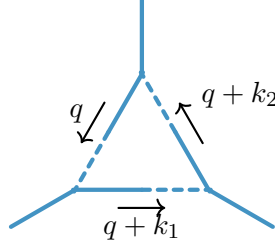


Figure 8: Triangle integral C_{PPP}

The solution to the above integral is given by

$$C_{PPP} = \begin{cases} \frac{2\pi}{(4\pi)^2} \frac{1}{\Sigma_c} \log \Lambda + \dots, & \text{if } k_1, k_2 \text{ span a spacelike subspace} \\ \frac{\Theta_{\text{overall}}}{8\sqrt{-\Sigma^2}}, & \text{else,} \end{cases}$$

where

$$\Theta_{\text{overall}} = \Theta(\omega_0 - m) \Theta\left(\omega_0 - \frac{\text{sgn}(k^0)}{\sqrt{-k^2}}(k_1 \cdot k)\right) \Theta\left(\omega_0 - \frac{\text{sgn}(k^0)}{\sqrt{-k^2}}(k_2 \cdot k)\right) \Theta(1 - |\beta|) \quad (5.2.6)$$

Given the above divergences, we compute correction to a vertex (e.g., σ_3) in open $\phi^3 + \phi^4$ theory.

5.2.2 Correction to σ_3 vertex due to triangle diagrams

There are 4^3 triangle diagrams contributing to the correction to σ_3 . However, many of these diagrams are obtained just by interchanging the external legs. We draw only those SK diagrams which cannot be obtained by interchanging the external legs. The diagrams can be found in figure 9, 10, 11, 12 and 13. For our convenience we have classified the triangle diagrams depending on type of propagator (R, L, P, M) that appear in a diagram.

1. All three propagators are same: These type of diagrams can be found in fig. 9.

The algebraic expression for all diagrams with all identical internal propagators is given by the following.

$$\mathcal{M}_I = (-i\lambda_3)^2 (-i\sigma_3) C_{RRR} + (i\lambda_3^*)(i\sigma_3^*)^2 C_{LLL} + (-i\sigma_3)^2 (i\sigma_3^*)(C_{MMM} + C_{PPP}) \quad (5.2.7)$$

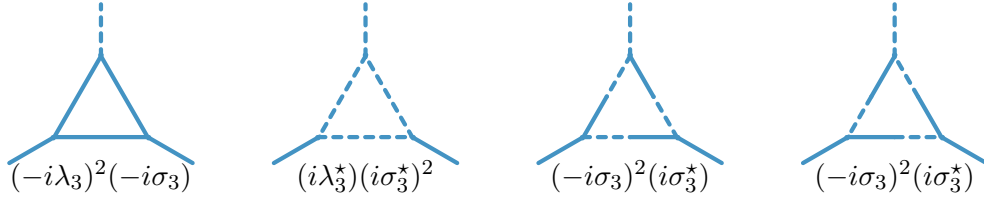


Figure 9: Feynman diagram for one loop renormalization to σ_3 - I. In these diagrams all of the internal propagators are same.

- Two propagators are same: These type of diagrams can be found in fig 10 and 11 and the expression being the following.

$$\begin{aligned}
\mathcal{M}_{II} = & (-i\sigma_3)^3 C_{RLR} + (-i\lambda_3)(-i\sigma_3)^2 (C_{RPR} + C_{RMR}) \\
& + (-i\lambda_3)(-i\sigma_3)(i\sigma_3^*) C_{PRP} + (-i\sigma_3)(i\sigma_3^*)^2 C_{PLP} + (-i\lambda_3)(i\sigma_3^*)^2 C_{PMP} \\
& + (i\lambda_3^*)(-i\sigma_3)^2 C_{LRL} + (i\lambda_3^*)(-i\sigma_3)(i\sigma_3^*) C_{LML} + (i\lambda_3^*)(-i\sigma_3)(i\sigma_3^*) C_{LPL} \\
& + (-i\sigma_3)(i\sigma_3^*)^2 C_{MLM} + (-i\lambda_3)(-i\sigma_3)(i\sigma_3^*) C_{MRM} + (-i\lambda_3)(i\sigma_3^*)^2 C_{MPM}
\end{aligned} \tag{5.2.8}$$

$$\begin{aligned}
\mathcal{M}_{III} = & (-i\lambda_3)(-i\sigma_3)(i\sigma_3^*) C_{RLR} + (-i\lambda_3)(-i\sigma_3)^2 (C_{RPR} + C_{RMR}) \\
& + (-i\lambda_3)(-i\sigma_3)(i\sigma_3^*) C_{PRP} + (i\lambda_3^*)(-i\sigma_3)^2 C_{PLP} + (-i\lambda_3)(i\lambda_3^*)(-i\sigma_3) C_{PMP} \\
& + (-i\sigma_3)(i\sigma_3^*)^2 C_{LRL} + (-i\sigma_3)(i\sigma_3^*)(i\lambda_3^*) C_{LML} + (i\sigma_3^*)^3 C_{LPL} \\
& + (-i\sigma_3)(i\sigma_3^*)^2 C_{MLM} + (-i\sigma_3)^3 C_{MRM} + (-i\sigma_3)^2 (i\sigma_3^*) C_{MPM} \\
& + \text{one channel } (p_2 \longleftrightarrow p_3).
\end{aligned} \tag{5.2.9}$$

- All three propagators are different: These type of diagrams can be found in fig 12, 13 and 14. The algebraic expression being the following.

$$\begin{aligned}
\mathcal{M}_{IV+V+VI} = & (-i\sigma_3)^2 (i\sigma_3^*) C_{RLP} + (-i\sigma_3)^2 (i\sigma_3^*) C_{RLM} + (-i\lambda_3)(-i\sigma_3)(i\sigma_3^*) C_{RPM} \\
& + (i\sigma_3^*)(i\lambda_3^*)(-i\lambda_3) C_{LMP} + \text{one more channel } (p_2 \longleftrightarrow p_3) \\
& + (-i\sigma_3)^2 (i\sigma_3^*) C_{RLP} + (-i\lambda_3)(i\sigma_3^*)^2 C_{RLM} + (-i\lambda_3)(-i\sigma_3)(i\sigma_3^*) C_{RPM} \\
& + (i\sigma_3^*)(i\lambda_3^*)(-i\lambda_3) C_{LMP} + \text{one more channel } (p_2 \longleftrightarrow p_3) \\
& + (-i\sigma_3)^2 (i\sigma_3^*) C_{RLP} + (-i\lambda_3)(-i\sigma_3)(i\lambda_3^*) C_{RLM} + (-i\lambda_3)^2 (i\lambda_3^*) C_{RPM} \\
& + (i\sigma_3^*)^2 (-i\sigma_3) C_{LMP} + \text{one more channel } (p_2 \longleftrightarrow p_3)
\end{aligned} \tag{5.2.10}$$

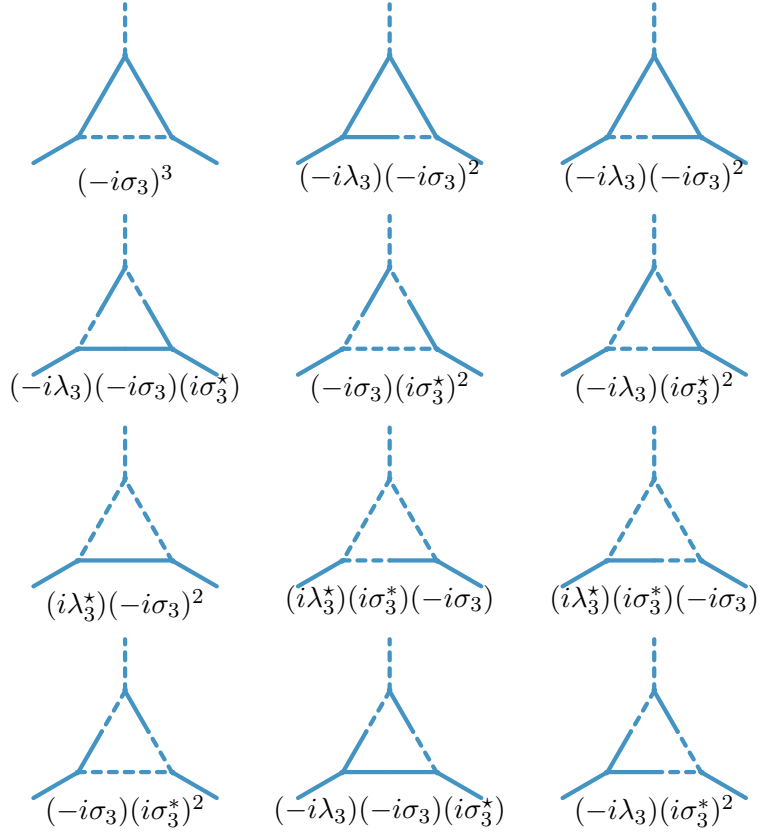


Figure 10: Feynman diagram for one loop renormalization to σ_3 - II. These set of diagrams consist of two identical propagators

Before we sum over all triangle diagrams described above, we summarise the domains of divergence of basis triangle diagrams so that we can choose suitable external momenta to simplify our computation. The domains of divergence are the following.

- C_{RRR} is convergent.
- C_{PRR} is divergent for all external momenta.
- C_{PPR} is divergent for space-like cut momentum and for all uncut momentum.
- C_{PPP} is divergent for only space-like cut momenta.

The correction to σ_3 vertex simplifies if we choose the cut or uncut momenta to be time-like. As a result, only single-cut diagrams contribute to the divergence structure.

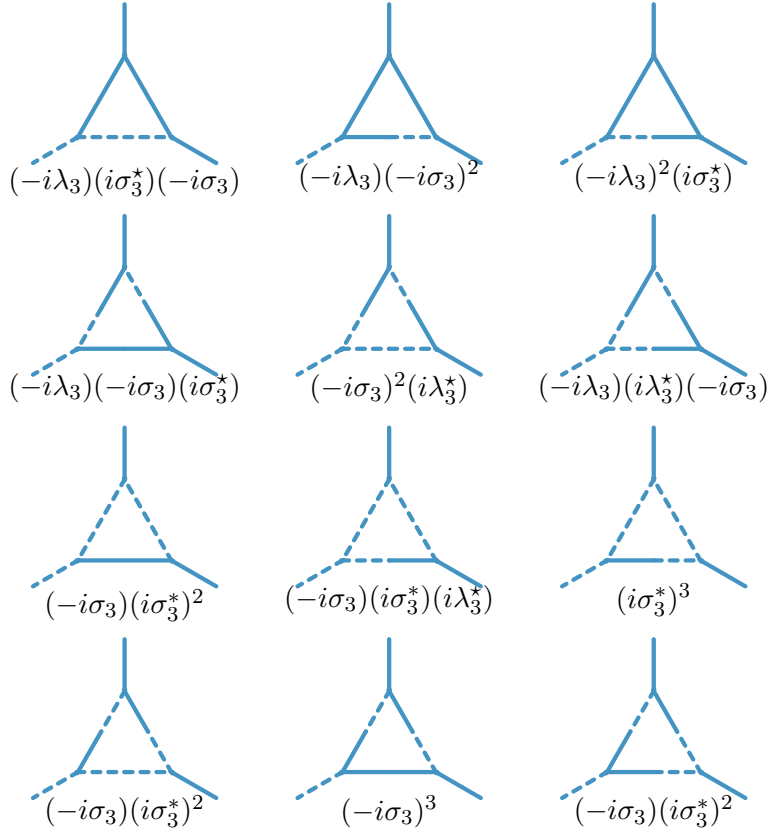


Figure 11: Feynman diagram for one loop renormalization to σ_3 - III.

Summing over all contribution we get

$$\begin{aligned}
& \mathcal{M}_I + \mathcal{M}_{II} + \mathcal{M}_{III} + \mathcal{M}_{IV} + \mathcal{M}_V + \mathcal{M}_{VI} \\
&= \left[(-i\sigma_3)^3 C_{RLR} + (-i\lambda_3)(-i\sigma_3)^2 (C_{RPR} + C_{RMR}) \right. \\
& \quad \left. + (i\lambda_3^*)(-i\sigma_3)^2 C_{LRL} + (i\lambda_3^*)(-i\sigma_3)(i\sigma_3^*) C_{LML} + (i\lambda_3^*)(-i\sigma_3)(i\sigma_3^*) C_{LPL} \right] \\
& \quad + \left[(-i\lambda_3)(-i\sigma_3)(i\sigma_3^*) C_{RLR} + (-i\lambda_3)(-i\sigma_3)^2 (C_{RPR} + C_{RMR}) \right. \\
& \quad \left. + (-i\sigma_3)(i\sigma_3^*)^2 C_{LRL} + (-i\sigma_3)(i\sigma_3^*)(i\lambda_3^*) C_{LML} + (i\sigma_3^*)^3 C_{LPL} \right. \\
& \quad \left. + \text{one channel } (p_2 \longleftrightarrow p_3) \right] \\
& \quad + \left[(-i\sigma_3)^2 (i\sigma_3^*) C_{RLP} + (-i\sigma_3)^2 (i\sigma_3^*) C_{RLM} + (-i\lambda_3)(-i\sigma_3)(i\sigma_3^*) C_{RPM} \right. \\
& \quad \left. + (i\sigma_3^*)(i\lambda_3^*)(-i\lambda_3) C_{LMP} + \text{one more channel } (p_2 \longleftrightarrow p_3) \right] \\
& \quad + \left[(-i\sigma_3)^2 (i\sigma_3^*) C_{RLP} + (-i\lambda_3)(i\sigma_3^*)^2 C_{RLM} + (-i\lambda_3)(-i\sigma_3)(i\sigma_3^*) C_{RPM} \right. \\
& \quad \left. + (i\sigma_3^*)(i\lambda_3^*)(-i\lambda_3) C_{LMP} + \text{one more channel } (p_2 \longleftrightarrow p_3) \right] \\
& \quad + \left[(-i\sigma_3)^2 (i\sigma_3^*) C_{RLP} + (-i\lambda_3)(-i\sigma_3)(i\lambda_3^*) C_{RLM} + (-i\lambda_3)^2 (i\lambda_3^*) C_{RPM} \right. \\
& \quad \left. + (i\sigma_3^*)^2 (-i\sigma_3) C_{LMP} + \text{one more channel } (p_2 \longleftrightarrow p_3) \right].
\end{aligned} \tag{5.2.11}$$

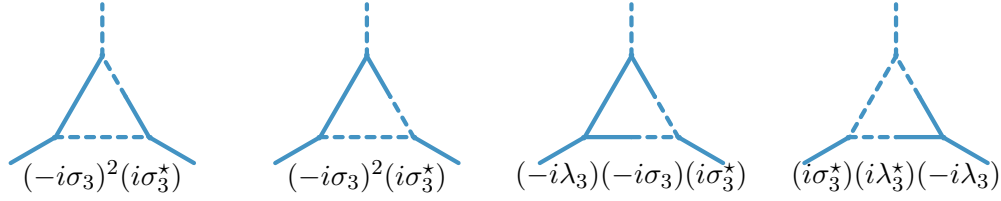


Figure 12: Feynman diagram for one loop renormalization to σ_3 - IV.

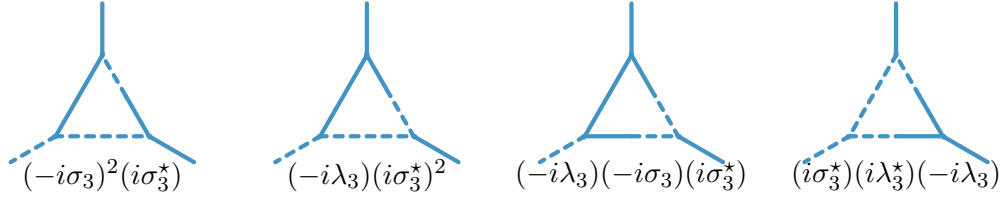


Figure 13: Feynman diagram for one loop renormalization to σ_3 - V.

Using the cutting identity ($R + L = P + M$) and relations given in C.3.4, the above expression can be simplified to

$$\begin{aligned}
& \mathcal{M}_I + \mathcal{M}_{II} + \mathcal{M}_{III} + \mathcal{M}_{IV} + \mathcal{M}_V + \mathcal{M}_{VI} \\
&= 2i \left[\sigma_3^3 - \lambda_3 \sigma_3^2 - \lambda_3^* \sigma_3^2 + \lambda_3^* \sigma_3 \sigma_3^* + \sigma_3^2 \sigma_3^* - \lambda_3 \sigma_3^{*2} \right] C_{RPR}(p_1, p_2, p_3) \\
&+ i \left[2\sigma_3 (\lambda_3 \sigma_3 - \lambda_3 \sigma_3^* + \sigma_3^{*2}) - \sigma_3^{*3} + \sigma_3 \sigma_3^* \lambda_3^* + \sigma_3^2 \sigma_3^* + \lambda_3 \sigma_3 \lambda_3^* \right] \\
&\quad \times [C_{RRP}(p_1, p_2, p_3) + C_{PRR}(p_1, p_2, p_3)] .
\end{aligned} \tag{5.2.12}$$

Since $C_{PRR}, C_{RPR}, C_{RRP}$ are non-local divergent, the above expression is also non-local divergent. Hence we conclude that non-local divergences do not cancel among diagrams in one loop correction to σ_3 in open $\phi^3 + \phi^4$ theory. We suspect that same conclusion holds true for any vertex correction.

5.3 Geometry of leading one-loop divergences in open QFTs

Taking cue from the kind of features we saw in §5.1, it is useful to define certain geometric objects that can be associated to a generic one loop diagram. These objects play an important role in analysis of one loop integrals. The geometry of loop integrals is a deep and a vast subject, especially as it relates to the structure of cuts singularity structures and the constraints due to unitarity [93, 94, 95, 96, 97, 98, 99].

As we have emphasised, the one loop integrals in open QFTs are very different objects with entirely different analytic structure and unfamiliar UV behaviours. Despite that fact, we will find

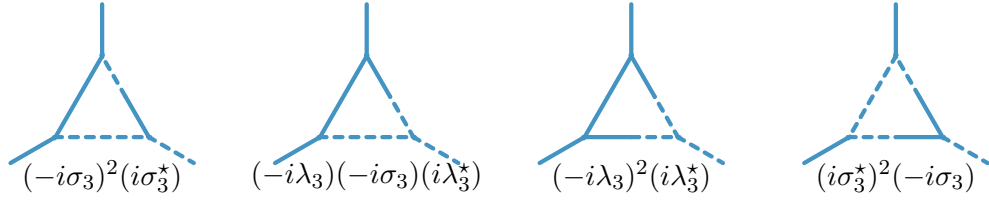


Figure 14: Feynman diagram for one loop renormalization to σ_3 - VI.

some striking resemblances to the geometric ideas that have appeared in the literature on unitary theories [96]. The crucial differences here arise from the enhanced degree of divergence in our loops arising from ‘linearisation’ of propagators by delta functions. As a result, quadric structures often get replaced by linear structures, simplifying the analysis in comparison to unitary theories.

The reader familiar with the unitary side, will hopefully find that whereas analysis differs very much in crucial details, the underlying philosophy is the same : the integrals are associated with geometric structures in the momentum space. Polytopes in momentum space and quadrics in Feynman parameters make their appearance, as in unitary theories [96], but in the somewhat unusual context of UV divergences.

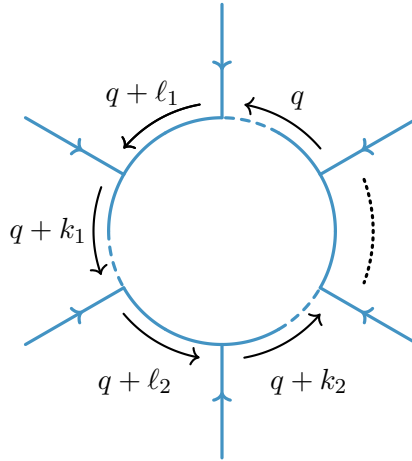


Figure 15: The $P^{N_c} R^{N-N_c}$ diagram : The cut Wightman propagators carry momenta $q^\mu, q + k_1^\mu, \dots, q + k_{N_c-1}^\mu$. The un-cut Feynman propagators carry momenta $q + \ell_1^\mu, \dots, q + \ell_{N-N_c}^\mu$.

Let us begin by considering a generic one-loop scalar diagram in D dimensions with N external legs, N_c number of Wightman/ P propagators and $N - N_c$ number of Feynman/ R propagators. We will denote this diagram by $P^{N_c} R^{N-N_c}$ and the corresponding integral by $\mathcal{I}[P^{N_c} R^{N-N_c}]$. This is a class of diagrams which in many senses capture the essential feature of one loop diagrams in

open QFTs. We will thus discuss these class of diagrams in detail in this section.

We label the internal momenta as shown in fig. 15. The momenta flowing through the cut/Wightman P propagators are $q, q + k_1, q + k_2, \dots, q + k_{N_c-1}$ respectively while the momenta flowing through the un-cut Feynman R propagators are $q + \ell_1, q + \ell_2, \dots, q + \ell_{N-N_c}$ respectively. We call the momenta $\{k_i\}$ as **cut** momenta since they flow through cut propagators while the momenta $\{\ell_i\}$ as **uncut** momenta since they flow through ordinary Feynman propagators. With these definitions in place, we can define several geometric objects associated to the cut and uncut momenta data. In what follows, we will assume the cut momenta to be linearly independent. As is usual in QFTs, at special kinematics of measure zero, the diagrams might show special kinds of divergences. But, we would be interested in divergences that happen for generic values of momenta of non-zero measure.

We define the following geometric objects for future convenience :

- **Cut momenta subspace, V_c :** This is the vector space spanned by the cut momenta $\{k_i\}$. It has a dimension of $N_c - 1$ (taking this to be less than spacetime dimension D , as we will assume from hereon). As we shall see later, this vector space controls one of the IR pre-factors in the open QFT divergences.
- **Parallelootope of cut momenta, \mathcal{P}_c :** The parallelootope (which is a higher dimensional generalisation of parallelogram) is formed out of the cut momenta and it lies within V_c . The inverse of the proper volume of this parallelootope appears in the non-local structure in the UV divergent diagram fig. 15. We will denote its proper volume by Σ_c .
- **Subspace transverse to the cut momenta, V_\perp :** This is also a vector space, which is the orthogonal complement of V_c . It has a dimension of $D - (N_c - 1)$. In open QFT diagrams with at least one cut/Wightman propagator, the dominant UV divergences come from fluctuations having momenta along V_c .
- **Positive Null cone transverse to the cut momenta, \mathcal{N}_\perp^+ :** This is the intersection of the positive null cone (i.e., the space of future-pointing light-like vectors) with the transverse space V_\perp . For the transverse space V_\perp to have null vectors at all, it has to be time-like. Equivalently, the span of cut momenta V_c has to be space-like. The physical significance of \mathcal{N}_\perp^+ lies in the statement that the leading divergences come from the loop momenta drawn from \mathcal{N}_\perp^+ .

With these basic definitions in hand, we would like to give a derivation of the leading UV divergence of a class of diagrams in open QFT in the rest of this section.

5.3.1 The parallelotope of cut momenta and its relativistic kinematics

In this subsection, we will describe in some detail how the geometry of the cut momenta appear in the IR pre-factors of open QFT divergences. Consider an integral of the form

$$\int \frac{d^D q}{(2\pi)^D} F[q, \ell_j] 2\pi \delta_+(q^2) \prod_{j=1}^{N_c-1} 2\pi \delta[2q \cdot k_j], \quad (5.3.1)$$

describing the leading UV behaviour of the diagram shown in fig. 15. Here, q^μ denotes the loop momentum to integrate with linear delta function constraints imposed on it by the cut-momenta $q + k_j$ of the Wightman propagators. We use the symbol $q + \ell_i$ to denote other un-cut momenta associated with Feynman propagators. Further, $F[q, \ell_j]$ is some Lorentz-invariant function of q^μ and the un-cut momenta. For the diagram above, it arises from the UV limit of Feynman propagators and it takes the form

$$F[q, \ell_j] = \frac{1}{\prod_{j=1}^{N-N_c} i(2q \cdot \ell_j - i\varepsilon)}. \quad (5.3.2)$$

Since, this particular form does not matter for the computation in this subsection, we will leave it implicit for now.

Our goal in this subsection would be to perform the integral over the delta functions to reduce the integral to a $D - N_c + 1$ dimensional integral. Without loss of generality, we will assume that k_j^μ are a set of $N_c - 1$ space-like vectors with $N_c < D$ such that their spatial parts are mutually orthogonal (i.e., $\mathbf{k}_i \cdot \mathbf{k}_j = 0$ if $i \neq j$). We will also assume that any linear combination of k_j^μ 's is also space-like.

- If their spatial parts were not mutually orthogonal to begin with, they can be made so by Gram-Schmidt procedure and the delta functions can be rearranged without changing the value of the integral.
- If they were not space-like, then the delta function with null-constraint $q^2 = 0$ would have no solutions. This follows from the fact that a vector transverse to a time-like vector should necessarily be a space-like vector (this is obvious by going to the rest-frame of the time-like vector in question). Thus, the above integral would evaluate to zero in that case. For the same reason, we require that any linear combination of k_j^μ 's should also space-like.

- If $N_c \geq D$, there would have been no solution again to the linear constraints imposed by the delta functions.

One of the main geometric objects of interest is the parallelotope formed by the momenta k_j^μ . We can define a Lorentz-invariant proper volume for this parallelotope by using the *Gram determinant*

$$\Sigma_c^2 \equiv \begin{vmatrix} k_1 \cdot k_1 & k_1 \cdot k_2 & \cdots & k_1 \cdot k_{N_c-1} \\ k_2 \cdot k_1 & k_2 \cdot k_2 & \cdots & k_2 \cdot k_{N_c-1} \\ \vdots & \vdots & \ddots & \vdots \\ k_{N_c-1} \cdot k_1 & k_{N_c-1} \cdot k_2 & \cdots & k_{N_c-1} \cdot k_{N_c-1} \end{vmatrix}. \quad (5.3.3)$$

Using the fact that \mathbf{k}_i are mutually orthogonal, we can do a short computation that yields the answer for the proper volume as

$$\Sigma_c^2 = (1 - \mathbf{v}^2) \prod_{j=1}^{N_c-1} \mathbf{k}_j^2. \quad (5.3.4)$$

Here the vector \mathbf{v} is defined by

$$\mathbf{v} \equiv \sum_{j=1}^{N_c} \frac{k_j^0}{|\mathbf{k}_j|^2} \mathbf{k}_j, \quad (5.3.5)$$

whose components along \mathbf{k}_j directions are given by

$$v_j \equiv \frac{k_j^0}{|\mathbf{k}_j|}. \quad (5.3.6)$$

To give a physical interpretation of \mathbf{v} , note the fact that we should have $\Sigma_c^2 > 0$ because the span of k_j^μ 's is space-like, by assumption. It follows that $|\mathbf{v}| < 1$ and \mathbf{v} can be thought of as a velocity. Note that we can use this velocity to write $k_j^0 = \mathbf{k}_j \cdot \mathbf{v}$. This in turn implies that, by boosting to a frame defined by the velocity, we can set to zero simultaneously all the time components of the momenta k_j^μ . Thus, the frame which is moving with this velocity is the frame of simultaneity for all k_j and is also the frame where the energy of all the cut propagators, viz., $(q + k_j)^0$ are equal. We can then recognise the relativistic/Lorentz-Fitzgerald contraction factor $\gamma_v \equiv \frac{1}{\sqrt{1-\mathbf{v}^2}}$ appearing in

$$\Sigma_c = \sqrt{1 - \mathbf{v}^2} \prod_{j=1}^{N_c-1} |\mathbf{k}_j|. \quad (5.3.7)$$

With these definitions in hand, let us now perform the integral over the delta functions. We will do this by choosing our co-ordinate axis appropriately : Let us choose the first $N_c - 1$ coordinates to be along $\mathbf{k}_{j=1,2,\dots,N_c-1}$. We will denote the components of the loop momentum along these directions as $q_{||,j=1,2,\dots,N_c-1}$. The rest of the $(D - N_c)$ spatial components perpendicular to \mathbf{k}_j are labelled as $q_{\perp,j=1,2,\dots,D-N_c}$.

$$\int \frac{dq^0}{2\pi} \int \frac{d^{D-N_c}q_{\perp}}{(2\pi)^{D-N_c}} \int \frac{d^{N_c-1}q_{||}}{(2\pi)^{N_c-1}} F[q^0, \mathbf{q}_{\perp}, \mathbf{q}_{||}, \ell_j] 2\pi\Theta(q^0) \delta(\mathbf{q}_{\perp}^2 + \mathbf{q}_{||}^2 - (q^0)^2) \times \prod_{j=1}^{N_c-1} 2\pi \delta[2q_{||,j}|\mathbf{k}_j| - q^0 k_j^0] . \quad (5.3.8)$$

Using $k_j^0 = v_j|\mathbf{k}_j|$, we can solve for the delta functions to get $\mathbf{q}_{||} = q^0\mathbf{v}$. We can then perform the integral over $\mathbf{q}_{||}$ which gives

$$\frac{1}{2^{N_c-1} \prod_{j=1}^{N_c-1} |\mathbf{k}_j|} \int \frac{dq^0}{2\pi} \int \frac{d^{D-N_c}q_{\perp}}{(2\pi)^{D-N_c}} 2\pi\Theta(q^0) \delta[\mathbf{q}_{\perp}^2 - (q^0)^2(1 - \mathbf{v}^2)] \times F[q^0, \mathbf{q}_{\perp}, \mathbf{q}_{||} = q^0\mathbf{v}, \ell_j^0, \ell_{j\perp}, \ell_{j||}] . \quad (5.3.9)$$

We will now simplify this integral further by moving to the frame of simultaneity of the space-like vectors k_j^μ , i.e., we boost by a velocity \mathbf{v} . The transverse/perpendicular components are invariant under the boost, whereas the parallel components become

$$\mathbf{q}_{||} = q^0\mathbf{v} \mapsto \left(1 - \frac{\mathbf{v}\mathbf{v}}{\mathbf{v}^2}\right) \cdot \mathbf{q}_{||} + \gamma_v \frac{\mathbf{v}\mathbf{v}}{\mathbf{v}^2} \cdot (\mathbf{q}_{||} - q^0\mathbf{v}) = 0 , \quad (5.3.10)$$

$$\ell_{j,||} \mapsto \left(1 - \frac{\mathbf{v}\mathbf{v}}{\mathbf{v}^2}\right) \cdot \ell_{j,||} + \gamma_v \frac{\mathbf{v}\mathbf{v}}{\mathbf{v}^2} \cdot (\ell_{j,||} - \ell_j^0\mathbf{v}) \equiv \tilde{\ell}_{j,||} .$$

We will denote the new time components in the frame of simultaneity of k_j^μ as q_{\perp}^0 and $\ell_{j\perp}^0$ respectively. We have

$$q^0 \mapsto \gamma_v(q^0 - \mathbf{v} \cdot \mathbf{q}_{||}) = q^0\sqrt{1 - \mathbf{v}^2} \equiv q_{\perp}^0 , \quad (5.3.11)$$

$$\ell_j^0 \mapsto \gamma_v(\ell_j^0 - \mathbf{v} \cdot \ell_{j,||}) \equiv \ell_{j\perp}^0 .$$

Using the Lorentz invariance of the function $F[q, \ell_j]$, we can then write

$$\frac{1}{2^{N_c-1}\sqrt{1 - \mathbf{v}^2} \prod_{j=1}^{N_c-1} |\mathbf{k}_j|} \int \frac{dq_{\perp}^0}{2\pi} \int \frac{d^{D-N_c}q_{\perp}}{(2\pi)^{D-N_c}} 2\pi\Theta(q_{\perp}^0) \delta[\mathbf{q}_{\perp}^2 - (q_{\perp}^0)^2] \times F[q_{\perp}^0, \mathbf{q}_{\perp}, \mathbf{q}_{||} = 0, \ell_{j\perp}^0, \ell_{j\perp}, \tilde{\ell}_{j,||}] . \quad (5.3.12)$$

We recognise here in the pre-factor, the inverse invariant volume of the cut momenta parallelepiped Σ_c . Further, if F is just a function of the dot product between q^μ and ℓ_j^μ and does not involve any factors of the form $\ell_i \cdot \ell_j$, then the dependence on $\tilde{\ell}_{j,||}$ completely drops out of the integral.

To summarise the main result of this subsection, we have proven the following useful identity

$$\boxed{\int \frac{d^D q}{(2\pi)^D} F[q, \ell_j] 2\pi \delta_+(q^2) \prod_{j=1}^{N_c-1} 2\pi \delta[2q \cdot k_j]} \quad (5.3.13)$$

$$= \frac{1}{2^{N_c-1} \Sigma_c} \int \frac{dq_{\perp}^0}{2\pi} \int \frac{d^{D-N_c} q_{\perp}}{(2\pi)^{D-N_c}} F_{\perp}[q_{\perp}, \ell_j] 2\pi \delta_+[q_{\perp}^2]$$

where the new loop function $F_{\perp}[q_{\perp}, \ell_j]$ is defined via

$$\boxed{F_{\perp}[q_{\perp}, \ell_j] \equiv F[q_{\perp}^0, \mathbf{q}_{\perp}, \mathbf{q}_{\parallel} \mapsto 0, \ell_j^0 \mapsto \gamma_v (\ell_j^0 - \mathbf{v} \cdot \ell_{j,\parallel}), \ell_{j\perp}, \ell_{j,\parallel} \mapsto \left(1 - \frac{\mathbf{v}\mathbf{v}}{v^2}\right) \cdot \ell_{j,\parallel} + \gamma_v \frac{\mathbf{v}\mathbf{v}}{v^2} \cdot (\ell_{j,\parallel} - \ell_j^0 \mathbf{v})]} \quad (5.3.14)$$

where the boost velocity to the frame of equal energy of the cut momenta (where k_j^{μ} are purely spatial) is given by

$$\boxed{\mathbf{v} \equiv \sum_{j=1}^{N_c} \frac{k_j^0}{|\mathbf{k}_j|^2} \mathbf{k}_j, \quad \gamma_v \equiv \frac{1}{\sqrt{1 - \mathbf{v}^2}},} \quad (5.3.15)$$

and Σ_c is the invariant volume polytope formed by k_j^{μ} :

$$\boxed{\Sigma_c \equiv \left| \begin{array}{cccc} k_1.k_1 & k_1.k_2 & \cdots & k_1.k_{N_c-1} \\ k_2.k_1 & k_2.k_2 & \cdots & k_2.k_{N_c-1} \\ \vdots & \vdots & \vdots & \vdots \\ k_{N_c-1}.k_1 & k_{N_c-1}.k_2 & \cdots & k_{N_c-1}.k_{N_c-1} \end{array} \right|^{1/2}} = \sqrt{1 - \mathbf{v}^2} \prod_{j=1}^{N_c-1} |\mathbf{k}_j|. \quad (5.3.16)$$

The essential complication in this formula is the physics of the boost factors which capture the relativistic kinematics. They simplify in the $\mathbf{v} \rightarrow 0$ limit, which is equivalent to working in the frame of simultaneity of k_j^{μ} from the start. Hereon, we will work in such a frame and the reader, if interested, can easily go back to a general frame using the formulae given above.

Ignoring these kinematic factors, the important dynamical lesson here is that the leading divergences arise completely from the interplay between

- IR pre-factor proportional to the inverse proper volume of cut momenta parallelepiped,
- UV divergences from transverse, future pointing, light-like fluctuations, with momenta along the transverse null-cone \mathcal{N}_{\perp}^+

We will next turn our attention to characterising the UV part of the loop integral.

5.3.2 The transverse null fluctuations and their contribution to the divergence

We now come back to the integral describing the leading UV divergence of the diagram shown in fig. 15 :

$$\begin{aligned} & \int \frac{d^D q}{(2\pi)^D} 2\pi \delta_+(q^2) \frac{\prod_{j=1}^{N_c-1} 2\pi \delta[2q \cdot k_j]}{\prod_{j=1}^{N-N_c} i(2q \cdot \ell_j - i\varepsilon)} \\ &= \frac{1}{2^{N_c-1} \Sigma_c} \int \frac{dq_{\perp}^0}{2\pi} \int \frac{d^{D-N_c} q_{\perp}}{(2\pi)^{D-N_c}} \frac{2\pi \delta_+[q_{\perp}^2]}{\prod_{j=1}^{N-N_c} i(2q_{\perp} \cdot \ell_{j\perp} - i\varepsilon)}. \end{aligned} \quad (5.3.17)$$

Here, we are working in a frame where all k_j^μ to be purely spatial, in order to simplify the relativistic kinematics. The corrected degree of divergence counting suggests that the above integral will diverge as

$$\frac{\Lambda^{D-N-1}}{\ell^{N-N_c} \Sigma_c},$$

and we would like to extract the precise form of this leading divergence.

Before we embark on a more detailed analysis of the integral, let us remark on the interesting structure of this integral and its UV divergences. The expression here bears striking similarities to the collinear divergences in scattering amplitudes dealt within the eikonal approximation (an idea at the heart of both heavy quark effective theory[100] and soft-collinear effective theory[101]). The integral above describes a hard particle world-line with momentum q^μ emitting soft/collinear particles with momenta ℓ_j^μ , suffering very little reduction in momentum. In the context of gauge theory, such an emission of gluons with its associated IR divergences can be exponentiated into a Wilson line. The difference here is that we are looking at a loop diagram and naively, the divergence here is not IR but UV.

Let us come back to evaluating the integral under question. We will begin by perform this integral by separating out the sphere integral over spatial parts of the loop momentum. We do this by writing $\mathbf{q}_{\perp} = |\mathbf{q}_{\perp}| \hat{n}$, where \hat{n} varies over the sphere $\mathbb{S}_{\perp}^{D-N_c-1}$, transverse to the cut momenta. This yields

$$\begin{aligned} & \frac{1}{2^{N_c-1} \Sigma_c} \int_0^{\Lambda} dq_{\perp}^0 \int_0^{\infty} |\mathbf{q}_{\perp}|^{D-N_c-1} d|\mathbf{q}_{\perp}| \delta[|\mathbf{q}_{\perp}|^2 - (q_{\perp}^0)^2] \\ & \times \frac{1}{(2\pi)^{D-N_c}} \int_{\hat{n} \in \mathbb{S}_{\perp}^{D-N_c-1}} \frac{1}{\prod_{j=1}^{N-N_c} i(2|\mathbf{q}_{\perp}| \hat{n} \cdot \ell_{j\perp} - 2q_{\perp}^0 \ell_{j\perp}^0 - i\varepsilon)}. \end{aligned} \quad (5.3.18)$$

Here

$$\int_{\hat{n} \in \mathbb{S}_{\perp}^{D-N_c-1}} \equiv \int_{\mathbb{S}_{\perp}^{D-N_c-1}} d\Omega[\hat{n}]$$

denotes the integral over the sphere $\mathbb{S}_\perp^{D-N_c-1}$.

We can now do the integral over $|\mathbf{q}_\perp|$ using the delta function. Since we are interested in the large q_\perp^0 contribution, we can then drop the small q_\perp^0 contributions and then write

$$\begin{aligned} & \frac{1}{2^{N_c-1}\Sigma_c} \int^\Lambda \frac{dq_\perp^0}{2q_\perp^0} (q_\perp^0)^{D-N-1} \\ & \times \frac{1}{(2\pi)^{D-N_c}} \int_{\hat{n} \in \mathbb{S}_\perp^{D-N_c-1}} \frac{1}{\prod_{j=1}^{N-N_c} i(2\hat{n} \cdot \ell_{j\perp} - 2\ell_{j\perp}^0 - i\varepsilon)}. \end{aligned} \quad (5.3.19)$$

Here, we have done the replacement $\varepsilon \mapsto \varepsilon q_\perp^0$ which is admissible at large positive q_\perp^0 . We see in the above expression a clean separation of the leading divergence into a product of three geometric factors as advertised :

1. First, we have the proper volume of cut parallelotope Σ_c , defined in the previous subsection, appearing in the denominator as

$$\frac{1}{2^{N_c-1}\Sigma_c}.$$

2. Next, we have the transverse sphere integral over the un-cut momenta

$$\boxed{\Xi_{uc\perp} \equiv \frac{1}{2(2\pi)^{D-N_c}} \int_{\hat{n} \in \mathbb{S}_\perp^{D-N_c-1}} \frac{1}{\prod_{j=1}^{N-N_c} i(2\hat{n} \cdot \ell_{j\perp} - 2\ell_{j\perp}^0 - i\varepsilon)}}. \quad (5.3.20)$$

This sphere integral is essentially an integral over the vectors $n^\mu \equiv (1, \hat{n})$ in the future light-cone. This can be made more explicit by introducing a time vector $t^\mu \equiv (1, \mathbf{0})$, to write

$$\boxed{\Xi_{uc\perp} \equiv \int \frac{d^{D-N_c}n}{(2\pi)^{D-N_c}} \frac{\delta(t \cdot n + 1)\delta_+(n^2)}{\prod_{j=1}^{N-N_c} i(2n \cdot \ell_{j\perp} - i\varepsilon)}}. \quad (5.3.21)$$

3. Lastly, we have a factor of

$$\int^\Lambda \frac{dq_\perp^0}{q_\perp^0} (q_\perp^0)^{D-N-1}$$

from high frequency light-like fluctuations which provide the UV divergence. The leading UV divergence of the diagram shown in fig. 15 then takes the form

$$\boxed{\frac{\Xi_{uc\perp}}{2^{N_c-1}\Sigma_c} \int^\Lambda \frac{dq_\perp^0}{q_\perp^0} (q_\perp^0)^{D-N-1}}. \quad (5.3.22)$$

This is the main result of this subsection.

As advertised, the leading divergence is consistent with the corrected degree of divergence $D - N - 1$ for open QFT loop. More precisely, from the formula above, we make the following observations about the degree of divergence:

- If $N_c = D$, then there will be no integration to perform, and hence the result will **always** be finite. This is simply because the delta functions/cut Wightman propagators of the loop integral eat up all the components of the loop momentum.
- If $N_c < D$, we have three cases
 1. If $D - N < 1$, there is no divergence.
 2. If $D - N = 1$, the divergence is **logarithmic** and there are **no** sub-leading divergences.
 3. If $D - N > 1$, the above result gives us the form of the **leading** universal divergence only. The sub-leading divergences will in general depend on the masses of the various propagators.
- If we restrict to the special case $N_c = D - 1$, the result above reduces back to the one described in the introduction. In that case, there are no leftover angular integrals to perform and the right answer is obtained by setting the volume of \mathbb{S}^0 to be $|\mathbb{S}^0|$ corresponding to the two branches of future light-cone.

5.4 Conclusion and discussion

We have shown in this chapter that a single scalar field theory exhibits non-local divergences in one-loop correction to vertices. These divergences appear in certain non-unitary one loop diagrams which have at least one cut internal propagator. While single cut diagrams always have this feature, multiple cut diagrams have non-local divergences only for certain choice of cut momenta (momenta flowing along cut propagators). The choice should be such that, there exists non-zero overlap of the light cone with the plane transverse to cut-momenta.

One can show that the leading divergence of a non-local divergent diagram (with some open-momenta and some unitary momenta) factorises into two parts. These parts admit an interesting geometric interpretation. The part which comes from cut momenta, can be interpreted as the inverse of volume of a parallelepiped, with its sides being the cut momenta.

One possibility of appearing these divergences is that the bath may not be completely decoupled from the system; some bath d.o.f. might be interacting with the high energy modes of system d.o.f. A way to resolve this would be to come up with a microscopic description of the effective action in weak-system-bath coupling limit. But we still lack such a description. One can also implement the

holographic construction [102, 103, 104] (will be discussed in the next chapter) to derive the SK effective action of a system coupled to a CFT bath and reconcile with the non-local divergences.

Chapter 6

Derivation of open effective action via holography

Holography provides a playground for study of strongly correlated systems where analytic techniques to compute response functions are limited. This approach has paid rich dividends over the past two decades: ranging from understanding thermalisation [74], linear response and hydrodynamics [105], to real-time transport computations [106]. Much of this success owes to the fact that black holes in asymptotically AdS spacetimes are dual to thermal QFTs.

Here we will study open quantum field theory using holography, where d.o.f. of the quantum system are non-trivially entangled with some external environment. The set-up we have in mind is the following: consider a QFT say with one Bosonic degree of freedom $\Psi(t, \mathbf{x})$ (for simplicity) which is our system of interest. We will model the environment by another field theory, now with many degrees of freedom $X_i(t, \mathbf{x})$. The unitary microscopic theory is of the form:

$$S_s[\Psi] + S_e[X_i] + S_{s-e}[\Psi, X_i]. \quad (6.0.1)$$

The combined system and environment is prepared in some initial state, which we may even take to be factorized between the respective degrees of freedom. Integrating out the environment degrees of freedom X_i we end up with a non-unitary evolution of our system. The question we ask is to find a local description of the open EFT (for our system degrees of freedom Ψ).

The set-up we have in mind is semi-holographic, cf., [107]. Say we wish to understand the dynamics of a single bosonic degree of freedom which we continue to call $\Psi(x)$ in d spacetime dimensions. We imagine coupling this to a strongly coupled thermal environment comprising of

some intrinsic microscopic degrees of freedom. For concreteness, one can imagine the environment to be the thermal large N , strongly coupled, $\mathcal{N} = 4$ Super Yang-Mills (SYM) theory (gauge group $SU(N)$) in $d = 4$, or a large c thermal CFT in $d = 2$. Following common practice, we will often refer to the system and the environment as the probe and the bath, respectively.

The coupling of the probe/system degree of freedom Ψ to the thermal bath is via a local coupling $\int d^d x \Psi(x) \mathcal{O}(x)$ where $\mathcal{O}(x)$ is a simple operator in the bath/environment theory. In the aforementioned examples \mathcal{O} could be a low lying single trace conformal primary operator. Crucially, the thermal bath theory is assumed to have a holographic dual. This will enable us model the environment by a dual black hole geometry. The influence phases of our system are then encoded in the real-time or Schwinger-Keldysh (SK) correlation functions of the environmental degrees of freedom. The computation of the latter, thanks to the holographic map, is one which can be carried out using classical fields propagating in a classical black hole background. From the holographic standpoint, the problem therefore boils down to developing a formalism for computing real-time observables in black hole backgrounds (or more generally in spacetimes with horizons).

Before commenting on the real-time computation let us first recall a well-known, but remarkable, fact of the Euclidean gravitational path integral. Thermal boundary conditions require that the Euclidean time (t_E) direction be compact with period given by the inverse temperature asymptotically. For the gravitational path integral these boundary conditions pick out the Wick rotated black hole solution as the Gibbons-Hawking saddle point solution [108]. This is unlike any non-gravitational system, where the Euclidean thermal circle is more of a computational aid, the background geometry being non-dynamical. Said differently, gravitational dynamics interplays non-trivially with thermal boundary conditions.

Given this solution, one way to pass to a real-time description is to slice open the Euclidean solution at some instant of real-time, say at $t = 0$, which exposes quite naturally two copies of the asymptotic region at ($t_E = 0$ and $t_E = \frac{\beta}{2}$, respectively). This initial data can then be evolved in real Lorentzian time to give the (future half) of the eternal black hole solution. This is the gravitational preparation of the thermofield double state in the doubled field theory Hilbert space, which in energy eigenbasis is expressed as

$$|\text{TFD}\rangle = \frac{1}{\sqrt{Z(\beta)}} \sum_n e^{-\frac{1}{2}\beta E_n} |E_n^R\rangle \otimes |E_n^L\rangle \quad (6.0.2)$$

where the $R(L)$ refers to the asymptotic boundaries at $t_E = 0$ ($t_E = \frac{\beta}{2}$).

Insofar as thermal equilibrium properties are concerned, the thermofield double construction proves ample. One gets to ask questions about correlation functions with operators inserted in either copy of the doubled system. One can therefore view the gravitational path integral as computing the following generating function for asymptotic observers (in asymptotically AdS spacetimes)

$$\mathcal{Z}_{\text{TFD}} [J_{\text{R}}, J_{\text{L}}] = \text{Tr} \mathcal{U}(J_{\text{R}}) \rho_{\beta}^{\frac{1}{2}} (\mathcal{U}[J_{\text{L}}])^{\dagger} \rho_{\beta}^{\frac{1}{2}} \quad (6.0.3)$$

The fact that we slice open the functional integral midway is what is responsible for the fractionation of the thermal density matrix ρ_{β} .

To obtain real-time response one then has to analytically continue these results to the real-time domain. In the absence of any sources deforming the state away from equilibrium there is in principle no obstacle to carrying out this analytic continuation. However, once one moves to the physics of systems in local equilibrium, or more generally out-of-equilibrium, which more pertinently applies to our discussion of computing influence functionals, the thermofield double state proves less useful. In this context the Schwinger-Keldysh formalism provides a cleaner and more natural way for computing real-time observables by keeping manifest causality and unitarity, without relying on the aforesaid analytic continuation. The Schwinger-Keldysh generating function does not fractionate the density matrix, but rather computes the generating function:

$$\mathcal{Z}_{\text{SK}} [J_{\text{R}}, J_{\text{L}}] = \text{Tr} \mathcal{U}(J_{\text{R}}) \rho_{\beta} (\mathcal{U}[J_{\text{L}}])^{\dagger}. \quad (6.0.4)$$

This fact is well-known in non-equilibrium QFTs where real-time observables, say linear response captured by viscosity, conductivity, etc., are always computed (using Kubo formulae) from the Schwinger-Keldysh formalism. The pictorial representation of the path integral contour shown in [1](#) provides a quick way to see the difference between the two constructions (cf., [\[73\]](#) for further discussion).

Given this fact, it is natural to ask how the Schwinger-Keldysh construction can be adopted to gravitational theories. We will primarily focus on situations where the system is prepared in a thermal state. We wish to know how the gravitational dynamics fills in an asymptotic Schwinger-Keldysh contour shown in [1\(b\)](#). This question has been considered by many authors in the AdS/CFT context over the years. In [\[109\]](#) the first proposal for computing real-time correlation functions was given. These authors posited that one should consider the future half of the domain of outer communication of a Lorentzian black hole spacetime, and impose ingoing boundary

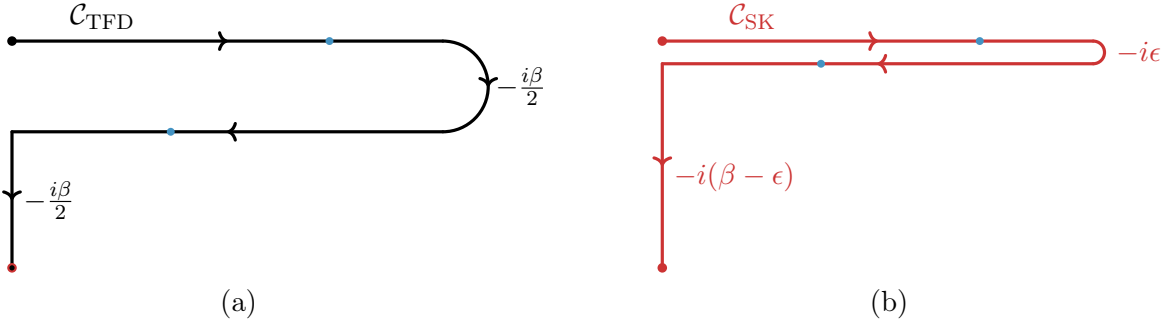


Figure 1: A comparison of the (a) thermofield double and (b) Schwinger-Keldysh complex time contours for a system prepared in a thermal state. The starting and end points of the contour are identified. The associated Euclidean (imaginary time) periodicity is set by the inverse temperature β .

conditions on the future horizon to extract causal observables (retarded Green’s functions). In addition they also argued for the absence of any boundary contribution from the horizon. This prescription was justified shortly thereafter in [110] using the maximal Kruskal extension of the black hole geometry (the logic was to exploit the analytic structure taking inspiration from the Euclidean thermofield double construction). One limitation of this approach was that it was well adapted to the computation of two-point functions, but it left implicit how to obtain higher point functions. Nevertheless, over the years, various authors have attempted to use this prescription for various applications [111, 112, 113, 114, 115].

In order to explain the subtlety let us remind the reader how Euclidean n -point correlation functions in AdS/CFT are computed via Witten diagrams [116]. One first computes the appropriate bulk-boundary propagators for various external operator insertions. These enable us to ‘evolve’ the corresponding fields into the bulk with sources set by the boundary conditions. One convolves the bulk fields thus obtained using the bulk interaction vertices which are dictated by gravitational dynamics. Since the fields interact locally, one has to integrate the position of the vertex over the entire Euclidean bulk manifold. Modulo the choice of temporal boundary conditions one expects something similar for the computation of real-time retarded observables. However, it is a-priori unclear what domain of the bulk geometry one ought to integrate the bulk interaction vertex over, even assuming that the ingoing boundary conditions serve to pick out the appropriate bulk-boundary propagator.

This issue was addressed in [103, 102] who gave a more detailed prescription for real-time computations, arguing that one should fill in asymptotic Schwinger-Keldysh contours with piece-

wise smooth geometries: real-time evolution sections of the boundary contour get filled in with Lorentzian geometries, and imaginary-time segments with Euclidean geometries. These geometries are glued together continuously along codimension-1 spacelike slices. The authors developed a robust holographic renormalization scheme for asymptotically AdS geometries [102]. Furthermore, the ingoing boundary condition for retarded correlation functions was derived quite cleanly using this prescription in [117]. This prescription was employed in the derivation of covariant holographic entanglement entropy proposal [118].

Per se, it is then clear that in order to carry out the computation of real-time correlation function of probe operators in a fixed state, one could simply use the prescription of [103, 102]. However, if one were to ask questions about dynamically evolving geometries, one realizes that the piecewise smooth geometries pose a potential issue in the presence of horizons. Physically, the question essentially becomes one of coming up with a prescription ensuring that effects of the outgoing Hawking quanta are correctly accounted for (see [113, 114] for attempts in this direction). While a complete answer to this question is still unclear, an interesting prescription was recently given by [104] to address this lacunae in the probe limit (see also [119]).

The prescription of [104] postulates that the gravitational dual of the asymptotic Schwinger-Keldysh contour is given by a complex two-sheeted spacetime. This geometry is made of two copies of the black hole exterior smoothly glued together across the future horizon, with a particular monodromy condition. One may view this as the statement that the asymptotic Schwinger-Keldysh contour gets filled in by a complex geometry. This can be motivated by the slicing open the Euclidean Gibbons-Hawking saddle [108] whilst incorporating the Schwinger-Keldysh boundary conditions, as we have attempted to illustrate in 2. The authors of [104] already demonstrated the efficacy of their prescription by obtaining the quadratic influence functional in a low frequency and momentum expansion for a bulk scalar field in the probe limit.¹

Subsequently, [120] explored how this prescription may be employed to study non-linear Langevin dynamics of a single particle degree of freedom in quantum mechanics. Their analysis subjected the prescription to the test of dealing with self-interacting fields in the bulk and demonstrated that it continues to give reasonable answers. Specifically, the authors of [120] modeled the Brownian particle using the holographic construction described in [121, 112]. Using the complex holographic

¹The authors of [104, 119] also addressed the problem of Maxwell gauge field in the probe limit. However, as pointed out in [104] many aspects of how the prescription works for gauge theories are still unclear.

geometry of [104] to compute influence functionals, they demonstrated that general expectations of non-linear Langevin dynamics explored in earlier [122, 123] was borne out. We will demonstrate in the course of our analysis that the prescription correctly captures real-time observables and can be used in the semi-holographic setting to model open effective field theories.

We have motivated the discussion in terms of invoking the holographic duality to learn about influence functionals in an open quantum system. It is instructive to also keep in mind that these influence functionals for holographic thermal baths in fact encode interesting semiclassical gravitational information about black holes. In the semi-holographic set-up we motivated above, the system degree of freedom Ψ gets imprinted upon by the characteristics of the environment. Since our thermal environment is provided by a black hole, we would effectively be encoding not only the dissipative behaviour of the horizon, which we know to be characterized linearly by quasinormal modes, but also the fluctuations of the horizon. The latter are nothing but the outgoing Hawking radiation. Since the quasinormal modes refer to the physical response of infalling matter we would effectively be capturing, in the non-Gaussian influence functionals, the interaction between infalling matter and the Hawking radiation.²

The coupling of AdS black holes to external systems has recently been of active interest in the context of the black hole information paradox [124, 125] (cf., [126]). In these examples the external system is treated as a passive reservoir wherein one captures the Hawking radiation. Our discussion applies in this context as well; the external system's observables will faithfully be able to diagnose the interaction of Hawking radiation with infalling matter. The structure we get to probe however is only the leading semiclassical pieces of the interaction. We are considering a single gravitational saddle point configuration, and not including contributions from non-trivial replica saddles which have been important in understanding the purification of the Hawking radiation and the reproduction of the Page curve for AdS black holes [127, 128].

In this paper, we will be considering the coupling of our probe/system (modeled by a single bosonic field) to a scalar operator in the holographic thermal system. Most of the technical computations we report will involve computing Schwinger-Keldysh correlation functions of a scalar field in an asymptotically AdS black hole background using the holographic Schwinger-Keldysh geometry of [104]. This work had already considered the computation of the two point function

²The non-Gaussian correlations we compute holographically using the semiclassical gravity approximation are suppressed in the planar expansion by powers of $1/N$, as indeed are all higher point functions in a large N (or large central charge) environment.

in a low-energy gradient expansion, i.e., perturbatively at low frequencies and momenta. We will extend this to higher point functions, but also show how to get results outside the gradient expansion in two dimensional CFTs.

6.1 grSK: the gravitational Schwinger-Keldysh saddle

The Schwinger-Keldysh contour for a thermal state is a complex time path running from $t = 0$ to $t = T$ and thence to $t = 0 - i\beta$ as depicted in 1(b). Thus we have a contour in a complex time plane for the temporal part of the action at the boundary for a holographic field theory. The proposal of [104] is to extend this contour to a codimension-1 hypersurface in the complexified bulk spacetime in gravity. To be specific, let us first introduce this geometry for stationary configurations with a timelike Killing field, such as the planar Schwarzschild-AdS_{d+1} black hole.

We start with the metric written in ingoing Eddington-Finkelstein coordinates, which are regular at the future horizon, viz.,

$$ds^2 = -r^2 f(r) dv^2 + 2 dv dr + r^2 d\mathbf{x}^2, \quad f(r) = 1 - \frac{r_h^d}{r^d}. \quad (6.1.1)$$

The coordinate v is identified with the time coordinate t on the boundary of the spacetime $r \rightarrow \infty$, which as we have argued, is to be interpreted as a curve in the complex plane. The idea is to also upgrade the radial coordinate to the complex domain and pick a codimension-1 slice through the resulting complex spacetime.

Operationally, we in fact upgrade radial tortoise coordinate to a complex variable, which we refer to as the *mock tortoise* coordinate, ζ . We define this coordinate by the differential relation:

$$\frac{dr}{d\zeta} = \frac{i\beta}{2} r^2 f(r), \quad (6.1.2)$$

where $\beta = \frac{4\pi}{dr_h}$ is the inverse temperature of the black hole. The rationale for introducing this coordinate is that ζ picks up a logarithmic branch cut from the integral about the zero of the emblickening function $f(r)$ of the black hole. The choice of normalization is such that the monodromy around this cut is set to unity. The coordinate ζ can be viewed as parameterizing a two-sheeted surface, each of which can be thought of as the bulk extension of the Schwinger-Keldysh contour. On each sheet ζ has an imaginary part running from 0 at the AdS boundary to ∞ at the horizon. In addition it has a real part which differentiates the two sheets and is given by the monodromy around the horizon. By convention we will choose one of the sheets to have vanishing real part,

and the other to have unit real part (this is based on our choice of normalization). We will also cut-off the AdS geometry at a radial cut-off $r = r_c$ for computational ease. With this choice, we have the two branches on which the mock tortoise coordinate asymptotes to

$$\zeta(r_c + i\varepsilon) = 0, \quad \zeta(r_c - i\varepsilon) = 1. \quad (6.1.3)$$

A section of geometry in the mock tortoise complex plane is illustrated in 3.

The metric then takes the form

$$ds^2 = -r^2 f(r) dv^2 + i\beta r^2 f(r) dv d\zeta + r^2 d\mathbf{x}^2, \quad f(r) = 1 - \frac{r_h^d}{r^d} \quad (6.1.4)$$

where we treat $r(\zeta)$ using (6.1.2). We will refer to this geometry as the *gravitational Schwinger-Keldysh (grSK) saddle or geometry*. One can integrate (6.1.2) explicitly to find that the mock tortoise coordinate for Schwarzschild-AdS $_{d+1}$ geometries in terms of a hypergeometric function, viz.,

$$\zeta + \zeta_c = \frac{id}{2\pi(d-1)} \left(\frac{r}{r_h}\right)^{d-1} {}_2F_1\left(1, \frac{d-1}{d}; 2 - \frac{1}{d}; \frac{r^d}{r_h^d}\right), \quad (6.1.5)$$

where ζ_c is chosen to make $\zeta = 0$ at $r = r_c + i\varepsilon$. The branch-cut of the hypergeometric function is taken to run from $r = r_h$ to ∞ .³

One can motivate the grSK geometry by recalling the Schwinger-Keldysh generating function (6.0.4) which computes casual response of the thermal state (as well as the fluctuations thereabout). In particular, it requires that we do not fractionate the thermal density matrix. Since the excursion into the complex time domain between the two segments of the contour on the boundary in 1(b) is infinitesimal, the gravity saddle point should respect this separation. One way to achieve this is to prepare the thermal state using the Euclidean path integral. The real-time part of the contour can thence be obtained by slicing open the Euclidean black hole solution around $t = i\varepsilon$ and $t = -i\beta + i\varepsilon$ and continue the geometry into the Lorentzian section. The evolution of the slice at $t = i\varepsilon$ will give a section of the domain of outer communication of the Lorentzian black hole geometry. The slice at $t = -i\beta + i\varepsilon$ will lead to something similar with a reversed temporal direction. These are the two slices of the geometry living at $\zeta = 0, 1$, respectively.

This basic picture was first espoused in [117], but the prescription of [104] has the added advantage of smoothly connecting the two slices across a ‘horizon-cap’. The resulting geometry is smooth and is coordinatized by (6.1.4). Pictorially, the construction is depicted in 2.

³It is actually convenient in explicit computations to work with a redefined radial coordinate $\varrho = \frac{r^d}{r_h^d}$, which is the argument of the hypergeometric function.

Now that we have identified the grSK geometry we can explain how to study dynamics thereupon. One should think of all the fields as residing on a complex ζ contour and upgrade the classical bulk action to a contour integral over the mock tortoise coordinate. We write:

$$S_{\text{bulk}} = \oint d\zeta \int d^d x \sqrt{-g} \mathcal{L}[g_{AB}, \Phi], \quad (6.1.6)$$

where x^μ are the boundary coordinates. We will use this form of the action for computations of influence functionals. Before we get to those however, we describe how to generalize our construction covariantly to spacetimes with a Killing horizon, and also explain some useful properties of the grSK geometries.

Covariant grSK spacetime: While we described the construction in a coordinate dependent manner, one can give a more covariant presentation of the same. We can describe this for any spacetime with a smooth future horizon. Pick some intrinsic coordinates on the spatial sections of the horizon, call them \mathbf{x} . One can let the temporal evolution be determined by the affine parameter, v , along the horizon generators. A natural radial coordinate r can be chosen by demanding that it be generated by the null normal to the horizon, normalized with respect to the horizon generators, i.e., $\partial_v \cdot \partial_r = 1$. For a non-degenerate horizon one has ∂_v being timelike outside the codimension-1 null hypersurface (the future horizon). In a local neighbourhood of the horizon one would then end up with a metric of the form (6.1.1) with $f(r)$ having a simple zero. The details of the rest of the geometry will depend on the asymptotics etc., but the part of the construction that matters for us is indeed the neighbourhood of the future horizon. One can now convert this classical geometry to a two-sheeted geometry with a gluing condition across the horizon as described above by replacing $r \rightarrow \zeta$.

To illustrate the construction more generally, it is sufficient to consider the near-horizon region of the spacetime. For non-degenerate black holes this is given by the Rindler geometry. In this case we have the familiar form of the geometry as well as the ingoing coordinatization to be given as:

$$ds^2 = -r^2 dt^2 + dr^2 = -r^2 dv^2 + 2r dv dr = 2dv d\rho - 2\rho dv^2. \quad (6.1.7)$$

Here we have defined $\rho \equiv \frac{1}{2} r^2$. It is then easy to explicitly identify the mock tortoise coordinate, $\zeta = \frac{1}{2\pi i} \log \rho$ on the primary branch (we work with the Rindler temperature normalized to be 2π). The grSK Rindler geometry would then take the form

$$ds^2 = 2e^{2\pi i \zeta} dv(2\pi i d\zeta - dv). \quad (6.1.8)$$

grSK time reversal: Before proceeding further, it is useful to note one useful feature of the grSK geometries. These geometries are not time reversal invariant as is indeed appropriate for the Schwinger-Keldysh dual. However, the Schwinger-Keldysh construction has a \mathbb{Z}_2 involution that can be thought of as time-reversal (cf., [73] for a discussion). As described in [120] the geometry does indeed have an involution which can be used to map ingoing solutions to outgoing ones. In the coordinates used in (6.1.4) the transformation takes the form:

$$v \rightarrow i\beta\zeta - v, \quad \omega \rightarrow -\omega \quad (6.1.9)$$

where ω is the frequency conjugate to v . More generally, on tensor valued fields the map acts via an idempotent $(1, 1)$ tensor:

$$\mathcal{T}_A^B \equiv \begin{pmatrix} 1 & i\beta & 0 \\ 0 & -1 & 0 \\ 0 & 0 & \delta_{ij} \end{pmatrix}, \quad \mathcal{T}_A^B \mathcal{T}_B^C = \delta_A^C. \quad (6.1.10)$$

Time reversal on tensors by contracting indices appropriately, which can be inferred from the action on one-forms and vectors, respectively. These are given to be:

$$\begin{aligned} \mathfrak{W}_A(v, \zeta, \mathbf{x}) &\mapsto \mathcal{T}_A^B \mathfrak{W}_B(i\beta\zeta - v, \zeta, \mathbf{x}), \\ \mathfrak{A}^A(v, \zeta, \mathbf{x}) &\mapsto \mathfrak{A}^B(i\beta\zeta - v, \zeta, \mathbf{x}) \mathcal{T}_A^B. \end{aligned} \quad (6.1.11)$$

It is useful to write these equations in terms of ingoing and outgoing modes explicitly, which we denote with superscripts ‘ \pm ’. So one has

$$\mathfrak{f}^-(v, \zeta, \mathbf{x}) = \mathfrak{f}^+(i\beta\zeta - v, \zeta, \mathbf{x}) \quad (6.1.12)$$

leading to the general tensor transformation:

$$(\mathfrak{T}^+)_{A_1 \dots A_n}^{B_1 \dots B_m} \mapsto \mathcal{T}_{A_1}^{C_1} \dots \mathcal{T}_{A_n}^{C_n} (\mathfrak{T}^-)_{C_1 \dots C_n}^{D_1 \dots D_m} \mathcal{T}_{D_1}^{B_1} \dots \mathcal{T}_{D_m}^{B_m}. \quad (6.1.13)$$

We will exploit this symmetry to construct solutions of the scalar wave equations in an asymptotically AdS grSK geometry to obtain the corresponding boundary-bulk Green’s functions.

6.2 Open scalar field theory and holographic baths

Our goal in this chapter is to construct the open effective field theory of a single scalar degree of freedom coupled to a holographic thermal field theory. We will start by describing the general set-up and then specialize to the case of two dimensional theories. We will first begin our description by

focusing on the ‘bath/environment’ theory with a holographic dual and how its real-time correlators can be computed via AdS/CFT. We will then describe how this computation amounts to deriving the open effective theory for the probe.

6.2.1 General set-up

Let us consider a scalar probe $\Psi(x)$ coupled to a d -dimensional field theory with fields denoted collectively by X . The latter is taken to be in a thermal state and we let $\mathcal{O} \equiv \mathcal{O}[X(x)]$ be a local gauge invariant operator in this theory. The action for our system is then

$$S = \int d^d x \left(\mathcal{L}[\Psi] + \mathcal{L}[X] + \Psi(x) \mathcal{O}(x) \right). \quad (6.2.1)$$

We wish to integrate out the thermal degrees of freedom characterized by X and derive an effective action for Ψ . The couplings in $S_{\text{eff}}[\Psi]$ are determined by standard sum rules in terms of the Schwinger-Keldysh thermal correlators of the environment variables X [22, 23] (see also [76]). So in what follows we will focus on computing thermal Schwinger-Keldysh observables for the environment, with the understanding that these feed into the effective action of our open quantum system. The implications for the open effective theory will be described below in 6.2.2.

The thermal field theory we consider will be taken to be holographic. For example we can consider $S[X]$ to refer to a strongly coupled, planar gauge theory in $d > 3$ (like $\mathcal{N} = 4$ SYM) or a large c 2d CFT. Concretely, in the familiar duality between $SU(N)$ $\mathcal{N} = 4$ Super Yang-Mills (SYM) and string theory on $\text{AdS}_5 \times \mathbf{S}^5$, the map between parameters is

$$g_{YM}^2 N \sim \left(\frac{\ell_{\text{AdS}}}{\ell_s} \right)^4, \quad N \sim \left(\frac{\ell_{\text{AdS}}}{\ell_p} \right)^4. \quad (6.2.2)$$

where ℓ_s is the string length scale, and ℓ_p the five-dimensional Planck scale. We will work in the regime $N \gg 1$ and $g_{YM}^2 N \gg 1$ whence the holographic system can be described by classical gravitational dynamics on $\text{AdS}_5 \times \mathbf{S}^5$.

The gravitational dual description is in terms of a planar Schwarzschild- AdS_{d+1} black hole, whose metric in ingoing coordinates was presented in (6.1.1). The scalar operator, \mathcal{O} , is characterized by its conformal dimension Δ and maps, under the AdS/CFT dictionary, to a scalar field Φ propagating on this black hole background with mass $m^2 \ell_{\text{AdS}}^2 = \Delta(\Delta - d)$. In particular, the marginal case $\Delta = d$ corresponds to $m^2 = 0$ in AdS. The correlation functions of the operator \mathcal{O} can be computed by studying the dynamics of Φ in the gravitational theory. For the purposes of

our discussion we will model the scalar dynamics by a minimally coupled scalar with a contact self-interaction. For the most part the self-interacting scalar action we work with takes the form:

$$S_\Phi = - \int d^{d+1}x \sqrt{-g} \left[\frac{1}{2} g^{AB} \partial_A \Phi \partial_B \Phi + \frac{1}{2} m^2 \Phi^2 + \frac{\lambda_n}{n!} \Phi^n \right]. \quad (6.2.3)$$

While this will be sufficient to illustrate the general features, it should be borne in mind that one can obtain in actual (top-down) holographic models, such effective action for the bulk fields using dimensional reduction from 10 or 11 dimensional supergravity.

The above discussion describes the basic set-up for any AdS/CFT computation. However, for the purposes of our real-time computation we would need to upgrade this action to reside on the gravitational Schwinger-Keldysh black hole geometry (6.1.4). This is readily done, for we simply change coordinates and rewrite the scalar action as a contour integral over the grSK geometry. To wit,

$$S_\Phi = - \oint d\zeta \int d^d x \sqrt{-g} \left[\frac{1}{2} g^{AB} \partial_A \Phi \partial_B \Phi + \frac{1}{2} m^2 \Phi^2 + \frac{\lambda_n}{n!} \Phi^n \right]. \quad (6.2.4)$$

We will study this problem in general dimensions, constructing first the boundary-bulk propagators on the grSK geometry. This involves only the quadratic part of the action; we essentially need to invert the kinetic terms on the grSK geometry.

The boundary to bulk propagators will be specified by suitable boundary conditions around the horizon-cap in the geometry (6.1.4) and non-normalizable boundary conditions characterizing sources on the AdS boundary. We will find that there are two types of propagators: *retarded (ingoing)* and *advanced (outgoing)*. They will be related in a simple manner by the time-reversal involution identified at the end of §6.1. These Green's functions can be obtained by solving the linear scalar wave equation on the grSK geometry. Working in momentum space variables allows mode decoupling as usual. For a general field \mathfrak{f} on the grSK geometry we adopt the following notational contrivance for Fourier transforms:

$$\mathfrak{f}(v, \zeta, \mathbf{x}) = \int \frac{d\omega}{2\pi} \frac{d^{d-1}\mathbf{k}}{(2\pi)^{d-1}} \mathfrak{f}(\omega, \zeta, \mathbf{k}) e^{-i\omega v + i\mathbf{k}\cdot\mathbf{x}} \equiv \int_k \mathfrak{f}_k e^{ikx}. \quad (6.2.5)$$

In general d dimensions we will not be able to solve for the propagator in an explicit analytic manner, as the wave equation on the Schwarzschild-AdS $_{d+1}$ black hole is not known to admit closed form solutions. Hence we will resort to a gradient expansion in the frequencies and momenta, aiming for a low-frequency, long-wavelength expansion. In $d = 2$ however we will be able to obtain closed form expressions for the propagators.

Once we have obtained the boundary to bulk propagators we can compute higher point functions using standard Witten diagram technology in the grSK geometry. Consider the computation of the 4-point function of the operator \mathcal{O} in the boundary theory on the Schwinger-Keldysh contour. Of the 4! Wightman functions with various time-orderings, 8 are computed by the Schwinger-Keldysh time-ordering. This is clear from the generating functional (6.0.4); on the Schwinger-Keldysh contour operators can be inserted either in the forward (R) or backward (L) segments, effectively doubling the number of correlators. These correlation functions are simply related via the Keldysh rules to sequences of nested commutators and anti-commutators of the operator \mathcal{O} with suitable time-ordering step-functions, see [63, 73]. Furthermore, the thermal KMS relations group the correlation functions into orbits of 4 elements (coming from cyclic symmetry of the thermal trace) [69].

It is convenient to introduce a couple of different basis of operators and sources which are convenient in the Schwinger-Keldysh formalism for various computations. First, we introduce the *average-difference* or *Keldysh* basis

$$\begin{aligned} \text{operators : } \quad \mathcal{O}_a &= \frac{1}{2} (\mathcal{O}_R + \mathcal{O}_L) , & \mathcal{O}_d &= \mathcal{O}_R - \mathcal{O}_L , \\ \text{sources : } \quad J_a &= \frac{1}{2} (J_R + J_L) , & J_d &= J_R - J_L . \end{aligned} \tag{6.2.6}$$

Within the Schwinger-Keldysh literature, the average/difference fields are also sometimes referred to as classical/quantum components respectively. The Keldysh basis naturally separates out an averaged mean field vs the corrections due to quantum/statistical fluctuations. Another useful basis which manifests the KMS relations is the *retarded-advanced* (RA) basis⁴

$$\begin{aligned} \bar{J}_F(\omega, \mathbf{k}) &\equiv - \left((1 + n_\omega) J_R(\omega, \mathbf{k}) - n_\omega J_L(\omega, \mathbf{k}) \right) , \\ \bar{J}_P(\omega, \mathbf{k}) &\equiv -n_\omega \left(J_R(\omega, \mathbf{k}) - J_L(\omega, \mathbf{k}) \right) , \end{aligned} \tag{6.2.7}$$

where n_ω is the Bose-Einstein statistical factor:

$$n_\omega \equiv \frac{1}{e^{\beta\omega} - 1} . \tag{6.2.8}$$

As we shall see below the distinction between the P and F combinations naturally shows up on the holographic side as the distinction between the ingoing modes and the outgoing modes.

⁴Per se, our definition of the retarded-advanced basis differs mildly from what is commonly used in the literature say in [63, 73]. The choice we make is inspired by certain simplifications for the spectral decomposition, not only of Schwinger-Keldysh observables, but also of the more general out-of-time-order correlation functions as described in [70].

The structure of the influence functionals we wish to extract can be now succinctly summarized as follows. Having solved for the field Φ in terms of sources J_R and J_L on the asymptotic boundaries of the AdS grSK geometry the influence functionals are obtained from the generating functional, assuming an n -point bulk contact interaction:

$$\begin{aligned}
S_{(n)} &\propto \prod_{i=1}^n \int_{k_i} \delta\left(\sum_{i=1}^n k_i\right) \oint d\zeta \prod_{i=1}^n \Phi(\zeta, k_i) \\
&\equiv \int \prod_{i=1}^n \frac{d^d k_i}{(2\pi)^d} (2\pi)^d \delta\left(\sum_i k_i\right) \oint d\zeta \prod_{i=1}^n \Phi(\zeta, k_i) \\
&= \int \prod_{i=1}^n \frac{d^d k_i}{(2\pi)^d} (2\pi)^d \delta\left(\sum_i k_i\right) \left[\mathfrak{I}_{p,n-p}(k_1, k_2, \dots, k_n) \prod_{i=1}^p J_a(k_i) \prod_{j=p+1}^n J_d(k_j) \right] \\
&= \int \prod_{i=1}^n \frac{d^d k_i}{(2\pi)^d} (2\pi)^d \delta\left(\sum_i k_i\right) \left[\mathcal{I}_{p,n-p}(k_1, k_2, \dots, k_n) \prod_{i=1}^p \bar{J}_F(k_i) \prod_{j=p+1}^n \bar{J}_P(k_j) \right].
\end{aligned} \tag{6.2.9}$$

In case there are lower-point contact interactions in the bulk, then we should also include tree level Witten diagrams where we have bulk-bulk propagators between the vertices of such lower order contact terms. While self-evident we nevertheless provide a brief argument for this prescription in Appendix D.3.

We have given the influence functionals both in the average-difference basis, denoted by \mathfrak{I} as well as in the retarded-advanced basis, denoted \mathcal{I} . We will later write down expressions for them directly in terms of scalar Green's functions. However, there are some general statements that one can make regarding their structural properties prior to any explicit computation, which follow directly from the generating function (6.0.4). In the average-difference basis the fact that $\mathcal{Z}_{\text{SK}}[J, J] = \text{Tr}(\rho_\beta)$ implies that

$$\mathfrak{I}_{a\dots a}(k_1, k_2, \dots, k_n) = 0. \tag{6.2.10}$$

This is reflection of the Schwinger-Keldysh collapse rule: the difference operators (equivalently the average source) cannot be futuremost.

In the retarded-advanced basis the fact that we have folded in the statistical factors makes not only the Schwinger-Keldysh collapse rule manifest, but also incorporates the KMS condition. We have

$$\mathcal{I}_{P\dots P}(k_1, k_2, \dots, k_n) = 0 = \mathcal{I}_{F\dots F}(k_1, k_2, \dots, k_n). \tag{6.2.11}$$

We shall see the holographic SK geometry naturally incorporates these relations through the smoothness of the solution across the future horizon cap region that glues together the two sheets

of grSK geometry.

6.2.2 Deriving an open EFT from holography

In 6.2.1 we have described how one could get a generating functional for Schwinger-Keldysh correlators from holography. This generating functional is evaluated in the presence of a source J for an operator \mathcal{O} in the theory with holographic dual. This selfsame generating functional has another physical interpretation as emphasized by Feynman and Vernon [22] in their seminal work on open quantum systems.

The form of the coupling between the probe and the bath systems in (6.2.1) suggests that we can interpret the source J of the operator \mathcal{O} as the probe field Ψ itself. Further assuming that the dynamics of our probe system is slow, we can then integrate out the ‘fast’ degrees of freedom which make up the environment. This will obtain for us an effective SK action for this probe, which was termed as the influence functional of the probe in [22]. The Schwinger-Keldysh generating functional of the CFT $\mathcal{Z}_{\text{SK}}[J_R, J_L]$ can hence be given an alternate interpretation as the influence functional of the probe $S_{\text{IF}}[\Psi_R, \Psi_L]$.

Various structural features we described above for the generating functional can then be re-interpreted as necessary features for the probe influence functional. If the environment is sufficiently forgetful, one would expect that a local influence functional could be written down for the probe. We will indeed see that the holographic influence functionals derived this way do satisfy this property. Given the difficulty of constructing local influence functionals from perturbative methods (see the introduction of this chapter), this is indeed a fortunate circumstance. We will show that a variety of open EFTs can be derived this way by using grSK geometry and holography.

The KMS conditions and Schwinger-Keldysh collapse rule then have a definite counterpart from the influence functional perspective. One can first of all construct a stochastic field theory that is dual to the influence functional of the open system. In this stochastic field theory, the structural features described above get re-interpreted as non-linear generalizations of fluctuation-dissipation theorems (FDTs). Our holographic construction naturally leads to these non-linear FDTs via the physics of the Hawking radiation and its interaction with the ingoing modes. As far as the authors are aware, this is the first instance where these non-linear FDTs are derived within a field theoretic setup by integrating out bath degrees of freedom.⁵

⁵The particle analogues of non-linear FDTs for a Brownian particle have for instance appeared in [122, 123,

The stochastic description for the dynamics of the open system degree of freedom which follows from the influence functionals $S_{\text{IF}}[\Psi_{\text{R}}, \Psi_{\text{L}}]$ can be obtained in the following manner. We work in the average/difference basis Ψ_a and Ψ_d defined analogously to (6.2.6) for the system variables. The idea is to write the dynamics of the average field Ψ_a as a Langevin equation after eliminating the difference or fluctuation field Ψ_d . We recall that the average field is the ‘classical’ variable, where the difference field is the ‘stochastic/fluctuation’ variable. One starts with the following ansatz for the Langevin dynamics

$$\begin{aligned} \mathcal{E}[\Psi_a, \eta] &= f \eta, \\ \mathcal{E}[\Psi_a, \eta] &\equiv (-K \partial_t^2 + D \nabla^2 + \gamma \partial_t) \Psi_a \\ &\quad + \sum_{k=1}^{n-1} \left(\theta_k \frac{\eta^{k-1}}{k!} \frac{\Psi_a^{n-k}}{(n-k)!} + \bar{\theta}_k \frac{\eta^{k-1}}{k!} \frac{\Psi_a^{n-k-1}}{(n-k-1)!} \partial_t \Psi_a \right). \end{aligned} \quad (6.2.12)$$

The parameters $\{K, D, \gamma, \theta_k, \bar{\theta}_k\}$ are coupling constants, to be determined in terms of the influence phase parameters. The variable η here is the thermal/stochastic noise, with strength f ; it is drawn from a non-Gaussian probability distribution

$$\mathcal{P}[\eta] \sim \exp \left(- \int d^d x \left(\frac{f}{2!} \eta^2 + \frac{\theta_n}{n!} \eta^n \right) \right). \quad (6.2.13)$$

To relate the Langevin ansatz (6.2.12) to an effective action arising from the influence functionals (see Eq. (6.5.1) for an explicit action) we follow the Martin-Siggia-Rose (MSR) trick [130], wherein one converts the stochastic Langevin equation into an effective action using a Lagrange multiplier field Ψ_d and the functional integral identity:

$$1 = \int \mathcal{D}\Psi_a \mathcal{D}\Psi_d \mathcal{D}\eta e^{-i \int d^d x (\mathcal{E}[\Psi_a, \eta] - f \eta) \Psi_d} \mathcal{P}[\eta]. \quad (6.2.14)$$

Integrating out the noise field η one obtains the SK effective action for Ψ_a and Ψ_d . To capture the leading order influence phase we only need to shift $\eta \rightarrow \eta + i \Psi_d$ and take the limit $\eta \rightarrow 0$. We then arrive at the Schwinger-Keldysh effective action for our probe system

$$\begin{aligned} S_{\Psi} &= - \int d^d x \Psi_d [-K \partial_t^2 + D \nabla^2 + \gamma \partial_t] \Psi_a \\ &\quad + i \int d^d x \left[-f \frac{(i \Psi_d)^2}{2!} + \sum_{k=1}^n \frac{(i \Psi_d)^k}{k!} (\theta_k + \bar{\theta}_k \partial_t) \frac{\Psi_a^{n-k}}{(n-k)!} \right]. \end{aligned} \quad (6.2.15)$$

Recall that the standard (linear) FDT relates the friction term γ and stochastic noise f via

$$\gamma = \frac{\beta f}{2}. \quad (6.2.16)$$

[129, 120].

We find that one obtains non-linear FDTs which relate the non-Gaussian couplings θ_k and $\bar{\theta}_k$ amongst each other in the form.

$$\frac{2}{\beta}\bar{\theta}_k + \theta_{k+1} + \frac{1}{4}\theta_{k-1} = 0. \quad (6.2.17)$$

This is the advertised FDT for which we will give a derivation once we have derived the influence functionals from holography in 6.5.

6.3 Scalar propagation in grSK geometries

We now turn to the solutions of the wave equations in diverse dimensions. We will first describe the general set-up, identifying various Green's functions of interest. Our goal is to determine the full solution for the scalar field with prescribed sources J_R and J_L on the two boundary segments of the grSK geometry. It will turn out that a useful way to proceed is to first identify the ingoing propagator G^+ , which solves the wave equation with infalling boundary conditions, and thence use time reversal to obtain the outgoing propagator G^- (or a linear combination, the Hawking propagator, G^H , that we introduce below).

Once we have the general framework we will exploit the relative simplicity in $d = 2$ where the BTZ black hole is a quotient of AdS_3 to find an explicit expression for our propagators. For $d > 2$ the Schwarzschild- AdS_{d+1} geometries do not admit closed form solutions to the scalar wave equation. However, one can solve for the propagators explicitly in a gradient expansion, i.e., order by order perturbatively in frequencies and momenta. We further elaborate on this gradient expansion scheme in D.1 exposing some useful technical tricks to organize the solution and extract the propagators.

In what follows we impose Dirichlet (standard) boundary conditions for our scalar field asymptotically (for simplicity), so the conformal dimension of the CFT operator and the mass of the field propagating in the grSK geometry are related by $\Delta = \frac{d}{2} + \sqrt{\frac{d^2}{4} + m^2 \ell_{\text{AdS}}^2}$.

6.3.1 Scalar boundary to bulk propagators in grSK geometry

The classical equation of motion for a minimally coupled scalar field

$$\partial_A (\sqrt{-g} g^{AB} \partial_B \Phi) - m^2 \Phi = 0, \quad (6.3.1)$$

in the grSK geometry (6.1.4). Written out explicitly in Fourier decomposition $\Phi(v, \zeta, \mathbf{x}) = \int_k \Phi_k(\zeta) e^{i k x}$ we find:

$$\frac{\partial}{\partial \zeta} \left(r^{d-1} \frac{\partial \Phi_k}{\partial \zeta} \right) + \frac{\beta \omega}{2} \left(r^{d-1} \frac{\partial \Phi_k}{\partial \zeta} + \frac{\partial}{\partial \zeta} (r^{d-1} \Phi_k) \right) + \frac{\beta^2}{4} r^{d-1} f(r) (|\mathbf{k}|^2 + r^2 m^2) \Phi_k = 0. \quad (6.3.2)$$

We can now proceed to solve this problem, but it is useful to understand some structural aspects first.

We wish to identify the boundary to bulk propagators for the wave equation (6.3.2), which allows us to evolve a non-normalizable source at the boundary of the spacetime into a field value at a bulk locale. We will start by first identifying the retarded or ingoing bulk to boundary Green's function G^+ and subsequently use information about the time reversal symmetry to extract the outgoing or advanced Green's function.

Let us first introduce a new pair of radial derivatives [120]

$$D_\zeta^\pm = \frac{\partial}{\partial \zeta} \pm \frac{\beta \omega}{2}, \quad (6.3.3)$$

which conjugate to each other in the form:

$$e^{\beta \omega \zeta} D_\zeta^+ e^{-\beta \omega \zeta} = D_\zeta^-. \quad (6.3.4)$$

Notice that D_ζ^\pm are related to each other by time reversal. The rationale for introducing them is that these derivatives allow us to absorb the odd powers of ω in the wave equation into themselves. Indeed, in terms of these derivations the scalar equation of motion takes the form:

$$D_\zeta^+ (r^{d-1} D_\zeta^+ \Phi_k) + \frac{\beta^2}{4} r^{d-1} (f |\mathbf{k}|^2 + r^2 f m^2 - \omega^2) \Phi_k = 0. \quad (6.3.5)$$

Ingoing boundary to bulk propagator: The ingoing Green's function $G_{in} \equiv G^+$ is a solution to (6.3.5) satisfying a regularity condition at the horizon and normalized to unity at the cut-off boundary of the spacetime.

$$G^+|_{r_c} = 1, \quad \left. \frac{dG^+}{d\zeta} \right|_{r_h} = 0. \quad (6.3.6)$$

The choice of boundary conditions is such that we are looking at infalling modes across the future horizon, which isolates for us the quasinormal modes (general solution being a superposition of these modes in a linear theory). As such the ingoing Green's function will be the one that was obtained in [109] who argue for the ingoing boundary conditions to compute the retarded propagator. We will shortly demonstrate how to obtain G^+ perturbatively in ω and $|\mathbf{k}|$, i.e., in a gradient expansion in general d and also obtain an explicit analytic form in $d = 2$.

Outgoing boundary to bulk propagator: Once one knows ingoing Green's function G^+ the advanced or outgoing Green function should be obtained by suitably time reversing it. As argued at the end of 6.1, while our coordinatization of the geometry is not time reversal invariant, there indeed an involution realized by the diffeomorphism (6.1.9). Let us see how this acts on the equation of motion (6.3.5). First, we note that after reversing the frequency dependence we obtain $G^-(\omega, \mathbf{k}) \equiv G^+(-\omega, \mathbf{k})$. Using the conjugation relation (6.3.4) we can then infer that the function $G^-(\omega, \mathbf{k})e^{-\beta\omega\zeta}$ satisfies the wave equation provided

$$D_{\zeta}^{-} (r^{d-1} D_{\zeta}^{-} G^{-}) + \frac{\beta^2}{4} r^{d-1} (f |\mathbf{k}|^2 + r^2 f m^2 - \omega^2) G^{-} = 0. \quad (6.3.7)$$

Note that (6.3.7) differs from (6.3.5) only in the signs of the temporal derivatives i.e., through $\omega \rightarrow -\omega$. It therefore follows that the outgoing Green's function can be obtained in Fourier domain as

$$G_{out}(\omega, |\mathbf{k}|) \equiv G^+(-\omega, |\mathbf{k}|)e^{-\beta\omega\zeta} \equiv G^-(\omega, |\mathbf{k}|)e^{-\beta\omega\zeta}. \quad (6.3.8)$$

Full solution and boundary conditions: Now that we have the formal expressions for the ingoing and outgoing Green's functions, we can take a suitable superposition to write down the general solution for the linear wave equation. The explicit form of the full solution takes the form

$$\Phi(\zeta, \omega, \mathbf{k}) = C_+(\omega, \mathbf{k}) G^+(\zeta, \omega, \mathbf{k}) + C_-(\omega, \mathbf{k}) G^-(\zeta, \omega, \mathbf{k})e^{-\beta\omega\zeta}. \quad (6.3.9)$$

We can now impose boundary conditions at the conformal boundary $r = r_c \pm i\varepsilon$ of the grSK geometry. We demand:

$$\Phi_k|_{\zeta=0} = J_L(\omega, \mathbf{k}), \quad \Phi_k|_{\zeta=1} = J_R(\omega, \mathbf{k}). \quad (6.3.10)$$

Using the fact that G^+ and G^- are normalized to unity at these boundaries, we find

$$C_+(\omega, \mathbf{k}) + C_-(\omega, \mathbf{k}) = J_L, \quad C_+(\omega, \mathbf{k}) + C_-(\omega, \mathbf{k})e^{-\beta\omega} = J_R. \quad (6.3.11)$$

which results in the solution

$$C_-(\omega, \mathbf{k}) = -(1 + n_\omega) (J_R - J_L), \quad C_+(\omega, \mathbf{k}) = (1 + n_\omega) J_R - n_\omega J_L. \quad (6.3.12)$$

Hence the general solution to the scalar wave equation (6.3.9) takes the form

$$\Phi_k(\zeta, \omega, \mathbf{k}) = G^+(\zeta, \omega, \mathbf{k}) \left((1 + n_\omega) J_R - n_\omega J_L \right) - G^-(\omega, \mathbf{k}) e^{\beta\omega(1-\zeta)} n_\omega \left(J_R - J_L \right). \quad (6.3.13)$$

where we have used the Bose-Einstein identity:

$$1 + n_\omega = e^{\beta\omega} n_\omega . \quad (6.3.14)$$

It is helpful, before proceeding further, to rewrite the result in terms of linear combinations of the L/R Schwinger-Keldysh sources. For instance, in the retarded-advanced basis (6.2.7) we find

$$\Phi(\zeta, \omega, \mathbf{k}) = -G^+(\zeta, \omega, \mathbf{k}) J_{\bar{F}} + G^-(\zeta, \omega, \mathbf{k}) e^{\beta\omega(1-\zeta)} J_{\bar{F}} . \quad (6.3.15)$$

More interesting to us is the solution in the average-difference basis:

$$\begin{aligned} \Phi(\zeta, \omega, \mathbf{k}) &= G^+(\zeta, \omega, \mathbf{k}) \left(J_a(\omega, \mathbf{k}) + \left(n_\omega + \frac{1}{2} \right) J_d(\omega, \mathbf{k}) \right) \\ &\quad - n_\omega e^{\beta\omega(1-\zeta)} G^-(\zeta, \omega, \mathbf{k}) J_d(\omega, \mathbf{k}) , \\ &\equiv G^+ J_a + \frac{1}{2} G^H J_d . \end{aligned} \quad (6.3.16)$$

In the last line we have isolated the contribution from the average and difference sources. The coefficient of the latter is a suitable admixture of the ingoing and outgoing modes which in fact deserves to be called the *Hawking Green's function* which is a solution to the wave equation with the boundary conditions

$$\lim_{\zeta \rightarrow 0} G^H = 1 \quad \text{and} \quad \lim_{\zeta \rightarrow 1} G^H = -1 . \quad (6.3.17)$$

Explicitly, it is given by:

$$G^H \equiv \coth\left(\frac{\beta\omega}{2}\right) G^- - e^{\frac{\beta\omega}{2}(1-2\zeta)} \operatorname{csch}\left(\frac{\beta\omega}{2}\right) G^- . \quad (6.3.18)$$

6.3.2 Propagators in $d = 2$

As a warm up we start with the BTZ geometry where $d = 2$. The metric we recall is

$$\begin{aligned} ds^2 &= -r^2 \left(1 - \frac{r_h^2}{r^2}\right) dv^2 + 2 dv dr + r^2 dx^2 \\ &= -r_h^2 \sinh^2 \rho dv^2 + 2r_h \sinh \rho dv d\rho + r_h^2 \cosh^2 \rho dx^2 , \end{aligned} \quad (6.3.19)$$

where we have written the metric in ingoing coordinates both in the standard AdS radial coordinate as well as in the BTZ adapted global coordinate $r = r_h \cosh \rho$. We have either by direct integration or by simplifying (6.1.5) the following expression for the mock tortoise coordinate

$$\frac{d\zeta}{dr} = \frac{r_h}{i\pi} \frac{1}{r^2 - r_h^2} \implies \sqrt{\frac{r - r_h}{r + r_h}} = \tanh \frac{\rho}{2} = e^{i\pi(\zeta + \zeta_c)} , \quad (6.3.20)$$

where accounted for the cut-off surface where we are imposing our boundary conditions.

We can solve the massive, minimally coupled, scalar wave equation (6.3.2) in terms of hypergeometric functions

$$\begin{aligned} & (\text{sech } \rho)^\Delta \left(1 + \tanh^2 \frac{\rho}{2}\right)^{\Delta - \mathbf{p}_+ - \mathbf{p}_-} {}_2F_1(\mathbf{p}_+, \mathbf{p}_-, 1 + \mathbf{p}_+ + \mathbf{p}_- - \Delta; \tanh^2 \rho), \\ & (\text{sech } \rho)^\Delta \left(\frac{\tanh^2 \frac{\rho}{2}}{1 + \tanh^2 \frac{\rho}{2}}\right)^{\Delta - \mathbf{p}_+ - \mathbf{p}_-} {}_2F_1(\Delta - \mathbf{p}_-, \Delta - \mathbf{p}_+, 1 + \Delta - \mathbf{p}_+ - \mathbf{p}_-; \tanh^2 \rho). \end{aligned} \quad (6.3.21)$$

The first of these is the solution that satisfies ingoing boundary conditions and is regular at the future horizon (near $\rho \sim 0$, we see that the linearly independent solutions are $\phi(\rho) = c_1 + c_2 \rho^{i\beta\omega}$ of which the constant behaviour is the correct ingoing mode). To keep expressions compact, we have introduced the lightcone like dimensionless combination of frequencies and momenta, including contributions from the dimension which will appear in the solutions below:

$$\mathbf{p}_+ = i \frac{\beta}{4\pi} (k - \omega) + \frac{\Delta}{2}, \quad \mathbf{p}_- = -i \frac{\beta}{4\pi} (k + \omega) + \frac{\Delta}{2}. \quad (6.3.22)$$

The ingoing Green's function of interest, normalized to unit at the AdS boundary $\zeta = 0$ or $\rho_c + i\epsilon$ can then be immediately inferred to be:

$$\begin{aligned} G^+(\zeta, \omega, k) &= \left(\frac{1 - e^{2\pi i(\zeta + \zeta_c)}}{1 + e^{2\pi i(\zeta + \zeta_c)}}\right)^\Delta \left(\frac{1 - e^{2\pi i\zeta_c}}{1 + e^{2\pi i\zeta_c}}\right)^{-\Delta} \left(\frac{1 + e^{2\pi i(\zeta + \zeta_c)}}{1 + e^{2\pi i\zeta_c}}\right)^{\Delta - \mathbf{p}_+ - \mathbf{p}_-} \\ &\quad \times \frac{{}_2F_1(\mathbf{p}_+, \mathbf{p}_-, \mathbf{p}_+ + \mathbf{p}_- - \Delta + 1; \sec^2 \pi(\zeta + \zeta_c))}{{}_2F_1(\mathbf{p}_+, \mathbf{p}_-, \mathbf{p}_+ + \mathbf{p}_- - \Delta + 1; \sec^2 \pi\zeta_c)}. \end{aligned} \quad (6.3.23)$$

We have written the answer in the mock tortoise coordinate which makes clear that the solution is continuous across the horizon-cap in the grSK geometry. The knowledge of the retarded Green's function is sufficient to obtain the full solution for the field Φ on the Schwinger-Keldysh contour using (6.3.16).

6.3.3 Propagators in $d > 2$: gradient expansion

In dimensions $d > 2$ the scalar wave equation (6.3.2) does not admit a simple closed form solution in the Schwarzschild-AdS $_{d+1}$ backgrounds. One can however make progress by solving the equations order by order in a low-energy, long-wavelength limit, i.e., we can expand our Green's function in the limit where $\beta\omega, \beta|\mathbf{k}| \ll 1$. We consider

$$G^+(\zeta, \omega, |\mathbf{k}|) = \sum_{n,m=0}^{\infty} G_{m,n}^+(\zeta) \left(\frac{\beta\omega}{2}\right)^m \left(\frac{\beta|\mathbf{k}|}{2}\right)^n, \quad (6.3.24)$$

where we continue to work with the dimensionless frequency and momenta. We have isolated the leading order term in the gradient expansion with some hindsight to simplify the computations.

To determine the solution for the scalar field, we first solve the equation (6.3.2) with ingoing boundary conditions. This amounts to imposing the following boundary conditions on the Green's function G^+ :

$$G^+ \Big|_{r=r_c} = 1, \quad \frac{dG^+}{d\zeta} \Big|_{r=r_h} = 0. \quad (6.3.25)$$

For the series coefficients in the gradient expansion this translates to the requirement

$$G_{0,0}^+ \Big|_{r=r_c} = 1, \quad G_{n,m}^+ \Big|_{r=r_c} = \frac{dG_{n,m}^+}{d\zeta} \Big|_{r=r_h} = 0, \quad \forall n, m \in \mathbb{Z}_+. \quad (6.3.26)$$

Some of the coefficients above are trivial, spatial reflection symmetry sets $G_{n,2m+1}^+ = 0$, so we do not encounter any terms which are odd in momenta.

It transpires that the knowledge of $G_{n,m}^+$ suffices to obtain the solution to the scalar wave equation in the average-difference basis in the long-wavelength gradient expansion. The final expression can be compactly summarized as

$$\Phi = \sum_{n,m=0}^{\infty} G_{n,2m}^+ \left(\frac{\beta^2 |\mathbf{k}|^2}{4} \right)^m (D_{\zeta}^+)^n \left\{ J_a - \frac{1}{2} J_d \left[(1 - 2\zeta) + \frac{\beta\omega}{2 \times 2!} ((1 - 2\zeta)^2 - 1) \cdots \right] \right\}. \quad (6.3.27)$$

An explicit derivation of the above as is outlined in D.1, but the basic strategy is easy to describe. We essentially introduce the bulk analog of the retarded-advanced sources and carry out the gradient expansion both for the Green's function and for the statistical factors that enter in the construction (6.2.7). We then use the time-reflection symmetry (6.1.9) to determine the outgoing Green's function, and employ (6.3.16) to assemble the pieces to give the solution to the wave equation.

Closed form solutions for the leading order terms in the gradient expansion can be obtained (see D.2). We present below of the basic data that we will use in the rest of the discussion.

$$\begin{aligned} G_{0,0}^+ &= \frac{P_{-\frac{d}{2}} \left(2 \frac{r^d}{r_h^d} - 1 \right)}{P_{-\frac{d}{2}} \left(2 \frac{r_c^d}{r_h^d} - 1 \right)}, \\ G_{1,0}^+ &= -G_{0,0}^+ \int_0^{\zeta} d\zeta' \left(1 - \left(\frac{G_{0,0}^+(\zeta h)}{G_{0,0}^+(\zeta')} \right)^2 \left(\frac{r_h}{r'} \right)^{d-1} \right), \\ G_{0,1}^+ &= 0. \end{aligned} \quad (6.3.28)$$

Higher order terms can similarly be obtained and we give some explicit expressions in [D.2](#); see for instance [\(D.2.23\)](#) for a massless scalar in arbitrary dimensions and [\(D.2.27\)](#) for an arbitrary scalar in $d = 2$.

6.4 Influence functionals

We now have all the pieces necessary to compute the influence functionals of interest. We first outline the computation of the quadratic effective action in [6.4.1](#). As is usual in AdS/CFT this is obtained as a boundary term in the on-shell action computation. For the higher order influence functionals we need to employ the standard Witten diagram technology on the grSK geometry (justified in [D.3](#)). Armed with these results we compute the n -point contact influence functions in [6.4.2](#). Along the way we will argue that the non-Gaussian contributions are well defined after a renormalization of the sources, and determine the appropriate counterterm action necessary to obtain the physical influence functionals. This will turn out to be crucial when our system couples to a marginal operator of the environment theory. We will give some explicit results for cubic and quartic self-interactions in [6.4.2](#). In [D.4](#) and [D.5](#) we compile various technical details underlying the results we present in this section.

6.4.1 Quadratic effective action

Let us begin with the evaluation of the quadratic part of the influence functional. Since we have solved for the field Φ on the grSK contour, it follows that result should be given by a boundary term. This is indeed the case, for starting with [\(6.2.4\)](#) with $\lambda = 0$ we have upon passing to momentum space

$$\begin{aligned}
S_{(2)} &= \frac{i}{\beta} \int \frac{d^d k_1}{(2\pi)^d} \int \frac{d^d k_2}{(2\pi)^d} (2\pi)^d \delta^d(k_1 + k_2) \\
&\quad \times \oint d\zeta r^{d-1} \left[D_\zeta^+ \Phi(k_1) D_\zeta^+ \Phi(k_2) - \Phi(k_1) \frac{\beta^2}{4} (f |\mathbf{k}_2|^2 + r^2 f m^2 - \omega_2^2) \Phi(k_2) \right] \\
&= \frac{i}{\beta} \int \frac{d^d k_1}{(2\pi)^d} \frac{d^d k_2}{(2\pi)^d} (2\pi)^d \delta^d(k_1 + k_2) \int_0^1 d\zeta \frac{d}{d\zeta} \left[r^{d-1} \Phi(k_1) D_\zeta^+ \Phi(k_2) \right] \\
&= \frac{i}{\beta} \int \frac{d^d k_1}{(2\pi)^d} \frac{d^d k_2}{(2\pi)^d} (2\pi)^d \delta^d(k_1 + k_2) \left[r^{d-1} \Phi(k_1) D_\zeta^+ \Phi(k_2) \right]_{\zeta=0}^{\zeta=1}.
\end{aligned} \tag{6.4.1}$$

In the second line we substituted the equation of motion [\(6.3.5\)](#) and performed the ζ contour integral in the final line, expressing the result as a pure boundary term on the grSK contour.

The general structure of the answer from evaluating the boundary term takes the following form in the average-difference basis:

$$S_{(2)} = \int \frac{d^d k}{(2\pi)^d} \left[\mathfrak{J}_{ad}(\omega, k) J_a(\omega, k) J_d(-\omega, -k) + \mathfrak{J}_{dd}(\omega, k) J_d(\omega, k) J_d(-\omega, -k) \right]. \quad (6.4.2)$$

We see that $\mathfrak{J}_{aa} = 0$ a consequence of Schwinger-Keldysh unitarity of the microscopic theory. This is because the coefficient of the average source is the ingoing Green's function which is manifestly regular on the grSK contour.

On-shell action in $d = 2$: Given our solution in the BTZ geometry it is straightforward to evaluate the boundary term. Using the normalized wavefunction built from (6.3.21), the boundary term contribution evaluates to

$$\begin{aligned} \mathfrak{J}_{ad}(\omega, k) = & \frac{4\pi^2}{\beta^2} \left\{ \mathfrak{p}_+ + \mathfrak{p}_- - \Delta \frac{r_c^2}{r_h^2} \right. \\ & \left. + \left(1 - \frac{r_h^2}{r_c^2} \right) \frac{{}_2\tilde{F}_1\left(1 + \mathfrak{p}_+, 1 + \mathfrak{p}_-, 2 - i \frac{\beta\omega}{2\pi}; 1 - \frac{r_h^2}{r_c^2}\right)}{{}_2\tilde{F}_1\left(\mathfrak{p}_+, \mathfrak{p}_-, 1 - i \frac{\beta\omega}{2\pi}; 1 - \frac{r_h^2}{r_c^2}\right)} \right\}_{\text{cf } r_c^{4-2\Delta}}. \end{aligned} \quad (6.4.3)$$

where ${}_2\tilde{F}_1(a, b, c, \xi)$ is the regularized hypergeometric function ${}_2\tilde{F}_1(a, b, c, \xi) = \frac{1}{\Gamma(c)} {}_2F_1(a, b, c, \xi)$.

The subscript at the end instructs us to extract the coefficient of $r_c^{4-2\Delta}$, which is the end result of carrying out a counterterm subtraction using standard holographic renormalization methods.⁶ To understand this recall that we have normalized $G^+(\zeta_c, \omega, k) = 1$ which means that the two point function is obtained from the term that scales like $\left(\frac{1}{r_c}\right)^{2\Delta-4}$ leading to the aforementioned prescription. A short calculation results in:

$$\begin{aligned} \mathfrak{J}_{ad}(\omega, k) = & 2 r_h^{2\Delta-2} \frac{\Gamma(\mathfrak{p}_+) \Gamma(\mathfrak{p}_-) \Gamma(2 - \Delta)}{\Gamma(\Delta - 1) \Gamma(\mathfrak{p}_+ + 1 - \Delta) \Gamma(\mathfrak{p}_- + 1 - \Delta)} \\ = & -\frac{2}{\pi} r_h^{2\Delta-2} \frac{1}{\Gamma(\Delta - 1)^2} \left| \Gamma(\mathfrak{p}_+) \Gamma(\mathfrak{p}_-) \right|^2 \frac{\sin(\pi(\mathfrak{p}_- - \Delta)) \sin(\pi(\mathfrak{p}_+ - \Delta))}{\sin(\pi\Delta)} \\ = & -\frac{1}{\pi} r_h^{2\Delta-2} \frac{1}{\Gamma(\Delta - 1)^2} \left| \Gamma\left(\frac{\Delta}{2} - i \frac{\beta(k + \omega)}{4\pi}\right) \Gamma\left(\frac{\Delta}{2} + i \frac{\beta(k - \omega)}{4\pi}\right) \right|^2 \\ & \times \left(\csc(\pi\Delta) \cosh\left(\frac{\beta k}{2}\right) - \cot(\pi\Delta) \cosh\left(\frac{\beta\omega}{2}\right) + i \sinh\left(\frac{\beta\omega}{2}\right) \right). \end{aligned} \quad (6.4.4)$$

This result is indeed the correct expression for the retarded Green's function $G_R(\omega, k)$ for a 2d CFT on the infinite line. One can obtain it directly by starting from the conformal 2-point

⁶We assume, for simplicity, that the field Φ satisfies standard (Dirichlet) boundary condition at infinity.

While this restricts us to $\Delta \geq \frac{d}{2}$, the result is unchanged for $\Delta \in (\frac{d}{2} - 1, \frac{d}{2})$ once we include additional boundary terms to account for the alternate (Neumann) boundary conditions.

function on the plane, conformally mapping it to the cylinder to obtain the (Euclidean) thermal correlator, and thence take the discontinuity across the lightcone branch cut while analytically continuing it to the timelike Lorentzian domain (using appropriate $i\epsilon$ prescription to do so). The result has been obtained in various places in the literature before. In [131] the computation of the Fourier transform was described and the imaginary part of the Green's function obtained (in the context of computing the absorption cross-section of D-branes). The first, principled, holographic derivation of the Green's function was given in [109].

The retarded Green's function $G_R(\omega, k)$ has poles in the lower half complex ω plane, at

$$\omega_{\text{qn}} = \pm k - 2\pi i T (\Delta + 2n), \quad n \in \mathbb{Z}_{\geq 0}. \quad (6.4.5)$$

These poles of course correspond to the BTZ quasinormal modes and set the characteristic scale for the decay of the response function in the time domain [74, 132]. Finally, we also note that the expression can be written in a form that is symmetric between the operator \mathcal{O} of dimension Δ and its shadow \mathcal{O}_s of dimension $\tilde{\Delta} = d - \Delta$ (with $d = 2$ here). To make the operator dimension's contribution to \mathbf{p}_{\pm} defined in (6.3.22) explicit we redefine the light-cone momenta:

$$\mathfrak{K}_+ = i \frac{\beta}{4\pi} (k - \omega) = \mathbf{p}_+ - \frac{\Delta}{2}, \quad \mathfrak{K}_- = -i \frac{\beta}{4\pi} (k + \omega) = \mathbf{p}_- - \frac{\Delta}{2}. \quad (6.4.6)$$

We can then write the 2-point influence functional in terms of the function

$$\mathfrak{G}(\mathfrak{K}_+, \mathfrak{K}_-, \Delta) \equiv \Gamma(\mathfrak{K}_+ + \frac{\Delta}{2}) \Gamma(\mathfrak{K}_- + \frac{\Delta}{2}) \Gamma(1 - \Delta), \quad (6.4.7)$$

as

$$\mathfrak{J}_{ad}(\omega, k) = \frac{2}{2 - \Delta} r_h^{2\Delta-2} \frac{\mathfrak{G}(\mathfrak{K}_+, \mathfrak{K}_-, \Delta)}{\mathfrak{G}(\mathfrak{K}_+, \mathfrak{K}_-, \tilde{\Delta})}. \quad (6.4.8)$$

We will find this notation useful in simplifying the analysis of the 3-point influence functional.

Having understood the computation of the influence functional \mathfrak{J}_{ad} we next can compute \mathfrak{J}_{dd} .

The computation proceeds along similar fashion lines and we obtain

$$\begin{aligned} \mathfrak{J}_{dd}(\omega, k) &= \frac{i}{4} \frac{\cos(\pi(\mathbf{p}_+ + \mathbf{p}_- - \Delta)) \sin(\pi\Delta)}{\sin(\pi(\mathbf{p}_- - \Delta)) \sin(\pi(\mathbf{p}_+ - \Delta))} \mathfrak{J}_{ad}(\omega, k) \\ &= \frac{r_h^{2\Delta-2}}{2\pi i} \frac{\cosh\left(\frac{\beta\omega}{2}\right)}{\Gamma(\Delta - 1)^2} \left| \Gamma\left(\frac{\Delta}{2} - i \frac{\beta(k + \omega)}{4\pi}\right) \Gamma\left(\frac{\Delta}{2} + i \frac{\beta(k - \omega)}{4\pi}\right) \right|^2 \\ &= \frac{i}{2} \coth\left(\frac{\beta\omega}{2}\right) \text{Im}(\mathfrak{J}_{ad}(\omega, k)). \end{aligned} \quad (6.4.9)$$

We have expressed the final result making manifest the fluctuation/dissipation relation. We recall that $\text{Im}(\mathfrak{J}_{ad})$ gives us the spectral function at finite temperature, see [63, 69] for further details.

On-shell action in gradient expansion: The analysis of the influence functionals in a gradient expansion is straightforward given our explicit expressions from before. It is however convenient in actuality to assemble the pieces somewhat differently and work in a basis that is better adapted to the bulk field Φ . We describe such a basis built from the even and odd parts of the ingoing Green's function in [D.1](#). The expressions of interest are the solution to the wave equation ([D.1.8](#)), the field radial gradient ([D.1.12](#)), and the expansion of the even and odd sources ([D.1.9](#)). To compute the quadratic influence functional, we need to evaluate the on-shell action as a boundary term ([6.4.1](#)). This amounts to knowledge of the values of $G_{n,m}^+$ and their derivatives at $\zeta = 0$. Explicitly, letting

$$G_{n,m}^+(0) = \begin{cases} 1, & n = m = 0 \\ 0, & (n, m) \neq (0, 0) \end{cases}, \quad \left. \frac{dG_{n,m}^+}{d\zeta} \right|_{\zeta=0} = \dot{g}_{n,m}, \quad (6.4.10)$$

the quadratic influence functional can be simplified to the form

$$\begin{aligned} \mathfrak{J}_{ad}(\omega, \mathbf{k}) &= \frac{i}{\beta} \left\{ r_c^{d-1} \left[(1 + \dot{g}_{1,0})\beta\omega + \frac{(\beta|\mathbf{k}|)^2}{2} \dot{g}_{0,2} + \frac{(\beta\omega)^2}{2} \dot{g}_{2,0} \right] \right\}_{\text{cf } r_c^{2(d-\Delta)}}, \\ \mathfrak{J}_{dd}(\omega, \mathbf{k}) &= \frac{i}{\beta} \left\{ r_c^{d-1} \left[(1 + \dot{g}_{1,0}) + \frac{(\beta\omega)^2}{12} (1 + \dot{g}_{1,0} + 3\dot{g}_{3,0}) + \frac{(\beta|\mathbf{k}|)^2}{4} \dot{g}_{1,2} \right] \right\}_{\text{cf } r_c^{2(d-\Delta)}}. \end{aligned} \quad (6.4.11)$$

We have been able to evaluate the expressions analytically to leading order in the gradient expansion. We recall that we have normalized $G_{0,0}^+(0) = 1$ and use the solution for $G_{1,0}^+$ given in ([6.3.28](#)), to learn that

$$r_c^{d-1} (1 + \dot{g}_{1,0}) = r_h^{d-1} \left[\frac{P_{-\frac{\Delta}{d}}(1)}{P_{-\frac{\Delta}{d}}\left(2\frac{r_c^d}{r_h^d} - 1\right)} \right]^2. \quad (6.4.12)$$

Expanding out the Legendre polynomial we pick up the a coefficient of the desired power of r_c , and find the influence functionals to be

$$\begin{aligned} \mathfrak{J}_{ad}(\omega, \mathbf{k}) &= i \frac{\Gamma\left(\frac{\Delta}{d}\right)^4}{\Gamma\left(2\frac{\Delta}{d} - 1\right)^2} r_h^{2\Delta-d-1} \omega, \\ \mathfrak{J}_{dd}(\omega, \mathbf{k}) &= \frac{i}{\beta} \frac{\Gamma\left(\frac{\Delta}{d}\right)^4}{\Gamma\left(2\frac{\Delta}{d} - 1\right)^2} r_h^{2\Delta-d-1}. \end{aligned} \quad (6.4.13)$$

While we are retaining terms only to leading order in the gradient expansion one can nevertheless see that the linearized version of the fluctuation dissipation relation ([6.4.9](#)) continues to hold quite generally (as is in fact readily inferred from ([6.4.11](#))).

The subleading terms in the influence functional \mathfrak{J}_{ad} are computable. While they do not seem to be amendable to a closed form analytic expression, we can easily extract the dependence on the

physical parameters. Using the results for the higher order terms in the gradient expansion given in [D.2](#) we can show that the quadratic order terms in \mathfrak{T}_{ad} are given by the following:

$$\begin{aligned} \left\{ \frac{i}{\beta} r_c^{d-1} \dot{g}_{0,2} \right\}_{\text{cf } r_c^{2(d-\Delta)}} &= -\frac{1}{2\pi\beta} \frac{\Gamma(\frac{\Delta}{d})^4}{\Gamma(2\frac{\Delta}{d}-1)^2} r_h^{2\Delta-d-1} \mathfrak{g}_{0,2}, \\ \left\{ \frac{i}{\beta} r_c^{d-1} \dot{g}_{2,0} \right\}_{\text{cf } r_c^{2(d-\Delta)}} &= \frac{1}{2\pi\beta} \frac{\Gamma(\frac{\Delta}{d})^4}{\Gamma(2\frac{\Delta}{d}-1)^2} r_h^{2\Delta-d-1} \mathfrak{g}_{2,0}. \end{aligned} \quad (6.4.14)$$

Here $\mathfrak{g}_{0,2}$ and $\mathfrak{g}_{2,0}$ are purely numerical coefficients and computed by the integral expressions involving Legendre functions; see [\(D.2.21\)](#) and [\(D.2.22\)](#), respectively. Specifically, they are

$$\begin{aligned} \mathfrak{g}_{0,2} &= \left[\int_1^{\varrho_c} d\varrho \varrho^{-\frac{2}{d}} \left(P_{-\frac{\Delta}{d}}(2\varrho-1) \right)^2 \right]_{\text{finite}} \\ \mathfrak{g}_{2,0} &= 2\pi i \frac{G_{1,0}^+(r_h)}{G_{0,0}^+(r_h)} + \mathfrak{g}_{0,2} + \left[\int_1^{\varrho_c} d\varrho \frac{\varrho^{-\frac{1}{d}}}{\varrho-1} \left(\varrho^{-\frac{1}{d}} P_{-\frac{\Delta}{d}}(2\varrho-1)^2 - 1 \right) \right]_{\text{finite}}. \end{aligned} \quad (6.4.15)$$

We have used [\(D.2.14\)](#) and expressed the answer as integrals over Legendre functions which can be evaluated numerically. For $\Delta \in (\frac{d}{2}, \frac{d}{2} + 1)$ the integrals are absolutely convergent and thus may be determined without need for a detailed counterterm analysis. Representative data for these quantities as a function of Δ in various dimensions is plotted in [4](#) within this window of conformal dimensions. We will exploit this structural form when writing down the effective action for the open quantum degree of freedom in [6.5](#).

6.4.2 Interactions: contact self-interaction

Using the standard Witten diagrams on the grSK contour, illustrated in [5](#) (we motivate this briefly in [D.3](#)), the influence functionals can be straightforwardly written down. A contact n -point self-interaction vertex in the bulk leads to the following contribution to the influence functional:

$$S_{(n)} = -\frac{\lambda_n}{n!} \int \prod_{i=1}^n \frac{d^d k_i}{(2\pi)^d} (2\pi)^d \delta \left(\sum_{i=1}^n k_i \right) \oint d\zeta \sqrt{-g} \prod_{i=1}^n \Phi(\zeta, k_i) \quad (6.4.16)$$

We can in general simplify expressions such as the above by using the fact that the contour integral over the mock tortoise coordinate can be done by basically integrating the discontinuity across the branch cut extending from the horizon over the radial coordinate. To wit, for any function on the grSK geometry $\mathfrak{L}(\zeta)$

$$\begin{aligned} \oint d\zeta \sqrt{-g} \mathfrak{L}(\zeta) &= \int_{\zeta_h}^{\zeta_c} d\zeta \sqrt{-g} \left(\mathfrak{L}(\zeta+1) - \mathfrak{L}(\zeta) \right) \\ &= \int_{r_h}^{r_c} dr r^{d-1} \left(\mathfrak{L}(\zeta(r)+1) - \mathfrak{L}(\zeta(r)) \right), \end{aligned} \quad (6.4.17)$$

where we used $\sqrt{-g} \frac{d\zeta}{dr} = r^{d-1}$. In the second line above, we have assumed that the integrand doesn't have a simple pole at $r = r_h$ and hence the horizon itself gives no contribution to the integral. Consequently, entire contribution arises from the discontinuity across the branch cut that extends from the horizon to the conformal boundary.

Influence functionals in the advanced-retarded basis

Using the explicit solution on the grSK contour (6.3.15) we identify from (6.2.9) the influence functionals in the retarded-advanced basis to be

$$\begin{aligned}
\mathcal{I}_{F\dots FP\dots P}(k_1, \dots, k_n) &= \text{coeff} \left(J_{\bar{F}}(k_1) \cdots J_{\bar{F}}(k_p) J_{\bar{P}}(k_{p+1}) \cdots J_{\bar{P}}(k_n) \right) \\
&= -\frac{\lambda_n}{p!(n-p)!} \oint d\zeta \sqrt{-g} (-)^p \prod_{i=1}^p G^+(\zeta, \omega_i, \mathbf{k}_i) \prod_{j=p+1}^n G^-(\zeta, \omega_j, \mathbf{k}_j) e^{\beta\omega_j(1-\zeta)} \\
&= \frac{\lambda_n (-)^{p+1}}{p!(n-p)!} \left(1 - e^{\beta \sum_{j=p+1}^n \omega_j} \right) \int_{r_h}^{r_c} dr r^{d-1} \prod_{i=1}^p G^+(\zeta, \omega_i, \mathbf{k}_i) \prod_{j=p+1}^n e^{-\beta\omega_j\zeta} G^+(\zeta, -\omega_j, \mathbf{k}_j).
\end{aligned} \tag{6.4.18}$$

One can evaluate the integrals directly given the solution to the Green's function on the grSK contour. Note that the causal structure of the influence function is completely manifest. The ingoing Green's function $G^+(\zeta, \omega, \mathbf{k})$ is manifestly regular in the upper-half ω plane, while its conjugate $G^-(\zeta, \omega, \mathbf{k})$ is regular on the lower-half plane by frequency reversal. The time-reversal also correctly incorporates the statistical factor which enters the final expression.

In the holographic setting, we expect the only singularities in $G^+(\zeta, \omega, \mathbf{k})$ to arise from quasinormal poles, while those of $G^-(\zeta, \omega, \mathbf{k})$ are attributable to the time-reversed anti-quasinormal poles. So the influence functional $\mathcal{I}_{F\dots FP\dots P}(k_1, \dots, k_n)$ will have quasinormal poles for all the ω_i with $i \in F$ and anti-quasinormal poles for ω_k with $k \in P$. We shall see an explicit illustration of this below.

The radial integral in the expression above, in general needs to be regulated. However, for a certain range of operator dimensions, specifically, for $\Delta < (1 - \frac{1}{n})d$ the integrals are absolutely convergent and need no regulating.⁷ In the discussion below we will focus on the case where the operator coupling to our system is sufficiently relevant to avoid introducing any regulators.

As an illustration consider the result for the 3-point influence function in a 2d CFT which can

⁷One can infer this by examining the asymptotic behaviour of the Green's functions. However, it is also worth noting that the UV divergences are determined by the CFT correlation functions in the vacuum, for which the criterion specified is well known, see eg., [133].

be obtained to be (using energy-momentum conservation to eliminate the ω_3 and \mathbf{k}_3)

$$\mathcal{I}_{FFP}(k_1, k_2, k_3) = -\lambda r_h^{3\Delta-4} (1 - e^{-\beta\omega_3}) \Gamma\left(1 + \frac{i\mathbf{w}_3}{\pi}\right) \sum_{\delta_i \in \{\Delta, \tilde{\Delta}\}} \mathfrak{J}_{FFP}^\delta(k_1, k_2, k_3) \quad (6.4.19)$$

where the function $\mathfrak{J}_{FFP}^\delta$ is given as an infinite sum involving generalized hypergeometric functions:

$$\begin{aligned} \mathfrak{J}_{FFP}^\delta(k_1, k_2, k_3) = & \frac{\mathfrak{G}(\mathfrak{K}_{1+}, \mathfrak{K}_{1-}, \delta_1) \mathfrak{G}(\mathfrak{K}_{2+}, \mathfrak{K}_{2-}, \delta_2)}{\mathfrak{G}(\mathfrak{K}_{1+}, \mathfrak{K}_{1-}, \tilde{\Delta}) \mathfrak{G}(\mathfrak{K}_{2+}, \mathfrak{K}_{2-}, \tilde{\Delta})} \left[\sum_{n=0}^{\infty} \frac{(-)^n \Gamma(1 - \delta_3 - n)}{\Gamma(n+1) \Gamma(1 - \delta_3 - 2n)} \right. \\ & \times \frac{\mathfrak{G}(\mathfrak{K}_{3+}^*, \mathfrak{K}_{3-}^*, \delta_3 + 2n)}{\mathfrak{G}(\mathfrak{K}_{3+}^*, \mathfrak{K}_{3-}^*, \tilde{\Delta})} \frac{\Gamma(-1 + n + \frac{\delta_1 + \delta_2 + \delta_3}{2})}{\Gamma(n + \frac{\delta_1 + \delta_2 + \delta_3}{2} + \frac{i\mathbf{w}_3}{\pi})} \\ & \times {}_3F_2 \left(\begin{matrix} \mathfrak{K}_{1+} + \frac{\delta_1}{2}, \mathfrak{K}_{1-} + \frac{\delta_1}{2}, -1 + \frac{\delta_1 + \delta_2 + \delta_3}{2} + n \\ \delta_1, \frac{\delta_1 + \delta_2 + \delta_3}{2} + n + \frac{i\mathbf{w}_3}{\pi} \end{matrix} ; 1 \right) \\ & \times {}_4F_3 \left(\begin{matrix} \mathfrak{K}_{2+} + \frac{\delta_2}{2}, \mathfrak{K}_{2-} + \frac{\delta_2}{2}, -n, 1 - n - \delta_3 \\ \delta_2, 1 - \mathfrak{K}_{3+}^* - \frac{\delta_3}{2} - n, 1 - \mathfrak{K}_{3-}^* - \frac{\delta_3}{2} - n \end{matrix} ; 1 \right) \left. \right]. \end{aligned} \quad (6.4.20)$$

This result is valid for $1 < \Delta < \frac{4}{3}$, chosen so that the radial integral was absolutely convergent. We have employed a notational contrivance to keep the expression simple – the above is actually a sum over eight terms with similar structure, where each of the three operators enters either as itself, or its shadow. This is indicated by using δ to sample the operator and shadow operator dimension as indicated in the summation. The lightcone momentum of the outgoing mode is conjugated because of time-reversal. We can use energy-momentum conservation to rewrite $\mathfrak{K}_{3\pm}^* = \mathfrak{K}_{12\pm}$ as a function of $\omega_1 + \omega_2$ and $k_1 + k_2$. Finally, we have chosen to write the final expression as a infinite sum, but one can equivalently have presented the result as set of contour integrals (which is where the sum is obtained from). We give a detailed derivation of this result in [D.4](#).

Let us focus on some of the features that the readily visible from the above parameterization of the influence functional. Firstly, the result is factorized into right and left movers. This is not manifest in when we consider the AdS radial integral representation, but is expected on grounds that the Euclidean thermal 3-point correlator factorizes into holomorphic and anti-holomorphic parts. Secondly, the influence functional, correctly captures the causality requirements noted above. The only singularities which can arise in the complex frequency plane are from the Gamma functions for ω_1 and ω_2 . One can also check that the generalized hypergeometric functions do not contribute any singularities (this is easier to see directly from the infinite sum or contour integral representation ([D.4.15](#))).

Of the eight possible choices of δ_i we note that there can only be poles when $\delta_i = \Delta$. When $\delta_i = 2 - \Delta$ the Gamma function in the denominator also a pole which cancels out the behaviour of the numerator leaving a finite answer. We conclude that the correlator is analytic in the upper half of the complex ω_1 and ω_2 planes and encounters the usual quasinormal type poles in the lower half-planes. So the influence functional only has simple poles at are at the following locations determined by the quasinormal modes.

$$\begin{aligned}\omega_1 &= \pm k_1 - 2\pi i T(2n_1 + 2m_1 + \Delta), & \omega_2 &= \pm k_2 - 2\pi i T(2n_2 + 2m_2 + \Delta), \\ \omega_1 + \omega_2 &= \pm(k_1 + k_2) - 2\pi i T(2n_3 + 2m_3 + \Delta).\end{aligned}\tag{6.4.21}$$

The last set translates upon using energy-momentum conservation to the anti-quasinormal modes of the advanced operator with frequency ω_3 .

We note in closing that one can give a closed form expression for the thermal real-time 3-point functions in 2d CFT in terms of Meijer G-functions. This has been derived by Fourier transforming the cylinder correlator of a 2d CFT to momentum space with an appropriate $i\epsilon$ prescription in [134]. We have not attempted to simplify our expression (6.4.19) to this form, though we note that the analytic structure does match between the two expressions (as it must).

Influence functionals in the average-difference basis

If we wish to evaluate the influence functionals in the average-difference basis we can simply implement the basis transformation to go from (6.2.7) to (6.2.6). While working in the long-wavelength gradient expansion however, one must also account for the statistical factor, which has been folded into (6.3.27). We will now use this expression to evaluate the influence functionals in the average-difference basis.

As noted above, depending on the nature of the operator \mathcal{O} we may need to incorporate counterterms to evaluate the influence functional which enter into the effective field theory of open system degrees of freedom. For the influence functionals to respect the microscopic unitarity, these counterterms must be both state independent and suitably factorized across the SK contour. We see that this is indeed possible, provided that we suitably renormalize the sources for the holographic operator \mathcal{O} obtain finite correlation functions. Operationally, from our discussion in 6.2.2 this means that we must renormalize our system degrees of freedom while constructing the open effective field theory.⁸

⁸We will continue here to write the expressions in terms of the boundary sources J of the holographic envi-

We will first describe the structure of the divergences encountered in the computation of the influence functionals themselves. These will appear from the bulk calculation in UV divergent terms from the radial integral, scaling with our radial cut-off r_c . We confine our attention to the leading order terms in the gradient expansion, so the results will be accurate to $\mathcal{O}(\beta\omega)$, for convenience. A more thorough analysis at arbitrary orders in the gradient expansion can be carried out along similar lines, and the details will appear elsewhere.

To begin with let us make the following two assertions about the non-linear influence functional.

1. First, the anharmonic influence phase to linear order in the coupling λ_n takes the form:

$$S_{(n)}^{\text{bare}} = -\lambda_n \int d^d x \sum_{k=1}^n \frac{1}{(n-k)!} \left(J_a^{\text{b}} + \frac{i}{8} \beta \partial_t J_d^{\text{b}} \right)^{n-k} \times \left[F_{n,k}^{\text{b}} \frac{(J_d^{\text{b}})^k}{k!} - F_{n,k+1}^{\text{b}} \frac{(J_d^{\text{b}})^{k-1}}{(k-1)!} \frac{i}{2} \beta \partial_t J_d^{\text{b}} \right]. \quad (6.4.22)$$

Here $F_{n,k}^{\text{b}}$ denotes the integral

$$F_{n,k}^{\text{b}} \equiv \oint d\zeta \sqrt{-g} (G_{0,0}^+)^n \left(\zeta - \frac{1}{2} + \frac{G_{1,0}^+}{G_{0,0}^+} \right)^k, \quad (6.4.23)$$

where $G_{m,n}^+$ to the desired order are given by the expressions in (6.3.28). We have anticipated the need for regulating the sources and the integrals and used the superscript **b** to denote that the above expressions are the bare results, prior to any renormalization prescription.

2. Second, the integrals $F_{n,k}^{\text{b}}$ appearing in the computation could be divergent. This depends on the conformal dimension Δ of the operator \mathcal{O} . We find:

- For $\Delta < (1 - \frac{1}{n})d$ the integrals involved in evaluating $F_{n,k}^{\text{b}}$ are convergent as noted in 6.4.2.
- For relevant operators with $\Delta \in [(1 - \frac{1}{n})d, d)$ we need to regulate some of the integrals. In particular, the integrals $F_{n,2k+1}^{\text{b}}$ with an odd argument are divergent. We can estimate them to behave as follows:

$$F_{n,2k+1}^{\text{b}} = F_{2k+1}^{\text{r}} + \frac{\Lambda_\Delta}{4^k}, \quad \Lambda_\Delta = \frac{r_c^{n\Delta - (n-1)d}}{n\Delta - (n-1)d}, \quad (6.4.24)$$

where $F_{n,k}^{\text{r}}$ denote the *renormalized* integrals which are completely finite and well-defined as $r_c \rightarrow \infty$.

ronment, leaving implicit the identification $\Psi_a \sim J_a$ and $\Psi_d \sim J_d$.

- Finally, for a marginal operator $\Delta = d$ all the integrals are divergent. The functions $F_{n,2k+1}^b$ are power-law divergent, but now for even argument $F_{n,2k}^b$ one encounters a logarithmic divergence.

$$F_{n,2k+1}^b = F_{2k+1}^r + \frac{\Lambda_d}{4^k}, \quad F_{n,2k}^b = F_{2k}^r + k \frac{\Lambda_l}{4^{k-1}}. \quad (6.4.25)$$

The divergences Λ_d and Λ_l are given by

$$\Lambda_d \equiv \frac{r_c^d}{d}, \quad \Lambda_l \equiv \frac{i}{\pi} r_h^d \log \frac{r_c}{r_h}. \quad (6.4.26)$$

We prove the aforementioned assertions regarding the structure of the bare influence functional and the divergences of the integrals appearing therein in [D.5](#).

Armed with these statements we can now assert the following result: define the *renormalized* probes J_a^r and J_d^r via

$$\begin{aligned} J_a^b &\equiv J_a^r & J_d^b &\equiv J_d^r, & \frac{d}{2} &\leq \Delta < d, \\ J_a^b &\equiv J_a^r - \frac{\Lambda_l}{2\Lambda_d} J_d^r, & J_d^b &\equiv J_d^r + \frac{\Lambda_l}{2\Lambda_d} i \beta \partial_t J_d^r, & \Delta &= d. \end{aligned} \quad (6.4.27)$$

While the integrals are divergent for some range of relevant operators, we will argue below that the divergences can be canceled by a standard counterterm. However, we see that there is a need for a non-trivial renormalization of the sources in the case of a marginal operator, arising primarily from the logarithmic divergence encountered in $F_{n,2k}^b$. Note that as $r_c \rightarrow \infty$ we have $\lim_{r_c \rightarrow \infty} \frac{\Lambda_l}{\Lambda_d} = 0$, i.e., the bare and the renormalized sources agree when the cutoff is removed. At finite cutoff however we need to renormalize the sources slightly; this is achieved by mixing them with difference probes in a temperature dependent manner. If the influence functional was completely finite, this deformation would disappear as we take $r_c \rightarrow \infty$ limit. But given the UV divergences in the case under consideration, this small renormalization, when ignored, can lead to new divergences which look like temperature-dependent divergences which cannot be canceled by unitary, state-independent counterterms factorized across the SK contour.

However, with respect to the renormalized sources there is no ambiguity and the result is consistent with the requirements delineated above. To see this, define the following counterterm action in terms of the renormalized probes that is unitary, state-independent, and factorized across the SK contour

$$S_{(n)}^{\text{c.t.}} = \int d^d x \frac{\lambda_n}{n!} \left[\left(J_a^r + \frac{1}{2} J_d^r \right)^n - \left(J_a^r - \frac{1}{2} J_d^r \right)^n \right]. \quad (6.4.28)$$

With this choice we obtain a manifestly finite influence functional to linear order in couplings λ_n and to linear order in derivatives, given by the expression

$$\begin{aligned}
S_{(n)} &\equiv - \lim_{r_c \rightarrow \infty} (S_{(n)}^{\text{bare}} + S_{(n)}^{\text{c.t.}}) \\
&= -\lambda_n \int d^d x \sum_{k=1}^n \frac{1}{(n-k)!} \left(J_a^r + \frac{i}{8} \beta \partial_t J_d^r \right)^{n-k} \left[F_{n,k}^r \frac{(J_d^r)^k}{k!} - F_{n,k+1}^r \frac{(J_d^r)^{k-1}}{(k-1)!} \frac{i}{2} \beta \partial_t J_d^r \right].
\end{aligned} \tag{6.4.29}$$

Once we have performed the renormalization described, we find that we have to evaluate the renormalized integrals $F_{n,k}^r$. We have been able to obtain closed form expressions for a marginal operator with $\Delta = d$ (see D.5.1). For the quartic influence functional, passing to momentum space and letting $\delta(k) = (2\pi)^d \delta^d(\sum_{i=1}^4 k_i)$, we find:

$$\begin{aligned}
\mathfrak{I}_{aaaa} &= 0, \\
\mathfrak{I}_{aaad} &= \frac{i\lambda_4}{3!} \frac{r_h^d}{d} \delta(k), \\
\mathfrak{I}_{aadd} &= \frac{-i\lambda_4}{4} \frac{r_h^d}{d} \delta(k) \frac{\beta\omega_4}{4}, \\
\mathfrak{I}_{ddda} &= \frac{i\lambda_4}{3!} \frac{r_h^d}{d} \delta(k) \left(\frac{1}{2} + \frac{3i\zeta(3)}{2\pi^3} \beta\omega_4 \right), \\
\mathfrak{I}_{dddd} &= \frac{i\lambda_4}{4!} \frac{r_h^d}{d} \delta(k) \left(\frac{3i\zeta(3)}{\pi^3} \right).
\end{aligned} \tag{6.4.30}$$

On the other hand closed form expressions for $\Delta < d$ are not easy to come by. One can however extract the overall dependence on the dimensionful parameters (r_h which sets the thermal scale) and obtain a result up to a numerical factor which is a function of the scaling dimension. These coefficients are given in terms of integrals of Legendre functions. More specifically, we find that the influence functionals are given in terms of the renormalized integrals

$$F_{n,k}^r = \frac{r_h^{n\Delta - (n-1)d}}{d} \frac{\Gamma\left(\frac{\Delta}{d}\right)^{2n}}{\Gamma\left(\frac{2\Delta}{d} - 1\right)^n} \mathfrak{F}_{n,k}(\Delta) \tag{6.4.31}$$

where

$$\begin{aligned}
\mathfrak{F}_{n,k}(\Delta) &= \int_1^\infty d\varrho \left[P_{-\frac{\Delta}{d}}(2\varrho - 1) \right]^n \left[\left(\frac{i}{\pi} \frac{Q_{-\frac{\Delta}{d}}(2\varrho - 1)}{P_{-\frac{\Delta}{d}}(2\varrho - 1)} + i \cot\left(\frac{\pi\Delta}{d}\right) + \frac{1}{2} \right)^k \right. \\
&\quad \left. - \left(\frac{i}{\pi} \frac{Q_{-\frac{\Delta}{d}}(2\varrho - 1)}{P_{-\frac{\Delta}{d}}(2\varrho - 1)} + i \cot\left(\frac{\pi\Delta}{d}\right) - \frac{1}{2} \right)^k \right].
\end{aligned} \tag{6.4.32}$$

To derive this expression we used the fact that one can solve for the combination $\zeta + \frac{G_{1,0}^+}{G_{0,0}^+}$ explicitly in terms of Legendre functions as we describe in (D.2.17). One can easily numerically estimate

these integrals entering the effective action. For the range of relevant operators where the integrals are convergent we quote results from a simple numerical integration in 6.

6.5 Stochastic description of the open effective field theory

Given that we have computed the influence functionals we can return to the problem of constructing the open effective field theory for our system degree of freedom $\Psi(x)$. As remarked in 6.2.2 this is easy, since all we need to do at the linear order is replace the sources J_a and J_d by the average and difference field $\Psi_a(x)$ and $\Psi_d(x)$, respectively. The renormalized effective action for when the operator Ψ couples to has a n -point contact interaction in the holographic set-up is then immediate to write down, using the results of 6.4.1 and 6.4.2. Collecting the results from (6.4.11), and (6.4.29) the effective action in position space reads:

$$\begin{aligned}
S_\Psi = \mathcal{N}_2 \int d^d x \left(-\partial_t \Psi_a \Psi_d + \frac{i}{\beta} \Psi_d^2 - \frac{\beta}{4\pi} \mathfrak{g}_{2,0} \partial_t \Psi_a \partial_t \Psi_d + \frac{\beta}{4\pi} \mathfrak{g}_{0,2} \nabla_i \Psi_a \nabla_i \Psi_d \right) \\
- \lambda_n \mathcal{N}_n \int d^d x \left[\sum_{k=1}^n \mathfrak{F}_{n,k}(\Delta) \frac{\Psi_a^{n-k}}{(n-k)!} \frac{\Psi_d^k}{k!} \right. \\
\left. - \frac{i\beta}{2} \sum_{k=1}^{n-1} \left(\mathfrak{F}_{n,k+1} - \frac{1}{4} \mathfrak{F}_{n,k-1} \right) \frac{\Psi_a^{n-k}}{(n-k)!} \frac{\Psi_d^{k-1}}{(k-1)!} \partial_t \Psi_d \right].
\end{aligned} \tag{6.5.1}$$

where

$$\mathcal{N}_2 = r_h^{2\Delta-d-1} \frac{\Gamma\left(\frac{\Delta}{d}\right)^4}{\Gamma\left(2\frac{\Delta}{d}-1\right)^2}, \quad \mathcal{N}_n = \frac{r_h^{n\Delta-(n-1)d}}{d} \frac{\Gamma\left(\frac{\Delta}{d}\right)^{2n}}{\Gamma\left(2\frac{\Delta}{d}-1\right)^n}. \tag{6.5.2}$$

The quantities $\mathfrak{g}_{0,2}$ and $\mathfrak{g}_{2,0}$ are finite numbers (they are functions of Δ and d) obtained from integral expressions in (6.4.14), as are $\mathfrak{F}_{n,k}(\Delta)$ which is given in (6.4.32). Sample values of these are also plotted in 4 and 6, respectively.

We can compare the effective action we have derived with the general expectation based on stochastic dynamics of the open system (6.2.12). The coupling constants of appearing in the Langevin effective action obtained earlier in (6.2.15) can be read off from (6.5.1). At the Gaussian order we have the relations

$$\begin{aligned}
\gamma = \mathcal{N}_2, & \quad f = \frac{2\gamma}{\beta}, \\
K = \frac{\beta}{4\pi} \mathfrak{g}_{2,0} \gamma, & \quad D = \frac{\beta}{4\pi} \mathfrak{g}_{0,2} \gamma
\end{aligned} \tag{6.5.3}$$

while the non-Gaussian terms lead to

$$\begin{aligned}\theta_k &= -\frac{\lambda_n}{i^{k+1}} \mathcal{N}_n \mathfrak{F}_{n,k}(\Delta), & \text{for } k \in \{1, \dots, n\}, \\ \bar{\theta}_k &= -\frac{\beta}{2} \frac{\lambda_n}{i^k} \mathcal{N}_n \left(\mathfrak{F}_{n,k+1}(\Delta) - \frac{1}{4} \mathfrak{F}_{n,k-1}(\Delta) \right), & \text{for } k \in \{1, \dots, n-1\}.\end{aligned}\tag{6.5.4}$$

The first set of these relations (6.5.3) capture the standard fluctuation dissipation relations expected from a Gaussian noise source. The fact that θ_k and $\bar{\theta}_k$ also owe their origins to the same set of influence functionals (and thus to the same underlying microscopic dynamics of the bath fields we integrated out) leads to a set of generalized FDTs quoted earlier in (6.2.17), which we reproduce here for convenience:

$$\frac{2}{\beta} \bar{\theta}_k + \theta_{k+1} + \frac{1}{4} \theta_{k-1} = 0.\tag{6.5.5}$$

6.6 Discussion

We have initiated the study of open quantum systems, where the environment/bath is modelled by a strongly correlated thermal medium with short relaxation times. We modelled the latter using holography, and used standard arguments to relate the real-time thermal observables of the bath to the influence functionals of the open effective field theory. For simplicity, our focus was on systems comprising of a single scalar degree of freedom, coupled to a gauge invariant operator of the bath theory of scaling dimension Δ .

As we have endeavoured to explain, it hitherto has been an unanswered question, at least within the remit of perturbative techniques, whether the dynamics of the system is described by a local influence functional, even assuming that the environment is sufficiently scrambling. As one might suspect, holographic systems, dual to black holes are maximally efficient in scrambling, and thus ought to be able to obtain local influence functions. This is indeed borne out by our explicit analysis, whereby the holographic influence functionals are manifestly local, and provide a proof-of-existence of such local open EFTs. We have furthermore shown that this open EFT can be given a stochastic interpretation, satisfying the required non-linear fluctuation-dissipation relations.

From a gravitational standpoint, the discussion also sheds further light on the semiclassical geometries that compute real-time observables in black hole backgrounds, providing further evidence to the proposal of [104]. In this context, we capture in the influence functionals, not only the

known dissipative physics contained in response functions, gravitationally encoded in the quasinormal modes, but also at the same time, learn about their interactions with the outgoing Hawking quanta. While earlier works, [120], demonstrated this in the context of a single Brownian particle degree of freedom, the present discussion generalises this to scalar probes of the black hole environment.

Finally, in the holographic setting, we have argued that one needs to carry out a suitable renormalization of the open system's degrees of freedom, in order to derive a local effective field theory, whilst respecting microscopic unitarity, state-independence, and factorization across the two legs of the Schwinger-Keldysh contour. This was starkly visible at leading order in the gradient expansion for the coupling of a bosonic degree of freedom to a marginal operator of the holographic thermal field theory. While we have analyzed the renormalization effects at leading order, developing a system holographic renormalization procedure, and understanding the requisite counter-terms, along the lines of [102], would be very helpful. For one these would be invaluable in attempting to construct a Wilsonian effective field theory for open systems (analogous to [135, 136]). Of particular interest in this context is to understand how strongly correlated thermal environments evade the issue of non-trivial (infra-red) divergences that appear to arise in perturbative open field theory computations [76, 4, 78, 137].

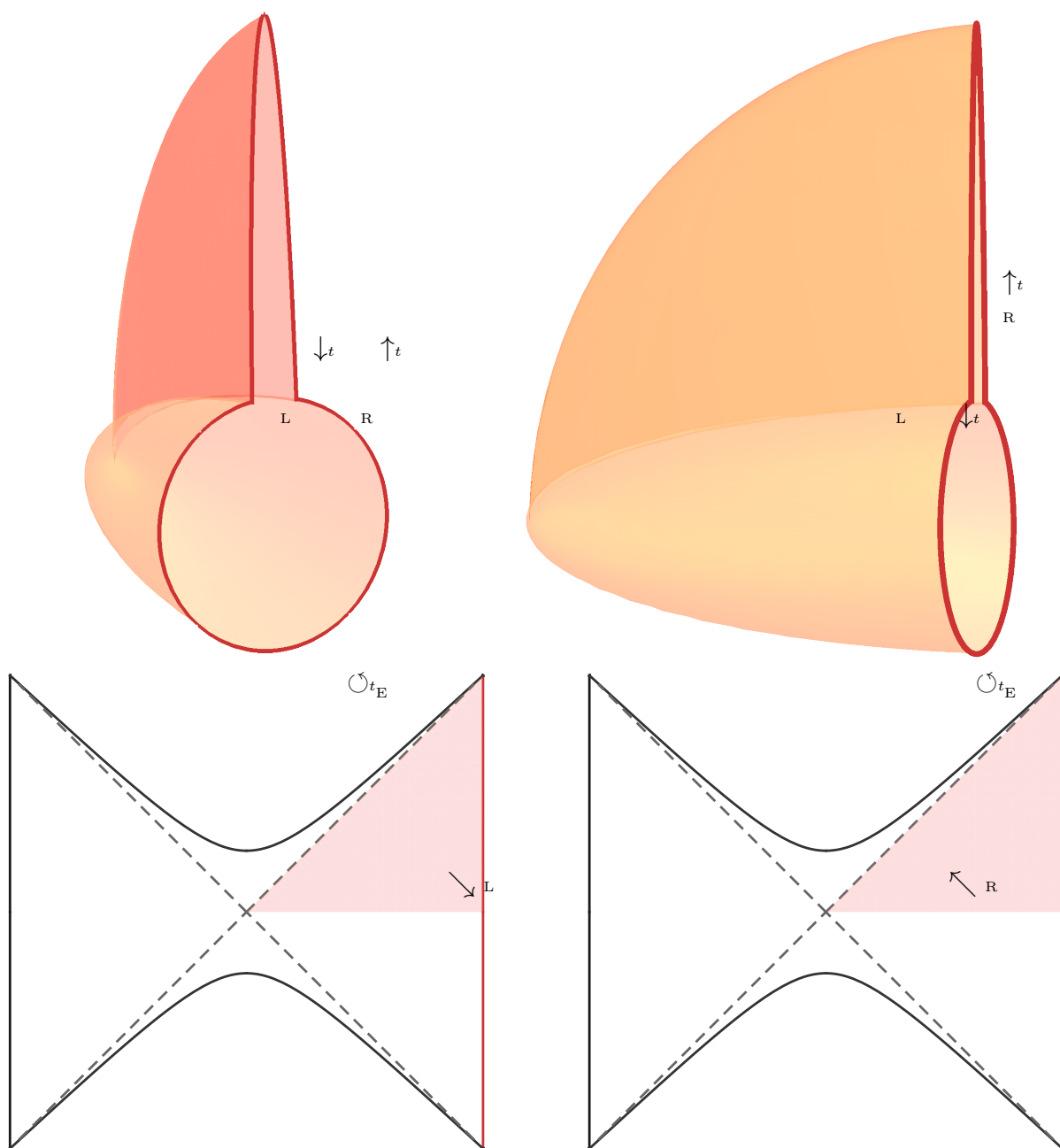


Figure 2: The two-sheeted complex grSK geometry shown from two different perspectives. On the top left we display the boundary thermal SK contour which is filled in the Euclidean portion by the Euclidean black hole geometry (the cigar) and in the Lorentzian section by two copies of the domain of outer communication of the Lorentzian black hole spacetime. The top right panel displays the bulk perspective to emphasize the smooth join of the two sheets of the Lorentzian section. On the bottom panel we illustrate the Lorentzian sections of the geometry on the Schwarzschild-AdSd+1 Penrose diagram, with the regions pertaining to the L and R sheets of the grSK spacetime shaded.

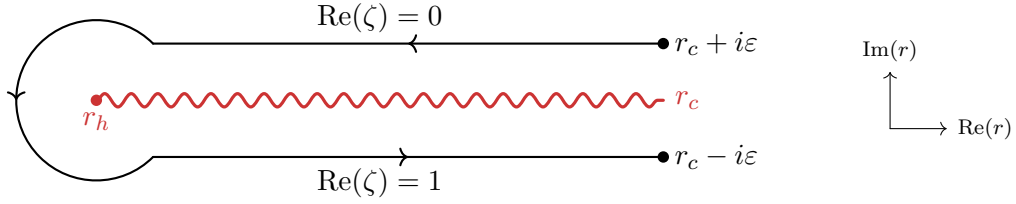


Figure 3: The complex r plane with the locations of the two boundaries and the horizon marked. The grSK contour is a codimension-1 surface in this plane (drawn at fixed v). The direction of the contour is as indicated counter-clockwise encircling the branch point at the horizon.

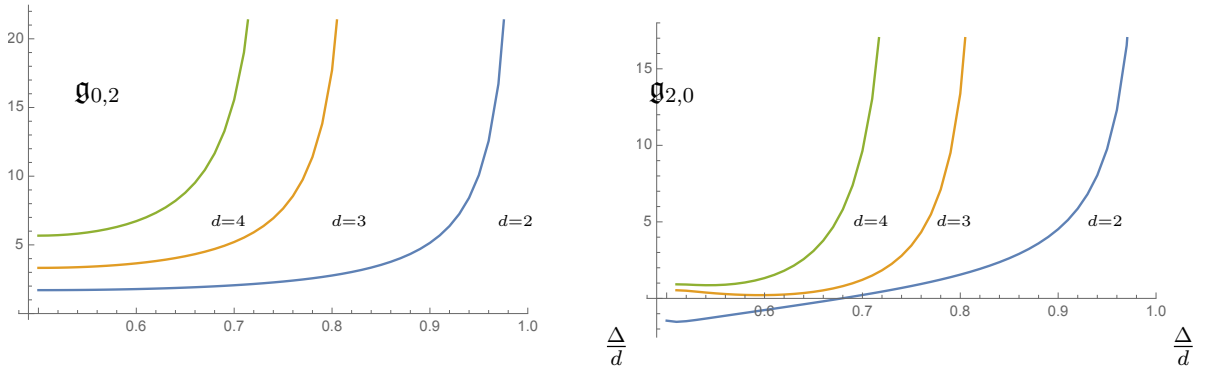


Figure 4: The numerical values of the quantities $g_{0,2}$ and $i g_{2,0}$ as a function of the conformal dimension Δ in dimensions 2, 3, and 4, respectively. We have confined attention to the case of relevant operators $\Delta \in (\frac{d}{2}, \frac{d}{2} + 1)$ when the integrals are convergent without need of additional counterterms.

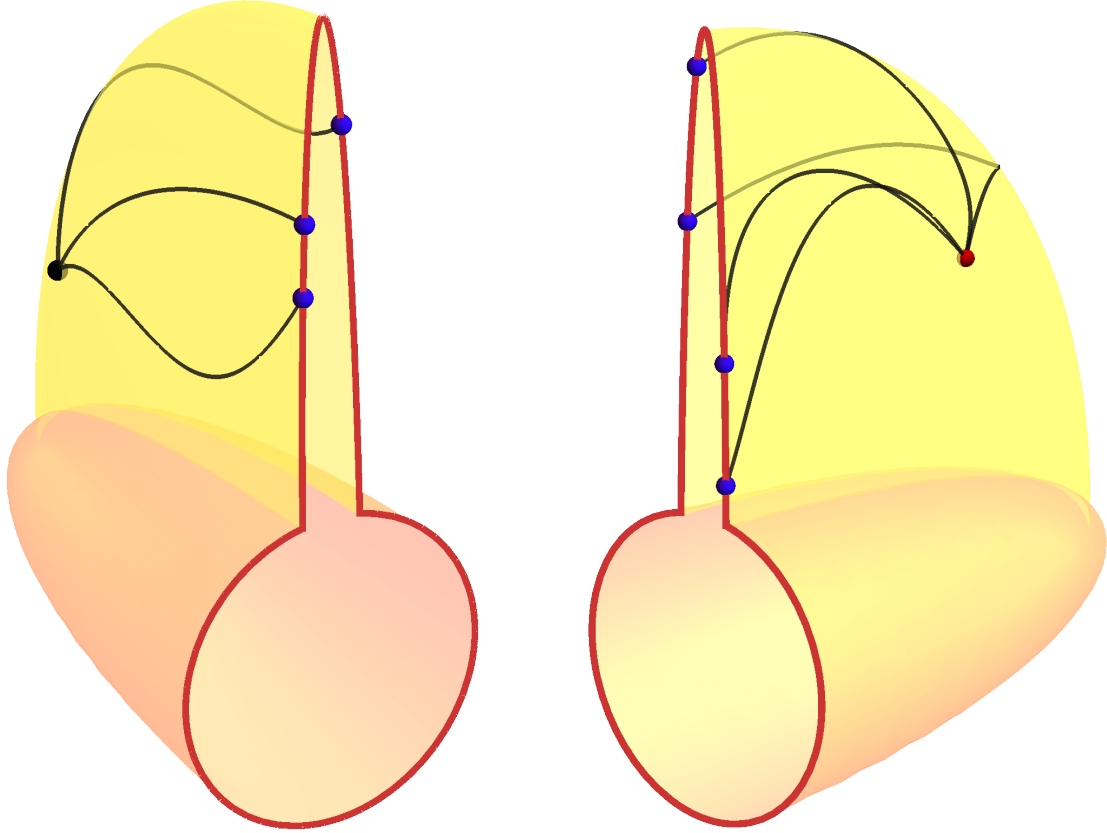


Figure 5: Illustration of Witten diagrams on the grSK geometry computing 3 and 4-point influence functions of the boundary field theory. The boundary operator insertions (blue) lie on the thermal SK contour. The bulk field is constructed using the boundary-bulk propagators, and the bulk vertex is integrated over the Lorentzian section of the grSK geometry.

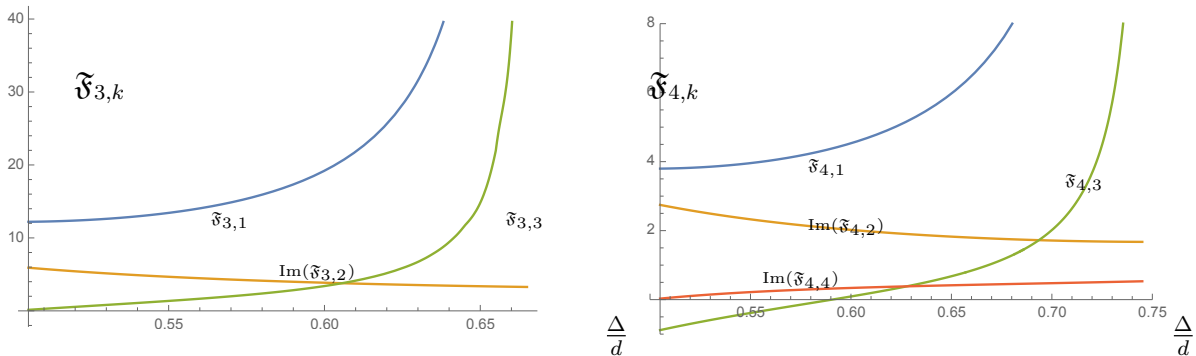


Figure 6: The numerical values of the quantities $\mathfrak{F}_{3,k}$ and $\mathfrak{F}_{4,k}$ as a function of the conformal dimension Δ (normalized by dimension). We have confined attention to the case of relevant operators $\Delta \in (\frac{d}{2}, \frac{n-1}{n}d)$ when the integrals are convergent without need of additional counterterms. We note that $\mathfrak{F}_{n,2k}$ are purely imaginary and $\mathfrak{F}_{n,2k+1}$ are real – we have thus plotted just the imaginary or real parts in the corresponding case.

Chapter 7

Discussion and Conclusion

We study various aspects of open QFTs in this thesis. First of all we argue that it is technically difficult to obtain EFT for an open QFT by integrating out its bath. As an alternative we assume an ansatz for open QFTs and then study its renormalisation along with other aspects of openness.

In this approach, we write the most general power-counting renormalisable action for open scalar field theory and study its renormalisation. We show that the theory is well behaved if one includes tadpole and bubble diagrams in the computation of β functions. We solve these β functions (analytically about the fixed points and numerically) and study scaling behaviour of parameters present in the theory.

However diagrams such as triangle, box, etc in open scalar QFTs furnish non-local divergent pieces which can not be regulated using local counter terms. These divergences in a generic scalar loop integral have interesting structures. To study these structures, we classify all one loop diagrams and write those in terms of few primitive diagrams. To demonstrate the divergence structure, we consider primitive loop integrals with $D - 1$ internal propagators in D space-time dimensions. We show that the divergences appear from certain domain of cut momenta (linear combination of external momenta flowing along a cut propagator); the cut momenta have to form a space-like hyper-surface perpendicular to null loop momentum. We also show that a Fermionic theory (open Yukawa theory) is not free from these divergences; even bubble diagrams in Fermion self-energy correction (unlike bubble diagram in scalar field theory) are non-local divergent.

A second approach to study open QFTs in thermal bath is holographic. We construct effective action of an open EFT in a bath of thermal CFT which has a gravitational dual. We integrate out the bath in AdS along gravitation SK contour. The effective action has various notable features

such as manifestly 'system+bath' unitarity, fluctuation-dissipation relations (both linear and non-linear) etc. The non-linear FDRs among parameters in the EFT emerge out of non-linear bath-bath interaction. These parameters are related to scattering amplitude of ingoing and Hawking modes in the AdS side. The SK EFT has a dual stochastic interpretation. In the stochastic description, we obtain a Langevin equation for the system field. The noise in this equation is drawn from a specific non-Gaussianity distribution which originates as a result of strong bath-bath correlation.

With this short summary, let us turn our attention to discuss non-local divergences in open field theories again. Since the physics of their appearance is not well understood, we revisit here the validity of the assumptions.

1. First of all, we assumed our theories to be Lorentz invariant. Thus any odd derivative term in the action is forbidden. We justify this assumption by the following argument. We are interested in relativistic open QFTs and their UV completion. If the energy scale is high enough, the vacuum contribution dominates over the excited states in the absence of non-unitary couplings. The Lorentz invariance breaking terms at such high energy is sub-dominant. We choose this Lorentz invariant vacuum as our initial state. Then we turn on Lorentz invariant non-unitary coupling perturbatively.

The above assumption has computational advantage - we do not know in general how to compute Green's function in field theory w.r.t. a generic state. But, in a Lorentz invariant open QFT, we can make use of the vacuum propagators to do loop computation as done in §§3 and §§4.

2. The second assumption is locality of the effective action. There is no prior reason for us to believe that the action should be local. However, as we will see in the next chapter, local description of open QFTs (probe) does exist in a bath of thermal CFT. If the bath temperature is high enough one obtain a local description of the probe QFT. But, if one pushes the temperature of the bath towards zero, locality breaks down.

If we stick to our assumptions, then the divergences should not be physical and there should be a way of absorbing those. For example, in holographic construction of open QFTs, we found some unusual divergences which can be absorbed by a renormalisation prescription for open systems (§6.4.2). A renormalisation of this sort might eliminate the non-local divergences.

The non-local divergences have similarities to the phenomenon dubbed 'UV-IR mixing' within non-commutative theories or open string theories [138, 139, 140]. If this analogy is taken seriously, our experience with those theories suggests the following resolution: the introduction of UV cutoff

and regularisation of these theories secretly also introduces an IR cutoff. The resultant UV divergences then have to be re-interpreted as IR divergences (which could indeed be non-local) and dealt with accordingly. A correct treatment of IR physics (which sometimes includes recognising hidden IR modes in the microscopic theory and adding them in explicitly in the Wilsonian theory [140]) then has potential to cure the divergences. Perhaps every open QFT also contains some IR degrees of freedom coming from their bath which do not quite decouple even when the bath has been integrated out. If so, the phenomenon of UV-IR mixing is perhaps more ubiquitous in nature than hitherto believed, and is behind the emergence of classical field theory from the underlying quantum description.

We conclude with the following open problems.

- First of all one can try understand the origin of non-local divergences and try to regularise those. Once this behaviour is understood, there are many follow up questions in this direction. One can study open version of gauge fields and analyse various aspects of QFT such as spontaneous symmetry breaking, anomaly etc.
- In the holographic setup there are several straightforward generalisations of our analysis such as discussion open system with spin degrees of freedom coupled to holographic matter [141]. More interesting are situation where the dynamics involves coupling the open system to conserved currents of the holographic theory. For instance, the open system could be coupled to a conserved R -current of the holographic field theory, or to the energy-momentum tensor. In either case, one has to examine the dynamics of gauge fields in the grSK geometries and compute the Schwinger-Keldysh correlators of these conserved currents. As mentioned in the introduction, there already exists an analysis in [104] for the dynamics of a Maxwell field in the grSK Schwarzschild-AdS geometry. However, there are several peculiarities of the gauge dynamics which deserve clarification (as already noted in the reference cited). Understanding probe gauge field dynamics is but a precursor to the more interesting question: how does one account for gravitational backreaction and consider holographic environments with non-trivial temporal evolution. A non-trivial example which would be worth analyzing is the coupling of our system to a holographic plasma which is spatially inhomogeneous and temporally evolving towards equilibrium. This would require us to understand the gravitational Schwinger-Keldysh construction for the fluid/gravity spacetimes [142].

- While we have focused on understanding the influence functionals that are computable by the Schwinger-Keldysh temporal ordering, some of these thermal observables are in turn related by the general KMS relations to certain out-of-time-order (OTO) observables [69]. For instance, all OTO three-point correlation functions can be generated from two Schwinger-Keldysh correlators, while many of the OTO four-point functions are related to ones with Schwinger-Keldysh ordering. A natural question is to encode these into the influence functionals, and use the system to probe OTO correlation functions of the holographic bath. This requires a suitable generalisation of the grSK geometry to an grOTO saddle, which would be interesting to analyze. Note that the imprints of OTO observables on a Brownian particle probe has been analysed hitherto in [122].
- A limitation of the grSK contour is that it is ignorant of the initial state of the probe. The initial state is required along with the action to compute real-time correlators. Therefore a prescription with the incorporation of grSK saddle and the initial state would be a complete prescription to study various non-equilibrium processes.

Appendices

Appendix A

Loop integrals in open scalar field theory

A.1 Notations and Conventions

Since more general diagrams can appear in this context we will introduce a suitable notation. Following the standard notation [88, 87], we will use A for tadpole diagrams and B for bubble diagrams. In addition, we will use R, L, P, M as subscripts to denote the corresponding propagators as present in the diagrams. 1.

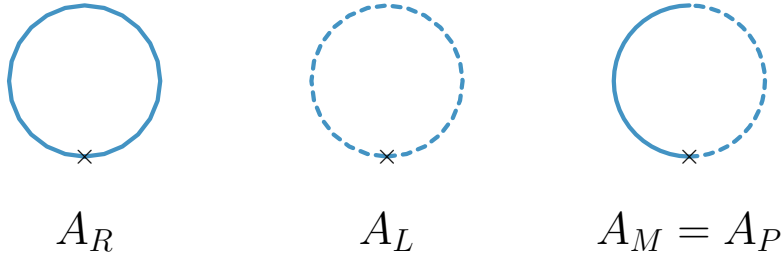


Figure 1: PV One loop A type integrals in SK theory

We are using slightly different normalization from [87] for Passarino-Veltman integrals. The relation between our integrals and the integrals in [87] is given below

$$A_0^{PV} = -(4\pi)^2 A_R \quad (\text{A.1.1})$$

$$B_0^{PV} = i(4\pi)^2 B_{RR} \quad (\text{A.1.2})$$

$$C_0^{PV} = (4\pi)^2 C_{RRR} \quad (\text{A.1.3})$$

$$D_0^{PV} = -i(4\pi)^2 D_{RRRR} \quad (\text{A.1.4})$$

We also note that Passarino-Veltman definitions use mostly negative metric $\eta_{\mu\nu} = \text{diag}(1, -1, -1, -1)$

, while in this work we use mostly positive metric $\eta_{\mu\nu} = \text{diag}(-1, 1, 1, 1)$. This fact has to be taken into account while comparing our expressions in terms of momentum-square against the standard expressions in discussions of PV integrals.

In SK theory there are four A type integrals. They are given by

$$\begin{aligned}
A_R(k) &\equiv \mu^{4-d} \int \frac{d^d p}{(2\pi)^{d_i}} \frac{1}{p^2 + m^2 - i\varepsilon} \\
A_L(k) &\equiv \mu^{4-d} \int \frac{d^d p}{(2\pi)^{d_i}} \frac{(-1)}{p^2 + m^2 + i\varepsilon} \\
A_P(k) &\equiv \mu^{4-d} \int \frac{d^d p}{(2\pi)^{d_i}} 2\pi i \delta_+(p^2 + m^2) \\
A_M(k) &\equiv \mu^{4-d} \int \frac{d^d p}{(2\pi)^{d_i}} 2\pi i \delta_-(p^2 + m^2)
\end{aligned} \tag{A.1.5}$$

Here

$$\delta_+(p^2 + m^2) \equiv \Theta(p^0) \delta(p^2 + m^2) \tag{A.1.6}$$

$$\delta_-(p^2 + m^2) \equiv \Theta(-p^0) \delta(p^2 + m^2) \tag{A.1.7}$$

In SK theory of one-scalar, there are ten B type integrals (compared to one B type integral in ordinary QFT of a single scalar). For the sake of generality, we will evaluate the most general scalar B-type integrals with unequal masses, m and \bar{m} , that can occur in an open EFT perturbation theory. These are 16 in number and they are defined as:

$$\begin{aligned}
B_{RR}(k) &\equiv \mu^{4-d} \int \frac{d^d p}{(2\pi)^{d_i}} \frac{d^d q}{(2\pi)^{d_i}} \frac{1}{p^2 + m^2 - i\varepsilon} \times \frac{1}{q^2 + \bar{m}^2 - i\varepsilon} \times (2\pi)^d \delta^d(p - q - k) \\
B_{LL}(k) &\equiv \mu^{4-d} \int \frac{d^d p}{(2\pi)^{d_i}} \frac{d^d q}{(2\pi)^{d_i}} \frac{(-1)}{p^2 + m^2 + i\varepsilon} \times \frac{(-1)}{q^2 + \bar{m}^2 + i\varepsilon} \times (2\pi)^d \delta^d(p - q - k) \\
B_{RL}(k) &\equiv \mu^{4-d} \int \frac{d^d p}{(2\pi)^{d_i}} \frac{d^d q}{(2\pi)^{d_i}} \frac{1}{p^2 + m^2 - i\varepsilon} \times \frac{(-1)}{q^2 + \bar{m}^2 + i\varepsilon} \times (2\pi)^d \delta^d(p - q - k) \\
B_{LR}(k) &\equiv \mu^{4-d} \int \frac{d^d p}{(2\pi)^{d_i}} \frac{d^d q}{(2\pi)^{d_i}} \frac{(-1)}{p^2 + m^2 + i\varepsilon} \times \frac{1}{q^2 + \bar{m}^2 - i\varepsilon} \times (2\pi)^d \delta^d(p - q - k)
\end{aligned} \tag{A.1.8}$$

$$\begin{aligned}
B_{PM}(k) &\equiv \mu^{4-d} \int \frac{d^d p}{(2\pi)^{d_i}} \frac{d^d q}{(2\pi)^{d_i}} 2\pi i \delta_+(p^2 + m^2) \times 2\pi i \delta_-(q^2 + \bar{m}^2) \times (2\pi)^d \delta^d(p - q - k) \\
B_{MP}(k) &\equiv \mu^{4-d} \int \frac{d^d p}{(2\pi)^{d_i}} \frac{d^d q}{(2\pi)^{d_i}} 2\pi i \delta_-(p^2 + m^2) \times 2\pi i \delta_+(q^2 + \bar{m}^2) \times (2\pi)^d \delta^d(p - q - k) \\
B_{PP}(k) &\equiv \mu^{4-d} \int \frac{d^d p}{(2\pi)^{d_i}} \frac{d^d q}{(2\pi)^{d_i}} 2\pi i \delta_+(p^2 + m^2) \times 2\pi i \delta_+(q^2 + \bar{m}^2) \times (2\pi)^d \delta^d(p - q - k) \\
B_{MM}(k) &\equiv \mu^{4-d} \int \frac{d^d p}{(2\pi)^{d_i}} \frac{d^d q}{(2\pi)^{d_i}} 2\pi i \delta_-(p^2 + m^2) \times 2\pi i \delta_-(q^2 + \bar{m}^2) \times (2\pi)^d \delta^d(p - q - k)
\end{aligned} \tag{A.1.9}$$

$$\begin{aligned}
B_{PR}(k) &\equiv \mu^{4-d} \int \frac{d^d p}{(2\pi)^{d_i}} \frac{d^d q}{(2\pi)^{d_i}} 2\pi i \delta_+(p^2 + m^2) \frac{1}{q^2 + \bar{m}^2 - i\varepsilon} \times (2\pi)^d \delta^d(p - q - k) \\
B_{MR}(k) &\equiv \mu^{4-d} \int \frac{d^d p}{(2\pi)^{d_i}} \frac{d^d q}{(2\pi)^{d_i}} 2\pi i \delta_-(p^2 + m^2) \frac{1}{q^2 + \bar{m}^2 - i\varepsilon} \times (2\pi)^d \delta^d(p - q - k) \\
B_{PL}(k) &\equiv \mu^{4-d} \int \frac{d^d p}{(2\pi)^{d_i}} \frac{d^d q}{(2\pi)^{d_i}} 2\pi i \delta_+(p^2 + m^2) \frac{(-1)}{q^2 + \bar{m}^2 + i\varepsilon} \times (2\pi)^d \delta^d(p - q - k) \\
B_{ML}(k) &\equiv \mu^{4-d} \int \frac{d^d p}{(2\pi)^{d_i}} \frac{d^d q}{(2\pi)^{d_i}} 2\pi i \delta_-(p^2 + m^2) \frac{(-1)}{q^2 + \bar{m}^2 + i\varepsilon} \times (2\pi)^d \delta^d(p - q - k)
\end{aligned} \tag{A.1.10}$$

$$\begin{aligned}
B_{RP}(k) &\equiv \mu^{4-d} \int \frac{d^d p}{(2\pi)^{d_i}} \frac{d^d q}{(2\pi)^{d_i}} \frac{1}{p^2 + m^2 - i\varepsilon} 2\pi i \delta_+(q^2 + \bar{m}^2) \times (2\pi)^d \delta^d(p - q - k) \\
B_{RM}(k) &\equiv \mu^{4-d} \int \frac{d^d p}{(2\pi)^{d_i}} \frac{d^d q}{(2\pi)^{d_i}} \frac{1}{p^2 + m^2 - i\varepsilon} 2\pi i \delta_-(q^2 + \bar{m}^2) \times (2\pi)^d \delta^d(p - q - k) \\
B_{LP}(k) &\equiv \mu^{4-d} \int \frac{d^d p}{(2\pi)^{d_i}} \frac{d^d q}{(2\pi)^{d_i}} \frac{(-1)}{p^2 + m^2 + i\varepsilon} 2\pi i \delta_+(q^2 + \bar{m}^2) \times (2\pi)^d \delta^d(p - q - k) \\
B_{LM}(k) &\equiv \mu^{4-d} \int \frac{d^d p}{(2\pi)^{d_i}} \frac{d^d q}{(2\pi)^{d_i}} \frac{(-1)}{p^2 + m^2 + i\varepsilon} 2\pi i \delta_-(q^2 + \bar{m}^2) \times (2\pi)^d \delta^d(p - q - k)
\end{aligned} \tag{A.1.11}$$

In the following appendix, we will evaluate these integrals and their divergences.

A.2 Evaluating Passarino-Veltman Loop Integrals for open $\phi^3 + \phi^4$ theory

In this section, we describe in some detail the loop integrals that appear in the perturbation theory of open $\phi^3 + \phi^4$ theory. While some of the integrals are familiar from usual QFT textbooks and a few other integrals occur in discussions of cutting rules, as far as the authors are aware, the majority of the integrals described in this section are not analyzed elsewhere. Hence, these

integrals are described in some detail with a special focus on the new kind of features that occur when we try to do integrals in the real time (most of the integrals in this section do not admit Wick rotation because of their unusual $i\epsilon$ prescriptions) .

A.2.1 Passarino-Veltman A type integrals

There are four A type PV integrals : A_R, A_L, A_P, A_M . They satisfy the following relations

$$A_R = A_L^* \quad A_P = A_P^* \quad (\text{A.2.1})$$

$$A_R + A_L = A_P + A_M \equiv 2A_P \quad (\text{A.2.2})$$

First we compute the integral A_R

$$\begin{aligned} A_R &= \mu^{4-d} \int \frac{d^d p}{(2\pi)^d} \frac{-i}{p^2 + m^2 - i\epsilon} = \int \frac{d^d p}{(2\pi)^{d_i}} \frac{1}{\omega_p^2 - (p^0)^2 - i\epsilon} \\ &= \mu^{4-d} \int \frac{d^{d-1} p}{(2\pi)^{d-1}} \frac{1}{2\omega_p} = \mu^{4-d} \frac{\text{Vol}(\mathbb{S}^{d-2})}{2(2\pi)^{d-1}} \int_m \left(\sqrt{\omega_p^2 - m^2} \right)^{d-3} d\omega_p \\ &= \Gamma\left[\frac{1}{2}(2-d)\right] \frac{m^2}{(4\pi)^2} \left(\frac{m^2}{4\pi\mu^2}\right)^{\frac{d-4}{2}} \quad (\text{A.2.3}) \\ &= \frac{m^2}{(4\pi)^2} \frac{2}{d-4} + \frac{m^2}{(4\pi)^2} \left\{ \ln \frac{m^2}{4\pi\mu^2 e^{-\gamma_E}} - 1 \right\} + O(d-4) \end{aligned}$$

Using this result and the relations (A.2.1)-(A.2.2), we can determine A_L and A_P . A_L, A_P and A_M are given by

$$A_R = A_L = A_P = A_M = \frac{m^2}{(4\pi)^2} \left(\frac{2}{d-4} + \ln \frac{m^2}{4\pi\mu^2 e^{-\gamma_E}} - 1 \right) \quad (\text{A.2.4})$$

A.2.2 Integrals $B_{PM}(k)$ and $B_{MP}(k)$

We will now consider the following two integrals

$$\begin{aligned} B_{PM}(k) &\equiv \mu^{4-d} \int \frac{d^d p}{(2\pi)^{d_i}} \frac{d^d q}{(2\pi)^{d_i}} 2\pi i \delta_+(p^2 + m^2) \times 2\pi i \delta_-(q^2 + \bar{m}^2) \times (2\pi)^d \delta^d(p - q - k) \\ B_{MP}(k) &\equiv \mu^{4-d} \int \frac{d^d p}{(2\pi)^{d_i}} \frac{d^d q}{(2\pi)^{d_i}} 2\pi i \delta_-(p^2 + m^2) \times 2\pi i \delta_+(q^2 + \bar{m}^2) \times (2\pi)^d \delta^d(p - q - k) \end{aligned} \quad (\text{A.2.5})$$

These integrals are well-known in discussions of cutting rules and we mainly discuss them here for completeness. They represent the amplitudes for the two body decay of a particle with mass $\sqrt{-k^2}$ to decay into two particles of mass m and \bar{m} . It follows that the integral $B_{PM}(k)$ vanishes unless k^μ

is future time-like, whereas $B_{MP}(k)$ is zero unless k^μ is past time-like. Since $B_{MP}(k) = B_{PM}(-k)$, it suffices to argue this for $B_{PM}(k)$. The mathematical reasoning is as follows : if k^μ were to be space-like, we can go to a frame where $k^0 = 0$ and the energy delta function then gives $\delta(\omega_p + \bar{\omega}_q) = 0$, thus reducing the amplitude to zero. If k^μ is time-like and we move to its rest frame by setting $k^\mu = \{M, \vec{0}\}$ where $M = \text{sgn}(k^0)\sqrt{-k^2}$. The energy delta function for $B_{PM}(k)$ then gives $\delta(\omega_p + \bar{\omega}_q - M) = 0$, thus forcing $M > 0$, i.e., k^μ should be future time-like.

By performing p^0 and q^0 integrals in the rest frame of k^μ , we can reduce both integrals to the two body phase space integral. Let us begin by defining the basic kinematics of a particle of mass $M = \sqrt{-k^2}$ decaying into two particles of mass m and \bar{m} . Let p_\star be the momentum with which these two particles fly away in the rest frame of M . Energy-momentum conservation then fixes

$$\begin{aligned}
p_\star &= \frac{1}{2M} \left[M^2 - (m + \bar{m})^2 \right]^{1/2} \left[M^2 - (m - \bar{m})^2 \right]^{1/2} \\
&= \frac{M}{2} \left[1 - 2 \left(\frac{m^2 + \bar{m}^2}{M^2} \right) + \left(\frac{m^2 - \bar{m}^2}{M^2} \right)^2 \right]^{1/2} \\
\omega_p^\star &\equiv \sqrt{p_\star^2 + m^2} = \frac{1}{2M} (M^2 + m^2 - \bar{m}^2) \\
\bar{\omega}_p^\star &\equiv \sqrt{p_\star^2 + \bar{m}^2} = \frac{1}{2M} (M^2 + \bar{m}^2 - m^2)
\end{aligned} \tag{A.2.6}$$

These expressions make sense only when the argument of the square root is positive, i.e., when $M \geq m + \bar{m}$ which is the condition for the two body decay to be kinematically possible. In this regime, ω_p^\star and $\bar{\omega}_p^\star$ are both positive as we would expect. Another useful identity is

$$\frac{1}{(2\omega_p)(2\bar{\omega}_p)} \delta(\omega_p + \bar{\omega}_p - M) = \frac{1}{4Mp_\star} \delta(|p| - p_\star) \tag{A.2.7}$$

Let us now compute this integral in terms of these kinematic variables. We have

$$\begin{aligned}
B_{PM}(k) &= \mu^{4-d} \int \frac{d^{d-1}p}{(2\pi)^{d-1}(2\omega_p)} \frac{d^{d-1}q}{(2\pi)^{d-1}(2\bar{\omega}_q)} \times (2\pi)^d \delta^{d-1}(\vec{p} - \vec{q}) \delta(\omega_p + \omega_q - M) \\
&= \mu^{4-d} \int \frac{d^{d-1}p}{(2\pi)^{d-1}(2\omega_p)(2\bar{\omega}_p)} 2\pi \delta(\omega_p + \bar{\omega}_p - M) \\
&= \mu^{4-d} \frac{\text{Vol}(\mathbb{S}^{d-2})}{(2\pi)^{d-2}} \int_0^\infty \frac{p^{d-2} d^d p}{(2\omega_p)(2\bar{\omega}_p)} \delta(\omega_p + \bar{\omega}_p - M) = \mu^{4-d} \frac{\text{Vol}(\mathbb{S}^{d-2}) p_\star^{d-3}}{4M(2\pi)^{d-2}} \\
&= \frac{\text{Vol}(\mathbb{S}^{d-2})}{32\pi^2} \left(\frac{M}{4\pi\mu} \right)^{d-4} \left(\frac{2p_\star}{M} \right)^{d-3}
\end{aligned} \tag{A.2.8}$$

which is the two-body phase space as advertised.

Restoring the kinematic constraints, we get

$$B_{PM}(k) = \frac{\text{Vol}(\mathbb{S}^{d-2})}{32\pi^2} \left(\frac{-k^2}{(4\pi\mu)^2} \right)^{\frac{d-4}{2}} \left[1 + 2 \left(\frac{m^2 + \bar{m}^2}{k^2} \right) + \left(\frac{m^2 - \bar{m}^2}{k^2} \right)^2 \right]^{\frac{d-3}{2}} \times \Theta(-k^2 - (m + \bar{m})^2) \Theta(k^0) \quad (\text{A.2.9})$$

The integral can then be expanded near $d = 4$ to get

$$B_{PM}(k) = \frac{\Theta(-k^2 - (m + \bar{m})^2) \Theta(k^0)}{8\pi} \left[1 + 2 \left(\frac{m^2 + \bar{m}^2}{k^2} \right) + \left(\frac{m^2 - \bar{m}^2}{k^2} \right)^2 \right]^{\frac{1}{2}} \quad (\text{A.2.10})$$

Replacing k^μ by $-k^\mu$ we get

$$B_{MP}(k) = \frac{\Theta(-k^2 - (m + \bar{m})^2) \Theta(-k^0)}{8\pi} \left[1 + 2 \left(\frac{m^2 + \bar{m}^2}{k^2} \right) + \left(\frac{m^2 - \bar{m}^2}{k^2} \right)^2 \right]^{\frac{1}{2}}. \quad (\text{A.2.11})$$

These two expressions can be added to get

$$B_{PM}(k) + B_{MP}(k) = \frac{\Theta(-k^2 - (m + \bar{m})^2)}{8\pi} \left[1 + 2 \left(\frac{m^2 + \bar{m}^2}{k^2} \right) + \left(\frac{m^2 - \bar{m}^2}{k^2} \right)^2 \right]^{\frac{1}{2}} \quad (\text{A.2.12})$$

When $m = \bar{m}$, we can write

$$\boxed{B_{PM}(k) = \frac{\Theta(k^0) \Theta(-k^2 - 4m^2)}{8\pi} \sqrt{1 + \frac{4m^2}{k^2}}} \quad (\text{A.2.13})$$

and

$$\boxed{B_{MP}(k) = \frac{\Theta(-k^0) \Theta(-k^2 - 4m^2)}{8\pi} \sqrt{1 + \frac{4m^2}{k^2}}} \quad (\text{A.2.14})$$

A.2.3 Integrals $B_{PP}(k)$ and $B_{MM}(k)$

We now turn to the ‘cross-cut’ integrals $B_{PP}(k)$ and $B_{MM}(k)$ which do not occur in the usual discussions of cutting rules in a unitary theory. They are loop integrals peculiar to open QFTs with their own characteristic kinematic behavior.

Time-like k^μ

We will begin by examining $B_{PP}(k)$ for time-like k^μ . In the rest frame of k^μ i.e., $k^\mu = (M, \vec{0})$, we can do similar manipulations as in the previous subsection to get

$$\begin{aligned}
B_{PP}(k) &\equiv \mu^{4-d} \int \frac{d^d p}{(2\pi)^{d_i}} \frac{d^d q}{(2\pi)^{d_i}} 2\pi i \delta_+(p^2 + m^2) 2\pi i \delta_+(q^2 + \bar{m}^2) (2\pi)^d \delta^d(p - q - k) \\
&= \mu^{4-d} \int \frac{d^{d-1} p}{(2\pi)^{d-1} 2\omega_p} \frac{d^{d-1} q}{(2\pi)^{d-1} 2\bar{\omega}_q} \delta(\omega_p - \bar{\omega}_q - M) (2\pi)^d \delta^{d-1}(\vec{p} - \vec{q}) \\
&= \mu^{4-d} \int \frac{d^{d-1} p}{(2\pi)^{d-2}} \frac{1}{2\omega_p} \frac{1}{2\bar{\omega}_p} \delta(\omega_p - \bar{\omega}_p - M) \\
&= \frac{\mu^{4-d} \text{Vol}(\mathbb{S}^{d-2})}{(2\pi)^{d-2}} \int_0^\infty \frac{p^{d-2} dp}{(2\omega_p)(2\bar{\omega}_p)} \delta(\omega_p - \bar{\omega}_p - M) = \frac{\text{Vol}(\mathbb{S}^{d-2})}{32\pi^2} \left(\frac{|M|}{4\pi\mu} \right)^{d-4} \left(\frac{2p_\star}{|M|} \right)^{d-3}
\end{aligned} \tag{A.2.15}$$

where we have used

$$\frac{1}{(2\omega_p)(2\bar{\omega}_p)} \delta(\omega_p - \bar{\omega}_p - M) = \frac{1}{4|M|p_\star} \delta(|p| - p_\star) \tag{A.2.16}$$

with p_\star being the appropriate momentum which solves the kinematics (see below).

For $M > 0$, i.e., k^μ being future time-like, we recognize the integral as the one describing the phase space for a deep in-elastic scattering process : \bar{m} with momentum p strikes against the target M at rest converting it into the particle m traveling with momentum p . The kinematics is solved by

$$\begin{aligned}
p_\star &= \frac{1}{2M} \left[(m + \bar{m})^2 - M^2 \right]^{1/2} \left[(m - \bar{m})^2 - M^2 \right]^{1/2} \\
&= \frac{M}{2} \left[1 - 2 \left(\frac{m^2 + \bar{m}^2}{M^2} \right) + \left(\frac{m^2 - \bar{m}^2}{M^2} \right)^2 \right]^{1/2} \\
\omega_p^\star &\equiv \sqrt{p_\star^2 + m^2} = \frac{1}{2M} (m^2 + M^2 - \bar{m}^2) \\
\bar{\omega}_p^\star &\equiv \sqrt{p_\star^2 + \bar{m}^2} = \frac{1}{2M} (m^2 - M^2 - \bar{m}^2)
\end{aligned} \tag{A.2.17}$$

which is sensible for $M < m - \bar{m}$. Thus, in this kinematic regime we get

$$\begin{aligned}
B_{PP}(k) &\ni \frac{\text{Vol}(\mathbb{S}^{d-2})}{32\pi^2} \left(\frac{-k^2}{(4\pi\mu)^2} \right)^{\frac{d-4}{2}} \left[1 + 2 \left(\frac{m^2 + \bar{m}^2}{k^2} \right) + \left(\frac{m^2 - \bar{m}^2}{k^2} \right)^2 \right]^{\frac{d-3}{2}} \\
&\quad \times \Theta((m - \bar{m})^2 + k^2) \Theta(k^0)
\end{aligned} \tag{A.2.18}$$

For $M < 0$, i.e., k^μ being past time-like, we recognize the integral as the one describing the phase space for the two body decay of \bar{m} into a particle of mass $|M|$ and m . The kinematics is

solved by

$$\begin{aligned}
p_\star &= \frac{1}{2|M|} \left[(m + \bar{m})^2 - M^2 \right]^{1/2} \left[(m - \bar{m})^2 - M^2 \right]^{1/2} \\
&= \frac{|M|}{2} \left[1 - 2 \left(\frac{m^2 + \bar{m}^2}{M^2} \right) + \left(\frac{m^2 - \bar{m}^2}{M^2} \right)^2 \right]^{1/2} \\
\omega_p^\star &\equiv \sqrt{p_\star^2 + m^2} = \frac{1}{2|M|} (\bar{m}^2 - m^2 - M^2) \\
\bar{\omega}_p^\star &\equiv \sqrt{p_\star^2 + \bar{m}^2} = \frac{1}{2|M|} (\bar{m}^2 - m^2 + M^2)
\end{aligned} \tag{A.2.19}$$

which is sensible for $\bar{m} > |M| + m$. Thus, in this kinematic regime we get

$$\begin{aligned}
B_{PP}(k) &\ni \frac{\text{Vol}(\mathbb{S}^{d-2})}{32\pi^2} \left(\frac{-k^2}{(4\pi\mu)^2} \right)^{\frac{d-4}{2}} \left[1 + 2 \left(\frac{m^2 + \bar{m}^2}{k^2} \right) + \left(\frac{m^2 - \bar{m}^2}{k^2} \right)^2 \right]^{\frac{d-3}{2}} \\
&\quad \times \Theta((\bar{m} - m)^2 + k^2) \Theta(-k^0)
\end{aligned} \tag{A.2.20}$$

Thus, we conclude that for time-like k^μ ,

$$\begin{aligned}
B_{PP}(k) &\ni \frac{\text{Vol}(\mathbb{S}^{d-2})}{32\pi^2} \left(\frac{-k^2}{(4\pi\mu)^2} \right)^{\frac{d-4}{2}} \left[1 + 2 \left(\frac{m^2 + \bar{m}^2}{k^2} \right) + \left(\frac{m^2 - \bar{m}^2}{k^2} \right)^2 \right]^{\frac{d-3}{2}} \\
&\quad \times \Theta((\bar{m} - m)^2 + k^2) \Theta(-k^2)
\end{aligned} \tag{A.2.21}$$

Note that $B_{PP}(k) = B_{PP}(-k)$ could have been directly deduced from the integral form.

Space-like k^μ

We will next study $B_{PP}(k)$ when k^μ is space-like. We set $k^\mu = \{0, Q = \sqrt{k^2}, \vec{0}_{d-2}\}$ where we take $Q > 0$ without loss of generality. We have

$$\begin{aligned}
B_{PP}(k) &\equiv \mu^{4-d} \int \frac{d^d p}{(2\pi)^{d_i}} \frac{d^d q}{(2\pi)^{d_i}} 2\pi i \delta_+(p^2 + m^2) 2\pi i \delta_+(q^2 + \bar{m}^2) (2\pi)^d \delta^d(p - q - k) \\
&= \mu^{4-d} \int \frac{d^{d-1} p}{(2\pi)^{d-1} (2\omega_p)} \frac{d^{d-1} q}{(2\pi)^{d-1} (2\bar{\omega}_q)} \times (2\pi)^d \delta^{d-2}(\vec{p}_\perp - \vec{q}_\perp) \delta(p_\parallel - q_\parallel - Q) \delta(\omega_p - \bar{\omega}_q) \\
&= \mu^{4-d} \int \frac{d^{d-1} p}{(2\pi)^{d-1} (2\omega_p) (2\bar{\omega}_{p\perp})} 2\pi \delta(\omega_p - \bar{\omega}_{p\perp}) = \frac{\mu^{4-d}}{(2Q)} \int \frac{d^{d-2} p_\perp}{(2\pi)^{d-2} (2\omega_{p\perp})}
\end{aligned} \tag{A.2.22}$$

where, in the penultimate step we have defined $\bar{\omega}_{p\perp} \equiv p_\perp^2 + (Q - p_\parallel)^2 + \bar{m}^2$. In the last step, we have used

$$\frac{1}{(2\omega_p)(2\bar{\omega}_{p\perp})} \delta(\omega_p - \bar{\omega}_{p\perp}) = \frac{1}{4Q\omega_{p\perp}} \delta(p_\parallel - p_\parallel^\star) \tag{A.2.23}$$

with the definitions

$$\begin{aligned}
p_{\parallel}^{\star} &\equiv \frac{1}{2Q}(\bar{m}^2 - m^2 + Q^2) \\
(\omega_{p_{\perp}})^2 &\equiv p_{\perp}^2 + (p_{\parallel}^{\star})^2 + m^2 = p_{\perp}^2 + \frac{1}{4Q^2} \left[(m + \bar{m})^2 + Q^2 \right] \left[(m - \bar{m})^2 + Q^2 \right].
\end{aligned} \tag{A.2.24}$$

The rest of the integral is $(d - 2)$ dimensional transverse phase space with the transverse mass given by

$$\begin{aligned}
m_{\perp} &\equiv \frac{1}{2Q} \left[(m + \bar{m})^2 + Q^2 \right]^{1/2} \left[(m - \bar{m})^2 + Q^2 \right]^{1/2} \\
&= \frac{Q}{2} \left[1 + 2 \left(\frac{m^2 + \bar{m}^2}{Q^2} \right) + \left(\frac{m^2 - \bar{m}^2}{Q^2} \right)^2 \right]^{1/2}
\end{aligned} \tag{A.2.25}$$

We thus get

$$\begin{aligned}
B_{PP}(k) &= \mu^{4-d} \frac{\text{Vol}(\mathbb{S}^{d-3})}{4Q(2\pi)^{d-2}} \int_{m_{\perp}}^{\infty} \left(\sqrt{\omega_{p_{\perp}}^2 - m_{\perp}^2} \right)^{d-4} d\omega_{p_{\perp}} \\
&= \mu^{4-d} \frac{\text{Vol}(\mathbb{S}^{d-2})}{(2\pi)^{d-1}} \frac{m_{\perp}^{d-3}}{4Q} \Gamma\left(\frac{3}{2} - \frac{d}{2}\right) \Gamma\left(\frac{d}{2} - \frac{1}{2}\right) \\
&= \frac{\text{Vol}(\mathbb{S}^{d-2})}{32\pi^2} \left(\frac{Q}{4\pi\mu} \right)^{d-4} \left(\frac{2m_{\perp}}{Q} \right)^{d-3} \frac{1}{2\pi} \Gamma\left(\frac{3}{2} - \frac{d}{2}\right) \Gamma\left(\frac{d}{2} - \frac{1}{2}\right)
\end{aligned} \tag{A.2.26}$$

Restoring the kinematical constraints, we get

$$\begin{aligned}
B_{PP}(k) &\ni \frac{\text{Vol}(\mathbb{S}^{d-2})}{32\pi^2} \left(\frac{k^2}{(4\pi\mu)^2} \right)^{\frac{d-4}{2}} \left[1 + 2 \left(\frac{m^2 + \bar{m}^2}{k^2} \right) + \left(\frac{m^2 - \bar{m}^2}{k^2} \right)^2 \right]^{\frac{d-3}{2}} \\
&\quad \times \Theta(k) \frac{1}{2\pi} \Gamma\left(\frac{3}{2} - \frac{d}{2}\right) \Gamma\left(\frac{d}{2} - \frac{1}{2}\right)
\end{aligned} \tag{A.2.27}$$

Putting together the various kinematical regimes, we obtain

$$\begin{aligned}
B_{PP}(k) &= \frac{\text{Vol}(\mathbb{S}^{d-2})}{32\pi^2} \left[1 + 2 \left(\frac{m^2 + \bar{m}^2}{k^2} \right) + \left(\frac{m^2 - \bar{m}^2}{k^2} \right)^2 \right]^{\frac{d-3}{2}} \\
&\quad \times \left\{ \Theta(k^2) \frac{1}{2\pi} \Gamma\left(\frac{3}{2} - \frac{d}{2}\right) \Gamma\left(\frac{d}{2} - \frac{1}{2}\right) \left(\frac{k^2}{(4\pi\mu)^2} \right)^{\frac{d-4}{2}} \right. \\
&\quad \left. + \Theta((\bar{m} - m)^2 + k^2) \Theta(-k^2) \left(\frac{-k^2}{(4\pi\mu)^2} \right)^{\frac{d-4}{2}} \right\}
\end{aligned} \tag{A.2.28}$$

Expanding around $d = 4$ we get

$$\begin{aligned}
B_{PP}(k) = B_{MM}(k) &= \frac{1}{8\pi} \left[1 + 2 \left(\frac{m^2 + \bar{m}^2}{k^2} \right) + \left(\frac{m^2 - \bar{m}^2}{k^2} \right)^2 \right]^{\frac{1}{2}} \\
&\quad \times \left\{ -\frac{1}{2} \Theta(k^2) + \Theta((\bar{m} - m)^2 + k^2) \Theta(-k^2) \right\}
\end{aligned} \tag{A.2.29}$$

where we have used $B_{MM}(k) = B_{PP}(-k) = B_{PP}(k)$. Taking $m = \bar{m}$, the second factor vanishes and we obtain

$$\boxed{B_{PP}(k) = B_{MM}(k) = \frac{[-\frac{1}{2} \Theta(k^2)]}{8\pi} \sqrt{1 + \frac{4m^2}{k^2}}} \quad (\text{A.2.30})$$

A.2.4 Reduction of divergent integrals to $B_{RP}(k)$

We now turn to the ‘quarter-cut’ integrals $B_{RP}(k)$, $B_{RM}(k)$, $B_{LP}(k)$ and $B_{LM}(k)$ which also do not occur in the usual discussions of cutting rules in a unitary theory. They are also loop integrals peculiar to open QFTs. However, unlike the integrals considered in the last section, they do not evaluate to on-shell phase space for various processes. This off-shell nature means that they exhibit UV divergences and hence are crucial to the issue of renormalizability of open QFTs. When the open QFT is renormalisable, these diagrams contribute to β functions of an open QFT. As before, we will evaluate this integrals in various kinematic regimes and then put together the answers at the end.

We will consider the integral

$$B_{RP}(k) = \mu^{4-d} \int \frac{d^d p}{(2\pi)^{d_i}} \int \frac{d^d q}{(2\pi)^{d_i}} \frac{1}{p^2 + m^2 - i\varepsilon} 2\pi i \delta_+(q^2 + \bar{m}^2) (2\pi)^d \delta^d(p - q - k) \quad (\text{A.2.31})$$

This is the characteristic integral which leads to UV divergences in open QFT. Before analyzing this integral further, we will show that the other divergent integrals can be reduced to this integral.

We start with

$$\begin{aligned} B_{RM}(k) &\equiv \mu^{4-d} \int \frac{d^d p}{(2\pi)^{d_i}} \int \frac{d^d q}{(2\pi)^{d_i}} \frac{1}{p^2 + m^2 - i\varepsilon} 2\pi i \delta_-(q^2 + \bar{m}^2) (2\pi)^d \delta^d(p - q - k) \\ &= B_{RP}(-k) \end{aligned} \quad (\text{A.2.32})$$

Similarly

$$\begin{aligned} B_{LP}(k) &\equiv \mu^{4-d} \int \frac{d^d p}{(2\pi)^{d_i}} \int \frac{d^d q}{(2\pi)^{d_i}} \frac{-1}{p^2 + m^2 + i\varepsilon} 2\pi i \delta_+(q^2 + \bar{m}^2) (2\pi)^d \delta^d(p - q - k) \\ &= [B_{RP}(k)]^* \\ B_{LM}(k) &\equiv \mu^{4-d} \int \frac{d^d p}{(2\pi)^{d_i}} \int \frac{d^d q}{(2\pi)^{d_i}} \frac{-1}{p^2 + m^2 + i\varepsilon} 2\pi i \delta_-(q^2 + \bar{m}^2) (2\pi)^d \delta^d(p - q - k) \\ &= [B_{RM}(k)]^* = [B_{RP}(-k)]^* \end{aligned} \quad (\text{A.2.33})$$

The integrals with the subscripts exchanged can be obtained by exchanging m and \bar{m} (thus exchanging p^μ and q^μ) and reversing k^μ . For example, $B_{PR}(k) = B_{RP}(-k)|_{m \leftrightarrow \bar{m}}$ and similarly for

other integrals :

$$\begin{aligned}
B_{PR}(k) &= B_{RP}(-k)|_{m \leftrightarrow \bar{m}} , & B_{MR}(k) &= B_{RP}(k)|_{m \leftrightarrow \bar{m}} , \\
B_{PL}(k) &= B_{RP}(-k)^*|_{m \leftrightarrow \bar{m}} , & B_{ML}(k) &= B_{RP}(k)^*|_{m \leftrightarrow \bar{m}} .
\end{aligned}
\tag{A.2.34}$$

It is convenient to define the following combination of integrals :

$$\begin{aligned}
B_{RL}^+(k) &\equiv B_{RP}(k) + B_{ML}(k) = B_{RP}(k) + [B_{RP}(k)]_{m \leftrightarrow \bar{m}}^* \\
B_{RR}^+(k) &\equiv \Theta(m > \bar{m})(B_{RM}(k) - B_{ML}(k)) + \Theta(m < \bar{m})(B_{PR}(k) - B_{LP}(k)) \\
&= \Theta(m > \bar{m})(B_{RP}(-k) - B_{RP}(k)_{m \leftrightarrow \bar{m}}^*) + \Theta(m < \bar{m})(B_{RP}(-k)_{m \leftrightarrow \bar{m}} - B_{RP}(k)^*)
\end{aligned}
\tag{A.2.35}$$

As we will see in next subsection, using these combinations, the rest of the divergent integrals can also be reduced to $B_{RP}(k)$.

Time-like k^μ : reduction of divergent integrals

We will begin with the case of time-like k^μ and move to the rest frame of k^μ i.e., set $k^\mu = (M, \vec{0})$.

Let us begin by evaluating

$$\begin{aligned}
B_{RP}(k) &= \mu^{4-d} \int \frac{d^d p}{(2\pi)^{d_i}} \int \frac{d^d q}{(2\pi)^{d_i}} \frac{1}{p^2 + m^2 - i\varepsilon} 2\pi i \delta_+(q^2 + \bar{m}^2) (2\pi)^d \delta^d(p - q - k) \\
&= \mu^{4-d} \int \frac{d^d p}{(2\pi)^{d_i}} \int \frac{d^{d-1} q}{(2\pi)^{d-1}(2\bar{\omega}_q)} \frac{1}{p^2 + m^2 - i\varepsilon} (2\pi)^d \delta^{d-1}(\vec{p} - \vec{q}) \delta(p^0 - \bar{\omega}_q - M) \\
&= \mu^{4-d} \int \frac{d^d p}{(2\pi)^{d_i}} \frac{1}{2\bar{\omega}_p} \frac{1}{p^2 + m^2 - i\varepsilon} 2\pi \delta(p^0 - \bar{\omega}_p - M) \\
&= \mu^{4-d} \int \frac{d^{d-1} p}{(2\pi)^{d-1} i} \frac{1}{2\bar{\omega}_p} \frac{1}{\omega_p^2 - (M + \bar{\omega}_p)^2 - i\varepsilon} \\
&= \frac{\mu^{4-d} \text{Vol}(\mathbb{S}^{d-2})}{2(2\pi)^{d-1} i} \int_{\bar{m}}^\infty d\bar{\omega}_p \frac{(\bar{\omega}_p^2 - \bar{m}^2)^{\frac{d-3}{2}}}{\omega_p^2 - (M + \bar{\omega}_p)^2 - i\varepsilon}
\end{aligned}
\tag{A.2.36}$$

We will now show how the rest of the one-loop integrals can be reduced to $B_{PR}(k)$ for time-like k^μ . We have

$$\begin{aligned}
B_{RL}(k) &\equiv \mu^{4-d} \int \frac{d^d p}{(2\pi)^{d_i}} \int \frac{d^d q}{(2\pi)^{d_i}} \frac{1}{p^2 + m^2 - i\varepsilon} \frac{-1}{q^2 + \bar{m}^2 + i\varepsilon} (2\pi)^d \delta^d(p - q - k) \\
&= -\mu^{4-d} \int \frac{d^d p}{(2\pi)^{d_i}} \frac{1}{p^2 + m^2 - i\varepsilon} \frac{1}{(p - k)^2 + \bar{m}^2 + i\varepsilon} \\
&= -\mu^{4-d} \int \frac{d^d p}{(2\pi)^{d_i}} \frac{1}{(\omega_p - i\varepsilon)^2 - (p^0)^2} \frac{1}{(\bar{\omega}_p + i\varepsilon)^2 - (p^0 - M)^2} \times e^{i\delta \frac{p^0}{M}}
\end{aligned}
\tag{A.2.37}$$

where in the last step, we have put ϵ, δ in different places to help in contour integration. Now we perform the contour integral by closing the contour in the upper half plane for $M > 0$ and in the lower half plane for $M < 0$. This gives

$$\begin{aligned}
B_{RL}(k) &= \mu^{4-d} \int \frac{d^{d-1}p}{(2\pi)^{d-1}i} \left(\frac{1}{\omega_p^2 - (|M| + \bar{\omega}_p)^2 - i\epsilon} \frac{1}{2\bar{\omega}_p} - \frac{1}{2\omega_p} \frac{1}{\bar{\omega}_p^2 - (|M| + \omega_p)^2 + i\epsilon} \right) \\
&= \frac{\mu^{4-d} \text{Vol}(\mathbb{S}^{d-2})}{2(2\pi)^{d-1}i} \left(\int_{\bar{m}}^{\infty} d\bar{\omega}_p \frac{(\bar{\omega}_p^2 - \bar{m}^2)^{\frac{d-3}{2}}}{\omega_p^2 - (|M| + \bar{\omega}_p)^2 - i\epsilon} - \int_m^{\infty} d\omega_p \frac{(\omega_p^2 - m^2)^{\frac{d-3}{2}}}{\bar{\omega}_p^2 - (|M| + \omega_p)^2 + i\epsilon} \right) \\
&= \Theta(k^0)[B_{RP}(k) + B_{ML}(k)] + \Theta(-k^0)[B_{RM}(k) + B_{PL}(k)] \\
&= \Theta(k^0) \left(B_{RP}(k) + [B_{RP}(k)]_{m \leftrightarrow \bar{m}}^* \right) + \Theta(-k^0) \left(B_{RP}(-k) + [B_{RP}(-k)]_{m \leftrightarrow \bar{m}}^* \right) \\
&= \Theta(k^0) B_{RL}^+(k) + \Theta(-k^0) B_{RL}^+(-k)
\end{aligned} \tag{A.2.38}$$

where we have used the definition given in equation(A.2.35). Next, we turn to

$$\begin{aligned}
B_{LR}(k) &\equiv \mu^{4-d} \int \frac{d^d p}{(2\pi)^{d_i}} \int \frac{d^d q}{(2\pi)^{d_i}} \frac{-1}{p^2 + m^2 + i\epsilon} \frac{1}{q^2 + \bar{m}^2 - i\epsilon} (2\pi)^d \delta^d(p - q - k) \\
&= B_{RL}(k)_{m \leftrightarrow \bar{m}} = \Theta(k^0)[B_{MR}(k) + B_{LP}(k)] + \Theta(-k^0)[B_{PR}(k) + B_{LM}(k)] \\
&= \Theta(k^0) \left(B_{RP}(k)_{m \leftrightarrow \bar{m}} + [B_{RP}(k)]^* \right) + \Theta(-k^0) \left(B_{RP}(-k)_{m \leftrightarrow \bar{m}} + [B_{RP}(-k)]^* \right) \\
&= \Theta(k^0)[B_{RL}^+(k)]^* + \Theta(-k^0)[B_{RL}^+(-k)]^*
\end{aligned} \tag{A.2.39}$$

We then look at

$$\begin{aligned}
B_{RR}(k) &= \mu^{4-d} \int \frac{d^d p}{(2\pi)^{d_i}} \int \frac{d^d q}{(2\pi)^{d_i}} \frac{1}{p^2 + m^2 - i\epsilon} \frac{1}{q^2 + \bar{m}^2 - i\epsilon} (2\pi)^d \delta^d(p + q - k) \\
&= \mu^{4-d} \int \frac{d^d p}{(2\pi)^d i^2} \frac{1}{p^2 + m^2 - i\epsilon} \frac{1}{(k-p)^2 + \bar{m}^2 - i\epsilon} \\
&= \mu^{4-d} \int \frac{d^d p}{(2\pi)^d i^2} \frac{1}{(\omega_p - i\epsilon)^2 - (p^0)^2} \frac{1}{(\bar{\omega}_p - i\epsilon)^2 - (p^0 - M)^2}
\end{aligned} \tag{A.2.40}$$

We want to now write the answer of the contour integral with a definite ϵ prescription. An examination of the sign of resulting ϵ 's shows that the form depends now on the sign of M as well as $m - \bar{m}$. A careful examination of ϵ 's give

$$\begin{aligned}
&B_{RR}(k) \\
&= \Theta(m > \bar{m}) \mu^{4-d} \int \frac{d^{d-1}p}{(2\pi)^{d-1}i} \left(\frac{1}{2\omega_p} \frac{1}{\bar{\omega}_p^2 - (|M| + \omega_p)^2 + i\epsilon} + \frac{1}{\omega_p^2 - (|M| - \bar{\omega}_p)^2 - i\epsilon} \frac{1}{2\bar{\omega}_p} \right) \\
&+ \Theta(m < \bar{m}) \mu^{4-d} \int \frac{d^{d-1}p}{(2\pi)^{d-1}i} \left(\frac{1}{2\omega_p} \frac{1}{\bar{\omega}_p^2 - (|M| - \omega_p)^2 - i\epsilon} + \frac{1}{\omega_p^2 - (|M| + \bar{\omega}_p)^2 + i\epsilon} \frac{1}{2\bar{\omega}_p} \right)
\end{aligned} \tag{A.2.41}$$

Transcribing it into B_{RP} integrals, we obtain

$$\begin{aligned}
& B_{RR}(k) \\
&= \Theta(k^0) \left\{ \Theta(m > \bar{m})(B_{RP}(-k) - B_{RP}(k)_{m \leftrightarrow \bar{m}}^*) + \Theta(m < \bar{m})(B_{RP}(-k)_{m \leftrightarrow \bar{m}} - B_{RP}(k)^*) \right\} \\
&\quad + \Theta(-k^0) \left\{ \Theta(m > \bar{m})(B_{RP}(k) - B_{RP}(-k)_{m \leftrightarrow \bar{m}}^*) + \Theta(m < \bar{m})(B_{RP}(k)_{m \leftrightarrow \bar{m}} - B_{RP}(-k)^*) \right\} \\
&= \Theta(k^0) B_{RR}^+(k) + \Theta(-k^0) B_{RR}^+(-k)
\end{aligned} \tag{A.2.42}$$

It follows that

$$\begin{aligned}
& B_{LL}(k) = B_{RR}(k)^* \\
&= \Theta(k^0) \left\{ \Theta(m > \bar{m})(B_{RP}(-k)^* - B_{RP}(k)_{m \leftrightarrow \bar{m}}) + \Theta(m < \bar{m})(B_{RP}(-k)_{m \leftrightarrow \bar{m}}^* - B_{RP}(k)) \right\} \\
&\quad + \Theta(-k^0) \left\{ \Theta(m > \bar{m})(B_{RP}(k)^* - B_{RP}(-k)_{m \leftrightarrow \bar{m}}) + \Theta(m < \bar{m})(B_{RP}(k)_{m \leftrightarrow \bar{m}}^* - B_{RP}(-k)) \right\} \\
&= \Theta(k^0) [B_{RR}^+(k)]^* + \Theta(-k^0) [B_{RR}^+(-k)]^*
\end{aligned} \tag{A.2.43}$$

We will now turn to the case of space-like k^μ to prove similar relations in that case.

Space-like k^μ : reduction of divergent integrals

We will study $B_{RP}(k)$ when k^μ is space-like. We set $k^\mu = \{0, Q = \sqrt{k^2}, \vec{0}_{d-2}\}$ where we can take $Q > 0$ without loss of generality.

$$\begin{aligned}
B_{RP}(k) &= \mu^{4-d} \int \frac{d^d p}{(2\pi)^{d_i}} \int \frac{d^d q}{(2\pi)^{d_i}} \frac{1}{p^2 + m^2 - i\varepsilon} 2\pi i \delta_+(q^2 + \bar{m}^2) (2\pi)^d \delta^d(p - q - k) \\
&= \mu^{4-d} \int \frac{d^d p}{(2\pi)^{d_i}} \int \frac{d^d q}{(2\pi)^{d_i}} \frac{1}{p^2 + m^2 - i\varepsilon} 2\pi i \delta_+(q^2 + \bar{m}^2) \\
&\quad \times (2\pi)^d \delta(p^0 - q^0) \delta(p_{\parallel} - q_{\parallel} - Q) \delta(p_{\perp} - q_{\perp}) \\
&= \mu^{4-d} \int \frac{d^{d-1} q}{(2\pi)^{d-1} i} \frac{1}{2\bar{\omega}_q} \frac{1}{q_{\perp}^2 + (Q + q_{\parallel})^2 + m^2 - \bar{\omega}_q^2 - i\varepsilon} \\
&= \mu^{4-d} \int \frac{d^{d-1} q}{(2\pi)^{d-1} i} \frac{1}{2\bar{\omega}_q} \frac{1}{m^2 - \bar{m}^2 + Q^2 + 2Qq_{\parallel} - i\varepsilon} \\
&= \frac{\mu^{4-d}}{4Q} \int \frac{d^{d-1} q}{(2\pi)^{d-1} i} \frac{1}{\bar{\omega}_q} \frac{1}{q_{\parallel}^* + q_{\parallel} - i\varepsilon}
\end{aligned} \tag{A.2.44}$$

where, we have defined

$$q_{\parallel}^* \equiv \frac{m^2 - \bar{m}^2 + Q^2}{2Q}.$$

Now, we move on to calculating $B_{RL}(k)$, given by

$$\begin{aligned}
B_{RL}(k) &= \mu^{4-d} \int \frac{d^d p}{(2\pi)^{d_i}} \int \frac{d^d q}{(2\pi)^{d_i}} \frac{1}{p^2 + m^2 - i\varepsilon} \frac{-1}{q^2 + \bar{m}^2 + i\varepsilon} (2\pi)^d \delta^d(p - q - k) \\
&= \mu^{4-d} \int \frac{d^d p}{(2\pi)^d} \frac{1}{p^2 + m^2 - i\varepsilon} \frac{1}{(p - k)^2 + \bar{m}^2 + i\varepsilon} \\
&= \mu^{4-d} \int \frac{d^d p}{(2\pi)^d} \frac{1}{\omega_p^2 - (p^0)^2 - i\varepsilon} \frac{1}{\bar{\omega}_{p_\perp}^2 + (Q - p_\parallel)^2 - (p^0)^2 + i\varepsilon} \\
&= \mu^{4-d} \int \frac{d^{d-1} p}{(2\pi)^{d-1} i} \left(-\frac{1}{2\omega_p} \frac{1}{\bar{m}^2 - m^2 + Q^2 - 2Qp_\parallel + i\varepsilon} \right. \\
&\quad \left. + \frac{1}{m^2 - \bar{m}^2 - Q^2 + 2Qp_\parallel - i\varepsilon} \frac{1}{2\bar{\omega}_{p-k}} \right)
\end{aligned} \tag{A.2.45}$$

Now, we take $p = -q$ in the first integral and $p = k + q$ for the second integral to write

$$\begin{aligned}
B_{RL}(k) &= \mu^{4-d} \int \frac{d^{d-1} q}{(2\pi)^{d-1} i} \left(-\frac{1}{2\omega_q} \frac{1}{\bar{m}^2 - m^2 + Q^2 + 2Qq_\parallel + i\varepsilon} \right. \\
&\quad \left. + \frac{1}{m^2 - \bar{m}^2 + Q^2 + 2Qq_\parallel - i\varepsilon} \frac{1}{2\bar{\omega}_q} \right) \\
&= B_{RP}(k)^*|_{m \leftrightarrow \bar{m}} + B_{RP}(k) = B_{RL}^+(k)
\end{aligned} \tag{A.2.46}$$

Similarly,

$$B_{LR}(k) = B_{RL}(k)_{m \leftrightarrow \bar{m}} = B_{RP}(k)|_{m \leftrightarrow \bar{m}} + B_{RP}(k)^* = [B_{RL}^+(k)]^* \tag{A.2.47}$$

Let us now do the $B_{RR}(k)$ integral for space-like k^μ :

$$\begin{aligned}
B_{RR}(k) &= \mu^{4-d} \int \frac{d^d p}{(2\pi)^{d_i}} \int \frac{d^d q}{(2\pi)^{d_i}} \frac{1}{p^2 + m^2 - i\varepsilon} \frac{1}{q^2 + \bar{m}^2 - i\varepsilon} (2\pi)^d \delta^d(p + q - k) \\
&= \mu^{4-d} \int \frac{d^d p}{(2\pi)^d} \frac{1}{i^2} \frac{1}{p^2 + m^2 - i\varepsilon} \frac{1}{(k - p)^2 + \bar{m}^2 - i\varepsilon} \\
&= \mu^{4-d} \int \frac{d^d p}{(2\pi)^d} \frac{1}{i^2} \frac{1}{\omega_p^2 - (p^0)^2 - i\varepsilon} \frac{1}{\bar{\omega}_{p_\perp}^2 + (Q - p_\parallel)^2 - (p^0)^2 - i\varepsilon} \\
&= \mu^{4-d} \int \frac{d^{d-1} p}{(2\pi)^{d-1} i} \left(\frac{1}{2\sqrt{\omega_{p_\perp}^2 + p_\parallel^2}} \frac{1}{\bar{m}^2 - m^2 + Q^2 - 2Qp_\parallel - i\varepsilon} \frac{1}{\text{sgn}(\bar{\omega}_{p_\perp} - \omega_{p_\perp})} \right. \\
&\quad \left. + \frac{1}{m^2 - \bar{m}^2 - Q^2 + 2Qp_\parallel - i\varepsilon} \frac{1}{\text{sgn}(\omega_{p_\perp} - \bar{\omega}_{p_\perp})} \frac{1}{2\sqrt{\bar{\omega}_{p_\perp}^2 + (Q - p_\parallel)^2}} \right)
\end{aligned} \tag{A.2.48}$$

Now, we take $p_{||} = -q_{||}$ in the first integral and $p_{||} = Q + q_{||}$ in the second, to get

$$\begin{aligned}
B_{RR}(k) &= \mu^{4-d} \int \frac{d^{d-1}q}{(2\pi)^{d-1}i} \left(\frac{1}{2\sqrt{\omega_{q_{\perp}}^2 + q_{||}^2}} \frac{1}{\bar{m}^2 - m^2 + Q^2 + 2Qq_{||} - i\varepsilon \operatorname{sgn}(\bar{\omega}_{p_{\perp}} - \omega_{p_{\perp}})} \right. \\
&\quad \left. + \frac{1}{m^2 - \bar{m}^2 + Q^2 + 2Qq_{||} - i\varepsilon \operatorname{sgn}(\omega_{q_{\perp}} - \bar{\omega}_{q_{\perp}})} \frac{1}{2\sqrt{\bar{\omega}_{q_{\perp}}^2 + q_{||}^2}} \right) \\
&= \Theta(m > \bar{m}) \mu^{4-d} \int \frac{d^{d-1}q}{(2\pi)^{d-1}i} \left(\frac{1}{m^2 - \bar{m}^2 + Q^2 - 2Qq_{||} - i\varepsilon} \frac{1}{2\bar{\omega}_q} \right. \\
&\quad \left. + \frac{1}{2\omega_q} \frac{1}{\bar{m}^2 - m^2 + Q^2 + 2Qq_{||} + i\varepsilon} \right) \\
&+ \Theta(m < \bar{m}) \mu^{4-d} \int \frac{d^{d-1}q}{(2\pi)^{d-1}i} \left(\frac{1}{2\omega_q} \frac{1}{\bar{m}^2 - m^2 + Q^2 - 2Qq_{||} - i\varepsilon} \right. \\
&\quad \left. + \frac{1}{m^2 - \bar{m}^2 + Q^2 + 2Qq_{||} + i\varepsilon} \frac{1}{2\bar{\omega}_q} \right) \\
&= \Theta(m > \bar{m})(B_{RP}(-k) - B_{RP}(k)_{m \leftrightarrow \bar{m}}^*) + \Theta(m < \bar{m})(B_{RP}(-k)_{m \leftrightarrow \bar{m}} - B_{RP}(k)^*) \\
&= B_{RR}^+(k)
\end{aligned} \tag{A.2.49}$$

Here, in the penultimate step, we have done some variable redefinitions to obtain an answer similar to the time-like case. We can finally compute

$$B_{LL}(k) = B_{RR}(k)^* = [B_{RR}^+(k)]^* . \tag{A.2.50}$$

Summary of divergent integrals

We can now put together various cases and write

$$\begin{aligned}
B_{RL}(k) &= \Theta(k^0)\Theta(-k^2)B_{RL}^+(k) + \Theta(-k^0)\Theta(-k^2)B_{RL}^+(-k) + \Theta(k^2)B_{RL}^+(k) \\
B_{LR}(k) &= \Theta(k^0)\Theta(-k^2)[B_{RL}^+(k)]^* + \Theta(-k^0)\Theta(-k^2)[B_{RL}^+(-k)]^* + \Theta(k^2)[B_{RL}^+(k)]^* \\
B_{RR}(k) &= \Theta(k^0)\Theta(-k^2)B_{RR}^+(k) + \Theta(-k^0)\Theta(-k^2)B_{RR}^+(-k) + \Theta(k^2)B_{RR}^+(k) \\
B_{LL}(k) &= \Theta(k^0)\Theta(-k^2)[B_{RR}^+(k)]^* + \Theta(-k^0)\Theta(-k^2)[B_{RR}^+(-k)]^* + \Theta(k^2)[B_{RR}^+(k)]^* .
\end{aligned} \tag{A.2.51}$$

where

$$\begin{aligned}
B_{RL}^+(k) &\equiv B_{RP}(k) + B_{ML}(k) = B_{RP}(k) + [B_{RP}(k)]_{m \leftrightarrow \bar{m}}^* \\
B_{RR}^+(k) &\equiv \Theta(m > \bar{m})(B_{RM}(k) - B_{ML}(k)) + \Theta(m < \bar{m})(B_{PR}(k) - B_{LP}(k)) \\
&= \Theta(m > \bar{m})(B_{RP}(-k) - B_{RP}(k)_{m \leftrightarrow \bar{m}}^*) + \Theta(m < \bar{m})(B_{RP}(-k)_{m \leftrightarrow \bar{m}} - B_{RP}(k)^*)
\end{aligned} \tag{A.2.52}$$

This is apart from the other divergent integrals :

$$\begin{aligned}
B_{RM}(k) &= B_{RP}(-k) , \\
B_{LP}(k) &= [B_{RP}(k)]^* , \quad B_{LM}(k) = [B_{RP}(-k)]^* , \\
B_{PR}(k) &= B_{RP}(-k)|_{m \leftrightarrow \bar{m}} , \quad B_{MR}(k) = B_{RP}(k)|_{m \leftrightarrow \bar{m}} , \\
B_{PL}(k) &= B_{RP}(-k)^*|_{m \leftrightarrow \bar{m}} , \quad B_{ML}(k) = B_{RP}(k)^*|_{m \leftrightarrow \bar{m}} .
\end{aligned} \tag{A.2.53}$$

We note that all these integrals can be written in terms of $B_{RP}(k)$ as advertised.

Reduction and identities due to largest time equations

A further reduction is possible using largest time equations and their concomitant cutting rules :

$$\begin{aligned}
B_{RR}(k) + B_{RL}(k) &= B_{RP}(k) + B_{RM}(k) \\
B_{LR}(k) + B_{LL}(k) &= B_{LP}(k) + B_{LM}(k) \\
B_{PR}(k) + B_{PL}(k) &= B_{PP}(k) + B_{MM}(k) \\
B_{MR}(k) + B_{ML}(k) &= B_{MP}(k) + B_{RM}(k)
\end{aligned} \tag{A.2.54}$$

From applying these identities, we can conclude that $\text{Re}[B_{RP}(k) + B_{RP}(-k)]$ and $\text{Im}[B_{RP}(k) - B_{RP}(-k)]$ is symmetric under $m \leftrightarrow \bar{m}$ exchange. Further, the real part(viz., the cut) of $B_{RP}(k)$ integral is given by

$$\begin{aligned}
B_{RP}(k) + B_{RP}(k)^* &= \text{Re } B_{RL}^+(k) \\
&= \frac{\text{Vol}(\mathbb{S}^{d-2})}{32\pi^2} \left[1 + 2 \left(\frac{m^2 + \bar{m}^2}{k^2} \right) + \left(\frac{m^2 - \bar{m}^2}{k^2} \right)^2 \right]^{\frac{d-3}{2}} \\
&\times \left\{ \Theta(k^2) \frac{1}{2\pi} \Gamma\left(\frac{3}{2} - \frac{d}{2}\right) \Gamma\left(\frac{d}{2} - \frac{1}{2}\right) \left(\frac{k^2}{(4\pi\mu)^2} \right)^{\frac{d-4}{2}} \right. \\
&\quad \left. + [\Theta(k^0) \Theta((\bar{m} - m)^2 + k^2) + \Theta(-k^0)] \Theta(-k^2) \left(\frac{-k^2}{(4\pi\mu)^2} \right)^{\frac{d-4}{2}} \right\}
\end{aligned} \tag{A.2.55}$$

These conditions in turn lead to the identities :

$$\begin{aligned}
B_{RP}(k) + B_{LP}(k) &= B_{MR}(k) + B_{ML}(k) \\
B_{RP}(k) + B_{LM}(k) &= B_{MR}(k) + B_{PL}(k) \\
B_{RP}(k) + B_{PR}(k) &= B_{RM}(k) + B_{MR}(k) \\
B_{PR}(k) + B_{PL}(k) &= B_{RM}(k) + B_{LM}(k) \\
B_{PR}(k) + B_{ML}(k) &= B_{RM}(k) + B_{LP}(k) \\
B_{LP}(k) + B_{PL}(k) &= B_{LM}(k) + B_{ML}(k)
\end{aligned} \tag{A.2.56}$$

From, these identities we get

$$\begin{aligned}
B_{RL}^+(k) &\equiv B_{RP}(k) + B_{ML}(k) = B_{RP}(k) + [B_{RP}(k)]_{m \leftrightarrow \bar{m}}^* \\
B_{RR}^+(k) &= B_{RP}(-k) - B_{RP}(k)_{m \leftrightarrow \bar{m}}^* = B_{RP}(-k)_{m \leftrightarrow \bar{m}} - B_{RP}(k)^*
\end{aligned} \tag{A.2.57}$$

which in turn obey

$$B_{RR}^+(k) + B_{RL}^+(k) = B_{RP}(k) + B_{RP}(-k) = B_{RP}(k) + B_{RM}(k) \tag{A.2.58}$$

Another implication is

$$\begin{aligned}
\text{Re } B_{RR}^+(k) &= \frac{\text{Vol}(\mathbb{S}^{d-2})}{32\pi^2} \left[1 + 2 \left(\frac{m^2 + \bar{m}^2}{k^2} \right) + \left(\frac{m^2 - \bar{m}^2}{k^2} \right)^2 \right]^{\frac{d-3}{2}} \\
&\times \frac{1}{2} [\Theta(k^0) - \Theta(-k^0)] \Theta(-(\bar{m} - m)^2 - k^2) \Theta(-k^2) \left(\frac{-k^2}{(4\pi\mu)^2} \right)^{\frac{d-4}{2}}
\end{aligned} \tag{A.2.59}$$

The following combination is symmetric under $m \leftrightarrow \bar{m}$ as well as $k \leftrightarrow -k$ exchange.

$$\begin{aligned}
&B_{RP}(k) + B_{RP}(k)^* + B_{PM}(k) \\
&= \frac{\text{Vol}(\mathbb{S}^{d-2})}{32\pi^2} \left[1 + 2 \left(\frac{m^2 + \bar{m}^2}{k^2} \right) + \left(\frac{m^2 - \bar{m}^2}{k^2} \right)^2 \right]^{\frac{d-3}{2}} \\
&\times \left\{ \Theta(k^2) \frac{1}{2\pi} \Gamma\left(\frac{3}{2} - \frac{d}{2}\right) \Gamma\left(\frac{d}{2} - 1\right) \left(\frac{k^2}{(4\pi\mu)^2} \right)^{\frac{d-4}{2}} \right. \\
&\quad \left. + \Theta(-k^2) \left(\frac{-k^2}{(4\pi\mu)^2} \right)^{\frac{d-4}{2}} \right\}
\end{aligned} \tag{A.2.60}$$

A.2.5 Evaluation of $B_{RP}(k)$

The basic integral $B_{RP}(k)$ has the following form on the time-like case :

$$\begin{aligned}
B_{RP}(k) &= \frac{\mu^{4-d} \text{Vol}(\mathbb{S}^{d-2})}{2(2\pi)^{d-1} i} \int_{\bar{m}}^{\infty} d\bar{\omega}_p \frac{(\bar{\omega}_p^2 - \bar{m}^2)^{\frac{d-3}{2}}}{\omega_p^2 - (M + \bar{\omega}_p)^2 - i\varepsilon} \\
&= \frac{\mu^{4-d} \text{Vol}(\mathbb{S}^{d-2})}{2(2\pi)^{d-1} i} \int_{\bar{m}}^{\infty} d\bar{\omega}_p \frac{(\bar{\omega}_p^2 - \bar{m}^2)^{\frac{d-3}{2}}}{2M(\bar{\omega}_p^* - \bar{\omega}_p) - i\varepsilon}
\end{aligned} \tag{A.2.61}$$

with

$$\bar{\omega}_p^* \equiv \frac{m^2 - \bar{m}^2 - M^2}{2M}.$$

The same integral in the space-like case takes the form

$$B_{RP}(k) = \frac{\mu^{4-d}}{2Q} \int \frac{d^{d-1}q}{(2\pi)^{d-1}i} \frac{1}{2\bar{\omega}_q} \frac{1}{q_{||}^* + q_{||} - i\varepsilon} \quad (\text{A.2.62})$$

where, we have defined

$$q_{||}^* \equiv \frac{m^2 - \bar{m}^2 + Q^2}{2Q}.$$

Our aim in this subsection is to evaluate these integrals and extract out the appropriate divergences.

Time-like k^μ : computation of divergences

We begin by setting $\bar{\omega}_p = \bar{m} \cosh \eta$ in the time-like case to get

$$\begin{aligned} B_{RP}(k) &= \frac{\mu^{4-d} \text{Vol}(\mathbb{S}^{d-2}) \bar{m}^{d-3}}{4M(2\pi)^{d-1} i} \int_0^\infty d\eta \frac{\sinh^{d-2} \eta}{\bar{\gamma} - \cosh \eta} \\ &= \frac{\text{Vol}(\mathbb{S}^{d-2}) \bar{m}}{32\pi^2} \frac{\bar{m}}{M} \left(\frac{\bar{m}^2}{4\pi\mu^2} \right)^{\frac{d-4}{2}} \int_0^\infty \frac{d\eta}{i\pi^{d/2-1}} \frac{\sinh^{d-2} \eta}{\bar{\gamma} - \cosh \eta} \end{aligned} \quad (\text{A.2.63})$$

where we have defined

$$\bar{\gamma} = \frac{\bar{\omega}_p^*}{\bar{m}} \equiv \frac{m^2 - \bar{m}^2 - M^2 - i\varepsilon}{2M\bar{m}}. \quad (\text{A.2.64})$$

Thus, we have reduced our analysis to the integral

$$F(\bar{\gamma}) \equiv \int_0^\infty \frac{d\eta}{i\pi^{d/2-1}} \frac{\sinh^{d-2} \eta}{\bar{\gamma} - \cosh \eta} \quad (\text{A.2.65})$$

This integral can then analyzed in detail to study the analytic structure of this integral. But, for our purposes, it is sufficient to extract the divergences.

For our computation of β function, we need to extract out the divergent part of these integrals.

Focusing on the large $\bar{\omega}_p$ contribution, we can approximate $B_{RP}(k)$ by

$$\begin{aligned} B_{RP}(k) &= \frac{\mu^{4-d} \text{Vol}(\mathbb{S}^{d-2})}{2(2\pi)^{d-1} i} \int_{\bar{m}}^\infty d\bar{\omega}_p (\bar{\omega}_p^2 - \bar{m}^2)^{\frac{d}{2}} \left[-\frac{1}{2M\bar{\omega}_p^4} + \frac{M^2 + \bar{m}^2 - m^2}{4M^2\bar{\omega}_p^5} + O(\bar{\omega}_p^{-6}) \right] \\ &= \frac{i}{128\pi^2} \frac{\Gamma\left(\frac{d+2}{2}\right)}{\Gamma\left(\frac{d-1}{2}\right)} \left(\frac{\bar{m}^2}{4\pi\mu^2} \right)^{\frac{d-4}{2}} \left\{ \frac{16\bar{m}}{3M} \Gamma\left(\frac{3-d}{2}\right) - \sqrt{\pi} \Gamma\left(\frac{4-d}{2}\right) \frac{M^2 + \bar{m}^2 - m^2}{M^2} + \dots \right\} \end{aligned} \quad (\text{A.2.66})$$

Near $d = 4$, this gives

$$B_{RP}(k) = \frac{i}{(4\pi)^2} \left\{ -\frac{16\bar{m}}{3M} + \frac{M^2 + \bar{m}^2 - m^2}{2M^2} \left[\frac{2}{d-4} + \ln\left(\frac{4\bar{m}^2}{4\pi\mu^2 e^{-\gamma_E}}\right) - \frac{1}{2} \right] + \dots \right\} \quad (\text{A.2.67})$$

so that

Space-like k^μ : computation of divergences

In this subsection, we will consider the space-like case and confirm that the divergence structure is same in the space-like case. Let us first get the real part of $B_{RP}(k)$, which is given by

$$B_{RP}(k) = \frac{\mu^{4-d} \text{Vol}(\mathbb{S}^{d-2})}{2(2\pi)^{d-1} i} \int_{\bar{m}}^{\infty} d\bar{\omega}_p \frac{(\bar{\omega}_p^2 - \bar{m}^2)^{\frac{d-3}{2}}}{2M(\bar{\omega}_p^* - \bar{\omega}_p) - i\varepsilon} \quad (\text{A.2.68})$$

$$\begin{aligned} B_{RP}(k) &= \frac{\mu^{4-d}}{2Q} \int \frac{d^{d-1}q}{(2\pi)^{d-1} i} \frac{1}{2\bar{\omega}_q} \frac{1}{q_{\parallel}^* + q_{\parallel} - i\varepsilon} \\ &= \frac{\mu^{4-d}}{4Q(2\pi)^{d-1} i} \int_{\bar{m}}^{\infty} d\bar{\omega}_{q_{\perp}} \bar{\omega}_{q_{\perp}} (\bar{\omega}_{q_{\perp}}^2 - \bar{m}^2)^{\frac{d-4}{2}} \int_{-\infty}^{\infty} dq_{\parallel} \frac{1}{\sqrt{\bar{\omega}_{q_{\perp}}^2 + q_{\parallel}^2}} \frac{1}{q_{\parallel}^* + q_{\parallel} - i\varepsilon} \end{aligned} \quad (\text{A.2.69})$$

where, we have defined

$$q_{\parallel}^* \equiv \frac{m^2 - \bar{m}^2 + Q^2}{2Q}.$$

Let us first get the real part of $B_{RP}(k)$, which is given by

$$\begin{aligned} &B_{RP}(k) \Big|_{\text{real part}} \\ &= \frac{\mu^{4-d}}{4Q(2\pi)^{d-1} i} \int_{\bar{m}}^{\infty} d\bar{\omega}_{q_{\perp}} \bar{\omega}_{q_{\perp}} (\bar{\omega}_{q_{\perp}}^2 - \bar{m}^2)^{\frac{d-4}{2}} \\ &\int_{-\infty}^{\infty} dq_{\parallel} \frac{1}{\sqrt{\bar{\omega}_{q_{\perp}}^2 + q_{\parallel}^2}} \left(\frac{1}{q_{\parallel}^* + q_{\parallel} - i\varepsilon} - \frac{1}{q_{\parallel}^* + q_{\parallel} + i\varepsilon} \right) \\ &= \frac{\mu^{4-d}}{4Q(2\pi)^{d-1} i} \int_{\bar{m}}^{\infty} d\bar{\omega}_{q_{\perp}} \bar{\omega}_{q_{\perp}} (\bar{\omega}_{q_{\perp}}^2 - \bar{m}^2)^{\frac{d-4}{2}} \int_{-\infty}^{\infty} dq_{\parallel} \frac{1}{\sqrt{\bar{\omega}_{q_{\perp}}^2 + q_{\parallel}^2}} 2\pi i \delta(q_{\parallel}^* + q_{\parallel}) \end{aligned} \quad (\text{A.2.70})$$

The above equation can easily be seen to be equal to $B_{PP}(k)$ for the space-like case in (A.2.22).

So, we have in the space-like case

$$B_{RP}(k) \Big|_{\text{real part}} = B_{PP}(k) \quad (\text{A.2.71})$$

Let us now get the imaginary part of $B_{RP}(k)$, which is also the divergent part. It is given by

$$B_{RP}(k) \Big|_{\text{imaginary part}} = \frac{i}{2(4\pi)^2} \frac{Q^2 + m^2 - \bar{m}^2}{Q^2} \left(\frac{2}{d-4} + \ln \frac{\bar{m}^2}{4\pi\mu^2 e^{-\gamma_E}} - 1 \right) + \dots \quad (\text{A.2.72})$$

when, $m = \bar{m}$, we get

$$B_{RP}(k) \Big|_{\text{imaginary part}} = \frac{i}{2(4\pi)^2} \left(\frac{2}{d-4} + \ln \frac{m^2}{4\pi\mu^2 e^{-\gamma_E}} - 1 \right) + \dots \quad (\text{A.2.73})$$

We see that these divergences are same as the time-like case.

Summary of divergences

We now summarize the divergences in various integrals. We start with

$$\text{div}[B_{RP}]_{\bar{m}s} = \frac{i}{(4\pi)^2} \frac{k^2 - \bar{m}^2 + m^2}{2k^2} \left[\frac{2}{d-4} + \ln\left(\frac{\bar{m}^2}{4\pi\mu^2 e^{-\gamma_E}}\right) \right] + \dots \quad (\text{A.2.74})$$

and

$$\begin{aligned} \text{div}[B_{RL}^+] &= \frac{i}{(4\pi)^2} \frac{m^2 - \bar{m}^2}{k^2} \left[\frac{2}{d-4} + \ln\left(\frac{m\bar{m}}{4\pi\mu^2 e^{-\gamma_E}}\right) \right] + \dots \\ \text{div}[B_{RR}^+] &= \frac{i}{(4\pi)^2} \left[\frac{2}{d-4} + \ln\left(\frac{m\bar{m}}{4\pi\mu^2 e^{-\gamma_E}}\right) \right] + \dots \end{aligned} \quad (\text{A.2.75})$$

Thus,

$$\begin{aligned} \text{div}[B_{RP}] &= \text{div}[B_{RM}] = \frac{i}{(4\pi)^2} \frac{k^2 - \bar{m}^2 + m^2}{2k^2} \left[\frac{2}{d-4} + \ln\left(\frac{\bar{m}^2}{4\pi\mu^2 e^{-\gamma_E}}\right) \right] \\ \text{div}[B_{PR}] &= \text{div}[B_{MR}] = \frac{i}{(4\pi)^2} \frac{k^2 + \bar{m}^2 - m^2}{2k^2} \left[\frac{2}{d-4} + \ln\left(\frac{m^2}{4\pi\mu^2 e^{-\gamma_E}}\right) \right] \\ \text{div}[B_{RL}] &= -\text{div}[B_{LR}] = \frac{i}{(4\pi)^2} \frac{m^2 - \bar{m}^2}{k^2} \left[\frac{2}{d-4} + \ln\left(\frac{m\bar{m}}{4\pi\mu^2 e^{-\gamma_E}}\right) \right] + \dots \\ \text{div}[B_{RR}] &= -\text{div}[B_{LL}] = \frac{i}{(4\pi)^2} \left[\frac{2}{d-4} + \ln\left(\frac{m\bar{m}}{4\pi\mu^2 e^{-\gamma_E}}\right) \right] + \dots \end{aligned} \quad (\text{A.2.76})$$

When $m = \bar{m}$, we can thus summarize the divergence of ‘quarter-cut’ integrals as

$$\begin{aligned} \text{div}[B_{RP}] &= \text{div}[B_{PR}] = \text{div}[B_{RM}] = \text{div}[B_{MR}] = \frac{i}{2(4\pi)^2} \left[\frac{2}{d-4} + \ln\left(\frac{m^2}{4\pi\mu^2 e^{-\gamma_E}}\right) \right] + \dots \\ \text{div}[B_{LP}] &= \text{div}[B_{PL}] = \text{div}[B_{LM}] = \text{div}[B_{ML}] = -\frac{i}{2(4\pi)^2} \left[\frac{2}{d-4} + \ln\left(\frac{m^2}{4\pi\mu^2 e^{-\gamma_E}}\right) \right] + \dots \end{aligned} \quad (\text{A.2.77})$$

This along with

$$\begin{aligned} \text{div}[B_{RR}] &= \frac{i}{(4\pi)^2} \left[\frac{2}{d-4} + \ln\left(\frac{m^2}{4\pi\mu^2 e^{-\gamma_E}}\right) - 1 \right] + \dots \\ \text{div}[B_{LL}] &= -\frac{i}{(4\pi)^2} \left[\frac{2}{d-4} + \ln\left(\frac{m^2}{4\pi\mu^2 e^{-\gamma_E}}\right) - 1 \right] + \dots \end{aligned} \quad (\text{A.2.78})$$

summarizes all the divergences needed in this work.

A.2.6 UV divergences and symmetry factors

In this subsection, we will collect the UV divergences of various B type diagrams for the convenience of the reader.

$$\text{div}[B_{RR}(k)] = \frac{i}{(4\pi)^2} \left[\frac{2}{d-4} + \ln\left(\frac{m^2}{4\pi\mu^2 e^{-\gamma_E}}\right) - 1 \right] \quad (\text{A.2.79a})$$

$$\text{div}[B_{LR}(k)] = 0 \quad (\text{A.2.79b})$$

$$\text{div}[B_{PP}(k)] = 0 \quad (\text{A.2.79c})$$

$$\text{div}[B_{PR}(k)] = \frac{1}{2}\text{div}[B_{RR}(k)] \quad (\text{A.2.79d})$$

Further, we have

$$\text{div}[B_{RR}] = \text{div}[B_{LL}]^* \quad (\text{A.2.80a})$$

$$\text{div}[B_{LR}] = \text{div}[B_{PM}]^* = \text{div}[B_{MP}] = \text{div}[B_{PP}] = 0 \quad (\text{A.2.80b})$$

$$\text{div}[B_{PR}] = \text{div}[B_{MR}] = \text{div}[B_{PL}]^* = \text{div}[B_{ML}]^* = \frac{1}{2}\text{div}[B_{RR}] \quad (\text{A.2.80c})$$

We also give below the symmetry factors of the corresponding diagrams in figure 3. The divergences given above along with the symmetry factors provides a quick way to write down appropriate β functions for the open QFT. In the ensuing figure 4 and figure 5, we tabulate a set of useful diagrammatic identities which relate the various SK loop integrals.

A.3 Passarino-Veltman diagrams in the average-difference basis

Let us now take a look at the Passarino-Veltman diagrams in average-difference basis. It's worth remembering here that only three out of the four propagators, in this basis, are non-vanishing: the ' d ' propagator vanishes. This means that we have lesser number of non-vanishing diagrams in this basis. As a matter of fact, some of the non-vanishing diagrams (in average-difference basis) do not diverge. All these facts add up to give only a few divergent one loop diagrams - only one A type and two B type integrals. Thus, computations for the beta functions greatly simplifies in this basis. We will not try to evaluate the PV integrals from scratch. We will express the integrals in the average-difference basis in terms of the integrals in the ϕ_R - ϕ_L basis and then, use the results from the previous sections to determine the former.

A.3.1 Passarino-Veltman A type integral in the average-difference basis

There are two A type PV integrals in this basis: A_a and $A_b = A_f$. Using the relations in equation (3.3.3) and equation (A.2.3)-(A.2.4), it's easy to check that we get

$$\begin{aligned}
 A_a &= \frac{1}{2}(A_R + A_L) = \frac{1}{(4\pi)^2} \left[\frac{2}{(d-4)} + \ln\left(\frac{m^2}{4\pi\mu^2 e^{-\gamma_E}}\right) - 1 \right] m^2 \\
 A_b &= A_R - A_M = 0 \\
 A_f &= A_R - A_P = 0
 \end{aligned}
 \tag{A.3.1}$$

A.3.2 Passarino-Veltman B type integral in the average-difference basis

There are six PV B type integrals in this basis: B_{aa} , B_{af} , B_{ab} , B_{bf} , B_{fb} and $B_{ff} = B_{bb}$. Using the relations given in equation (3.3.3), it is easy to check that

$$\begin{aligned}
 B_{aa} &= \frac{1}{4}(B_{RR} + B_{RL} + B_{LR} + B_{LL}) \\
 B_{af} &= \frac{1}{2}(B_{RR} - B_{RP} + B_{LR} - B_{LP}) \\
 B_{ab} &= \frac{1}{2}(B_{RR} - B_{RM} + B_{LR} - B_{LM}) \\
 B_{fb} &= B_{RR} - B_{RM} - B_{MR} + B_{MM} \\
 B_{bf} &= B_{RR} - B_{RL} - B_{LR} + B_{LL} \\
 B_{ff} &= B_{bb} = B_{RR} - B_{RM} - B_{MR} + B_{MP}
 \end{aligned}
 \tag{A.3.2}$$

To compute the divergences for the above-mentioned integrals, we use the results given in equations (A.2.79a)-(A.2.80c) in section A.2.6. So, we have

$$\begin{aligned}
 \text{div}[B_{aa}] &= 0 \\
 \text{div}[B_{af}] &= \frac{1}{2}\text{div}[B_{RR}] = \frac{i}{2(4\pi)^2} \left[\frac{2}{d-4} + \ln\left(\frac{m^2}{4\pi\mu^2 e^{-\gamma_E}}\right) - 1 \right] \\
 \text{div}[B_{ab}] &= \frac{1}{2}\text{div}[B_{RR}] = \frac{i}{2(4\pi)^2} \left[\frac{2}{d-4} + \ln\left(\frac{m^2}{4\pi\mu^2 e^{-\gamma_E}}\right) - 1 \right] \\
 \text{div}[B_{fb}] &= 0 \\
 \text{div}[B_{bf}] &= 0 \\
 \text{div}[B_{ff}] &= \text{div}[B_{bb}] = 0
 \end{aligned}
 \tag{A.3.3}$$

We shall use these results for the computations in section 3.3 and in the next section.

A.4 Computations in the average-difference basis

In section 3.3, we have already computed the beta functions for the Lindblad violating combinations in the average-difference basis and we found that it matches with our computations in the ϕ_R - ϕ_L basis. For the sake of completion, we calculate the beta function for rest of the mass terms and the rest of the coupling constants in this basis. This computation enables one to verify the beta functions computed in ϕ_R - ϕ_L basis. We shall start off by providing the set of Feynman rules in this basis.

The propagators in this basis are given in equation (3.3.3). The vertex factors in this basis are given by

| Vertex | Factor |
|---------------------|---|
| ϕ_d^3 | $\frac{(-i)}{4}(\text{Re } \lambda_3 - 3 \text{ Re } \sigma_3)(2\pi)^d \delta(\sum p)$ |
| ϕ_a^3 | $2(\text{Im } \lambda_3 + 3 \text{ Im } \sigma_3)(2\pi)^d \delta(\sum p)$ |
| $\phi_d^2 \phi_a$ | $\frac{1}{2}(\text{Im } \lambda_3 - \text{Im } \sigma_3)(2\pi)^d \delta(\sum p)$ |
| $\phi_d \phi_a^2$ | $(-i)(\text{Re } \lambda_3 + \text{Re } \sigma_3)(2\pi)^d \delta(\sum p)$ |
| ϕ_d^4 | $\frac{1}{8}(\text{Im } \lambda_4 - 4 \text{ Im } \sigma_4 - 3\lambda_\Delta)(2\pi)^d \delta(\sum p)$ |
| ϕ_a^4 | $2(\text{Im } \lambda_4 + 4 \text{ Im } \sigma_4 - 3\lambda_\Delta)(2\pi)^d \delta(\sum p)$ |
| $\phi_d^3 \phi_a$ | $\frac{(-i)}{4}(\text{Re } \lambda_4 - 2 \text{ Re } \sigma_4)(2\pi)^d \delta(\sum p)$ |
| $\phi_d \phi_a^3$ | $(-i)(\text{Re } \lambda_4 + 2 \text{ Re } \sigma_4)(2\pi)^d \delta(\sum p)$ |
| $\phi_d^2 \phi_a^2$ | $\frac{1}{2}(\text{Im } \lambda_4 + \lambda_\Delta)(2\pi)^d \delta(\sum p)$ |

A.4.1 Beta functions for the mass terms

In order to compute the beta functions of the masses $\text{Re } m^2$, $\text{Im } m^2$ and m_Δ^2 , we need to compute three different correlators. As usual, we omit all the finite terms which are irrelevant for beta function computation.

We have chosen the following three correlators:

ϕ_a^2 vertex

First we consider $\phi_a \rightarrow \phi_a$ via ϕ_a^2 vertex. There are three divergent one loop contribution, as depicted in the first row of the figure 9. The total contribution is given by

$$\begin{aligned}
& 2(\text{Im } m^2 - m_\Delta^2) + (2 \text{ diagrams}) \times 2(\text{Im } \lambda_3 + 3 \text{ Im } \sigma_3) \times (-i)(\text{Re } \lambda_3 + \text{Re } \sigma_3) \frac{i}{(4\pi)^2} \frac{1}{d-4} \\
& + \frac{1}{2} \times 2(\text{Im } \lambda_4 + 4 \text{ Im } \sigma_4 - 3\lambda_\Delta) \frac{\text{Re } m^2}{(4\pi)^2} \frac{2}{d-4}
\end{aligned} \tag{A.4.1}$$

where, the first term is from tree level contribution and the rest are from loop level. Thus, from equation (A.4.1), the beta function for $(\text{Im } m^2 - m_\Delta^2)$ is given by

$$\frac{d}{d\ln \mu} (\text{Im } m^2 - m_\Delta^2) = \frac{2}{(4\pi)^2} (\text{Im } \lambda_3 + 3 \text{ Im } \sigma_3) (\text{Re } \lambda_3 + \text{Re } \sigma_3) + \frac{\text{Re } m^2}{(4\pi)^2} (\text{Im } \lambda_4 + 4 \text{ Im } \sigma_4 - 3\lambda_\Delta) \tag{A.4.2}$$

$\phi_a\phi_d$ vertex

Next we consider $\phi_a \rightarrow \phi_a$ via $\phi_a\phi_d$ vertex. It has same divergent diagrams as that of (A.4.1), but with different vertex factors. The corresponding Feynman diagrams are depicted in the second row of the figure 9. The total contribution is given by

$$\begin{aligned}
& (-i)\text{Re } m^2 + (-i)(\text{Re } \lambda_3 + \text{Re } \sigma_3) \times (-i)(\text{Re } \lambda_3 + \text{Re } \sigma_3) \frac{i}{(4\pi)^2} \frac{1}{d-4} \\
& + 2(\text{Im } \lambda_3 + 3 \text{ Im } \sigma_3) \times \frac{1}{2} (\text{Im } \lambda_3 - \text{Im } \sigma_3) \frac{i}{(4\pi)^2} \frac{1}{d-4} \\
& + \frac{1}{2} \times (-i)(\text{Re } \lambda_4 + 2 \text{ Re } \sigma_4) \frac{\text{Re } m^2}{16\pi^2} \frac{2}{d-4}
\end{aligned} \tag{A.4.3}$$

Again, the first term is the tree level and the rest are the one loop contributions. Thus, from (A.4.3) the beta function for $(\text{Re } m^2)$ is as follows

$$\begin{aligned}
\frac{d}{d\ln \mu} \text{Re } m^2 &= \frac{1}{(4\pi)^2} (\text{Re } \lambda_3 + \text{Re } \sigma_3)^2 - \frac{1}{(4\pi)^2} (\text{Im } \lambda_3 + 3 \text{ Im } \sigma_3) (\text{Im } \lambda_3 - \text{Im } \sigma_3) \\
& + \frac{\text{Re } m^2}{(4\pi)^2} (\text{Re } \lambda_4 + 2 \text{ Re } \sigma_4)
\end{aligned} \tag{A.4.4}$$

ϕ_d^2 vertex

The Feynman diagrams for $\phi_a \rightarrow \phi_a$ via ϕ_d^2 vertex are depicted in the third row of the figure 9.

The tree level and one loop contributions are given by

$$\begin{aligned} & \frac{1}{2}(\text{Im } m^2 + m_\Delta^2) + (2 \text{ diagrams}) \times \frac{1}{2}(\text{Im } \lambda_3 - \text{Im } \sigma_3) \times (-i)(\text{Re } \lambda_3 + \text{Re } \sigma_3) \frac{i}{(4\pi)^2} \frac{1}{d-4} \\ & + \frac{1}{2} \times \frac{1}{2}(\text{Im } \lambda_4 + \lambda_\Delta) \frac{\text{Re } m^2}{16\pi^2} \frac{2}{d-4} \end{aligned} \quad (\text{A.4.5})$$

From this equation we obtain the beta function for $(\text{Im } m^2 + m_\Delta^2)$

$$\frac{d}{d\ln \mu}(\text{Im } m^2 + m_\Delta^2) = \frac{2}{(4\pi)^2}(\text{Im } \lambda_3 - \text{Im } \sigma_3)(\text{Re } \lambda_3 + \text{Re } \sigma_3) + \frac{\text{Re } m^2}{(4\pi)^2}(\text{Im } \lambda_4 + \lambda_\Delta) \quad (\text{A.4.6})$$

Final β function

The beta functions of m^2 ($= \text{Re } m^2 + i \text{Im } m^2$) and m_Δ^2 can be obtained from the equations (A.4.2), (A.4.4) and (A.4.6)

$$\begin{aligned} \frac{dm^2}{d\ln \mu} &= \frac{1}{(4\pi)^2}(\lambda_3 + \sigma_3^*)(\lambda_3 + \sigma_3 + 2i \text{Im } \sigma_3) + \frac{m^2}{(4\pi)^2} \left[\lambda_4 + 2\sigma_4 - i\lambda_\Delta \right] \\ \frac{dm_\Delta^2}{d\ln \mu} &= -\frac{4}{(4\pi)^2} \text{Im } \sigma_3 (\text{Re } \lambda_3 + \text{Re } \sigma_3) + \frac{2}{(4\pi)^2} \text{Re} \left[m^2(\lambda_\Delta + i\sigma_4) \right] \end{aligned} \quad (\text{A.4.7})$$

A.4.2 Beta functions for the cubic couplings

We have four cubic coupling constants and the corresponding vertices are ϕ_a^3 , $\phi_a^2\phi_d$, $\phi_a\phi_d^2$, ϕ_d^3 and we need to compute four correlators. In each case, we will keep only the divergent parts as before.

ϕ_a^3 vertex

The tree level and one loop Feynman diagram for $\phi_d \rightarrow \phi_d\phi_d$ via ϕ_a^3 vertex is depicted in the first row of the figure 10. These contributions are given by

$$\begin{aligned} & 2(\text{Im } \lambda_3 + 3 \text{Im } \sigma_3) \\ & + (3 \text{ channels}) \times 2(\text{Im } \lambda_3 + 3 \text{Im } \sigma_3) \times (-i)(\text{Re } \lambda_4 + 2 \text{Re } \sigma_4) \times \frac{i}{(4\pi)^2} \frac{1}{d-4} \\ & + (3 \text{ channels}) \times 2(\text{Im } \lambda_4 + 4 \text{Im } \sigma_4 - 3\lambda_\Delta) \times (-i)(\text{Re } \lambda_3 + \text{Re } \sigma_3) \times \frac{i}{(4\pi)^2} \frac{1}{d-4} \end{aligned} \quad (\text{A.4.8})$$

and from this equation we determine the beta function for $\text{Im } \lambda_3 + 3 \text{ Im } \sigma_3$

$$\begin{aligned} \frac{d}{d \ln \mu} (\text{Im } \lambda_3 + 3 \text{ Im } \sigma_3) &= \frac{3}{(4\pi)^2} (\text{Im } \lambda_3 + 3 \text{ Im } \sigma_3) (\text{Re } \lambda_4 + 2 \text{ Re } \sigma_4) \\ &+ \frac{3}{(4\pi)^2} (\text{Im } \lambda_4 + 4 \text{ Im } \sigma_4 - 3\lambda_\Delta) (\text{Re } \lambda_3 + \text{Re } \sigma_3) \end{aligned} \quad (\text{A.4.9})$$

$\phi_a^2 \phi_d$ **vertex**

Now we compute $\phi_d \rightarrow \phi_a \phi_a$ via $\phi_a^2 \phi_d$ vertex. The relevant tree level and one loop Feynman diagrams are shown in the second row of the figure 10 and these contributions are given by

$$\begin{aligned} &(-i)(\text{Re } \lambda_3 + \text{Re } \sigma_3) \\ &+ (3 \text{ diagrams}) \times (-i)(\text{Re } \lambda_3 + \text{Re } \sigma_3) \times (-i)(\text{Re } \lambda_4 + 2 \text{ Re } \sigma_4) \times \frac{i}{(4\pi)^2} \frac{1}{d-4} \\ &+ (1 \text{ diagram}) \times 2(\text{Im } \lambda_4 + 4 \text{ Im } \sigma_4 - 3\lambda_\Delta) \times \frac{1}{2}(\text{Im } \lambda_3 - \text{Im } \sigma_3) \times \frac{i}{(4\pi)^2} \frac{1}{d-4} \\ &+ (2 \text{ diagram}) \times \frac{1}{2}(\text{Im } \lambda_4 + \lambda_\Delta) \times 2(\text{Im } \lambda_3 + 3 \text{ Im } \sigma_3) \times \frac{i}{(4\pi)^2} \frac{1}{d-4} \end{aligned} \quad (\text{A.4.10})$$

This implies that the beta function for $(\text{Re } \lambda_3 + \text{Re } \sigma_3)$ is given by

$$\begin{aligned} \frac{d}{d \ln \mu} (\text{Re } \lambda_3 + \text{Re } \sigma_3) &= \frac{3}{(4\pi)^2} (\text{Re } \lambda_3 + \text{Re } \sigma_3) (\text{Re } \lambda_4 + 2 \text{ Re } \sigma_4) \\ &- \frac{1}{(4\pi)^2} (\text{Im } \lambda_4 + 4 \text{ Im } \sigma_4 - 3\lambda_\Delta) (\text{Im } \lambda_3 - \text{Im } \sigma_3) \\ &- \frac{2}{(4\pi)^2} (\text{Im } \lambda_4 + \lambda_\Delta) (\text{Im } \lambda_3 + 3 \text{ Im } \sigma_3) \end{aligned} \quad (\text{A.4.11})$$

$\phi_a \phi_d^2$ **vertex**

The contribution (upto one loop) to $\phi_a \rightarrow \phi_a \phi_a$ via $\phi_a \phi_d^2$ vertex is given by

$$\begin{aligned} &\frac{1}{2}(\text{Im } \lambda_3 - \text{Im } \sigma_3) \\ &+ (3 \text{ diagrams}) \times (-i)(\text{Re } \lambda_3 + \text{Re } \sigma_3) \times \frac{1}{2}(\text{Im } \lambda_4 + \lambda_\Delta) \times \frac{i}{(4\pi)^2} \frac{1}{d-4} \\ &+ (2 \text{ diagrams}) \times (-i)(\text{Re } \lambda_4 + 2 \text{ Re } \sigma_4) \times \frac{1}{2}(\text{Im } \lambda_3 - \text{Im } \sigma_3) \times \frac{i}{(4\pi)^2} \frac{1}{d-4} \\ &+ \frac{(-i)}{4} (\text{Re } \lambda_4 - 2 \text{ Re } \sigma_4) \times 2(\text{Im } \lambda_3 + 3 \text{ Im } \sigma_3) \times \frac{i}{(4\pi)^2} \frac{1}{d-4} \end{aligned} \quad (\text{A.4.12})$$

The corresponding Feynman diagram can be found in the third row of the figure 10. Hence the beta function for $(\text{Im } \lambda_3 - \text{Im } \sigma_3)$ is as follows

$$\begin{aligned} \frac{d}{d\ln \mu}(\text{Im } \lambda_3 - \text{Im } \sigma_3) &= \frac{3}{(4\pi)^2}(\text{Re } \lambda_3 + \text{Re } \sigma_3)(\text{Im } \lambda_4 + \lambda_\Delta) \\ &+ \frac{2}{(4\pi)^2}(\text{Re } \lambda_4 + 2 \text{Re } \sigma_4)(\text{Im } \lambda_3 - \text{Im } \sigma_3) \\ &+ \frac{1}{(4\pi)^2}(\text{Re } \lambda_4 - 2 \text{Re } \sigma_4)(\text{Im } \lambda_3 + 3 \text{Im } \sigma_3) \end{aligned} \quad (\text{A.4.13})$$

ϕ_d^3 vertex

The tree level and the one loop Feynman diagrams for $\phi_a \rightarrow \phi_a \phi_a$ via ϕ_d^3 vertex is depicted in the fourth row of the figure 10 and the contribution from these diagrams are given by

$$\begin{aligned} &\frac{-i}{4}(\text{Re } \lambda_3 - 3 \text{Re } \sigma_3) \\ &+ (3 \text{ channels}) \times (-i)(\text{Re } \lambda_3 + \text{Re } \sigma_3) \times \frac{(-i)}{4}(\text{Re } \lambda_4 - 2 \text{Re } \sigma_4) \times \frac{i}{(4\pi)^2} \frac{1}{d-4} \\ &+ (3 \text{ channels}) \times \frac{1}{2}(\text{Im } \lambda_4 + \lambda_\Delta) \times \frac{1}{2}(\text{Im } \lambda_3 - \text{Im } \sigma_3) \times \frac{i}{(4\pi)^2} \frac{1}{d-4} \end{aligned} \quad (\text{A.4.14})$$

which leads to the following beta function for $(\text{Re } \lambda_3 - 3 \text{Re } \sigma_3)$

$$\begin{aligned} \frac{d}{d\ln \mu}(\text{Re } \lambda_3 - 3 \text{Re } \sigma_3) &= \frac{3}{(4\pi)^2}(\text{Re } \lambda_3 + \text{Re } \sigma_3)(\text{Re } \lambda_4 - 2 \text{Re } \sigma_4) \\ &- \frac{3}{(4\pi)^2}(\text{Im } \lambda_4 + \lambda_\Delta)(\text{Im } \lambda_3 - \text{Im } \sigma_3) \end{aligned} \quad (\text{A.4.15})$$

Final β function

From the equations (A.4.9), (A.4.11), (A.4.13) and (A.4.15) we can compute the beta functions of λ_3, σ_3

$$\begin{aligned} \frac{d\lambda_3}{d\ln \mu} &= \frac{3}{(4\pi)^2} \left[\lambda_4(\lambda_3 + \sigma_3) + \sigma_4(\lambda_3 + \sigma_3^*) + i\lambda_\Delta(\sigma_3 - \sigma_3^*) \right] \\ \frac{d\sigma_3}{d\ln \mu} &= \frac{1}{(4\pi)^2} \left[(\lambda_4 + 2\sigma_4^*)(\sigma_3 - \sigma_3^*) + \sigma_4(\lambda_3^* + 2\lambda_3 + 3\sigma_3) - i\lambda_\Delta(\lambda_3^* + 2\lambda_3 + 3\sigma_3^*) \right] \end{aligned} \quad (\text{A.4.16})$$

A.4.3 Beta functions for the quartic couplings

In this subsection we compute the beta functions for the quartic couplings in the average-difference basis. There are five different quartic coupling constants: these are the coupling constants multiplying the operators $\phi_a^4, \phi_a^3 \phi_d, \phi_a^2 \phi_d^2, \phi_a \phi_d^3, \phi_d^4$. For all these couplings there are two distinct

divergent diagrams (similar to the cubic coupling constants). As in the last subsection, we keep only the divergent terms from the one loop contributions.

ϕ_a^4 vertex

We start by computing $\phi_d\phi_d \rightarrow \phi_d\phi_d$ via ϕ_a^4 vertex. The Feynman diagrams are depicted in the first row of the figure 11 and the corresponding contributions are given by

$$\begin{aligned}
& 2(\text{Im } \lambda_4 + 4 \text{ Im } \sigma_4 - 3\lambda_\Delta) \\
& + (2 \text{ diagrams})(3 \text{ channels}) \times 2(\text{Im } \lambda_4 + 4 \text{ Im } \sigma_4 - 3\lambda_\Delta) \times (-i)(\text{Re } \lambda_4 + 2 \text{ Re } \sigma_4) \times \frac{i}{32\pi^2} \frac{2}{d-4} \\
& = 2(\text{Im } \lambda_4 + 4 \text{ Im } \sigma_4 - 3\lambda_\Delta) + 2(\text{Im } \lambda_4 + 4 \text{ Im } \sigma_4 - 3\lambda_\Delta) \times (\text{Re } \lambda_4 + 2 \text{ Re } \sigma_4) \times \frac{6}{(4\pi)^2} \frac{1}{d-4}
\end{aligned} \tag{A.4.17}$$

Thus the beta function for $(\text{Im } \lambda_4 + 4 \text{ Im } \sigma_4 - 3\lambda_\Delta)$ is given by

$$\frac{d}{d\ln \mu} (\text{Im } \lambda_4 + 4 \text{ Im } \sigma_4 - 3\lambda_\Delta) = \frac{6}{(4\pi)^2} (\text{Im } \lambda_4 + 4 \text{ Im } \sigma_4 - 3\lambda_\Delta) (\text{Re } \lambda_4 + 2 \text{ Re } \sigma_4) \tag{A.4.18}$$

$\phi_a^3\phi_d$ vertex

Next we compute $\phi_d\phi_d \rightarrow \phi_a\phi_d$ via $\phi_a^3\phi_d$ vertex, which is depicted in the second row of the figure 11. The tree level and one loop contributions from these Feynman diagrams are given by

$$\begin{aligned}
& \frac{d}{d\ln \mu} (\text{Re } \lambda_4 + 2 \text{ Re } \sigma_4) + (3 \text{ channels}) \times 2(\text{Im } \lambda_4 + 4 \text{ Im } \sigma_4 - 3\lambda_\Delta) \times \frac{1}{2}(\text{Im } \lambda_4 + \lambda_\Delta) \times \frac{i}{32\pi^2} \frac{2}{d-4} \\
& + (3 \text{ channels}) \times (-i)(\text{Re } \lambda_4 + 2 \text{ Re } \sigma_4) \times (-i)(\text{Re } \lambda_4 + 2 \text{ Re } \sigma_4) \times \frac{i}{32\pi^2} \frac{2}{d-4} \\
& = (-i)(\text{Re } \lambda_4 + 2 \text{ Re } \sigma_4) + i(\text{Im } \lambda_4 + 4 \text{ Im } \sigma_4 - 3\lambda_\Delta)(\text{Im } \lambda_4 + \lambda_\Delta) \frac{3}{(4\pi)^2} \frac{1}{d-4} \\
& \quad - i(\text{Re } \lambda_4 + 2 \text{ Re } \sigma_4)^2 \times \frac{3}{(4\pi)^2} \frac{1}{d-4}
\end{aligned} \tag{A.4.19}$$

we can determine the beta function for $(\text{Re } \lambda_4 + 2 \text{ Re } \sigma_4)$ -

$$\frac{d}{d\ln \mu} (\text{Re } \lambda_4 + 2 \text{ Re } \sigma_4) = \frac{3}{(4\pi)^2} \left[(\text{Re } \lambda_4 + 2 \text{ Re } \sigma_4)^2 - (\text{Im } \lambda_4 + 4 \text{ Im } \sigma_4 - 3\lambda_\Delta)(\text{Im } \lambda_4 + \lambda_\Delta) \right] \tag{A.4.20}$$

$\phi_a^2 \phi_d^2$ vertex

The tree level and one loop Feynman diagrams for $\phi_a \phi_a \rightarrow \phi_a \phi_a$ via $\phi_a^2 \phi_d^2$ vertex, which is depicted in the third row of the figure 11, contributes as follows

$$\begin{aligned}
& \frac{1}{2}(\text{Im } \lambda_4 + \lambda_\Delta) \\
& + (3 \text{ channels}) \times \frac{1}{2}(\text{Im } \lambda_4 + \lambda_\Delta) \times (-i)(\text{Re } \lambda + 2 \text{ Re } \sigma_4) \times \frac{i}{32\pi^2} \frac{2}{d-4} \\
& + (2 \text{ channels}) \times \frac{1}{2}(\text{Im } \lambda_4 + \lambda_\Delta) \times (-i)(\text{Re } \lambda_4 + 2 \text{ Re } \sigma_4) \times \frac{i}{32\pi^2} \frac{2}{d-4} \\
& + 2(\text{Im } \lambda_4 + 4 \text{ Im } \sigma_4 - 3\lambda_\Delta) \times \frac{(-i)}{4}(\text{Re } \lambda_4 - 2 \text{ Re } \sigma_4) \times \frac{i}{32\pi^2} \frac{2}{d-4} \\
& = \frac{1}{2}(\text{Im } \lambda_4 + \lambda_\Delta) + (\text{Im } \lambda_4 + \lambda_\Delta)(\text{Re } \lambda_4 + 2 \text{ Re } \sigma_4) \frac{5}{2(4\pi)^2} \frac{1}{d-4} \\
& \quad + (\text{Im } \lambda_4 + 4 \text{ Im } \sigma_4 - 3\lambda_\Delta)(\text{Re } \lambda_4 - 2 \text{ Re } \sigma_4) \frac{1}{2(4\pi)^2} \frac{1}{d-4}
\end{aligned} \tag{A.4.21}$$

From this equation we evaluate the beta function for $(\text{Im } \lambda_4 + \lambda_\Delta)$,

$$\begin{aligned}
\frac{d}{d \ln \mu} (\text{Im } \lambda_4 + \lambda_\Delta) = \frac{1}{(4\pi)^2} \left[5(\text{Im } \lambda_4 + \lambda_\Delta)(\text{Re } \lambda_4 + 2 \text{ Re } \sigma_4) \right. \\
\left. + (\text{Im } \lambda_4 + 4 \text{ Im } \sigma_4 - 3\lambda_\Delta)(\text{Re } \lambda_4 - 2 \text{ Re } \sigma_4) \right]
\end{aligned} \tag{A.4.22}$$

$\phi_a \phi_d^3$ vertex

Here we determine the tree level and one loop contribution to $\phi_a \phi_a \rightarrow \phi_a \phi_a$ via $\phi_a \phi_d^3$ vertex. The Feynman diagrams can be found in the fourth row in figure 11 and the corresponding contributions are

$$\begin{aligned}
& \frac{(-i)}{4}(\text{Re } \lambda_4 - 2 \text{ Re } \sigma_4) \\
& + (3 \text{ channels}) \times \frac{1}{2}(\text{Im } \lambda_4 + \lambda_\Delta) \times \frac{1}{2}(\text{Im } \lambda_4 + \lambda_\Delta) \times \frac{i}{32\pi^2} \frac{2}{d-4} \\
& + (3 \text{ channels}) \times \frac{(-i)}{4}(\text{Re } \lambda_4 - 2 \text{ Re } \sigma_4) \times (-i)(\text{Re } \lambda_4 + 2 \text{ Re } \sigma_4) \times \frac{i}{32\pi^2} \frac{2}{d-4} \\
& = \frac{(-i)}{4}(\text{Re } \lambda_4 - 2 \text{ Re } \sigma_4) + i(\text{Im } \lambda_4 + \lambda_\Delta)^2(\text{Re } \lambda_4 + 2 \text{ Re } \sigma_4) \frac{3}{4(4\pi)^2} \frac{1}{d-4} \\
& \quad - i(\text{Re } \lambda_4 - 2 \text{ Re } \sigma_4)(\text{Re } \lambda_4 + 2 \text{ Re } \sigma_4) \frac{3}{4(4\pi)^2} \frac{1}{d-4}
\end{aligned} \tag{A.4.23}$$

The beta function for $(\text{Re } \lambda_4 - 2 \text{ Re } \sigma_4)$ is given by

$$\frac{d}{d \ln \mu} (\text{Re } \lambda_4 - 2 \text{ Re } \sigma_4) = \frac{3}{(4\pi)^2} \left[(\text{Re } \lambda_4 - 2 \text{ Re } \sigma_4)(\text{Re } \lambda_4 + 2 \text{ Re } \sigma_4) - (\text{Im } \lambda_4 + \lambda_\Delta)^2 \right] \tag{A.4.24}$$

ϕ_d^4 vertex

The last computation of this section is $\phi_a\phi_a \rightarrow \phi_a\phi_a$ via ϕ_d^4 vertex, which is depicted in the fifth row in figure 11. The tree level and one loop contribution to this process is given by

$$\begin{aligned} & \frac{1}{8}(\text{Im } \lambda_4 - 4 \text{ Im } \sigma_4 - 3\lambda_\Delta) \\ & + (2 \text{ diagrams})(3 \text{ channels}) \times \frac{1}{2}(\text{Im } \lambda_4 + \lambda_\Delta) \times \frac{(-i)}{4}(\text{Re } \lambda_4 - 2 \text{ Re } \sigma_4) \times \frac{i}{32\pi^2} \frac{2}{d-4} \quad (\text{A.4.25}) \\ & = \frac{1}{8}(\text{Im } \lambda_4 - 4 \text{ Im } \sigma_4 - 3\lambda_\Delta) + (\text{Im } \lambda_4 + \lambda_\Delta) \times (\text{Re } \lambda_4 - 2 \text{ Re } \sigma_4) \times \frac{3}{4(4\pi)^2} \frac{1}{d-4} \end{aligned}$$

this equation determines the the beta function for $(\text{Im } \lambda_4 - 4 \text{ Im } \sigma_4 - 3\lambda_\Delta)$ and it is given by

$$\frac{d}{d\ln \mu}(\text{Im } \lambda_4 - 4 \text{ Im } \sigma_4 - 3\lambda_\Delta) = \frac{6}{(4\pi)^2}(\text{Im } \lambda_4 + \lambda_\Delta) \times (\text{Re } \lambda_4 - 2 \text{ Re } \sigma_4) \quad (\text{A.4.26})$$

Final β functions

From the five equations - (A.4.18), (A.4.20), (A.4.22), (A.4.24) and (A.4.26) we can determine the beta functions of $\lambda_4 (= \text{Re } \lambda_4 + i \text{ Im } \lambda_4)$, $\sigma_4 (= \text{Re } \sigma_4 + i \text{ Im } \sigma_4)$ and λ_Δ and they are given by

$$\begin{aligned} \frac{d\lambda_4}{d\ln \mu} &= \frac{3}{(4\pi)^2} \left[\lambda_4^2 + 2 \sigma_4(\lambda_4 + i\lambda_\Delta) + \lambda_\Delta^2 \right] = \frac{3}{(4\pi)^2}(\lambda_4 + 2 \sigma_4 - i\lambda_\Delta)(\lambda_4 + i\lambda_\Delta) \\ \frac{d\sigma_4}{d\ln \mu} &= \frac{3}{(4\pi)^2} \left[\sigma_4^2 + (\lambda_4 + \sigma_4^*)(\sigma_4 - i\lambda_\Delta) + \lambda_\Delta^2 \right] = \frac{3}{(4\pi)^2}(\lambda_4 + \sigma_4 + \sigma_4^* + i\lambda_\Delta)(\sigma_4 - i\lambda_\Delta) \\ \frac{d\lambda_\Delta}{d\ln \mu} &= \frac{1}{(4\pi)^2 i} \left[\lambda(\sigma_4^* + i\lambda_\Delta) - 2\sigma_4^2 + 5i\sigma_4\lambda_\Delta - \lambda_4^*(\sigma_4 - i\lambda_\Delta) + 2(\sigma_4^*)^2 + 5i\sigma_4^*\lambda_\Delta \right] \quad (\text{A.4.27}) \\ &= \frac{1}{(4\pi)^2 i} \left[(\lambda_4 + 2\sigma_4^*)(\sigma_4^* + i\lambda_\Delta) + 3i\sigma_4\lambda_\Delta - c.c. \right] \end{aligned}$$

A.5 Tadpoles

In this appendix we compute various one loop tadpoles in this theory.

ϕ_R 1 loop tadpole The Feynman diagrams contributing to one loop tadpole of ϕ_R is being drawn in figure 12. The sum of the contribution from all the Feynman diagrams is given by

$$i\mathcal{M} = +\frac{(-i\lambda_3)}{2}A_R + \frac{(i\sigma_3^*)}{2}A_L + (-i\sigma_3)A_M \quad (\text{A.5.1})$$

Now using result from appendix A.2 we get the following divergent contribution

$$= \frac{-i\text{Re} [m^2]}{(4\pi)^2} \left[\frac{\lambda_3 - \sigma_3^* + 2\sigma_3}{2} \right] \left(\frac{2}{d-4} + \ln \frac{m^2}{4\pi\mu^2 e^{-\gamma_E}} - 1 \right) \quad (\text{A.5.2})$$

This can be removed a counter term of the form

$$\kappa = \frac{-i\text{Re}[m^2]}{(4\pi)^2} \left[\frac{\text{Re}\lambda_3 + \text{Re}\sigma_3 + i(\text{Im}\lambda_3 + 3\text{Im}\sigma_3)}{2} \right] \left(\frac{2}{d-4} + \ln \frac{m^2}{4\pi\mu^2 e^{-\gamma_E}} - 1 \right) \quad (\text{A.5.3})$$

Checking lindblad condition Now we want to check whether the counter terms that were added to remove the tadpoles satisfy the Lindblad condition or not.

$$i[\kappa - a\kappa^*] = \frac{-1}{(4\pi)^2} [\text{Im}\lambda_3 + 3\text{Im}\sigma_3] \left(\frac{2}{d-4} + \ln \frac{m^2}{4\pi\mu^2 e^{-\gamma_E}} - 1 \right) \text{Re}[m^2] \quad (\text{A.5.4})$$

So, the counter-terms obey Lindblad condition if there is no Lindblad violating cubic couplings.

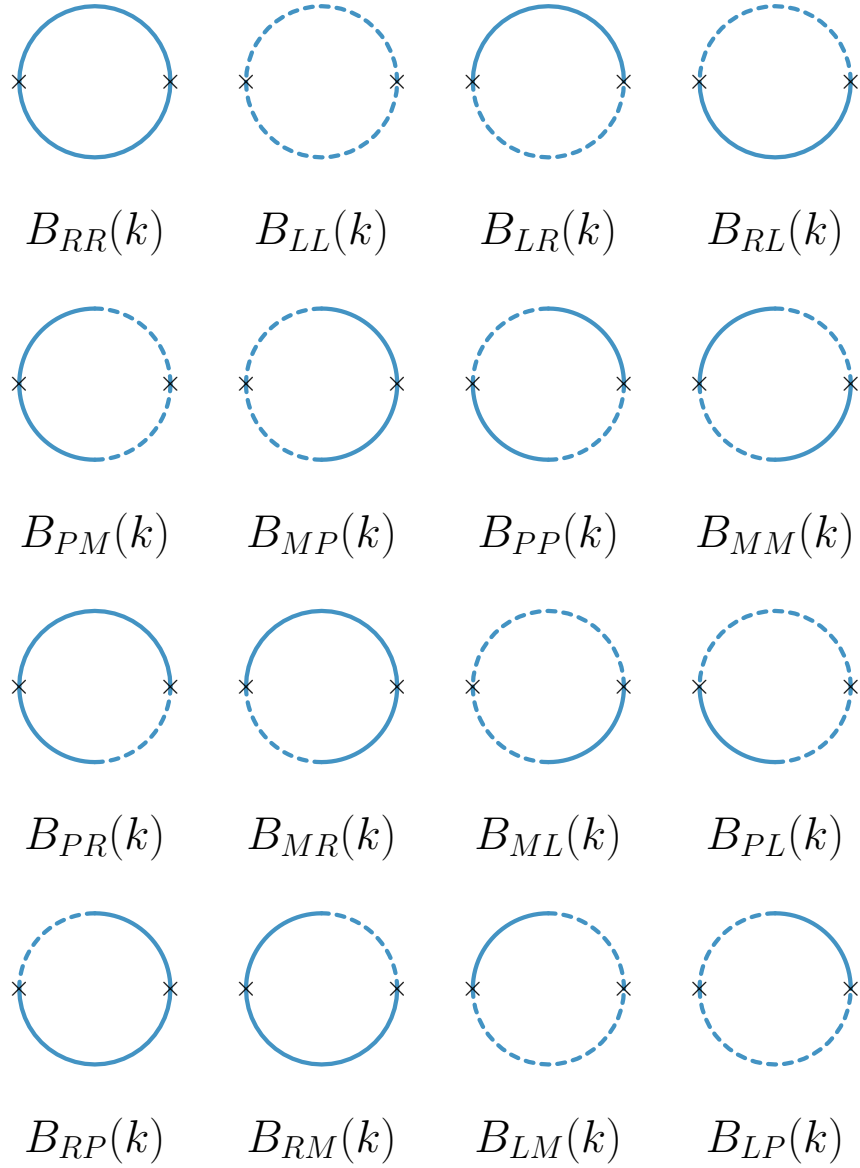


Figure 2: PV one loop B type integrals in SK theory. The momentum and mass corresponding to the lower propagator is denoted by p^μ and m respectively, whereas the momentum and mass corresponding to the upper propagator are q^μ and \bar{m} respectively. The momenta p and q are taken to flow anti-clockwise in the loop.

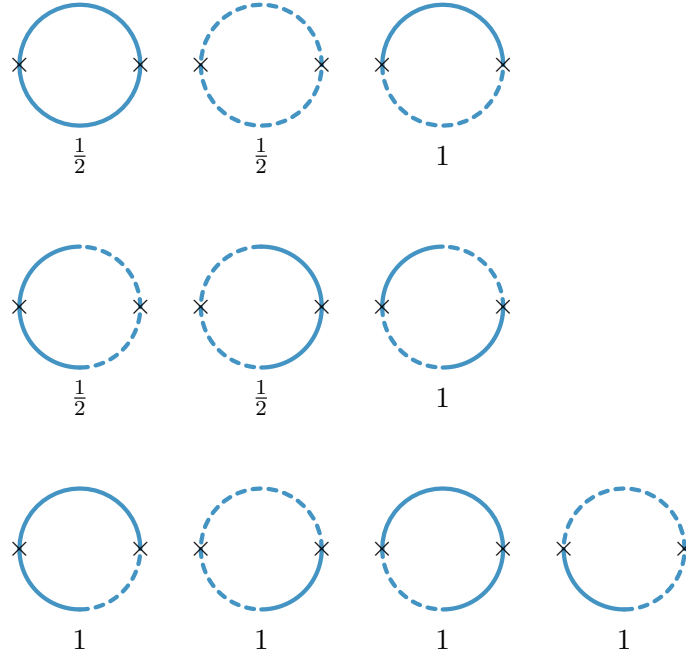


Figure 3: Symmetry factors for all the ten one loop integrals

$$\begin{aligned}
 & \begin{array}{c} \text{Solid circle} \\ B_{RR}(k) \end{array} + \begin{array}{c} \text{Dashed circle} \\ B_{LL}(k) \end{array} + 2 \begin{array}{c} \text{Dashed circle} \\ 2B_{LR}(k) \end{array} \\
 &= \begin{array}{c} \text{Dashed circle} \\ B_{PM}(k) \end{array} + \begin{array}{c} \text{Solid circle} \\ B_{MP}(k) \end{array} + 2 \begin{array}{c} \text{Solid circle} \\ 2B_{PP}(k) \end{array}
 \end{aligned}$$

Figure 4: Cutting identity of one loop integrals

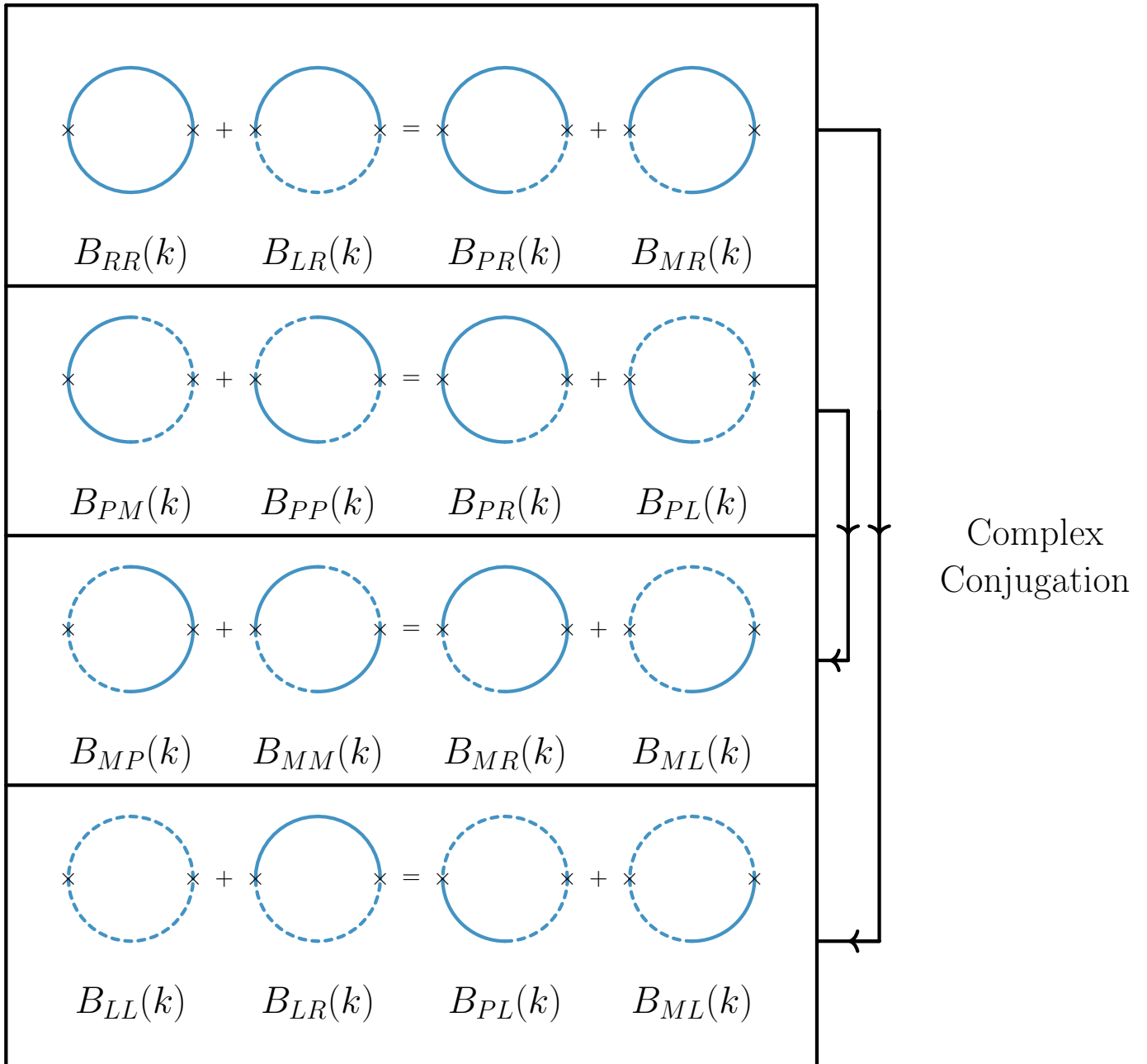
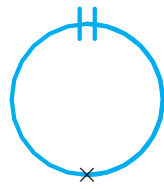
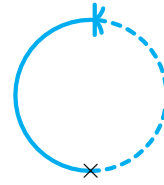


Figure 5: Identities between the ten one loop B type integrals

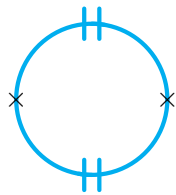


$$A_a$$

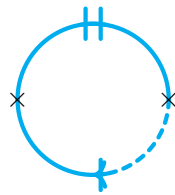


$$A_b = A_f = 0$$

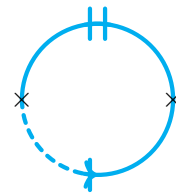
Figure 6: PV one loop A type integrals in the average-difference basis



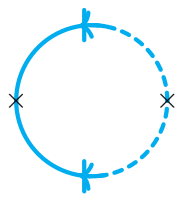
$$B_{aa}$$



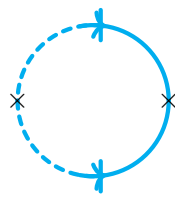
$$B_{ab}$$



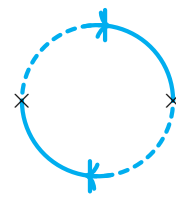
$$B_{af}$$



$$B_{bf}$$



$$B_{fb}$$



$$B_{ff} = B_{bb} = 0$$

Figure 7: PV one loop B type integrals in the average-difference basis

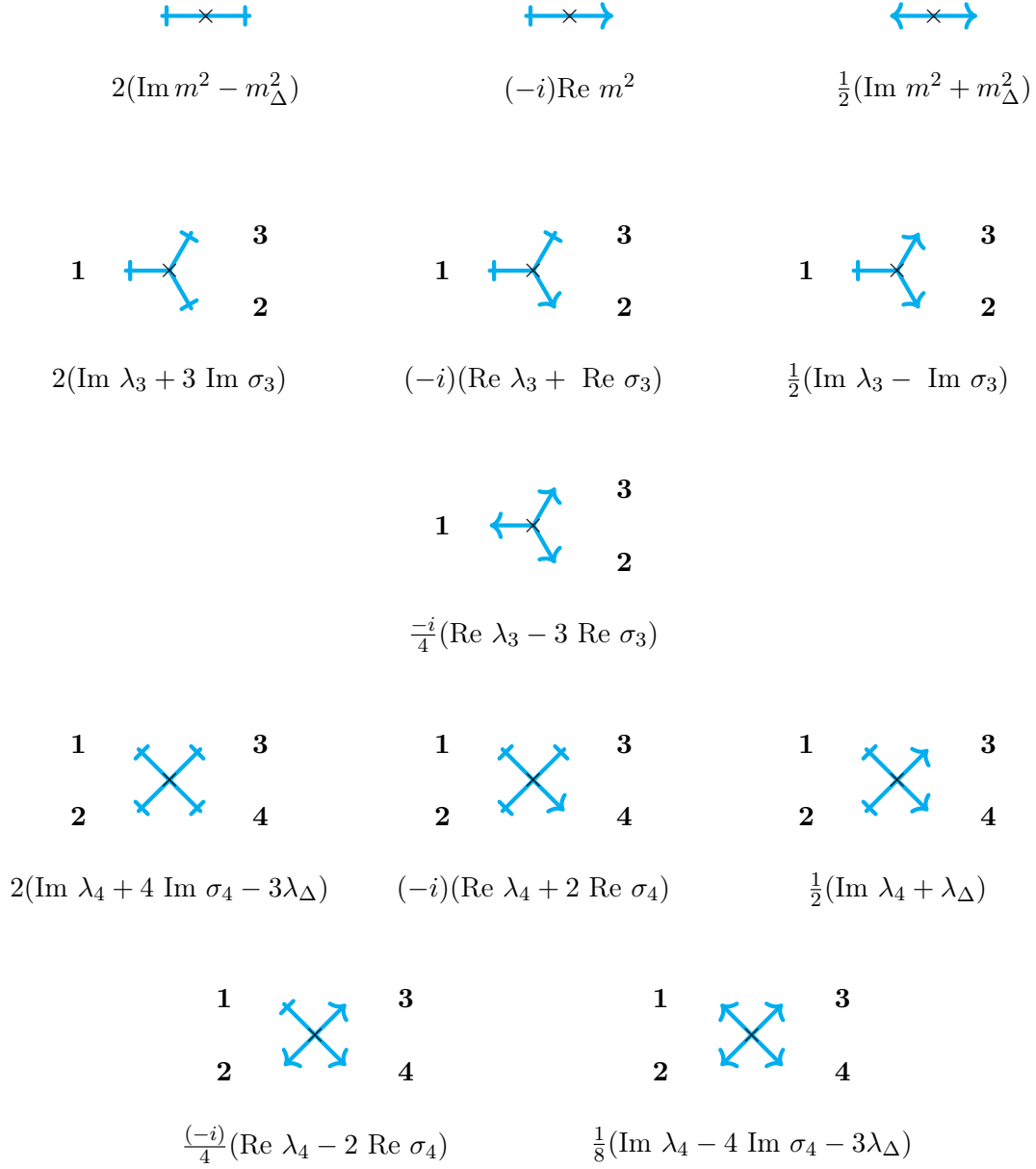


Figure 8: Feynman rules in the average-difference basis

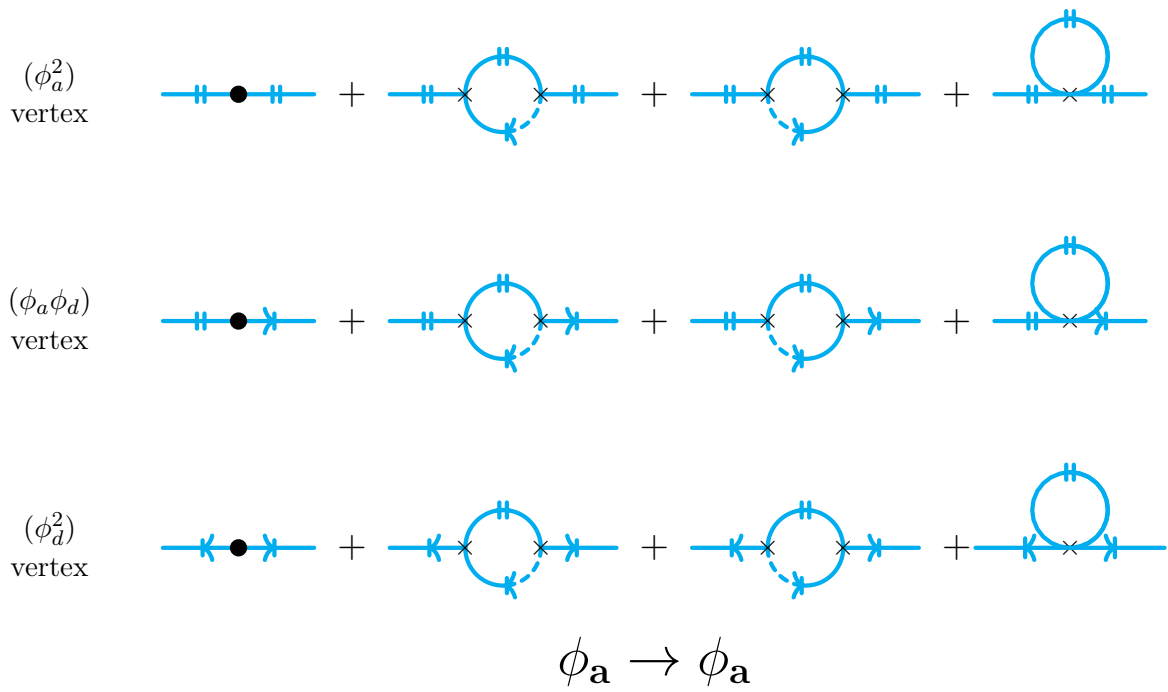


Figure 9: Mass renormalization in the average-difference basis

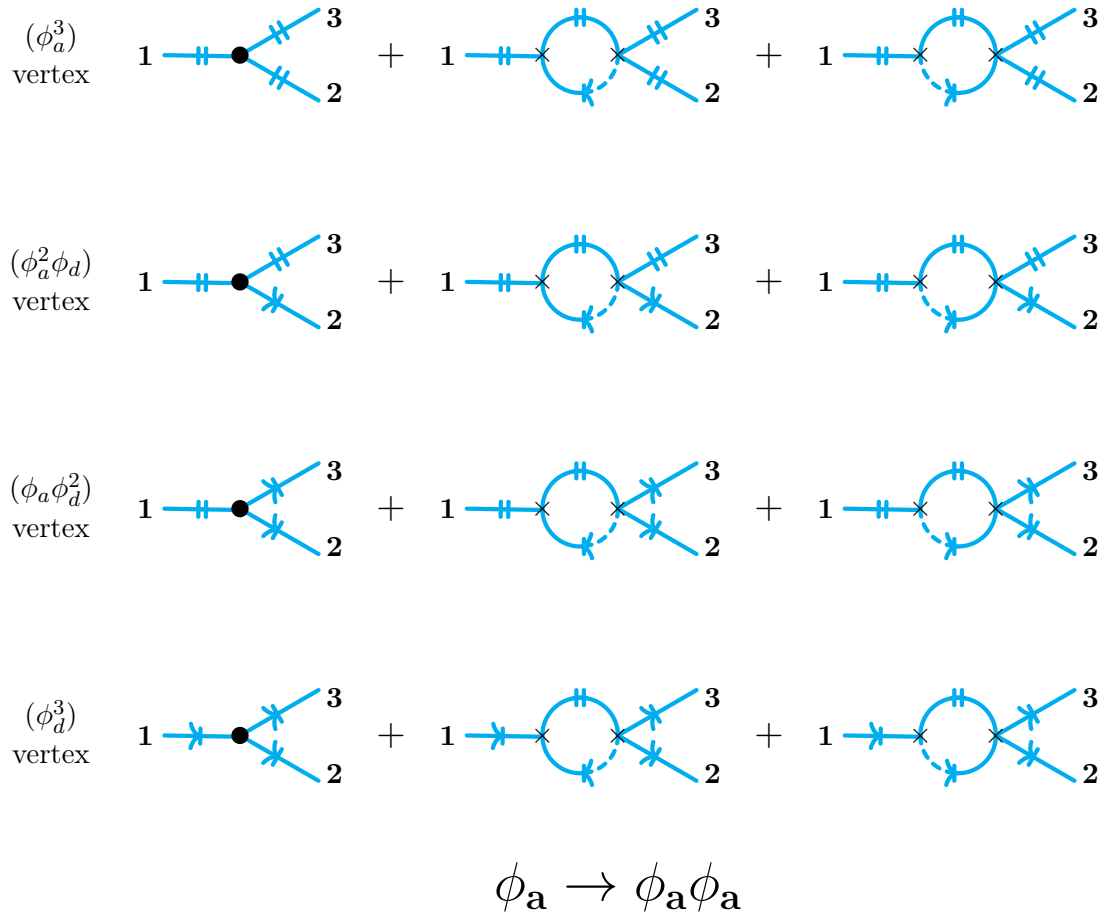


Figure 10: Renormalization of the cubic couplings in the average-difference basis

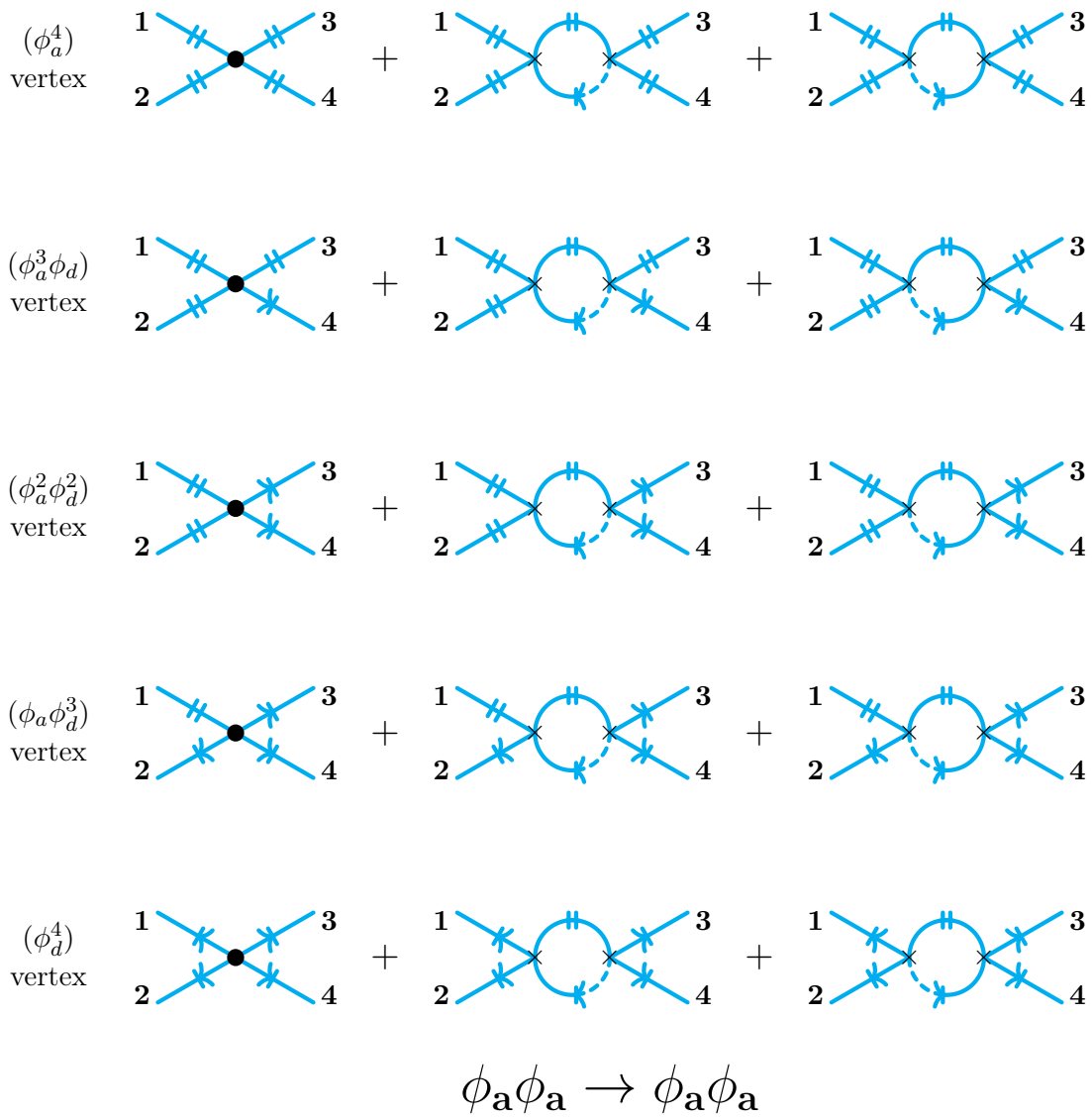


Figure 11: Renormalization of the quartic couplings in the average-difference basis

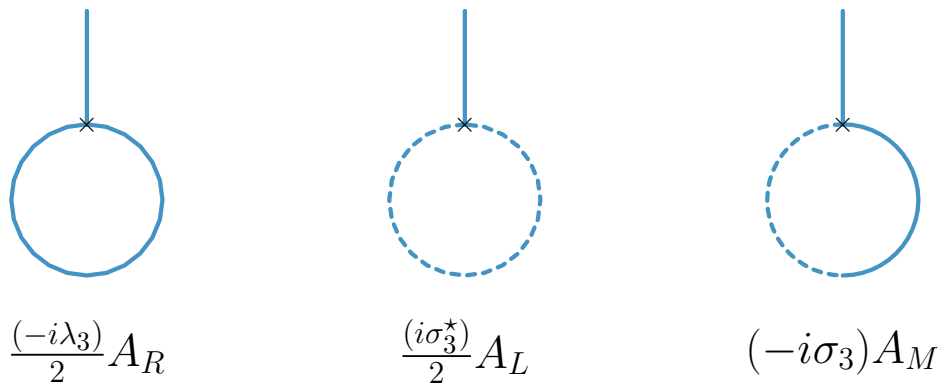


Figure 12: 1 loop tadpole to ϕ_R

Appendix B

PV reduction in open Yukawa theory

Passarino-Veltman (PV) reduction [87, 88, 143, 144] is a procedure to write tensor loop integrals in terms of scalar loop integrals. We implement PV reduction to SK loop integrals that appear in self energy correction to Fermion. The SK diagrams which contribute to the self energy are of B_{ab}^f type. Here $a, b \in \{R, L, P, M\}$. The 'f' superscript in B_{ab}^f denotes that one of the internal propagators is Fermionic - the other being scalar. We define the following quantity for future convenience.

$$\Delta \equiv -k^2 + m_\psi^2 - m_\phi^2, \quad (\text{B.0.1})$$

The PV reduction formula for B^f integrals with no cut propagator are given by

$$\begin{aligned} B_{RR}^f(k, m_\psi, m_\phi) &= m_\psi B_{RR}(k, m_\psi, m_\phi) - \not{k} \frac{i A_R(m_\psi) - i A_R(m_\phi) - \Delta B_{RR}(k, m_\psi, m_\phi)}{2k^2}, \\ B_{LL}^f(k, m_\psi, m_\phi) &= m_\psi B_{LL}(k, m_\psi, m_\phi) - \not{k} \frac{-i A_L(m_\psi) + i A_L(m_\phi) - \Delta B_{LL}(k, m_\psi, m_\phi)}{2k^2}, \\ B_{RL}^f(k, m_\psi, m_\phi) &= m_\psi B_{RL}(k, m_\psi, m_\phi) - \not{k} \frac{-i A_R(m_\psi) - i A_L(m_\phi) - \Delta B_{RL}(k, m_\psi, m_\phi)}{2k^2}, \\ B_{LR}^f(k, m_\psi, m_\phi) &= m_\psi B_{LR}(k, m_\psi, m_\phi) - \not{k} \frac{i A_R(m_\psi) + i A_L(m_\phi) - \Delta B_{LR}(k, m_\psi, m_\phi)}{2k^2}. \end{aligned} \quad (\text{B.0.2})$$

Consider reduction formula for B^f with two cut propagators. Those are given by

$$\begin{aligned} B_{PM}^f(k, m_\psi, m_\phi) &= m_\psi B_{PM}(k, m_\psi, m_\phi) + \not{k} \frac{\Delta B_{PM}(k, m_\psi, m_\phi)}{2k^2}, \\ B_{MP}^f(k, m_\psi, m_\phi) &= m_\psi B_{MP}(k, m_\psi, m_\phi) + \not{k} \frac{\Delta B_{MP}(k, m_\psi, m_\phi)}{2k^2}, \\ B_{PP}^f(k, m_\psi, m_\phi) &= m_\psi B_{PP}(k, m_\psi, m_\phi) + \not{k} \frac{\Delta B_{PP}(k, m_\psi, m_\phi)}{2k^2}, \\ B_{MM}^f(k, m_\psi, m_\phi) &= m_\psi B_{MM}(k, m_\psi, m_\phi) + \not{k} \frac{\Delta B_{MM}(k, m_\psi, m_\phi)}{2k^2}. \end{aligned} \quad (\text{B.0.3})$$

The remaining B^f integrals with one cut propagator are given by

$$\begin{aligned}
B_{RP}^f(k, m_\psi, m_\phi) &= m_\psi B_{RP}(k, m_\psi, m_\phi) - \not{k} \frac{-i A_P(m_\phi) - \Delta B_{RP}(k, m_\psi, m_\phi)}{2k^2}, \\
B_{PR}^f(k, m_\psi, m_\phi) &= m_\psi B_{PR}(k, m_\psi, m_\phi) - \not{k} \frac{i A_P(m_\psi) - \Delta B_{PR}(k, m_\psi, m_\phi)}{2k^2}, \\
B_{RM}^f(k, m_\psi, m_\phi) &= m_\psi B_{RM}(k, m_\psi, m_\phi) - \not{k} \frac{-i A_M(m_\phi) - \Delta B_{RM}(k, m_\psi, m_\phi)}{2k^2}, \\
B_{MR}^f(k, m_\psi, m_\phi) &= m_\psi B_{MR}(k, m_\psi, m_\phi) - \not{k} \frac{i A_M(m_\psi) - \Delta B_{MR}(k, m_\psi, m_\phi)}{2k^2}, \\
B_{LP}^f(k, m_\psi, m_\phi) &= m_\psi B_{LP}(k, m_\psi, m_\phi) - \not{k} \frac{i A_P(m_\phi) - \Delta B_{LP}(k, m_\psi, m_\phi)}{2k^2}, \\
B_{PL}^f(k, m_\psi, m_\phi) &= m_\psi B_{PL}(k, m_\psi, m_\phi) - \not{k} \frac{-i A_P(m_\psi) - \Delta B_{PL}(k, m_\psi, m_\phi)}{2k^2}, \\
B_{LM}^f(k, m_\psi, m_\phi) &= m_\psi B_{LM}(k, m_\psi, m_\phi) - \not{k} \frac{i A_M(m_\phi) - \Delta B_{LM}(k, m_\psi, m_\phi)}{2k^2}, \\
B_{ML}^f(k, m_\psi, m_\phi) &= m_\psi B_{ML}(k, m_\psi, m_\phi) - \not{k} \frac{-i A_M(m_\psi) - \Delta B_{ML}(k, m_\psi, m_\phi)}{2k^2}.
\end{aligned} \tag{B.0.4}$$

Substituting the divergences of all scalar A and B type integrals given in (A.2.4) and A.2.5, we find that B_{RL}^f , B_{LR}^f and all single-cut integrals in (B.0.3) are non-local divergent. They remain so even in the equal mass limit ($m_\phi = m_\psi = m$). The divergence structure of B_{RL} , B_{LR} in the equal mass limit, are given by

$$\begin{aligned}
B_{RL}^f(k, m, m) &= \frac{i \not{k}}{k^2} \frac{m^2}{(4\pi)^2} \frac{2}{d-4} + \dots, \\
B_{LR}^f(k, m, m) &= -\frac{i \not{k}}{k^2} \frac{m^2}{(4\pi)^2} \frac{2}{d-4} + \dots.
\end{aligned} \tag{B.0.5}$$

The divergence structure of single-cut loop integrals in the equal mass limit, are given by

$$\begin{aligned}
B_{RP}^f(k, m, m) &= \frac{i}{(4\pi)^2} \left(m - \frac{\not{k}}{2} + \frac{\not{k}m^2}{k^2} \right) \frac{1}{d-4}, \\
B_{PR}^f(k, m, m) &= \frac{i}{(4\pi)^2} \left(m - \frac{\not{k}}{2} - \frac{\not{k}m^2}{k^2} \right) \frac{1}{d-4}, \\
\dots &= \dots.
\end{aligned} \tag{B.0.6}$$

Appendix C

Non-local divergences in scalar loops

C.1 Leading divergence in open QFTs

We summarise the general form of the non-local log divergences in [Table C.1](#) appearing in cut diagrams in D spacetime dimensions. In D dimensions there are a total of $D - 1$ types of non-local log divergent diagrams viz. $PR^{D-2}, P^2R^{D-3}, P^3R^{D-4}, \dots, P^{D-1}$ all of which have $D - 1$ external legs. The extreme cases in this list are the single cut PR^{D-2} and the totally cut P^{D-1} . These $D - 1$ types *completely* classify non-local log divergences at one-loop in D dimensions. Any non-local log divergent diagram in D dimensions will fall into one of these classes, meaning it will have structure of non-local divergence similar to one from the set $\{P^{N_c}R^{D-N_c-1}\}_{N_c=1}^{D-1}$.

| Diagram | Name | Divergence condition | Divergence structure ¹ |
|--------------------|-----------------------|---|--|
| Single cut | PR^{D-2} | No condition | $\frac{i^{D-2} \text{Vol}(\mathbb{S}^{D-2})}{2^{D-1}(2\pi)^{D-1}} \int_{\Delta^{D-3}} \prod_{i=1}^{D-2} dx_i \frac{\text{sgn}^{D-2}(\tilde{k}^0)}{(-\tilde{k}^2)^{\frac{D-2}{2}}} \ln(\Lambda)$ |
| Almost totally cut | $P^{D-2}R$ | $\Sigma_c^2 > 0, (\Sigma_{cut}^{space})^2 \neq 0$ | $\frac{i}{2^D \pi} \frac{\text{sgn}(\tilde{\Sigma}_{cut}^0 _{x=1})}{\sqrt{-\tilde{\Sigma}_{cut}^2 _{x=1}}} \ln(\Lambda)$ |
| Totally cut | P^{D-1} | $\Sigma_c^2 > 0, (\Sigma_{cut}^{space})^2 \neq 0$ | $\frac{1}{2^{D-1} \pi} \frac{1}{\Sigma_c} \ln(\Lambda)$ |
| Multiple cut | $P^{N_c} R^{D-N_c-1}$ | $\Sigma_c^2 > 0, (\Sigma_{cut}^{space})^2 \neq 0$ | $\frac{i^{D-N_c-1}}{2^{D-1}(2\pi)^{D-N_c}} \text{Vol}(\mathbb{S}^{D-N_c-1}) \Sigma_c^{D-N_c-2} \times$ $\int_{\Delta^{D-N_c-2}} \prod_{i=1}^{D-N_c-1} dx_i \frac{\text{sgn}^{D-N_c-1}(\tilde{\Sigma}_{cut}^0)}{(-\tilde{\Sigma}_{cut}^2)^{\frac{D-N_c-1}{2}}} \ln(\Lambda)$ |

Table C.1: Non-local log divergences in one-loop diagrams with $D - 1$ external legs in D spacetime dimensions; Λ is a UV cutoff.

Examples

The $D = 4$ case has already been done explicitly in [section C.3](#). Here we use the formulae listed in [Table C.1](#) to write down all the non-local divergences in $D = 3, 4$ dimensions. For $D = 4$, this will serve as a consistency check against our explicit computations.

- $D = 3$: There are two non-local log divergent bubble diagrams PR, P^2 .

| Diagram | Divergence condition | Divergence structure |
|---------|----------------------|---|
| PR | None | $\frac{i}{8\pi} \frac{\text{sgn}(k^0)}{\sqrt{-k^2}} \ln(\Lambda)$ |
| P^2 | $k^2 > 0$ | $\frac{1}{4\pi} \frac{1}{\sqrt{k^2}} \ln(\Lambda)$ |

Table C.2: Non-local log divergences at one-loop in $D = 3$ spacetime dimensions; Λ is a UV cutoff

¹For the multiple cut case, the result given here should be multiplied by 2 if $N_c = D - 1$ which is nothing but the totally cut case

- $D = 4$: There are three non-local log divergent triangle (C -type) diagrams viz. PR^2 , P^2R , P^3 .

| Diagram | Divergence condition | Divergence structure |
|---------|------------------------------|--|
| PR^2 | None | $\frac{1}{16\pi^2\sqrt{\Sigma_c^2}} \arctan\left(\frac{\sqrt{\Sigma_c^2}}{k_1 \cdot k_2}\right) \ln \Lambda$ |
| P^2R | $k_1^2 > 0$ | $\frac{i}{16\pi\sqrt{-\Sigma_c^2}} \text{sgn} \left(\begin{array}{cc} k_2^0 & k_1^0 \\ \mathbf{k}_2 \cdot \mathbf{k}_1 & \mathbf{k}_1 \cdot \mathbf{k}_1 \end{array} \right) \ln \Lambda$ |
| P^3 | Span of k_i^μ space-like | $\frac{1}{8\pi\Sigma_c} \ln \Lambda$ |

Table C.3: Leading Non-local log divergences at one-loop in $D = 4$ spacetime dimensions. Here Λ is a UV cutoff and $\Sigma_c^2 \equiv k_1^2 k_2^2 - (k_1 \cdot k_2)^2$.

For the diagram P^2R in Table C.3, the answer seems to be apparently different from the one calculated in Equation C.3.9. The mismatch is reconciled if we recall that the explicit computation was done in a special frame where $k_1^0 = 0$ (since k_1 is space-like). In the result above, if we substitute $k_1^0 = 0$, we find that the two results agree as expected.

C.2 Feynman parameterisation of $\Xi_{uc\perp}$

The light-cone/sphere integral representation of $\Xi_{uc\perp}$ in (5.3.20) can be converted to a Feynman parameter integral by using some well-known Dirichlet-type integral identities. The Feynman parameter representation will be used to explicitly compute $\Xi_{uc\perp}$ for various log divergent C -type diagrams in the next appendix.

The covariant light-cone integral expression for $\Xi_{uc\perp}$ is

$$\Xi_{uc\perp} = \int \frac{d^{D-N_c}n}{(2\pi)^{D-N_c}} \frac{\delta(t \cdot n + 1)\delta_+(n^2)}{\prod_{j=1}^{N-N_c} i(2n \cdot \ell_{j\perp} - i\varepsilon)} \quad (\text{C.2.1})$$

Since all the denominators in the above expression have non-zero imaginary parts of the same sign, we can combine them by Feynman parameter trick.

$$\Xi_{uc\perp} = \int \frac{d^{D-N_c}n}{(2\pi)^{D-N_c}} \int_{[0,1]^{N-N_c}} dX_{N-N_c} \frac{\delta(t \cdot n + 1)\delta_+(n^2)}{i^{N-N_c}(2n \cdot \mathcal{L} - i\varepsilon)^{N-N_c}}, \quad (\text{C.2.2})$$

where $dX_{N-N_c} \equiv \prod_{j=1}^{N-N_c} dx_j \delta(1 - \sum x) \Gamma(N - N_c)$, is the Feynman parameter integration measure (or more precisely the probability measure for a *uniform Dirichlet distribution*) for $N - N_c$ Feynman parameters, while $\mathcal{L}^\mu \equiv \sum_{j=1}^{N-N_c} x_j \ell_{j\perp}^\mu$ is the Feynman parameter averaged momenta.

Written as a sphere integral, (C.2.2) takes the form

$$\Xi_{uc\perp} = \frac{1}{2(2\pi)^{D-N_c}} \int_{\hat{n} \in \mathbb{S}_\perp^{D-N_c-1}} \int_{[0,1]^{N-N_c}} \frac{dX_{N-N_c}}{i^{N-N_c}(2\hat{n} \cdot \mathcal{L} - 2\mathcal{L}^0 - i\varepsilon)^{N-N_c}}, \quad (\text{C.2.3})$$

C.2.1 Leading log divergence

Let us consider the case where $N = D - 1$, i.e., the diagrams where the leading UV divergence is expected to be logarithmic (according to the modified degree of divergence). The sphere integral can be performed in this case, using the Dirichlet-type identity

$$\frac{1}{|\mathbb{S}^d|} \int_{\hat{n} \in \mathbb{S}^d} \frac{1}{(1 + \mathbf{A} \cdot \hat{n})^d} = \left(\frac{1}{\sqrt{1 - \mathbf{A}^2}} \right)^d \quad (\text{C.2.4})$$

The identity can be proven by writing

$$\frac{1}{|\mathbb{S}^d|} \int_{\hat{n} \in \mathbb{S}^d} \frac{1}{(1 + \mathbf{A} \cdot \hat{n})^d} = \frac{|\mathbb{S}^{d-1}|}{|\mathbb{S}^d|} \int_0^\pi \frac{(\sin \vartheta)^{d-1} d\vartheta}{(1 + \sqrt{\mathbf{A}^2} \cos \vartheta)^d}. \quad (\text{C.2.5})$$

A binomial expansion yields an Euler-Beta integral, which in turn gives the result quoted above. Using the identity quoted above, we can write (C.2.3) as

$$\Xi_{uc\perp} \Big|_{N=D-1} = \frac{|\mathbb{S}_\perp^{D-N_c-1}|}{(4\pi)^{D-N_c} (-i)^{D-N_c-1}} \mathbb{E} \left[\left\{ \frac{\text{csgn}(\mathcal{L}^0)}{\sqrt{-\mathcal{L}^2}} \right\}^{D-N_c-1} \right] \quad (\text{C.2.6})$$

where by \mathcal{L}^0 we really mean complexified \mathcal{L}^0 viz. $\mathcal{L}^0 + i\varepsilon$. Thus, $\mathcal{L}^2 = -(\mathcal{L}^0 + i\varepsilon)^2 + \mathcal{L}^2$ and

$$\mathbb{E} \left[\left\{ \frac{\text{csgn}(\mathcal{L}^0)}{\sqrt{-\mathcal{L}^2}} \right\}^{D-N_c-1} \right] \equiv \int_{[0,1]^{D-N_c-1}} dX_{D-N_c-1} \left\{ \frac{\text{csgn}(\mathcal{L}^0)}{\sqrt{-\mathcal{L}^2}} \right\}^{D-N_c-1} \quad (\text{C.2.7})$$

is the expectation of the $D - N_c - 1$ power of *signed* (determined by sign of \mathcal{L}^0) inverse length, $\frac{\text{csgn}(\mathcal{L}^0)}{\sqrt{-\mathcal{L}^2}}$ with respect to a uniform Dirichlet distribution.

The above expression thus lends a nice geometric interpretation of $\Xi_{uc\perp}$, in the case of log divergent diagrams. It can be viewed as being proportional to the $D - N_c - 1$ *moment (with respect to a uniform Dirichlet distribution) of signed inverse length of vectors in the convex hull of the transverse uncut momenta*.

C.2.2 Leading power divergence

In this section we will consider the case of power law divergences i.e. when $N < D - 1$.

One can generalize the d dimensional sphere integral identity (C.2.4) to the case where the degree of the denominator is some generic value $s < d$. The result of such an integral is a Gauss hypergeometric function, that can also be interpreted as a beta distribution weighted average.

$$\begin{aligned} \frac{1}{|\mathbb{S}^d|} \int_{\mathbb{S}^d} \frac{1}{(1 + \mathbf{A} \cdot \hat{n})^s} &= {}_2F_1 \left(\frac{s}{2}, \frac{s+1}{2}; \frac{d+1}{2}; \mathbf{A}^2 \right) \\ &= \int_0^1 \frac{db_{d,s}}{(1 - (\mathbf{A}\sqrt{t})^2)^{\frac{s}{2}}} \end{aligned} \quad (\text{C.2.8})$$

where $db_{d,s} \equiv dt f_{\text{beta}}(t; \frac{s+1}{2}, \frac{d-s}{2}) \equiv dt \frac{t^{\frac{s+1}{2}-1} (1-t)^{\frac{d-s}{2}-1}}{B(\frac{s+1}{2}, \frac{d-s}{2})}$ is the probability measure corresponding to the normalized beta distribution $f_{\text{beta}}(t; \frac{s+1}{2}, \frac{d-s}{2})$.

Using the identity quoted above and defining $\mathcal{L}_t \equiv (\mathcal{L}^0 + i\varepsilon, \mathbf{L}\sqrt{t})$ we can write (C.2.3) as

$$\Xi_{uc\perp} \Big|_{N < D-1} = \frac{|\mathbb{S}_{\perp}^{D-N_c-1}|}{2(-2i)^{N-N_c} (2\pi)^{D-N_c}} \mathbb{E} \left[\left\{ \frac{\text{csgn}(\mathcal{L}_t^0)}{\sqrt{-\mathcal{L}_t^2}} \right\}^{N-N_c} \right] \quad (\text{C.2.9})$$

where the expectation is with respect to the joint distribution of Feynman parameters (uniform Dirichlet distribution) and the fractional spatial scaling parameter (beta distribution).

$$\mathbb{E} \left[\left\{ \frac{\text{csgn}(\mathcal{L}_t^0)}{\sqrt{-\mathcal{L}_t^2}} \right\}^{N-N_c} \right] \equiv \int_{[0,1]^{N-N_c+1}} db_{D-N_c-1, N-N_c} dX_{N-N_c} \left\{ \frac{\text{csgn}(\mathcal{L}_t^0)}{\sqrt{-\mathcal{L}_t^2}} \right\}^{N-N_c} \quad (\text{C.2.10})$$

Thus the above expression also admits a geometric interpretation, similar to the log divergent case. $\Xi_{uc\perp}$ is proportional to the $N - N_c$ *moment of the signed inverse length of vectors in the set of*

convex hulls $\{\mathcal{L}_t|t \in [0, 1]\}$, where the Feynman parameters follow a uniform Dirichlet distribution while the fractional spatial scaling parameter follows a beta distribution.

C.3 Evaluation of C -type triangle diagrams

We compute C type loop integrals in four dimensions. As we shall see, the diagrams may be convergent or divergent (with non-local structure) depending on the choice of external momenta. In the case of divergent integrals, we only extract the leading divergent piece. By virtue of cutting relations, it suffices to focus our attention on a basis set of integrals viz. the single-cut C_{PRR} , the double-cut C_{PPR} and the triple-cut C_{PPP} .

C.3.1 Single-cut C -type diagram

In this section we will compute the single-cut C -type diagram C_{PRR} . The diagram corresponding to C_{PRR} is shown in figure (1).

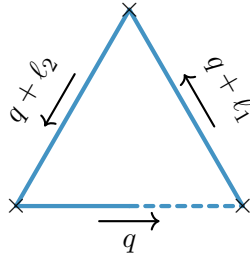


Figure 1: C_{PRR}

The integral expression is

$$C_{PRR} = \int \frac{d^4q}{(2\pi)^4} \frac{2\pi\delta_+(q^2 + m^2)}{i^2 [(q + l_1)^2 + m^2 - i\varepsilon] [(q + l_2)^2 + m^2 - i\varepsilon]} \quad (\text{C.3.1})$$

This integral is log divergent from corrected power counting arguments we discussed in the introduction. The leading divergence can be extracted and we borrow the results from the general analysis in 5.3 to first note the three contributions to the overall divergence.

We have $D = 4, N = 3, N_c = 1$

1. Cut momenta geometric factor:

$$\frac{1}{2^{1-1}\Sigma_c} = 1$$

$\Sigma_c = 1$ as there is no cut momenta

2. **Transverse uncut momenta geometric factor:** Referring to the Feynman parameter representation of $\Xi_{uc\perp}$ in (C.2.6)

$$\frac{|\mathbb{S}^2|}{(4\pi)^{4-1}(-i)^{4-1-1}} \int_0^1 \int_0^1 dx_1 dx_2 \delta(1-x_1-x_2) \frac{\Gamma(2)}{-\mathcal{L}^2}$$

where $\mathcal{L}^2 = (\ell_1 x_1 + \ell_2 x_2)^2$. Note that the Feynman $i\varepsilon$ prescription translates to shifting the ℓ_j^0 by $i\varepsilon$ i.e. $\ell_j^0 \rightarrow \ell_j^0 + i\varepsilon$

The Feynman parameter integral can be done exactly to yield

$$\frac{1}{(4\pi)^2 \sqrt{-\Sigma_{uc}^2}} \left[\tanh^{-1} \left(\frac{\ell_1 \cdot \ell_2 - \ell_1^2}{\sqrt{-\Sigma_{uc}^2}} \right) + \tanh^{-1} \left(\frac{\ell_1 \cdot \ell_2 - \ell_2^2}{\sqrt{-\Sigma_{uc}^2}} \right) \right] = \frac{1}{(4\pi)^2 \sqrt{-\Sigma_{uc}^2}} \tanh^{-1} \left(\frac{\sqrt{-\Sigma_{uc}^2}}{\ell_1 \cdot \ell_2} \right)$$

where $\Sigma_{uc} \equiv \sqrt{\ell_1^2 \ell_2^2 - (\ell_1 \cdot \ell_2)^2}$ is the area of the parallelogram made out of the uncut momenta. Algebraically, $-4\Sigma_{uc}^2$ is the discriminant of the quadratic form \mathcal{L}^2 .

3. **UV lightlike fluctuations of transverse loop momentum:** Since $D-N = 1$, the leading divergence is logarithmic

$$\int^\Lambda \frac{dq_\perp^0}{q_\perp^0} = \log \Lambda$$

We can now combine all the three parts to write down the full leading divergence

$$\text{div}(C_{PRR}) = \frac{1}{(4\pi)^2} \frac{1}{\sqrt{-\Sigma_{uc}^2}} \tanh^{-1} \left(\frac{\sqrt{-\Sigma_{uc}^2}}{\ell_1 \cdot \ell_2} \right) \log \Lambda \quad (\text{C.3.2})$$

C.3.2 Double-cut C -type diagram

Consider the double-cut C -type diagram C_{PPR} . The diagram is shown in figure (2) and the integral expression is

$$C_{PPR} = \int \frac{d^4 q}{(2\pi)^4} \frac{2\pi\delta_+(q^2 + m^2) 2\pi\delta_+((q+k)^2 + m^2)}{i[(q+\ell)^2 + m^2 - i\varepsilon]} \quad (\text{C.3.3})$$

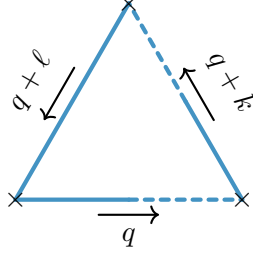


Figure 2: C_{PRR}

To integrate the above loop integral, we have two cases to consider:

- k is *spacelike*
- k is *timelike*

Spacelike cut momentum k :

The three geometric parts of the divergence (similar analysis done in case of C_{PRR}) are listed below.

We have $D = 4, N = 3, N_c = 2$

1. Cut momenta geometric factor:

$$\frac{1}{2^{2-1}\Sigma_c} = \frac{1}{2\sqrt{k^2}}$$

2. Transverse uncut momenta geometric factor:

Referring to the Feynman parameter representation of $\Xi_{uc\perp}$ in (C.2.6), the contribution is

$$\frac{|\mathbb{S}^1|}{(4\pi)^{4-2}(-i)^{4-2-1}} \frac{\text{csgn}(\ell_{\perp}^0 + i\epsilon)}{\sqrt{-\ell_{\perp}^2}} = \frac{2\pi i}{(4\pi)^2} \frac{\text{csgn}(k^2\ell^0 - (\ell \cdot k)k^0 + i\epsilon)\sqrt{k^2}}{\sqrt{-\Sigma_{c,uc}^2}}$$

where $\Sigma_{c,uc} \equiv \sqrt{\ell^2 k^2 - (\ell \cdot k)^2}$ is the area of the parallelogram formed out of the cut momentum k and uncut momentum ℓ .

3. UV lightlike fluctuations of transverse loop momentum: Since $D - N = 1$, the leading divergence is logarithmic

$$\int^{\Lambda} \frac{dq_{\perp}^0}{q_{\perp}^0} = \log \Lambda$$

Putting all the three together we get

$$\text{div}(C_{PPR}) \Big|_{\text{spacelike } k} = \frac{i\pi}{(4\pi)^2} \frac{\text{csgn}(k^2 \ell^0 - (\ell \cdot k)k^0 + i\varepsilon)}{\sqrt{-\Sigma_{c,uc}^2}} \log \Lambda \quad (\text{C.3.4})$$

Timelike cut momentum k :

Let us work in the rest frame of the cut momentum k i.e. $k^\mu \equiv (M, \mathbf{0})$.

The kinematics of the scattering process is solved by

$$q^0 = \omega_{\mathbf{q}} = -\frac{M}{2} \equiv \omega_0 \quad (\text{C.3.5})$$

provided

$$\omega_0 > m, \quad \omega_0 + M > 0 \quad (\text{C.3.6})$$

The above two conditions cannot be simultaneously satisfied and hence the integral vanishes.

Thus we conclude that the loop integral corresponding to C_{PPR} vanishes for timelike k .

$$C_{PPR} \Big|_{\text{timelike } k} = 0 \quad (\text{C.3.7})$$

C.3.3 Triple cut C -type diagram

Here we will calculate C_{PPP} from the list of all possible triple cut C -type diagrams. The diagram is shown in figure (3).

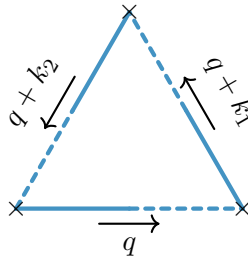


Figure 3: C_{PPP}

The integral expression for C_{PPP} is the following.

$$C_{PPP} = \int \frac{d^4 q}{(2\pi)^4} (2\pi)\delta_+(q^2 + m^2)(2\pi)\delta_+((q + k_1)^2 + m^2)(2\pi)\delta_+((q + k_2)^2 + m^2) \quad (\text{C.3.8})$$

We consider two possible cases:

1. k_1, k_2 span a *spacelike* subspace i.e. their span consists of only spacelike vectors (or $\Sigma_c^2 > 0$)
2. k_1, k_2 span a *timelike* subspace i.e. their span contains a timelike vector (or $\Sigma_c^2 < 0$)

k_1, k_2 span a spacelike subspace

The three geometric parts of the divergence are listed below. We have $D = 4, N = 3, N_c = 3$

1. **Cut momenta geometric factor:**

$$\frac{1}{2^{3-1}\Sigma_c} = \frac{1}{4\sqrt{k_1^2 k_2^2 - (k_1 \cdot k_2)^2}}$$

2. **Transverse uncut momenta geometric factor:** There is no uncut momentum. So the contribution is just

$$\frac{|\mathbb{S}^0|}{(4\pi)^{4-3}(-i)^{4-3-1}} = \frac{2}{4\pi}$$

3. **UV lightlike fluctuations of transverse loop momentum:** Since $D - N = 1$, the leading divergence is logarithmic

$$\int^\Lambda \frac{dq_\perp^0}{q_\perp^0} = \log \Lambda$$

Putting all the three together we get

$$\left. \text{div}(C_{PPP}) \right|_{k_1, k_2 \text{ span a spacelike subspace}} = \frac{2\pi}{(4\pi)^2} \frac{1}{\Sigma_c} \log \Lambda \quad (\text{C.3.9})$$

k_1, k_2 span a timelike subspace

In this case $\Sigma_c^2 < 0$. This means k_1 and k_2 are linearly independent and there exists a timelike vector in their linear span. We will perform the integral in the rest frame of that timelike vector.

Let $k \equiv \alpha_1 k_1 + \alpha_2 k_2$ be a timelike vector in the span of the cut momenta k_1 and k_2 . Let us now work in the rest frame of k i.e. $k^\mu \equiv (M, \mathbf{0})$. Without loss of generality, we will assume k_1 to

have non-zero spatial part in the rest frame of k^2 . It then follows that $\alpha_2 \neq 0$ ³. We can thus take $\alpha_2 = 1$ and call α_2 as α . So $k = \alpha k_1 + k_2$.

Next we determine an α such that k is timelike.

Let \mathbf{k}_1 be along the \hat{z} direction and the angle between \mathbf{q} and \mathbf{k}_1 be θ . We will use $\omega_{\mathbf{q}}$ to denote the expression $\sqrt{\mathbf{q}^2 + m^2}$.

The kinematics of the scattering process is solved by

$$\begin{aligned} q^0 = \omega_{\mathbf{q}} &= \frac{\alpha k_1^2 + k_2^2}{2M} \equiv \omega_0 \\ \cos \theta &= \frac{2k_1^0 \omega_0 - k_1^2}{2|\mathbf{k}_1| \sqrt{\omega_0^2 - m^2}} \equiv \beta \end{aligned} \quad (\text{C.3.10})$$

provided

$$\begin{aligned} \omega_0 &> m, \quad \omega_0 + k_1^0 > 0, \quad \omega_0 + k_2^0 > 0, \\ |\beta| &< 1 \end{aligned} \quad (\text{C.3.11})$$

The delta functions in the kinematically admissible domain can be written as

$$\begin{aligned} \delta_+(q^2 + m^2) &= \frac{\delta(q^0 - \omega_0)}{2\omega_{\mathbf{q}}} \\ \delta_+((q + k_1)^2 + m^2) &= \frac{\delta(\cos \theta - \beta)}{2|\mathbf{q}||\mathbf{k}_1|} \\ \delta_+((q + k_2)^2 + m^2) &= \frac{\delta(\omega_{\mathbf{q}} - \omega_0)}{2|M|} \end{aligned} \quad (\text{C.3.12})$$

After performing the q^0, θ and $\omega_{\mathbf{q}}$ integrals with the delta functions above, we are left with a one dimensional phase space integral

$$C_{PPP} = \frac{1}{2\pi} \frac{1}{2^3 |\mathbf{k}_1| |M|} \int_0^{2\pi} d\phi = \frac{1}{8 |\mathbf{k}_1| |M|} \quad (\text{C.3.13})$$

To rewrite everything in terms of the original frame data, we make the following substitutions:

$$\begin{aligned} M &= \text{sgn}(k^0) \sqrt{-k^2} \\ k_1^0 &= - \frac{\text{sgn}(k^0)}{\sqrt{-k^2}} (k_1 \cdot k) \\ k_2^0 &= - \frac{\text{sgn}(k^0)}{\sqrt{-k^2}} (k_2 \cdot k) \\ |\mathbf{k}_1| &= \frac{\sqrt{-\Sigma^2}}{\sqrt{-k^2}} \end{aligned} \quad (\text{C.3.14})$$

²In the rest frame of k , both \mathbf{k}_1 and \mathbf{k}_2 cannot be simultaneously zero, otherwise k_1 and k_2 become linearly dependent and hence $\Sigma_c^2 = 0$

³ $\alpha_2 = 0 \implies \alpha_1 = 0$ since $\mathbf{k}_1 \neq 0$. Then k becomes the 0 vector, which is not possible

where $\Sigma^2 \equiv k^2 k_1^2 - (k \cdot k_1)^2 < 0$ since k is timelike and computes the squared area of the parallelogram formed by the cut momentum k_1 and the timelike vector k .

We will now argue that $\Sigma^2 = \Sigma_c^2$. If $\alpha = 0$, then the fact that $\Sigma^2 = \Sigma_c^2$ is trivially true. Let us then consider the case when $\alpha \neq 0$. Then we can write⁴

$$\Sigma^2 = \frac{1}{\alpha^2} \{k^2(\alpha k_1)^2 - (k \cdot \alpha k_1)^2\} = \frac{1}{\alpha^2} \{k_2^2(\alpha k_1)^2 - (k_2 \cdot \alpha k_1)^2\} = \Sigma_c^2 \quad (\text{C.3.15})$$

Restoring the kinematical constraints, we have the following finite covariant expression for the loop integral

$$C_{PPP} = \frac{\Theta_{\text{overall}}}{8\sqrt{-\Sigma_c^2}} \quad (\text{C.3.16})$$

where

$$\Theta_{\text{overall}} = \Theta(\omega_0 - m) \Theta\left(\omega_0 - \frac{\text{sgn}(k^0)}{\sqrt{-k^2}}(k_1 \cdot k)\right) \Theta\left(\omega_0 - \frac{\text{sgn}(k^0)}{\sqrt{-k^2}}(k_2 \cdot k)\right) \Theta(1 - |\beta|) \quad (\text{C.3.17})$$

$$C_{PPP} \Big|_{k_1, k_2 \text{ span a timelike subspace}} = \frac{\Theta_{\text{overall}}}{8\sqrt{-\Sigma_c^2}} \quad (\text{C.3.18})$$

C.3.4 Summary of divergences of C -type integrals

We summarise the divergences of all divergent C -type integrals. The divergences of integrals with one-cut propagator is given by the following.

$$\begin{aligned} C_{PLL} = C_{MLL} = C_{MRR} = C_{PRR} &= \frac{1}{(4\pi)^2} \frac{\text{arctanh}\left[\frac{\Sigma_{uc}(p_1, p_2)}{-p_1 \cdot p_2}\right]}{\Sigma_{uc}(p_1, p_2)} \ln \Lambda, \\ C_{LPL} = C_{LML} = C_{RMR} = C_{RPR} &= \frac{1}{(4\pi)^2} \frac{\text{arctanh}\left[\frac{\Sigma_{uc}(p_2, p_3)}{-p_2 \cdot p_3}\right]}{\Sigma_{uc}(p_2, p_3)} \ln \Lambda, \\ C_{LLP} = C_{LLM} = C_{RRM} = C_{RRP} &= \frac{1}{(4\pi)^2} \frac{\text{arctanh}\left[\frac{\Sigma_{uc}(p_1, p_3)}{-p_1 \cdot p_3}\right]}{\Sigma_{uc}(p_1, p_3)} \ln \Lambda, \end{aligned} \quad (\text{C.3.19})$$

⁴here we use the basic linear algebra fact that $\Sigma_{v_1+v_2, v_1}^2 = \Sigma_{v_2, v_1}^2$ where $v_1 = \alpha k_1, v_2 = k_2$

where $\Sigma_{uc}^2(p_1, p_2) = (p_1 \cdot p_2)^2 - p_1^2 p_2^2$.

Integrals with two cut propagators have the following divergences.

$$\begin{aligned}
-C_{LMM} &= C_{RMM} = -C_{PPL} = C_{PPR} = \frac{i\pi}{(4\pi)^2} \frac{\text{sgn}(-p_1^0)}{\Sigma_{c,uc}(p_1, p_2)} \log \Lambda, \\
-C_{MML} &= C_{MMR} = -C_{PLP} = C_{PRP} = \frac{i\pi}{(4\pi)^2} \frac{\text{sgn}(-p_3^0)}{\Sigma_{c,uc}(p_2, p_3)} \log \Lambda, \\
-C_{MLM} &= C_{MRM} = -C_{LPP} = C_{RPP} = \frac{i\pi}{(4\pi)^2} \frac{\text{sgn}(-p_2^0)}{\Sigma_{c,uc}(p_1, p_3)} \log \Lambda,
\end{aligned} \tag{C.3.20}$$

where $\Sigma_{c,uc}^2(p_1, p_2) \equiv (p_1 \cdot p_2)^2 - p_1^2 p_2^2$.

The divergent pieces of all tripple-cut diagrams are the following.

$$\begin{aligned}
C_{PPP} &= \frac{2\pi}{(4\pi)^2 \Sigma_c(p_1, p_2)} \log \Lambda, \\
C_{MMM} &= \frac{2\pi}{(4\pi)^2 \Sigma_c(p_1, p_2)} \log \Lambda,
\end{aligned} \tag{C.3.21}$$

where $\Sigma_c^2(p_1, p_2) \equiv (p_1 \cdot p_2)^2 - p_1^2 p_2^2$.

A point to note that the rest of integrals are not all convergent. But the divergences of those integrals can be constructed using cutting identity that $R + L = P + M$. We list two of such integrals.

$$\begin{aligned}
C_{RLP} &= C_{RPP} + C_{RMP} - C_{RRP}, \\
C_{LLR} &= C_{LLP} + C_{LLM} - C_{LLL},
\end{aligned} \tag{C.3.22}$$

...

where C_{RMP}, C_{LLL} are convergent.

Appendix D

Open effective field theory via holography: detailed computation

D.1 Gradient expansion on the grSK contour

In the main text we defined the retarded-advanced basis for the sources on the boundary. It is useful to extend this to the bulk and define two related combinations:

$$\begin{aligned}
 J_{even} &\equiv -J_{\bar{F}} + e^{\beta\omega(1-\zeta)} J_{\bar{P}} = \left[J_a - \left(\frac{e^{\beta\omega(1-\zeta)} - 1}{e^{\beta\omega} - 1} - \frac{1}{2} \right) J_d \right] \\
 &= (1 - e^{-\beta\omega\zeta}) (n_\omega + 1) J_R + (e^{\beta\omega(1-\zeta)} - 1) n_\omega J_L, \\
 J_{odd} &\equiv -J_{\bar{F}} - e^{\beta\omega(1-\zeta)} J_{\bar{P}} = \left[J_a + \left(\frac{e^{\beta\omega(1-\zeta)} + 1}{e^{\beta\omega} - 1} + \frac{1}{2} \right) J_d \right] \\
 &= (1 + e^{-\beta\omega\zeta}) (n_\omega + 1) J_R - (e^{\beta\omega(1-\zeta)} + 1) n_\omega J_L.
 \end{aligned} \tag{D.1.1}$$

The solution for Φ can then be written as with this simple change of basis as

$$\Phi = G_{even} J_{even} + G_{odd} J_{odd}, \tag{D.1.2}$$

where

$$G_{even} \equiv \frac{1}{2} (G^+ + G^-), \quad G_{odd} \equiv \frac{1}{2} (G^+ - G^-). \tag{D.1.3}$$

Note that G_{even}^+ , G_{odd}^+ are obtained by separating the ingoing Green function G^+ into even and odd parts under frequency reversal once we recall that $G^-(\zeta, \omega, \mathbf{k}) = G^+(\zeta, -\omega, \mathbf{k})$.

The advantage of the combinations J_{even} and J_{odd} lies in the following fact: given the ingoing Green function G^+ in a boundary gradient expansion, one can obtain the solution on the full grSK

contour by a simple substitution. We simply multiply the even frequency part of the Green's function by J_{even} and the odd frequency part by J_{odd} , i.e.,

$$\Phi(\zeta, \omega, \mathbf{k}) = \sum_{n,m=0}^{\infty} \left(G_{2n,m}^+(\zeta) J_{even} + G_{2n+1,m}^+(\zeta) \mathfrak{w} J_{odd} \right) \mathfrak{w}^{2n} \mathfrak{q}^m, \quad (\text{D.1.4})$$

where we resort to the truncated notation:

$$\mathfrak{w} = \frac{\beta\omega}{2}, \quad \mathfrak{q} = \frac{\beta|\mathbf{k}|}{2}. \quad (\text{D.1.5})$$

There is another useful property obeyed by the even and odd combinations which is worth highlighting:

$$D_{\zeta}^+ J_{even} = \mathfrak{w} J_{odd}, \quad D_{\zeta}^+ J_{odd} = \mathfrak{w} J_{even}. \quad (\text{D.1.6})$$

This can be established by a direct differentiation of the definitions above. It follows that J_{even} and J_{odd} are solutions of the time-reversal invariant differential equation

$$\left((D_{\zeta}^+)^2 - \mathfrak{w}^2 \right) \Phi = 0. \quad (\text{D.1.7})$$

This equation involves no spatial boundary derivatives and hence should be thought of as a differential equation on each ingoing Eddington-Finkelstein tube in the grSK contour (the terminology comes from the fluid/gravity correspondence, cf., [142]). We can then define J_{even} as the solution that interpolates between J_L at $\zeta = 0$ to J_R at $\zeta = 1$. The odd combination J_{odd} is obtained by differentiation $D_{\zeta}^+ J_{even} = \mathfrak{w} J_{odd}$ as given from (D.1.6). More explicitly, we have

$$\Phi = \sum_{n,m=0}^{\infty} G_{n,m}^+ \mathfrak{q}^m (D_{\zeta}^+)^n J_{even}. \quad (\text{D.1.8})$$

For computations involving the full solution written down in a derivative expansion we can use the following gradient expansions of the even and odd sources:

$$\begin{aligned} J_{even} &= J_a - \frac{1}{2} J_d \left[y + \frac{\mathfrak{w}}{2!} (y^2 - 1) + \frac{\mathfrak{w}^2}{3!} y (y^2 - 1) + \frac{\mathfrak{w}^3}{4!} (y^2 - 1)^2 + \dots \right] \\ 2 \mathfrak{w} J_{odd} &= 2 \mathfrak{w} J_a + J_d \left[2 + \mathfrak{w} y + \frac{1}{2!} (\mathfrak{w})^2 \left(y^2 + \frac{1}{3} \right) + \frac{1}{3!} (\mathfrak{w})^3 y (y^2 - 1) \right. \\ &\quad \left. + \frac{1}{4!} (\mathfrak{w})^4 \left(y^4 - 2y^2 - \frac{1}{15} \right) + \dots \right]. \end{aligned} \quad (\text{D.1.9})$$

Here we have introduced a new bulk variable y defined as

$$y = 1 - 2\zeta, \quad (\text{D.1.10})$$

to simplify the expressions somewhat. Using the gradient expansion of J_{even} given above, in (D.1.8) we end up the result (6.3.27) quoted in the main text. For certain computations it is helpful to have the solution in the gradient expansion directly in position space. One can verify that (6.3.27) can be simplified to the following form, accurate to linear order in the derivative expansion

$$\begin{aligned} \Phi = & \left(G_{0,0}^+ + \frac{i}{2} G_{1,0}^+ \beta \partial_t \right) \left\{ J_a + \frac{i}{8} \beta \partial_t J_d + J_d \left(\zeta - \frac{1}{2} + \frac{G_{1,0}^+}{G_{0,0}^+} \right) \right. \\ & \left. - \frac{i}{2} \beta \partial_t J_d \left(\zeta - \frac{1}{2} + \frac{G_{1,0}^+}{G_{0,0}^+} \right)^2 \right\} + \mathcal{O}((\beta \partial_t)^2). \end{aligned} \quad (\text{D.1.11})$$

It is also useful to record here a simple expression for the D_ζ derivative of the field which enters into the computation of the quadratic influence functional. It is

$$D_\zeta^+ \Phi = \sum_{n=0}^{\infty} \sum_{m=0}^{\infty} \mathbf{q}^m \left(\frac{dG_{n,m}^+}{d\zeta} + G_{n-1,m}^+ \right) (D_\zeta^+)^n J_{even}, \quad (\text{D.1.12})$$

with $G_{-1,m}^+ \equiv 0$.

Note that, by construction, J_{odd} occurs in the full solution with at least one $\beta\omega$ factor multiplying it. It follows that if G^+ has a derivative expansion, so does the full solution on the grSK contour written in *average-difference*/Keldysh basis. Note also that when the even part of the ingoing solution is lifted to the holographic SK contour, the order of the derivative expansion is maintained. In contrast, when the odd part of the ingoing solution is lifted to the holographic SK contour, the source J_d occurs with one less time derivative.

D.2 Gradient expansion of the Green's functions

For a massive scalar field $m^2 = \Delta(\Delta - d) \neq 0$ on the grSK geometry we now analyze the wave equation (6.3.1) in a gradient expansion (6.3.24). It is helpful to introduce a new radial coordinate

$$\varrho \equiv \frac{r^d}{r_h^d} \implies \frac{d}{d\zeta} = 2\pi i \varrho^{\frac{1}{d}} (\varrho - 1) \frac{d}{d\varrho}, \quad (\text{D.2.1})$$

and re-express (6.3.1) as

$$\left(\frac{d}{d\varrho} \left(\varrho(\varrho - 1) \frac{d}{d\varrho} \right) - \nu(\nu - 1) \right) \Phi = \mathfrak{w} \mathcal{S}_1[\Phi] + \mathbf{q}^2 \mathcal{S}_2[\Phi], \quad (\text{D.2.2})$$

in terms of the following operators:

$$\begin{aligned} \mathcal{S}_1[\Phi] &= -\frac{1}{2\pi i} \frac{1}{\Phi} \frac{d}{d\varrho} \left(\varrho^{1-\frac{1}{d}} \Phi^2 \right), \\ \mathcal{S}_2[\Phi] &= \frac{1}{(2\pi)^2} \varrho^{-\frac{2}{d}} \Phi. \end{aligned} \quad (\text{D.2.3})$$

We have also defined a rescaled conformal dimension

$$\nu = \frac{\Delta}{d} \quad (\text{D.2.4})$$

which will be the only parameter entering our expressions. Upon plugging in the expansion (6.3.24) we immediately find the recursion relation:

$$\left(\frac{d}{d\varrho} \left(\varrho(\varrho - 1) \frac{d}{d\varrho} \right) - \nu(\nu - 1) \right) G_{m,n}^+ = \mathcal{S}_1[G_{m-1,n}^+] + \mathcal{S}_2[G_{m,n-2}^+], \quad (\text{D.2.5})$$

with the understanding that $G_{m,n}^+ = 0$ for either $m < 0$ or $n < 0$. We will now solve this order by order sequentially.

We first note that the leading order term in the expansion, the zero-mode or the DC part, $G_{0,0}^+$ satisfies the homogeneous equation with no sources:

$$\left(\frac{d}{d\varrho} \left(\varrho(\varrho - 1) \frac{d}{d\varrho} \right) - \nu(\nu - 1) \right) G_{0,0}^+ = 0. \quad (\text{D.2.6})$$

We can exploit this fact to simplify our recursion relation, remove the contribution arising from the mass, and rewrite the differential part of the expression as a total derivative, amenable to integration by quadratures. Define the ratio

$$\tilde{G}_{m,n}^+ = \frac{G_{m,n}^+}{G_{0,0}^+}, \quad (\text{D.2.7})$$

which one can check satisfies the following equation

$$\frac{d}{d\varrho} \left(\varrho(\varrho - 1) (G_{0,0}^+)^2 \frac{d\tilde{G}_{m,n}^+}{d\varrho} \right) = G_{0,0}^+ (\mathcal{S}_1[G_{m-1,n}^+] + \mathcal{S}_2[G_{m,n-2}^+]), \quad (\text{D.2.8})$$

where we have exploited the fact that $G_{0,0}^+$ is in the kernel of the differential operator. We impose regular boundary condition at the horizon and normalization at the conformal boundary at each order in perturbation theory as described in (6.3.26). The general solution can then be immediately written down:

$$\tilde{G}_{m,n}^+ = \int_{\varrho_c}^{\varrho} \frac{d\varrho'}{\varrho'(\varrho' - 1) (G_{0,0}^+(\varrho'))^2} \int_1^{\varrho'} d\bar{\varrho} G_{0,0}^+(\bar{\varrho}) (\mathcal{S}_1[G_{m-1,n}^+] + \mathcal{S}_2[G_{m,n-2}^+]), \quad (\text{D.2.9})$$

where the inner integral has its constant of integration chosen to ensure that the pole at $\varrho' = 1$ is canceled.

Zeroth order solution: Let us examine some of the leading order terms in the gradient expansion explicitly. The differential operator appearing on the l.h.s. of (D.2.2) is the Legendre differential operator. Consequently, $G_{0,0}^+$ satisfies the homogeneous Legendre differential equation (D.2.6) which has the general solution¹

$$G_{0,0}^+ = c_1 P_{-\nu}(2\varrho - 1) + c_2 Q_{-\nu}(2\varrho - 1), \quad (\text{D.2.11})$$

It is easy to check that the Legendre function of second kind $Q_{-\nu}(2\varrho - 1)$ diverges at the horizon, $\varrho = 1$. Hence the normalized solution obeying our boundary conditions is simply

$$G_{0,0}^+ = \frac{P_{-\nu}(2\varrho - 1)}{P_{-\nu}(2\varrho_c - 1)}. \quad (\text{D.2.12})$$

This is the result quoted in (6.3.28).

First order solution: At the next order it is immediate to see that $G_{0,1}^+$ (or for that matter any $G_{m,2n+1}^+$) vanishes. We then have to solve for $G_{1,0}^+$ which can be ascertained to satisfy the inhomogeneous equation

$$\frac{d}{d\varrho} \left((\varrho^2 - \varrho) (G_{0,0}^+)^2 \frac{d\tilde{G}_{1,0}^+}{d\varrho} \right) = -\frac{1}{2\pi i} \frac{d}{d\varrho} \left(\varrho^{1-\frac{1}{d}} (G_{0,0}^+)^2 \right), \quad (\text{D.2.13})$$

which gives a solution by quadratures

$$\tilde{G}_{1,0}^+ = -\frac{1}{2\pi i} \int_{\varrho_c}^{\varrho} d\varrho' \left(\frac{1}{\varrho'^{\frac{1}{d}} (\varrho' - 1)} - \frac{1}{(\varrho'^2 - \varrho') P_{-\nu}(2\varrho' - 1)^2} \right), \quad (\text{D.2.14})$$

where constants of integration have been chosen to ensure regularity at the horizon $\varrho = 1$ and vanishing of the function at the cut-off surface. We have in addition also made use (D.2.12) to write the result as an integral over Legendre functions. It is useful to massage this to the form:

$$\zeta + \tilde{G}_{1,0}^+ = \frac{1}{2\pi i} \int_{\varrho_c}^{\varrho} \frac{d\varrho'}{\varrho' (\varrho' - 1)} \left(\frac{1}{P_{-\nu}(2\varrho' - 1)} \right)^2, \quad (\text{D.2.15})$$

¹We define the associated Legendre function of the second kind as in [145, Eq. 14.3.7] which disambiguates the various definition for this function employed in the literature. In particular, we define it in terms of the regularized hypergeometric function as

$$Q_{\nu}(x) = \sqrt{\pi} \frac{\Gamma(\nu + 1)}{(2x)^{\nu+1}} {}_2\tilde{F}_1 \left(\frac{\nu}{2} + \frac{1}{2}, \frac{\nu}{2} + 1, \nu + \frac{3}{2}, \frac{1}{x^2} \right). \quad (\text{D.2.10})$$

This expression is well defined for $x \in (1, \infty)$ which is the domain of interest to us.

which will enter in the computation of the influence functionals in the gradient expansion. This integral can be explicitly evaluated in terms of Legendre functions of the second kind. In terms of $x = 2\varrho - 1$ we find after a small algebraic manipulation, the following simple relation

$$\begin{aligned} P_{-\nu}(x)^2 \frac{d}{dx} \left(\zeta + \tilde{G}_{1,0}^+ \right) &= \frac{1}{i\pi} \frac{1}{x^2 - 1} \\ &= -\frac{1}{i\pi} \text{Wr}\{P_{-\nu}(x), Q_{-\nu}(x)\} \\ &= -\frac{1}{i\pi} P_{-\nu}(x)^2 \frac{d}{dx} \left(\frac{Q_{-\nu}(x)}{P_{-\nu}(x)} \right), \end{aligned} \quad (\text{D.2.16})$$

where we have identified the Wronskian of the Legendre functions, see [145, Eq. 14.2.10]. It then follows that

$$\zeta + \tilde{G}_{1,0}^+ = \frac{i}{\pi} \frac{Q_{-\nu}(2\varrho - 1)}{P_{-\nu}(2\varrho - 1)} + i \cot \pi\nu, \quad \nu \notin \mathbb{Z}_+ \quad (\text{D.2.17})$$

where we fixed the constant by matching the asymptotics of the integral and the Legendre functions. Note that the integral is convergent for $\nu > \frac{1}{2}$, though in the main text we will often restrict attention to $\nu \in (\frac{1}{2}, 1]$. The bound on ν arises from our focus on relevant and marginal operators (a detailed analysis of convergence properties is given in D.5).

Second order solution: At the next order in the gradient expansion we first solve for $G_{0,2}^+$ which satisfies the inhomogeneous equation

$$\frac{d}{d\varrho} \left((\varrho^2 - \varrho) (G_{0,0}^+)^2 \frac{d\tilde{G}_{0,2}^+}{d\varrho} \right) = \frac{1}{(2\pi)^2} \varrho^{-\frac{2}{d}} (G_{0,0}^+)^2. \quad (\text{D.2.18})$$

Integrating this and imposing our boundary conditions (6.3.26) we find the integral expression

$$\tilde{G}_{0,2}^+(\varrho) = \frac{1}{(2\pi)^2} \int_{\varrho_c}^{\varrho} \frac{d\varrho'}{\varrho'(\varrho' - 1) (G_{0,0}^+(\varrho'))^2} \int_1^{\varrho'} d\bar{\varrho} \bar{\varrho}^{-\frac{2}{d}} (G_{0,0}^+(\bar{\varrho}))^2. \quad (\text{D.2.19})$$

Similarly, one finds for the temporal component $G_{2,0}^+$ the following expression:

$$\tilde{G}_{2,0}^+(\varrho) = -\frac{1}{2\pi i} \int_{\varrho_c}^{\varrho} \frac{d\varrho'}{\varrho'(\varrho' - 1) (G_{0,0}^+(\varrho'))^2} \int_1^{\varrho'} d\bar{\varrho} \frac{G_{0,0}^+(\bar{\varrho})}{G_{1,0}^+(\bar{\varrho})} \frac{d}{d\bar{\varrho}} \left(\bar{\varrho}^{1-\frac{1}{d}} (G_{1,0}^+(\bar{\varrho}))^2 \right). \quad (\text{D.2.20})$$

For the computation of the quadratic influence functional, we do not need the precise form of these functions. Having their derivatives at the cut-off surface suffices to determine the quantities $\dot{g}_{0,2}$ and $\dot{g}_{2,0}$ entering $\mathfrak{J}_{ad}(\omega, \mathbf{k})$ in (6.4.11). These can be computed straightforwardly as we have:

$$\begin{aligned} \dot{g}_{0,2} &= \left. \frac{dG_{0,2}^+}{d\zeta} \right|_{\zeta=0} = \frac{2\pi i}{(2\pi)^2} \frac{\varrho_c^{\frac{1}{d}-1}}{G_{0,0}^+(\varrho_c)} \int_1^{\varrho_c} d\varrho \varrho^{-\frac{2}{d}} (G_{0,0}^+(\varrho))^2 \\ &= \frac{i}{2\pi} \frac{\varrho_c^{\frac{1}{d}-1}}{P_{-\nu}(2\varrho_c - 1)^2} \int_1^{\varrho_c} d\varrho \varrho^{-\frac{2}{d}} P_{-\nu}(2\varrho - 1)^2, \end{aligned} \quad (\text{D.2.21})$$

and

$$\begin{aligned}
\dot{g}_{2,0} &= \left. \frac{dG_{2,0}^+}{d\zeta} \right|_{\zeta=0} = -\varrho_c^{\frac{1}{d}-1} \int_1^{\varrho_c} d\varrho \frac{1}{\tilde{G}_{1,0}^+(\varrho)} \frac{d}{d\varrho} \left(\varrho^{1-\frac{1}{d}} \tilde{G}_{1,0}^+(\varrho)^2 G_{0,0}^+(\varrho)^2 \right) \\
&= -\frac{\varrho_c^{\frac{1}{d}-1}}{P_{-\nu}(2\varrho_c-1)^2} \int_1^{\varrho_c} d\varrho \left(\frac{d}{d\varrho} \left(\varrho^{1-\frac{1}{d}} \tilde{G}_{1,0}^+ P_{-\nu}(2\varrho-1)^2 \right) \right. \\
&\quad \left. + \varrho^{1-\frac{1}{d}} P_{-\nu}(2\varrho-1)^2 \frac{d\tilde{G}_{1,0}^+}{d\varrho} \right) \tag{D.2.22} \\
&= -\frac{\varrho_c^{\frac{1}{d}-1}}{P_{-\nu}(2\varrho_c-1)^2} \left[-\tilde{G}_{1,0}^+(1) - \frac{1}{2\pi i} \int_1^{\varrho_c} d\varrho \varrho^{-\frac{2}{d}} P_{-\nu}(2\varrho-1)^2 \right. \\
&\quad \left. - \frac{1}{2\pi i} \int_1^{\varrho_c} d\varrho \frac{\varrho^{-\frac{1}{d}}}{\varrho-1} \left(\varrho^{-\frac{1}{d}} P_{-\nu}(2\varrho-1)^2 - 1 \right) \right],
\end{aligned}$$

where we have integrated by parts and used (D.2.14) to simplify the integral. These are the expressions that are compiled in (6.4.14) and (6.4.15).

Explicit solutions for massless fields: The expressions are in fact simplest for $d|\Delta$, i.e., $\nu \in \mathbb{Z}_+$, since then the Legendre functions are simple polynomials (note that $P_{-\nu}(x) = P_{\nu-1}(x)$ from the Legendre differential equation). For instance, carrying out the exercise we find for a massless, minimally coupled field $m^2 = 0$ or $\Delta = d$:

$$\begin{aligned}
G_{0,0}^+ &= 1 \\
G_{1,0}^+ &= -\int_0^\zeta d\zeta' \left(1 - \left(\frac{r_h}{r'} \right)^{d-1} \right) \\
G_{0,1}^+ &= 0 \\
G_{2,0}^+ &= \int_0^\zeta d\zeta' \int_{\zeta_h}^{\zeta'} d\zeta'' \left(1 + \left(\frac{r''}{r'} \right)^{d-1} \right) \left(1 - \left(\frac{r_h}{r''} \right)^{d-1} \right) \tag{D.2.23} \\
&\quad + \int_0^{\zeta_h} d\zeta' \left(1 - \left(\frac{r_h}{r'} \right)^{d-1} \right) \int_0^\zeta d\zeta'' \left(1 - \left(\frac{r_h}{r''} \right)^{d-1} \right) \\
G_{0,2}^+ &= -\int_0^\zeta d\zeta' \int_{\zeta_h}^{\zeta'} d\zeta'' \left(\frac{r''}{r'} \right)^{d-1} f(r'').
\end{aligned}$$

Solutions in the BTZ geometry: It would not be a surprise to reader to know that the above expressions can be integrated in $d = 2$. We can alternately use the knowledge of the hypergeometric series to aid in expanding out (6.3.23).

$${}_2F_1(a, b, c; z) = \sum_{n=0}^{\infty} \frac{(a)_n (b)_n}{(c)_n n!} z^n \tag{D.2.24}$$

to aid the expansion, but note that we have resum the terms to get the perturbative contributions. The resummation can be done in terms of polylogarithms. For example:

$${}_2F_1(\epsilon a, \epsilon b, 1 + \epsilon c; z) = 1 + \epsilon^2 a b \text{Li}_2(z) + \mathcal{O}(\epsilon^3) \quad (\text{D.2.25})$$

Using this we can expand $G^+(\omega, k)$ to the desired order, for

$$G^+(\zeta, \omega, k) = \left[1 + i \frac{1}{\pi} \mathfrak{w} \log \left(\frac{1 + e^{2\pi i(\zeta + \zeta_c)}}{1 + e^{2\pi i \zeta_c}} \right) - \frac{1}{2\pi^2} \mathfrak{w}^2 \left(\log \left(\frac{1 + e^{2\pi i \zeta}}{1 + e^{2\pi i \zeta_c}} \right) \right)^2 + \dots \right] \times \left[1 + \frac{1}{4\pi^2} (\mathfrak{q}^2 - \mathfrak{w}^2) (\text{Li}_2(\sec^2 \pi(\zeta + \zeta_c)) - \text{Li}_2(\sec^2 \pi \zeta_c)) + \dots \right] \quad (\text{D.2.26})$$

where we have kept terms to $\mathcal{O}(\mathfrak{w}^2)$ and $\mathcal{O}(\mathfrak{q}^2)$, respectively. In other words, the analog of (D.2.23) now reads to quadratic order:

$$\begin{aligned} G_{0,0}^+ &= 1 \\ G_{1,0}^+ &= \frac{i}{\pi} \log \left(\frac{1 + e^{2\pi i(\zeta + \zeta_c)}}{1 + e^{2\pi i \zeta_c}} \right) \\ G_{2,0}^+ &= -\frac{1}{2\pi^2} \left[\log \left(\frac{1 + e^{2\pi i(\zeta + \zeta_c)}}{1 + e^{2\pi i \zeta_c}} \right) \right]^2 - \frac{1}{4\pi^2} (\text{Li}_2(\sec^2 \pi(\zeta + \zeta_c)) - \text{Li}_2(\sec^2 \pi \zeta_c)) \\ G_{0,2}^+ &= \frac{1}{4\pi^2} (\text{Li}_2(\sec^2 \pi(\zeta + \zeta_c)) - \text{Li}_2(\sec^2 \pi \zeta_c)) . \end{aligned} \quad (\text{D.2.27})$$

D.3 Witten diagrams on the grSK contour

In this Appendix we give a short argument in favour of using Witten diagrams on the grSK contour. Per se the argument is no different from the one used in the standard AdS/CFT context on a single sheeted geometry, but for completeness we give a brief account. Consider the action (6.2.4) whose equation of motion is:

$$\frac{1}{\sqrt{-g}} \partial_A [\sqrt{-g} g^{AB} \partial_B \Phi] - m^2 \Phi - \frac{\lambda_n}{(n-1)!} \Phi^{n-1} = 0 . \quad (\text{D.3.1})$$

We can solve this equation perturbatively with λ as a perturbation parameter, viz.,

$$\Phi = \Phi_0 + \lambda \Phi_1 + \dots . \quad (\text{D.3.2})$$

Here Φ_0 solves (6.3.2) while Φ_1 satisfies the following inhomogeneous equation

$$\frac{1}{\sqrt{-g}} \partial_A [\sqrt{-g} g^{AB} \partial_B \Phi_1] - m^2 \Phi_1 = \lambda_n \frac{1}{(n-1)!} \Phi_0^{n-1} . \quad (\text{D.3.3})$$

It will be helpful for our analysis to fix the boundary conditions in a manner that is well adapted to this perturbation theory, so that a minimal number of terms contribute in the evaluation of the action. We pick:

$$\Phi_0(\zeta = 0, k) = J_L(k), \quad \Phi_0(\zeta = 1, k) = J_R(k), \quad \Phi_i(\zeta = 0, k) = 0 \quad \forall i > 0. \quad (\text{D.3.4})$$

Assuming that we have the solution to a desired order we can then evaluate the on-shell action. For instance, if we compute the action up to $\mathcal{O}(\lambda_n)$, as appropriate for a contact bulk interaction, we will simply find the contribution from the zeroth order solution, for:

$$\begin{aligned} S_{os} &= - \int d^d x \oint d\zeta \sqrt{-g} \left[\frac{g^{AB}}{2} (\partial_A \Phi_0 \partial_B \Phi_0 + 2\lambda_n \partial_A \Phi_1 \partial_B \Phi_0) + \frac{\lambda_n}{n!} \Phi_0^n \right] + \mathcal{O}(\lambda_n^2), \\ &= - \int d^d x \oint d\zeta \left[\frac{1}{2} \partial_A (\sqrt{-g} g^{AB} (\Phi_0 + 2\lambda_n \Phi_1) \partial_B \Phi_0) \right. \\ &\quad \left. - \lambda_n \Phi_1 [\partial_B (\sqrt{-g} g^{AB} \partial_A \Phi_0) - \sqrt{-g} m^2 \Phi_0] + \frac{\lambda_n}{n!} \sqrt{-g} \Phi_0^n \right] + \mathcal{O}(\lambda_n^2) \\ &= - \int d^d x \oint d\zeta \left[\frac{1}{2} \partial_A (\sqrt{-g} g^{AB} \Phi_0 \partial_B \Phi_0) + \frac{\lambda_n}{n!} \sqrt{-g} \Phi_0^n \right]. \end{aligned} \quad (\text{D.3.5})$$

In passing from the first to the second line we plugged in the equation of motion. We then see that as expected the first term in the second line is a total derivative, and thus a boundary term. Since our boundary conditions (6.3.26) set $\Phi_1 = 0$ at the conformal boundary, so its contribution to the boundary term vanishes. The other term in the expression is the Φ_0 equation of motion which vanishes on-shell. The action with the surviving terms is the expression which only cares about Φ_0 and indeed the contribution to the interaction can be obtained by writing out $\Phi_0(\zeta, x)$ in terms of the boundary values using boundary-bulk propagators. Given this, we have chosen drop the subscript ‘0’ from Φ_0 in the main text.

D.4 Cubic influence functionals in 2d CFTs

The computation of the influence functional in the RA basis in a two-dimensional CFT is quite general, since conformal invariance on the plane fixes the 3-point function in Euclidean space. One can obtain the thermal correlation function by conformally mapping the complex plane onto the cylinder. A further analytic continuation with suitable $i\epsilon$ prescription gives the result in Lorentz signature. For a certain choice of operator ordering the result is given in momentum space in

[134]. We will now derive the general influence functions in momentum space from the bulk BTZ geometry. It is worth emphasizing that while holography provides a simple way to get the answer, the result is not particularly holographic, since it is constrained entirely by the underlying conformal symmetry.

For definiteness we will compute the result for three scalar primary operators \mathcal{O}_i with conformal dimensions Δ_i with $i = 1, 2, 3$. We will assume that the OPE coefficient is C_{123} which sets the strength of the bulk vertex (the result presented in the main text corresponds to the special case $\Delta_1 = \Delta_2 = \Delta_3 = \Delta$). We take the bulk action to be given by

$$S = - \sum_{i=1}^3 \oint d\zeta \int d^3x \sqrt{-g} \left[\frac{1}{2} g^{AB} \partial_A \Phi_i \partial_B \Phi_i + \frac{1}{2} \Delta_i (\Delta_i - 2) \Phi_i^2 \right] - C_{123} \int \prod_{i=1}^2 \frac{d^3k_i}{(2\pi)^3} (2\pi)^3 \delta \left(\sum_{i=1}^3 k_i \right) \oint d\zeta \sqrt{-g} \prod_{i=1}^3 \Phi_i(\zeta, k_i). \quad (\text{D.4.1})$$

The cubic influence functional \mathcal{I}_{FFP} is then given by

$$\begin{aligned} \mathcal{I}_{FFP}(k_1, k_2, k_3) &= C_{123} \oint d\zeta \sqrt{-g} G_{\Delta_1}^+(\zeta, \omega_1, k_1) G_{\Delta_2}^+(\zeta, \omega_2, k_2) G_{\Delta_3}^-(\zeta, \omega_3, k_3) e^{\beta\omega_3(1-\zeta)} \\ &= C_{123} (1 - e^{\beta\omega_3}) \int_{r_h}^{r_c} dr r G_{\Delta_1}^+(r, \omega_1, k_1) G_{\Delta_2}^+(r, \omega_2, k_2) G_{\Delta_3}^-(r, \omega_3, k_3) \left(\frac{r - r_h}{r + r_h} \right)^{i \frac{\beta\omega_3}{2\pi}}, \end{aligned} \quad (\text{D.4.2})$$

where the BTZ Green's function in radial coordinates is given by

$$\begin{aligned} G_{\Delta}^+(r, \omega, k) &= \mathcal{N} \left(\frac{r_h}{r} \right)^{\Delta} \left(\frac{r}{r + r_h} \right)^{\Delta - \mathbf{p}_+ - \mathbf{p}_-} {}_2\tilde{F}_1 \left(\mathbf{p}_+, \mathbf{p}_-, \mathbf{p}_+ + \mathbf{p}_- + 1 - \Delta; 1 - \frac{r_h^2}{r^2} \right) \\ \mathcal{N} &\equiv \frac{\Gamma(\mathbf{p}_+) \Gamma(\mathbf{p}_-)}{\Gamma(\Delta - 1)}, \end{aligned} \quad (\text{D.4.3})$$

where we have included the normalization factors which set the source term to unit on the boundary of the spacetime.² In the second line we have written out the discontinuity across the branch cut which includes a factor of $e^{-2\beta\omega_3\zeta}$ in terms of the standard BTZ radial coordinate.

²This normalization is different from what is used in the main part of the discussion where we have left the cut-off explicit. Here we choose to normalize the propagator by demanding that $\lim_{r \rightarrow \infty} r^{d-\Delta} G_{\Delta}^+ = 1$. If one uses this normalization then the computation of the two point function proceeds as described in 6.4.1 with some minor changes. Firstly, we should pick up the constant term in the asymptotic expansion to compute $S_{(2)}$. Secondly, there is a renormalization of the operator – the 2-point functions computed in this fashion are rescaled by a factor of $\frac{\Delta}{2(\Delta-1)}$ relative to the result in (6.4.4). For the computation of the 3-point function, we should supply a factor $r_h^{\Delta_1 + \Delta_2 + \Delta_3 - 6}$ at the end to ensure that we have the correct scaling of the correlator.

The non-normalizable mode in G_{Δ}^{\pm} leads to a $r^{\Delta-2}$ fall-off. This can be seen from the fact that (with $\epsilon = \frac{r_h}{r}$)

$${}_2\tilde{F}_1\left(\mathbf{p}_+, \mathbf{p}_-, 1 - i\frac{\mathbf{w}}{\pi}; 1 - \epsilon^2\right) \xrightarrow{\epsilon \rightarrow 0} \frac{1}{\mathcal{N}} \epsilon^{2-2\Delta} + \frac{\Gamma(1-\Delta)}{\Gamma(\mathbf{p}_+ + 1 - \Delta)\Gamma(\mathbf{p}_- + 1 - \Delta)} + \dots \quad (\text{D.4.4})$$

This implies that the radial integral is absolutely convergent³ if $\Delta_1 + \Delta_2 + \Delta_3 < 4$. We will restrict to this range of conformal dimensions to avoid introducing UV regulators in the computation for the present (a discussion of the regulators can be found in D.5).

One way to proceed is to use the contour integral representation of the hypergeometric function. A variant of the Barnes integral representation [145, 15.6.7] gives

$$\begin{aligned} {}_2\tilde{F}_1(a, b, c; z) &= \mathcal{M}(a, b, c) \int_{\mathcal{C}} \frac{ds}{2\pi i} \Gamma(s) \Gamma(c - a - b + s) \Gamma(a - s) \Gamma(b - s) (1 - z)^{-s}, \\ \mathcal{M}(a, b, c) &= \frac{1}{\Gamma(a)\Gamma(b)} \frac{1}{\Gamma(c - a)\Gamma(c - b)}. \end{aligned} \quad (\text{D.4.5})$$

This is valid for $|\arg(1 - z)| < \pi$ and the choice of the contour \mathcal{C} is as follows. One separates the poles of the Gamma functions in the integrand into two sets. The first set includes the poles of $\Gamma(s)$ and $\Gamma(c - a - b + s)$ i.e., $s \in \mathcal{P}_{\text{left}} = \{-n, -n + a + b - c \mid n = 0, 1, 2, \dots\}$. The second set comprises the poles of $\Gamma(a - s)$ and $\Gamma(b - s)$ i.e., $s \in \mathcal{P}_{\text{right}} = \{a - n, b - n \mid n = 0, 1, 2, \dots\}$. The contour \mathcal{C} is chosen as a separatrix between $\mathcal{P}_{\text{left}}$ and $\mathcal{P}_{\text{right}}$. Depending on the range of z and the parameters a, b, c one can either take it to be a vertical contour between $\mathcal{P}_{\text{left}}$ and $\mathcal{P}_{\text{right}}$, or a contour that encircles the poles of one of the sets.

For the BTZ Green's function we can write the ingoing Green's function using (6.4.6) and (6.4.7) as

$$\begin{aligned} G_{\Delta}^+(r, \omega, k) &= \frac{1}{\mathfrak{G}(\mathfrak{K}_{\pm}, \tilde{\Delta})} \left(\frac{r}{r + r_h}\right)^{\frac{i}{\pi} \mathbf{w}} \int_{\mathcal{C}} \frac{ds}{2\pi i} \mathcal{G}_{\Delta}(\mathfrak{K}, \Delta, s) \left(\frac{r_h}{r}\right)^{\Delta - 2s}, \\ \mathcal{G}_{\Delta}(\mathfrak{K}_{\pm}, s) &= \Gamma(s) \Gamma(1 - \Delta + s) \Gamma(\mathfrak{K}_+ + \frac{\Delta}{2} - s) \Gamma(\mathfrak{K}_- + \frac{\Delta}{2} - s). \end{aligned} \quad (\text{D.4.6})$$

We also have shortened the notation for functions of both \mathfrak{K}_+ and \mathfrak{K}_- and written the dependence into simply \mathfrak{K}_{\pm} to allow for more compact formulae below. We will do likewise for $\mathfrak{G}(\mathfrak{K}_{\pm}, \Delta)$.

The contour we want to pick is one which encircles the poles in the left set

$$\mathcal{P}_{\text{left}} = \{-n, -n + \Delta - 1 \mid n = 0, 1, 2, \dots\}, \quad (\text{D.4.7})$$

³In general dimensions the conformal three-point function in momentum space has a convergent integral representation for $\Delta_1 + \Delta_2 + \Delta_3 < 2d$, see [133].

and is anchored at $-\infty$. As expected the leading divergence comes from the rightmost pole located at $s = \Delta - 1$ which gives us the asymptotic behaviour in (D.4.4). Taking then $s_i \leq \Delta_i - 1$ for $i = 1, 2, 3$ we see that the influence functional receives contribution from the following radial integral

$$\begin{aligned} \int_{r_h}^{\infty} r dr \left(\frac{r_h}{r}\right)^{\sum_{i=1}^3 (\Delta_i - 2s_i)} \left(\frac{r}{r+r_h}\right)^{\frac{i}{\pi}(\mathfrak{w}_1 + \mathfrak{w}_2 - \mathfrak{w}_3)} \left(\frac{r-r_h}{r+r_h}\right)^{\frac{i\mathfrak{w}_3}{\pi}} \\ = r_h^2 \Gamma\left(1 + \frac{i\mathfrak{w}_3}{\pi}\right) \frac{\Gamma\left(-1 + \sum_{i=1}^3 \frac{\Delta_i}{2} - s_i\right)}{2\Gamma\left(\frac{i\mathfrak{w}_3}{\pi} + \sum_{i=1}^3 \frac{\Delta_i}{2} - s_i\right)}. \end{aligned} \quad (\text{D.4.8})$$

We have explicitly used the fact that the integral is absolutely convergent when

$$\text{Re}\left(\sum_{i=1}^3 (2s_i - \Delta_i)\right) < -2 \implies \Delta_1 + \Delta_2 + \Delta_3 < 4, \quad (\text{D.4.9})$$

as argued earlier and have employed momentum conservation to eliminate \mathfrak{w}_2 . The integral as defined appears to have poles when $\mathfrak{w}_3 = i\pi$, but note that the prefactor $(1 - e^{\beta\omega_3})$ also vanishes at that point rendering this harmless.

Putting all the pieces together we find:

$$\begin{aligned} \mathcal{I}_{FFP}(k_1, k_2, k_3) = \frac{C_{123} r_h^2 (1 - e^{\beta\omega_3}) \Gamma\left(1 + \frac{i\mathfrak{w}_3}{\pi}\right)}{\mathfrak{G}(\mathfrak{K}_{1\pm}, \tilde{\Delta}_1) \mathfrak{G}(\mathfrak{K}_{2\pm}, \tilde{\Delta}_2) \mathfrak{G}(\mathfrak{K}_{3\pm}^*, \tilde{\Delta}_3)} \left[\prod_{i=1}^3 \int_{\mathcal{C}_i} \frac{ds_i}{2\pi i} K(s_1, s_2, s_3) \right], \\ K(s_1, s_2, s_3) = \mathcal{G}_{\Delta_1}(\mathfrak{K}_{1\pm}, s_1) \mathcal{G}_{\Delta_2}(\mathfrak{K}_{2\pm}, s_2) \mathcal{G}_{\Delta_3}(\mathfrak{K}_{3\pm}^*, s_3) \frac{\Gamma\left(-1 + \sum_{i=1}^3 \frac{\Delta_i}{2} - s_i\right)}{2\Gamma\left(\frac{i\mathfrak{w}_3}{\pi} + \sum_{i=1}^3 \frac{\Delta_i}{2} - s_i\right)}. \end{aligned} \quad (\text{D.4.10})$$

In writing the above expression we have used the fact that the sign reversal of ω_3 owing to the contribution coming from outgoing Green's function $G^-(r, \omega_3, k_3)$ can be expressed by complex conjugation of the lightcone momenta, for $\mathfrak{K}_{\pm}^*(\omega, k) = \mathfrak{K}_{\mp}(-\omega, k)$.

The main point to note is that the choice of parameters we have made is such that the contribution from the hypergeometric function arising from the radial integral is completely regular in s_i . This means that we can close the contours \mathcal{C}_i to the left picking up the contributions from the poles in \mathcal{P}_+^i for $i = 1, 2, 3$. This implies that we can write the final result as a triple sum:

$$\begin{aligned} \mathfrak{J}(k_1, k_2, k_3) &\equiv \left(\prod_{i=1}^3 \int_{\mathcal{C}_i} \frac{ds_i}{2\pi i} \right) K(s_1, s_2, s_3) \\ &= \sum_{n_1, n_2, n_3}^{\infty} \left(\prod_{i=1}^3 \frac{(-)^{n_i} \Gamma(1 - \delta_i - n_i)}{\Gamma(1 + n_i) \Gamma(1 - \delta_i - 2n_i)} \right) \frac{\Gamma\left(-1 + \sum_{i=1}^3 \frac{\delta_i + 2n_i}{2}\right)}{2\Gamma\left(\sum_{i=1}^3 \frac{\delta_i + 2n_i}{2} + \frac{i\mathfrak{w}_3}{\pi}\right)} \\ &\quad \times \mathfrak{G}(\mathfrak{K}_{1\pm}, \delta_1 + 2n_1) \mathfrak{G}(\mathfrak{K}_{2\pm}, \delta_2 + 2n_2) \mathfrak{G}(\mathfrak{K}_{3\pm}^*, \delta_3 + 2n_3). \end{aligned} \quad (\text{D.4.11})$$

We have written this result in a shorthand notation: accounting for the poles from $s_i = -n_i$ and from $s_i = -n_i + \Delta_i - 1$ is tantamount to picking contributions involving either the operator dimension or that of its shadow for each i . This is encoded in binary choice of our parameter δ_i , viz.,

$$\delta_i \in \{\Delta_i, 2 - \Delta_i\}. \quad (\text{D.4.12})$$

The result is expressed in terms of the function \mathfrak{G} introduced during the analysis of the 2-point function, Eq. (6.4.7), for brevity. To be explicit

$$\mathfrak{G}(\mathfrak{K}_\pm, \delta + 2n) = \Gamma\left(\frac{i(\mathfrak{q} - \mathfrak{w})}{2\pi} + \frac{\delta + 2n}{2}\right) \Gamma\left(-\frac{i(\mathfrak{q} + \mathfrak{w})}{2\pi} + \frac{\delta + 2n}{2}\right) \Gamma(1 - \delta - 2n). \quad (\text{D.4.13})$$

Note that the first term in the parenthesis in the second line of (D.4.11) contains the residues from the poles and includes a ratio arising from our having expressed the result in terms of the functions \mathfrak{G} defined above.

To understand the analytic structure it is helpful to reinstate ω_2 and use energy-momentum conservation to eliminate ω_3 instead. Noting that

$$\mathfrak{K}_{3\pm}^* = \mp i \frac{\mathfrak{q}_3 \mp \mathfrak{w}_3}{2\pi} = \pm i \frac{\mathfrak{q}_1 + \mathfrak{q}_2 \mp (\mathfrak{w}_1 + \mathfrak{w}_2)}{2\pi} \equiv \mathfrak{K}_{12\pm}, \quad (\text{D.4.14})$$

we can write the three-point influence functional by replacing $\mathfrak{G}(\mathfrak{K}_{3+}^*, \mathfrak{K}_{3-}^*, \delta_3 + 2n_3)$ with the simpler expression $\mathfrak{G}(\mathfrak{K}_{12+}, \mathfrak{K}_{12-}, \delta_3 + 2n_3)$.

The full influence functional then can be expressed as (after supplying the factors of r_h for dimensional reasons, see 2)

$$\begin{aligned} \mathcal{I}_{FFP}(k_1, k_2) = & C_{123} r_h^{\Delta_1 + \Delta_2 + \Delta_3 - 4} (1 - e^{-\beta(\omega_1 + \omega_2)}) \Gamma\left(1 - \frac{i(\mathfrak{w}_1 + \mathfrak{w}_2)}{\pi}\right) \\ & \left[\sum_{n_1, n_2, n_3}^{\infty} \left(\prod_{i=1}^3 \frac{(-)^{n_i} \Gamma(1 - \delta_i - n_i)}{\Gamma(1 + n_i) \Gamma(1 - \delta_i - 2n_i)} \right) \frac{\Gamma(-1 + \sum_{i=1}^3 \frac{\delta_i + 2n_i}{2})}{2\Gamma(\sum_{i=1}^3 \frac{\delta_i + 2n_i}{2} + \frac{i\mathfrak{w}_3}{\pi})} \right. \\ & \left. \times \frac{\mathfrak{G}(\mathfrak{K}_{1\pm}, \delta_1 + 2n_1) \mathfrak{G}(\mathfrak{K}_{2\pm}, \delta_2 + 2n_2) \mathfrak{G}(\mathfrak{K}_{12\pm}, \delta_3 + 2n_3)}{\mathfrak{G}(\mathfrak{K}_{1\pm}, \tilde{\Delta}_1) \mathfrak{G}(\mathfrak{K}_{2\pm}, \tilde{\Delta}_2) \mathfrak{G}(\mathfrak{K}_{12\pm}, \tilde{\Delta}_3)} \right]. \quad (\text{D.4.15}) \end{aligned}$$

The analytic structure of the influence function can be read off without further effort. The terms on the second line of $\mathcal{I}_{FFP}(k_1, k_2)$ involving the sum of n_i are regular as a function of ω_1 and ω_2 . The only singularities are from the Gamma functions containing $\mathfrak{p}_{k\pm} = \mathfrak{K}_{k\pm} + \frac{\Delta}{2}$, i.e., the pieces that occur already in the 2-point function. Of the eight possible choices of δ_i we note that there can only be poles when $\delta_i = \Delta_i$. When $\delta_i = 2 - \Delta_i$ the Gamma functions in the denominator factor also have a pole which cancels against that of the numerator leaving a finite answer. We

conclude that the correlator is analytic in the upper half of the complex ω_1 and ω_2 planes and encounters the usual quasinormal type poles in the lower half-planes.

One can in fact carry out the two of the three sums by realizing that some of the sums are the defining expressions for the generalized hypergeometric function. For instance, the sum over n_1 leads to ${}_3F_2$ with arguments comprising of the combination $n_2 + n_3$:

$$\begin{aligned} & \sum_{n_1=0}^{\infty} \frac{(-)^{n_1}}{\Gamma(n_1 + 1)} \Gamma(1 - \delta_1 - n_1) \Gamma(\mathfrak{K}_{1+} + \frac{\delta_1}{2} + n_1) \Gamma(\mathfrak{K}_{1-} + \frac{\delta_1}{2} + n_1) \frac{\Gamma(-1 + \sum_{i=1}^3 \frac{\delta_i + 2n_i}{2})}{2\Gamma(\sum_{i=1}^3 \frac{\delta_i + 2n_i}{2} + \frac{i\mathfrak{w}_3}{\pi})} \\ &= \mathfrak{G}(\mathfrak{K}_{1\pm}, \delta_1) \frac{\Gamma(-1 + \frac{\delta_1 + \delta_2 + \delta_3}{2} + n_2 + n_3)}{2\Gamma(\frac{\delta_1 + \delta_2 + \delta_3}{2} + n_2 + n_3 + \frac{i\mathfrak{w}_3}{\pi})} \\ & \quad \times {}_3F_2 \left(\begin{matrix} \mathfrak{K}_{1+} + \frac{\delta_1}{2}, \mathfrak{K}_{1-} + \frac{\delta_1}{2}, -1 + \frac{\delta_1 + \delta_2 + \delta_3}{2} + n_2 + n_3 \\ \delta_1, \frac{\delta_1 + \delta_2 + \delta_3}{2} + n_2 + n_3 + \frac{i\mathfrak{w}_3}{\pi} \end{matrix} ; 1 \right). \end{aligned} \quad (\text{D.4.16})$$

One can then carry out the sum over n_2 after a shift $n_3 + n_2 = n$, which allows performing the n_2 sum. The result is given as

$$\begin{aligned} \mathfrak{J}(k_1, k_2, k_3) &= \mathfrak{G}(\mathfrak{K}_{1\pm}, \delta_1) \mathfrak{G}(\mathfrak{K}_{2\pm}, \delta_2) \sum_{n=0}^{\infty} \frac{(-)^n \Gamma(1 - \delta_3 - n)}{\Gamma(n + 1) \Gamma(1 - \delta_3 - 2n)} \frac{\Gamma(-1 + n + \frac{\delta_1 + \delta_2 + \delta_3}{2})}{2\Gamma(n + \frac{\delta_1 + \delta_2 + \delta_3}{2} + \frac{i\mathfrak{w}_3}{\pi})} \\ & \quad \times \mathfrak{G}(\mathfrak{K}_{3\pm}^*, \delta_3 + 2n) {}_3F_2 \left(\begin{matrix} \mathfrak{K}_{1+} + \frac{\delta_1}{2}, \mathfrak{K}_{1-} + \frac{\delta_1}{2}, -1 + \frac{\delta_1 + \delta_2 + \delta_3}{2} + n \\ \delta_1, \frac{\delta_1 + \delta_2 + \delta_3}{2} + n + \frac{i\mathfrak{w}_3}{\pi} \end{matrix} ; 1 \right) \\ & \quad \times {}_4F_3 \left(\begin{matrix} \mathfrak{K}_{2+} + \frac{\delta_2}{2}, \mathfrak{K}_{2-} + \frac{\delta_2}{2}, -n, 1 - n - \delta_3 \\ \delta_2, 1 - \mathfrak{K}_{3+}^* - \frac{\delta_3}{2} - n, 1 - \mathfrak{K}_{3-}^* - \frac{\delta_3}{2} - n \end{matrix} ; 1 \right). \end{aligned} \quad (\text{D.4.17})$$

This is the expression quoted in the main text in (6.4.19) and (6.4.20), modulo a reversion to our standard notation and accounting for a symmetry factor from the $k_1 \leftrightarrow k_2$ swap of the F -type sources.

D.5 Counterterm analysis for influence functionals

We prove the statements made in 6.4.2 regarding the renormalization of the nonlinear influence functional. We will demonstrate the divergence of the integrals noted in the main text and then argue that a suitable temperature dependent mixing of the difference source into the average source serves to give a counterterm action that is consistent with microscopic unitarity.

The starting point of our analysis is the time-domain solution of the free massless scalar equation on the gravitational SK contour (D.1.11) which we reproduce here with the bare sources explicitly

marked.

$$\begin{aligned} \Phi = & \left(G_{0,0}^+ + \frac{i}{2} G_{1,0}^+ \beta \partial_t \right) \left\{ J_a^b + \frac{i}{8} \beta \partial_t J_d^b + J_d^b \left(\zeta - \frac{1}{2} + \tilde{G}_{1,0}^+ \right) \right. \\ & \left. - \frac{i}{2} \beta \partial_t J_d^b \left(\zeta - \frac{1}{2} + \tilde{G}_{1,0}^+ \right)^2 \right\} + \mathcal{O}((\beta \partial_t)^2) \end{aligned} \quad (\text{D.5.1})$$

where we are using (D.2.7). We work to linear order in the gradients, leaving a more detailed analysis of the gradient expansion for the future.

To compute the influence phase to linear order in perturbation theory, this unperturbed solution is sufficient. Taking the n^{th} power of this solution, we obtain

$$\begin{aligned} \frac{\Phi^n}{n!} = & \left\{ \sum_{k=0}^n \frac{1}{(n-k)!} (G_{0,0}^+)^n \left(J_a^b + \frac{i}{8} \beta \partial_t J_d^b \right)^{n-k} \right. \\ & \left. \times \frac{1}{k!} \left[J_d^b \left(\zeta - \frac{1}{2} + \tilde{G}_{1,0}^+ \right) - \frac{i}{2} \beta \partial_t J_d^b \left(\zeta - \frac{1}{2} + \tilde{G}_{1,0}^+ \right)^2 \right]^k \right\} \\ & + n \frac{i}{2} \beta \partial_t \left[(G_{0,0}^+)^{n-1} G_{1,0}^+ \left(J_a^b + J_d^b \left(\zeta - \frac{1}{2} + \tilde{G}_{1,0}^+ \right) \right) \right] + \mathcal{O}((\beta \partial_t)^2) . \end{aligned} \quad (\text{D.5.2})$$

Note that in the above expression we have expanded the solution accurately to linear order in time-derivatives and we have combined all the contributions coming from $\frac{i}{2} G_{1,0}^+ \beta \partial_t$ into a total derivative using Leibniz rule.

We now compute the integral over the bulk gravitational SK contour. Only the terms with branch cuts can contribute to the radial integral: this implies we can drop the $k = 0$ term in the sum above since it is analytic. As expected we get no contribution involving only the average sources. We can also drop the total time derivative in the last line since it gives a boundary contribution to the influence functional (this is partially the reason for working in coordinate space). Thus, we have

$$\begin{aligned} \int d^d x \oint d\zeta \sqrt{-g} \frac{\Phi^n}{n!} = & \int d^d x \oint d\zeta \sqrt{-g} \left\{ \sum_{k=1}^n \frac{1}{(n-k)!} (G_{0,0}^+)^n \left(J_a^b + \frac{i}{8} \beta \partial_t J_d^b \right)^{n-k} \right. \\ & \left. \times \left[\frac{(J_d^b)^k}{k!} \left(\zeta - \frac{1}{2} + \tilde{G}_{1,0}^+ \right)^k - \frac{i}{2} \beta \partial_t J_d^b \frac{(J_d^b)^{k-1}}{(k-1)!} \left(\zeta - \frac{1}{2} + \tilde{G}_{1,0}^+ \right)^{k+1} \right] \right\} \\ & + \mathcal{O}((\beta \partial_t)^2) . \end{aligned} \quad (\text{D.5.3})$$

Defining the integrals

$$\begin{aligned}
F_{n,k}^{\text{b}} &\equiv \oint d\zeta \sqrt{-g} (G_{0,0}^+)^n \left(\zeta + \tilde{G}_{1,0}^+ - \frac{1}{2} \right)^k \\
&= \oint dr r^{d-1} (G_{0,0}^+)^n \left(\zeta + \tilde{G}_{1,0}^+ - \frac{1}{2} \right)^k,
\end{aligned} \tag{D.5.4}$$

we get the following contribution to the influence functional

$$\begin{aligned}
&\int d^d x \oint d\zeta \sqrt{-g} \frac{\Phi^n}{n!} \\
&= \int d^d x \sum_{k=1}^n \frac{1}{(n-k)!} \left(J_a^{\text{b}} + \frac{i}{8} \beta \partial_t J_d^{\text{b}} \right)^{n-k} \left[F_{n,k}^{\text{b}} \frac{(J_d^{\text{b}})^k}{k!} - F_{n,k+1}^{\text{b}} \frac{(J_d^{\text{b}})^{k-1}}{(k-1)!} \frac{i}{2} \beta \partial_t J_d^{\text{b}} \right].
\end{aligned} \tag{D.5.5}$$

To proceed we need to estimate the integrals. Since we have explicit expressions for the massless scalar field we will first describe the computation in that case, before outlining the general story.

D.5.1 Divergence structure for a marginal operator

For the massless scalar, for which the radial functions appearing in the gradient expansion are given in (D.2.23) we can simplify the integrals $F_{n,k}$ defined in (D.5.4) since $G_{0,0}^+ = 1$. Dropping the subscript n , since it is unnecessary, we focus on the integrals F defined in (6.4.23), viz.,

$$F_k^{\text{b}} = \oint dr r^{d-1} \left(\zeta + G_{1,0}^+ - \frac{1}{2} \right)^k \tag{D.5.6}$$

We then can use the explicit form of $G_{1,0}^+$ in (D.2.23)

$$G_{1,0}^+ = - \int_0^\zeta d\zeta' \left(1 - \left(\frac{r_h}{r'} \right)^{d-1} \right) \tag{D.5.7}$$

and immediately obtain $\zeta + G_{1,0}^+ \sim \frac{1}{r^d}$. Furthermore, since $G_{1,0}^+$ is continuous across the grSK contour the integrals F_k^{b} are simply:

$$F_k^{\text{b}} = \int_{r_h}^{r_c} dr r^{d-1} \left[\left(\zeta + G_{1,0}^+ + \frac{1}{2} \right)^k - \left(\zeta + G_{1,0}^+ - \frac{1}{2} \right)^k \right]. \tag{D.5.8}$$

To understand the divergence structure it is sufficient to use the asymptotic expansion, though we will use the explicit form.

First consider the situation with the argument k being an odd integer. Then,

$$F_{2k+1}^{\text{b}} \sim \int^{r_c} dr r^{d-1} \left[\frac{1}{4^k} + \binom{2k+1}{2} \frac{1}{4^{k-1}} (\zeta + G_{1,0}^+)^2 + \dots \right] = \frac{1}{4^k d} r_c^d + \mathcal{O}(r_c^{-1}) \tag{D.5.9}$$

To check that the other terms do not contribute realize that

$$\begin{aligned} \int^{r_c} dr r^{d-1} \log^2 \left(\frac{1 - \left(\frac{r_h}{r}\right)^d}{1 - \left(\frac{r_h}{r_c}\right)^d} \right) &= \frac{r^d}{d} \log^2 \left(\frac{1 - \left(\frac{r_h}{r}\right)^d}{1 - \left(\frac{r_h}{r_c}\right)^d} \right) \Big|^{r_c} \\ &- 2 \int^{r_c} dr \frac{r_h^d}{r^2} \frac{1}{1 - \left(\frac{r_h}{r}\right)^d} \log \left(\frac{1 - \left(\frac{r_h}{r}\right)^d}{1 - \left(\frac{r_h}{r_c}\right)^d} \right) \end{aligned} \quad (\text{D.5.10})$$

The first term vanishes at the cut-off and the second is a convergent integral. Thus we have established the first of the relations given in (6.4.26), for indeed

$$F_{2k+1}^b = F_{2k+1}^r + \frac{1}{4^k} \frac{r_c^d}{d} \quad (\text{D.5.11})$$

When the argument k is even case we have a divergence when we pick up the linear term in $\zeta + G_{1,0}^+$, for integrating by parts we find

$$\begin{aligned} F_{2k}^b &\sim \int^{r_c} dr r^{d-1} \left[2 \binom{2k}{1} \frac{1}{2^{2k-1}} (\zeta + G_{1,0}^+) + \dots \right] \\ &= \frac{k}{4^{k-1} \pi i} \int^{r_c} dr r^{d-1} \log \left(\frac{1 - \left(\frac{r_h}{r}\right)^d}{1 - \left(\frac{r_h}{r_c}\right)^d} \right) \\ &= -\frac{k}{4^{k-1} \pi i} \int^{r_c} dr \frac{r_h^d}{r} \frac{1}{1 - \left(\frac{r_h}{r}\right)^d} \\ &= -\frac{k}{4^{k-1} \pi i} r_h^d \log \frac{r_c}{r_h} + \mathcal{O}(1). \end{aligned} \quad (\text{D.5.12})$$

thus proving the second relation in (6.4.26)

$$F_{2k}^b = F_{2k}^r + \frac{i}{\pi 4^{k-1}} r_h^d \log \frac{r_c}{r_h}. \quad (\text{D.5.13})$$

For completeness let us record the integrals for the massless scalar that enter into the computation of the quartic influence functional. In intermediate steps we define a rescaled radial variable

$$y = \frac{1}{\varrho} = \left(\frac{r_h}{r} \right)^d$$

which helps simplify the integration.

$$F_1^b = \oint dr r^{d-1} \left(\zeta + G_{1,0}^+ - \frac{1}{2} \right) = \int_{r_h}^{r_c} dr r^{d-1} = \frac{1}{d} (r_c^d - r_h^d). \quad (\text{D.5.14})$$

$$\begin{aligned}
F_2^b &= \oint dr r^{d-1} \left(\zeta + G_{1,0}^+ - \frac{1}{2} \right)^2 = 2 \int_{r_h}^{r_c} dr r^{d-1} (\zeta + G_{1,0}^+) \\
&= \frac{1}{2\pi i} \frac{r_h^d}{d} \int_{y_c}^1 \frac{dy}{y^2} \log \left(\frac{1-y}{1-y_c} \right) = -\frac{r_h^d}{\pi i} \log \frac{r_c}{r_h}.
\end{aligned} \tag{D.5.15}$$

$$\begin{aligned}
F_3^b &= \oint dr r^{d-1} \left(\zeta + G_{1,0}^+ - \frac{1}{2} \right)^3 = \int_{r_h}^{r_c} dr r^{d-1} \left[\frac{1}{4} + 3(\zeta + G_{1,0}^+)^2 \right] \\
&= \frac{r_c^d}{4d} - \frac{r_h^d}{4d} + \frac{r_h^d}{d} \frac{3}{(2\pi i)^2} \int_{y_c}^1 \frac{dy}{y^2} \log^2 \left(\frac{1-y}{1-y_c} \right) = \frac{r_c^d}{4d} - \frac{r_h^d}{2d}.
\end{aligned} \tag{D.5.16}$$

$$\begin{aligned}
F_4^b &= \oint dr r^{d-1} \left(\zeta + G_{1,0}^+ - \frac{1}{2} \right)^4 = \int_{r_h}^{r_c} dr r^{d-1} [4(\zeta + G_{1,0}^+)^3 + (\zeta + G_{1,0}^+)] \\
&= \frac{r_h^d}{d} \left[\frac{4}{(2\pi i)^3} \int_{y_c}^1 \frac{dy}{y^2} \log^3 \frac{1-y}{1-y_c} + \frac{1}{2\pi i} \int_{y_c}^1 \frac{dy}{y^2} \log \frac{1-y}{1-y_c} \right] \\
&= \frac{1}{2\pi i} \frac{r_h^d}{d} \left(\log(y_c) + \frac{6}{\pi^2} \text{Li}_3(1-y_c) \right) \\
&= -\frac{r_h^d}{2\pi i} \log \frac{r_c}{r_h} + \frac{1}{2\pi i} \frac{r_h^d}{d} \frac{6}{\pi^2} \zeta(3) + \mathcal{O}(r_c^{-d}).
\end{aligned} \tag{D.5.17}$$

D.5.2 Divergence structure for relevant operators

We shall now generalize the discussion of the divergence structure to an arbitrary operator of dimension Δ . We have derived hitherto the general expressions for the functions entering the gradient expansion in (D.2.9). While there are still integrals to be done, for the purposes of analyzing the divergence structure, it suffices to exploit the standard AdS asymptotics to extract the leading behaviour.

We recall that, $G_{0,0}^+$ solves the massive wave equation in the Schwarzschild-AdS $_{d+1}$ geometry and thus has both the non-normalizable $r^{\Delta-d}$ and the normalizable $r^{-\Delta}$ fall-offs. As written in (D.2.12) from the explicit solution we can see the asymptotic behaviour to be given by

$$\varrho_c^{\nu-1} G_{0,0}^+ = \varrho^{\nu-1} \left(1 - \frac{\nu-1}{2} \frac{1}{\varrho} + \dots \right) + \frac{\Gamma(\nu)^2 \Gamma(1-2\nu)}{\Gamma(1-\nu)^2 \Gamma(-1+2\nu)} \varrho^{-\nu} \left(1 + \frac{\nu}{2} \frac{1}{\varrho} + \dots \right) \tag{D.5.18}$$

where $\nu = \frac{\Delta}{d}$ was defined earlier in (D.2.4). We recognize the leading term as the non-normalizable mode $\varrho^{\nu-1} \sim r^{\Delta-d}$ and the second series as the normalizable mode $\varrho^{-\nu} \sim r^{-\Delta}$. Often it is convenient to normalize the Green's function to have a unit source, which would imply:

$$\begin{aligned}
G_{0,0}^+ &= \frac{1}{r^{d-\Delta}} (1 + \mathcal{O}(r^{-d})) + s_\Delta \frac{1}{r^\Delta} (1 + \mathcal{O}(r^{-d})) \\
s_\Delta &= \frac{\Gamma(\nu)^2 \Gamma(1-2\nu)}{\Gamma(1-\nu)^2 \Gamma(-1+2\nu)} r_h^{2\Delta-d}.
\end{aligned} \tag{D.5.19}$$

Notice that the subleading term in the source expansion appears at the order $r^{\Delta-2d}$ which is faster than the normalizable fall-off of $r^{-\Delta}$ provided $\Delta < d$. So for all relevant operators we can ignore the subleading term in the expansion of the source. The special case of a marginal operator $\Delta = d$ was dealt with explicitly above in [D.5.1](#).

To proceed we need estimates for the combination $\zeta + \tilde{G}_{1,0}^+$ which appears in the functions $F_{n,k}^b$ defined in [\(D.5.4\)](#). We recall that this is the combination we solved for in [\(D.2.17\)](#). Expanding out the integrand for large ρ we discern the asymptotic behaviour, directly from [\(D.2.15\)](#),

$$\zeta + \tilde{G}_{1,0}^+ \sim \int \frac{d\bar{\rho}}{\bar{\rho}^{2\nu}} = \frac{d}{d-2\Delta} \left(\frac{r_h}{r}\right)^{2\Delta-d} + \dots \quad (\text{D.5.20})$$

In deriving this expression we have used $P_{-\nu}(\varrho = 1) = 1$ and also accounted for the normalization factors in the source term of $G_{0,0}^+$. Note that the most delicate case is when $\Delta = \frac{d}{2}$ for then $G_{0,0}^+ \sim \frac{\log r}{r^{\frac{d}{2}}}$, which is nevertheless convergent. Recall that we are sticking to standard AdS boundary conditions, so $\Delta \geq \frac{d}{2}$.

Armed with this information we can proceed to estimate the integrals $F_{n,k}^b$ given in [\(D.5.4\)](#). We again note that the Green's functions $G_{n,m}^+$ are continuous on the grSK contour, so the only contribution to the contour integral comes from the explicit factor of ζ . We can therefore write

$$F_{n,k}^b = \int dr r^{d-1} (G_{0,0}^+)^n \left[\left(\zeta + \tilde{G}_{1,0}^+ + \frac{1}{2}\right)^k - \left(\zeta + \tilde{G}_{1,0}^+ - \frac{1}{2}\right)^k \right]. \quad (\text{D.5.21})$$

The leading divergence comes from the bare contribution in the case of odd argument, whence

$$F_{n,2k+1}^b \sim \frac{1}{4^k} \int^{r_c} dr r^{d-1} (G_{0,0}^+)^n \sim \frac{1}{4^k} \int^{r_c} dr r^{d-1-n(d-\Delta)}. \quad (\text{D.5.22})$$

This is absolutely convergent when

$$(1-n)d + n\Delta - 1 < -1 \implies \Delta < \frac{n-1}{n}d, \quad (\text{D.5.23})$$

but otherwise predicts a divergence

$$F_{n,2k+1}^b \sim \frac{1}{4^k} \frac{r_c^{n\Delta-(n-1)d}}{n\Delta - (n-1)d} + \text{regular} \quad (\text{D.5.24})$$

On the other hand for even argument we would estimate:

$$F_{n,2k}^b \sim \frac{2k}{4^{k-1}} \int^{r_c} dr r^{d-1} (G_{0,0}^+)^n \left(\zeta + \tilde{G}_{1,0}^+\right) \sim \frac{2k}{4^{k-1}} \int^{r_c} dr r^{-1+(n-2)(\Delta-d)} \quad (\text{D.5.25})$$

leading to

$$F_{n,2k}^b \sim \frac{2k}{4^{k-1}} \frac{r_c^{(n-2)(\Delta-d)}}{(n-2)(\Delta-d)} + \dots . \quad (\text{D.5.26})$$

For $n > 3$ we thus end up with a convergent integral for all relevant operators ($\Delta < d$). So the only renormalization necessary for a relevant operator is to remove the power-law divergence in the functions $F_{n,2k+1}^b$ for the range of Δ specified above.

Bibliography

- [1] W. H. Zurek, “Decoherence, einselection, and the quantum origins of the classical,” *Rev. Mod. Phys.* **75** (May, 2003) 715–775.
<https://link.aps.org/doi/10.1103/RevModPhys.75.715>.
- [2] M. Schlosshauer, “Decoherence, the measurement problem, and interpretations of quantum mechanics,” *Rev. Mod. Phys.* **76** (2004) 1267–1305, [arXiv:quant-ph/0312059](https://arxiv.org/abs/quant-ph/0312059) [quant-ph].
- [3] G. Bacciagaluppi, “The role of decoherence in quantum mechanics,” in *The Stanford Encyclopedia of Philosophy*, E. N. Zalta, ed. Metaphysics Research Lab, Stanford University, summer 2020 ed., 2020.
- [4] C. Agón and A. Lawrence, “Divergences in open quantum systems,” *JHEP* **04** (2018) 008, [arXiv:1709.10095](https://arxiv.org/abs/1709.10095) [hep-th].
- [5] C. Agon, V. Balasubramanian, S. Kasko, and A. Lawrence, “Coarse Grained Quantum Dynamics,” [arXiv:1412.3148](https://arxiv.org/abs/1412.3148) [hep-th].
- [6] E. Braaten, H. W. Hammer, and G. P. Lepage, “Open Effective Field Theories from Deeply Inelastic Reactions,” *Phys. Rev.* **D94** no. 5, (2016) 056006, [arXiv:1607.02939](https://arxiv.org/abs/1607.02939) [hep-ph].
- [7] E. Braaten, H.-W. Hammer, and G. P. Lepage, “Open Effective Field Theories from Highly Inelastic Reactions,” *PoS ICHEP2016* (2016) 350, [arXiv:1612.08047](https://arxiv.org/abs/1612.08047) [hep-ph].
- [8] E. Braaten, H. W. Hammer, and G. P. Lepage, “Lindblad Equation for the Inelastic Loss of Ultracold Atoms,” *Phys. Rev.* **A95** no. 1, (2017) 012708, [arXiv:1607.08084](https://arxiv.org/abs/1607.08084) [cond-mat.quant-gas].
- [9] D. Boyanovsky, “Effective Field Theory out of Equilibrium: Brownian quantum fields,” *New J. Phys.* **17** no. 6, (2015) 063017, [arXiv:1503.00156](https://arxiv.org/abs/1503.00156) [hep-ph].

- [10] D. Boyanovsky, “Information loss in effective field theory: entanglement and thermal entropies,” *Phys. Rev.* **D97** no. 6, (2018) 065008, [arXiv:1801.06840 \[hep-th\]](#).
- [11] C. Burrage, C. Käding, P. Millington, and J. Minář, “Open quantum dynamics induced by light scalar fields,” [arXiv:1812.08760 \[hep-th\]](#).
- [12] C. Burrage, C. Käding, P. Millington, and J. Minář, “Influence functionals, decoherence and conformally coupled scalars,” in *9th International Conference: Spacetime - Matter - Quantum Mechanics: From discrete structures and dynamics to top-down causation (DICE2018) Castiglioncello, Tuscany, Italy, September 17-21, 2018*. 2019. [arXiv:1902.09607 \[hep-th\]](#).
- [13] J.-O. Gong and M.-S. Seo, “Quantum non-linear evolution of inflationary tensor perturbations,” *JHEP* **05** (2019) 021, [arXiv:1903.12295 \[hep-th\]](#).
- [14] G. León, A. Pujol, S. J. Landau, and M. P. Piccirilli, “Observational constraints on inflationary potentials within the quantum collapse framework,” *Phys. Dark Univ.* (2019) 100285, [arXiv:1902.08696 \[astro-ph.CO\]](#).
- [15] J. Martin and V. Vennin, “Non Gaussianities from Quantum Decoherence during Inflation,” *JCAP* **1806** (2018) 037, [arXiv:1805.05609 \[astro-ph.CO\]](#).
- [16] J. Martin and V. Vennin, “Observational constraints on quantum decoherence during inflation,” *JCAP* **1805** (2018) 063, [arXiv:1801.09949 \[astro-ph.CO\]](#).
- [17] S. Shandera, N. Agarwal, and A. Kamal, “Open quantum cosmological system,” *Phys. Rev.* **D98** no. 8, (2018) 083535, [arXiv:1708.00493 \[hep-th\]](#).
- [18] B. O. Kerbikov, “Lindblad and Bloch equations for conversion of a neutron into an antineutron,” *Nucl. Phys.* **A975** (2018) 59–72, [arXiv:1704.07117 \[hep-ph\]](#).
- [19] K. Dixit, J. Naikoo, S. Banerjee, and A. Kumar Alok, “Study of coherence and mixedness in meson and neutrino systems,” *Eur. Phys. J.* **C79** no. 2, (2019) 96, [arXiv:1809.09947 \[hep-ph\]](#).
- [20] J. S. Schwinger, “Brownian motion of a quantum oscillator,” *J. Math. Phys.* **2** (1961) 407–432.

- [21] L. V. Keldysh, “Diagram technique for nonequilibrium processes,” *Zh. Eksp. Teor. Fiz.* **47** (1964) 1515–1527. [Sov. Phys. JETP20,1018(1965)].
- [22] R. P. Feynman and F. L. Vernon, Jr., “The Theory of a general quantum system interacting with a linear dissipative system,” *Annals Phys.* **24** (1963) 118–173. [Annals Phys.281,547(2000)].
- [23] A. Caldeira and A. Leggett, “Path integral approach to quantum Brownian motion,” *Physica A* **121** (1983) 587–616.
- [24] V. Gorini, A. Kossakowski, and E. C. G. Sudarshan, “Completely Positive Dynamical Semigroups of N Level Systems,” *J. Math. Phys.* **17** (1976) 821.
- [25] G. Lindblad, “On the Generators of Quantum Dynamical Semigroups,” *Commun. Math. Phys.* **48** (1976) 119.
- [26] Á. Rivas and S. Huelga, *Open Quantum Systems: An Introduction*. SpringerBriefs in Physics. Springer Berlin Heidelberg, 2011.
<https://books.google.co.in/books?id=FGCuYsIZAA0C>.
- [27] H. P. Breuer and F. Petruccione, *The theory of open quantum systems*. Oxford University Press, Great Clarendon Street, 2002.
- [28] A. Kamenev, *Field Theory of Non-Equilibrium Systems*. Cambridge University Press, Cambridge, 1985. <http://www.cambridge.org/us/academic/subjects/physics/condensed-matter-physics-nanoscience-and-mesoscopic-physics/field-theory-non-equilibrium-systems?format=HB&isbn=9780521760829>.
- [29] P. Jurcevic, H. Shen, P. Hauke, C. Maier, T. Brydges, C. Hempel, B. P. Lanyon, M. Heyl, R. Blatt, and C. F. Roos, “Direct observation of dynamical quantum phase transitions in an interacting many-body system,” *Phys. Rev. Lett.* **119** (Aug, 2017) 080501.
<https://link.aps.org/doi/10.1103/PhysRevLett.119.080501>.
- [30] R. Alicki, “Decoherence and the appearance of a classical world in quantum theory,” *Journal of Physics A: Mathematical and General* **37** (02, 2004) 1948.

- [31] S. Braun, M. Friesdorf, S. S. Hodgman, M. Schreiber, J. P. Ronzheimer, A. Riera, M. del Rey, I. Bloch, J. Eisert, and U. Schneider, “Emergence of coherence and the dynamics of quantum phase transitions,” *Proceedings of the National Academy of Sciences* **112** no. 12, (2015) 3641–3646, <https://www.pnas.org/content/112/12/3641.full.pdf>.
<https://www.pnas.org/content/112/12/3641>.
- [32] E. Nicklas, M. Karl, M. Höfer, A. Johnson, W. Muessel, H. Strobel, J. Tomkovič, T. Gasenzer, and M. K. Oberthaler, “Observation of scaling in the dynamics of a strongly quenched quantum gas,” *Phys. Rev. Lett.* **115** (Dec, 2015) 245301.
<https://link.aps.org/doi/10.1103/PhysRevLett.115.245301>.
- [33] J. Kasprzak, M. Richard, S. Kundermann, A. Baas, P. Jeambrun, J. M. J. Keeling, F. M. Marchetti, M. H. Szymańska, R. André, J. L. Staehli, V. Savona, P. B. Littlewood, B. Deveaud, and L. S. Dang, “Bose–einstein condensation of exciton polaritons,” *Nature* **443** no. 7110, (2006) 409–414. <https://doi.org/10.1038/nature05131>.
- [34] M. Fitzpatrick, N. M. Sundaresan, A. C. Y. Li, J. Koch, and A. A. Houck, “Observation of a dissipative phase transition in a one-dimensional circuit qed lattice,” *Phys. Rev. X* **7** (Feb, 2017) 011016. <https://link.aps.org/doi/10.1103/PhysRevX.7.011016>.
- [35] U. C. Tauber, “Field Theory Approaches to Nonequilibrium Dynamics,” *arXiv e-prints* (Nov., 2005) cond-mat/0511743, [arXiv:cond-mat/0511743](https://arxiv.org/abs/cond-mat/0511743) [cond-mat.stat-mech].
- [36] A. A. Starobinsky, *Stochastic de Sitter (inflationary) Stage in the Early Universe*, vol. 246, p. 107. 1986.
- [37] R. H. Brandenberger, R. Laflamme, and M. Mijic, “Classical Perturbations From Decoherence of Quantum Fluctuations in the Inflationary Universe,” *Mod. Phys. Lett. A* **5** (1990) 2311–2318.
- [38] A. A. Starobinsky and J. Yokoyama, “Equilibrium state of a selfinteracting scalar field in the De Sitter background,” *Phys. Rev. D* **50** (1994) 6357–6368, [arXiv:astro-ph/9407016](https://arxiv.org/abs/astro-ph/9407016).
- [39] E. Calzetta and B. Hu, “Quantum fluctuations, decoherence of the mean field, and structure formation in the early universe,” *Phys. Rev. D* **52** (1995) 6770–6788, [arXiv:gr-qc/9505046](https://arxiv.org/abs/gr-qc/9505046).

- [40] J. Lesgourgues, D. Polarski, and A. A. Starobinsky, “Quantum to classical transition of cosmological perturbations for nonvacuum initial states,” *Nucl. Phys. B* **497** (1997) 479–510, [arXiv:gr-qc/9611019](#).
- [41] C. Kiefer, D. Polarski, and A. A. Starobinsky, “Quantum to classical transition for fluctuations in the early universe,” *Int. J. Mod. Phys. D* **7** (1998) 455–462, [arXiv:gr-qc/9802003](#).
- [42] C. Kiefer and D. Polarski, “Emergence of classicality for primordial fluctuations: Concepts and analogies,” *Annalen Phys.* **7** (1998) 137–158, [arXiv:gr-qc/9805014](#).
- [43] F. C. Lombardo and D. Lopez Nacir, “Decoherence during inflation: The Generation of classical inhomogeneities,” *Phys. Rev. D* **72** (2005) 063506, [arXiv:gr-qc/0506051](#).
- [44] J. W. Sharman and G. D. Moore, “Decoherence due to the Horizon after Inflation,” *JCAP* **11** (2007) 020, [arXiv:0708.3353 \[gr-qc\]](#).
- [45] C. P. Burgess, R. Holman, G. Tasinato, and M. Williams, “EFT Beyond the Horizon: Stochastic Inflation and How Primordial Quantum Fluctuations Go Classical,” *JHEP* **03** (2015) 090, [arXiv:1408.5002 \[hep-th\]](#).
- [46] C. P. Burgess, R. Holman, and G. Tasinato, “Open EFTs, IR effects & late-time resummations: systematic corrections in stochastic inflation,” *JHEP* **01** (2016) 153, [arXiv:1512.00169 \[gr-qc\]](#).
- [47] D. Boyanovsky, “Effective field theory during inflation. II. Stochastic dynamics and power spectrum suppression,” *Phys. Rev.* **D93** (2016) 043501, [arXiv:1511.06649 \[astro-ph.CO\]](#).
- [48] D. Boyanovsky, “Effective field theory during inflation: Reduced density matrix and its quantum master equation,” *Phys. Rev.* **D92** no. 2, (2015) 023527, [arXiv:1506.07395 \[astro-ph.CO\]](#).
- [49] D. Boyanovsky, “Fermionic influence on inflationary fluctuations,” *Phys. Rev.* **D93** no. 8, (2016) 083507, [arXiv:1602.05609 \[gr-qc\]](#).

- [50] T. J. Hollowood and J. I. McDonald, “Decoherence, discord and the quantum master equation for cosmological perturbations,” *Phys. Rev.* **D95** no. 10, (2017) 103521, [arXiv:1701.02235 \[gr-qc\]](#).
- [51] T. J. Hollowood, “Unravelling Cosmological Perturbations,” *Phys. Lett.* **B785** (2018) 254–261, [arXiv:1804.07637 \[gr-qc\]](#).
- [52] R. D. Jordan, “Effective Field Equations for Expectation Values,” *Phys. Rev.* **D33** (1986) 444–454.
- [53] E. Calzetta and B. L. Hu, “Closed Time Path Functional Formalism in Curved Space-Time: Application to Cosmological Back Reaction Problems,” *Phys. Rev.* **D35** (1987) 495.
- [54] S. Weinberg, “Quantum contributions to cosmological correlations,” *Phys. Rev.* **D72** (2005) 043514, [arXiv:hep-th/0506236 \[hep-th\]](#).
- [55] E. A. Calzetta and B.-L. B. Hu, *Nonequilibrium Quantum Field Theory*. Cambridge Monographs on Mathematical Physics. Cambridge University Press, 2008. <http://www.cambridge.org/mw/academic/subjects/physics/theoretical-physics-and-mathematical-physics/nonequilibrium-quantum-field-theory?format=AR>.
- [56] N. Iqbal, H. Liu, and M. Mezei, “Lectures on holographic non-Fermi liquids and quantum phase transitions,” in *Theoretical Advanced Study Institute in Elementary Particle Physics: String theory and its Applications: From meV to the Planck Scale*, pp. 707–816. 10, 2011. [arXiv:1110.3814 \[hep-th\]](#).
- [57] S. A. Hartnoll, A. Lucas, and S. Sachdev, “Holographic quantum matter,” [arXiv:1612.07324 \[hep-th\]](#).
- [58] D. Bernard and B. Doyon, “Energy flow in non-equilibrium conformal field theory,” *Journal of Physics A: Mathematical and Theoretical* **45** no. 36, (Aug, 2012) 362001. <https://doi.org/10.1088%2F1751-8113%2F45%2F36%2F362001>.
- [59] A. Kundu and S. Kundu, “Steady-state Physics, Effective Temperature Dynamics in Holography,” *Phys. Rev. D* **91** no. 4, (2015) 046004, [arXiv:1307.6607 \[hep-th\]](#).

- [60] B. Doyon, A. Lucas, K. Schalm, and M. J. Bhaseen, “Non-equilibrium steady states in the Klein–Gordon theory,” *Journal of Physics A: Mathematical and Theoretical* **48** no. 9, (Feb, 2015) 095002. <https://doi.org/10.1088%2F1751-8113%2F48%2F9%2F095002>.
- [61] M. Spillane and C. P. Herzog, “Relativistic hydrodynamics and non-equilibrium steady states,” *Journal of Statistical Mechanics: Theory and Experiment* **2016** no. 10, (Oct, 2016) 103208. <https://doi.org/10.1088%2F1742-5468%2F2016%2F10%2F103208>.
- [62] H. Liu and J. Sonner, “Holographic systems far from equilibrium: a review,” *Reports on Progress in Physics* **83** no. 1, (Dec, 2019) 016001. <https://doi.org/10.1088%2F1361-6633%2Fab4f91>.
- [63] K.-C. Chou, Z.-B. Su, B.-l. Hao, and L. Yu, “Equilibrium and Nonequilibrium Formalisms Made Unified,” *Phys. Rept.* **118** (1985) 1.
- [64] J. Rammer, *Quantum Field Theory of Non-Equilibrium States*. 01, 2007.
- [65] M. J. G. Veltman, “Unitarity and causality in a renormalizable field theory with unstable particles,” *Physica* **29** (1963) 186–207.
- [66] G. ’t Hooft and M. J. G. Veltman, “Diagrammar,” *NATO Sci. Ser. B* **4** (1974) 177–322. <http://cds.cern.ch/record/186259/files/?ln=en>.
- [67] F. L. Vernon, Jr., *The theory of a general quantum system interacting with a linear dissipative system*. Dissertation (Ph.D.), California Institute of Technology, 1959. http://thesis.library.caltech.edu/737/1/Vernon_fl_1959.pdf.
- [68] F. M. Haehl, R. Loganayagam, P. Narayan, and M. Rangamani, “Classification of out-of-time-order correlators,” [arXiv:1701.02820](https://arxiv.org/abs/1701.02820) [hep-th].
- [69] F. M. Haehl, R. Loganayagam, P. Narayan, A. A. Nizami, and M. Rangamani, “Thermal out-of-time-order correlators, KMS relations, and spectral functions,” *JHEP* **12** (2017) 154, [arXiv:1706.08956](https://arxiv.org/abs/1706.08956) [hep-th].
- [70] S. Chaudhuri, C. Chowdhury, and R. Loganayagam, “Spectral Representation of Thermal OTO Correlators,” *JHEP* **02** (2019) 018, [arXiv:1810.03118](https://arxiv.org/abs/1810.03118) [hep-th].

- [71] A. I. Larkin and Y. N. Ovchinnikov, “Quasiclassical method in the theory of superconductivity,” *Sov.Phys.JETP* **28** no. 6, (1969) 1200–1205.
- [72] M. J. G. Veltman, “Diagrammatica: The Path to Feynman rules,” *Cambridge Lect. Notes Phys.* **4** (1994) 1–284.
- [73] F. M. Haehl, R. Loganayagam, and M. Rangamani, “Schwinger-Keldysh formalism. Part I: BRST symmetries and superspace,” *JHEP* **06** (2017) 069, [arXiv:1610.01940 \[hep-th\]](#).
- [74] G. T. Horowitz and V. E. Hubeny, “Quasinormal modes of AdS black holes and the approach to thermal equilibrium,” *Phys. Rev.* **D62** (2000) 024027, [arXiv:hep-th/9909056 \[hep-th\]](#).
- [75] F. Lombardo and F. D. Mazzitelli, “Coarse graining and decoherence in quantum field theory,” *Phys. Rev. D* **53** (1996) 2001–2011, [arXiv:hep-th/9508052](#).
- [76] A. Baidya, C. Jana, R. Loganayagam, and A. Rudra, “Renormalization in open quantum field theory. Part I. Scalar field theory,” *JHEP* **11** (2017) 204, [arXiv:1704.08335 \[hep-th\]](#).
- [77] P. Gao, P. Glorioso, and H. Liu, “Ghostbusters: Unitarity and Causality of Non-equilibrium Effective Field Theories,” *JHEP* **03** (2020) 040, [arXiv:1803.10778 \[hep-th\]](#).
- [78] Avinash, C. Jana, and A. Rudra, “Renormalisation in Open Quantum Field theory II: Yukawa theory and PV reduction,” [arXiv:1906.10180 \[hep-th\]](#).
- [79] L. M. Sieberer, M. Buchhold, and S. Diehl, “Keldysh Field Theory for Driven Open Quantum Systems,” *Rept. Prog. Phys.* **79** no. 9, (2016) 096001, [arXiv:1512.00637 \[cond-mat.quant-gas\]](#).
- [80] H. P. Breuer and F. Petruccione, *The theory of open quantum systems*. Oxford, UK: Univ. Pr. (2002) 625 p, 2002. <https://global.oup.com/academic/product/the-theory-of-open-quantum-systems-9780198520634?cc=us&lang=en&>.
- [81] U. Weiss, *Quantum Dissipative Systems*. Series in modern condensed matter physics. World Scientific, 2008. <https://books.google.co.in/books?id=4NfnaEsbQq4C>.

- [82] H. Carmichael, *An Open Systems Approach to Quantum Optics: Lectures Presented at the Université Libre de Bruxelles, October 28 to November 4, 1991*. Lecture Notes in Physics Monographs. Springer Berlin Heidelberg, 2009.
https://books.google.co.in/books?id=uor_CAAAQBAJ.
- [83] G. Schaller, *Open Quantum Systems Far from Equilibrium*. Lecture Notes in Physics. Springer International Publishing, 2014.
<https://books.google.co.in/books?id=deS5BQAAQBAJ>.
- [84] Avinash, C. Jana, R. Loganayagam, and A. Rudra, “ work in progress ,”.
- [85] R. P. Feynman, “Closed Loop and Tree Diagrams (Talk),”.
- [86] K. Symanzik, “A field theory with computable large-momenta behaviour,” *Lettere al Nuovo Cimento (1971-1985)* **6** no. 2, (1973) 77–80. <http://dx.doi.org/10.1007/BF02788323>.
- [87] G. Passarino and M. J. G. Veltman, “One Loop Corrections for $e^+ e^-$ Annihilation Into $\mu^+ \mu^-$ in the Weinberg Model,” *Nucl. Phys.* **B160** (1979) 151–207.
- [88] G. 't Hooft and M. J. G. Veltman, “Scalar One Loop Integrals,” *Nucl. Phys.* **B153** (1979) 365–401.
- [89] N. Bogoliubov and D. Shirkov, *Introduction to the Theory of Quantized Fields [by] N.N. Bogoliubov [and] D.V. Shirkov: Authorized English Ed., Rev. and Enl. by the Authors*. Interscience monographs in physics and astronomy, v.3. Interscience Publishers, 1959.
<https://books.google.co.in/books?id=mL7bngEACAAJ>.
- [90] K. Hepp, “Proof of the bogoliubov-parasiuk theorem on renormalization,” *Communications in Mathematical Physics* **2** no. 1, (1966) 301–326.
- [91] W. Zimmermann, “Convergence of bogoliubov’s method of renormalization in momentum space,” *Communications in Mathematical Physics* **15** no. 3, (1969) 208–234.
- [92] M. E. Peskin and D. V. Schroeder, *An Introduction to quantum field theory*. Addison-Wesley, Reading, USA, 1995.
- [93] H. Elvang and Y.-t. Huang, “Scattering Amplitudes,” [arXiv:1308.1697](https://arxiv.org/abs/1308.1697) [hep-th].

- [94] J. M. Henn and J. C. Plefka, *Scattering Amplitudes in Gauge Theories*, vol. 883. Springer, Berlin, 2014.
- [95] N. Arkani-Hamed, J. L. Bourjaily, F. Cachazo, A. B. Goncharov, A. Postnikov, and J. Trnka, *Grassmannian Geometry of Scattering Amplitudes*. Cambridge University Press, 4, 2016. [arXiv:1212.5605](https://arxiv.org/abs/1212.5605) [hep-th].
- [96] N. Arkani-Hamed and E. Y. Yuan, “One-Loop Integrals from Spherical Projections of Planes and Quadrics,” [arXiv:1712.09991](https://arxiv.org/abs/1712.09991) [hep-th].
- [97] C. Kacser, “The discontinuities of the triangle graph as a function of an internal mass. ii,” *Journal of Mathematical Physics* **7** no. 11, (1966) 2008–2025, <https://doi.org/10.1063/1.1704884>. <https://doi.org/10.1063/1.1704884>.
- [98] I. J. R. Aitchison, “Dispersion theory model of three-body production and decay processes,” *Phys. Rev.* **137** (Feb, 1965) B1070–B1084. <https://link.aps.org/doi/10.1103/PhysRev.137.B1070>.
- [99] I. J. R. Aitchison and C. Kacser, “Singularities and discontinuities of the triangle graph, as a function of an internal mass,” *Il Nuovo Cimento A (1965-1970)* **40** no. 2, (1965) 576–588.
- [100] N. Brambilla, M. Krämer, R. Mussa, A. Vairo, G. Bali, G. T. Bodwin, E. Braaten, E. Eichten, S. Eidelman, S. Godfrey, A. Hoang, M. Jamin, D. Kharzeev, M. P. Lombardo, C. Lourenco, A. B. Meyer, V. Papadimitriou, C. Patrignani, M. Rosati, M. A. Sanchis-Lozano, H. Satz, J. Soto, D. Z. Besson, D. Bettoni, A. Böhrer, S. Boogert, C. H. Chang, P. Cooper, P. Crochet, S. Datta, C. Davies, A. Deandrea, R. Faustov, T. Ferguson, R. Galik, F. A. Harris, O. Iouchtchenko, O. Kaczmarek, F. Karsch, M. Kienzle, V. V. Kiselev, S. R. Klein, P. Kroll, A. Kronfeld, Y. P. Kuang, V. Laporta, J. Lee, A. Leibovich, J. P. Ma, P. Mackenzie, L. Maiani, M. L. Mangano, A. Meyer, X. H. Mo, C. Morningstar, A. Nairz, J. Napolitano, S. Olsen, A. Penin, P. Petreczky, F. Piccinini, A. Pineda, A. D. Polosa, L. Ramello, R. Rapp, J. M. Richard, V. Riquer, S. Ricciardi, E. Robutti, O. Schneider, E. Scomparin, J. Simone, T. Skwarnicki, G. Stancari, I. W. Stewart, Y. Sumino, T. Teubner, J. Tseng, R. Vogt, P. Wang, B. Yabsley, C. Z. Yuan, F. Zantow, Z. G. Zhao, and A. Zieminski, “Heavy Quarkonium Physics,” *arXiv e-prints* (Dec., 2004) hep-ph/0412158, [arXiv:hep-ph/0412158](https://arxiv.org/abs/hep-ph/0412158) [hep-ph].

- [101] C. W. Bauer, S. Fleming, D. Pirjol, and I. W. Stewart, “An Effective field theory for collinear and soft gluons: Heavy to light decays,” *Phys. Rev. D* **63** (2001) 114020, [arXiv:hep-ph/0011336](#).
- [102] K. Skenderis and B. C. van Rees, “Real-time gauge/gravity duality: Prescription, Renormalization and Examples,” *JHEP* **05** (2009) 085, [arXiv:0812.2909 \[hep-th\]](#).
- [103] K. Skenderis and B. C. van Rees, “Real-time gauge/gravity duality,” *Phys. Rev. Lett.* **101** (2008) 081601, [arXiv:0805.0150 \[hep-th\]](#).
- [104] P. Glorioso, M. Crossley, and H. Liu, “A prescription for holographic Schwinger-Keldysh contour in non-equilibrium systems,” [arXiv:1812.08785 \[hep-th\]](#).
- [105] G. Policastro, D. T. Son, and A. O. Starinets, “From AdS / CFT correspondence to hydrodynamics,” *JHEP* **09** (2002) 043, [arXiv:hep-th/0205052 \[hep-th\]](#).
- [106] C. P. Herzog, P. Kovtun, S. Sachdev, and D. T. Son, “Quantum critical transport, duality, and M-theory,” *Phys. Rev.* **D75** (2007) 085020, [arXiv:hep-th/0701036 \[hep-th\]](#).
- [107] T. Faulkner and J. Polchinski, “Semi-Holographic Fermi Liquids,” *JHEP* **06** (2011) 012, [arXiv:1001.5049 \[hep-th\]](#).
- [108] G. W. Gibbons and S. W. Hawking, “Action Integrals and Partition Functions in Quantum Gravity,” *Phys. Rev.* **D15** (1977) 2752–2756.
- [109] D. T. Son and A. O. Starinets, “Minkowski space correlators in AdS / CFT correspondence: Recipe and applications,” *JHEP* **09** (2002) 042, [arXiv:hep-th/0205051 \[hep-th\]](#).
- [110] C. P. Herzog and D. T. Son, “Schwinger-Keldysh propagators from AdS/CFT correspondence,” *JHEP* **03** (2003) 046, [arXiv:hep-th/0212072 \[hep-th\]](#).
- [111] E. Barnes, D. Vaman, C. Wu, and P. Arnold, “Real-time finite-temperature correlators from AdS/CFT,” *Phys. Rev.* **D82** (2010) 025019, [arXiv:1004.1179 \[hep-th\]](#).
- [112] D. T. Son and D. Teaney, “Thermal Noise and Stochastic Strings in AdS/CFT,” *JHEP* **07** (2009) 021, [arXiv:0901.2338 \[hep-th\]](#).

- [113] S. Caron-Huot, P. M. Chesler, and D. Teaney, “Fluctuation, dissipation, and thermalization in non-equilibrium AdS₅ black hole geometries,” *Phys. Rev.* **D84** (2011) 026012, [arXiv:1102.1073 \[hep-th\]](#).
- [114] P. M. Chesler and D. Teaney, “Dynamical Hawking Radiation and Holographic Thermalization,” [arXiv:1112.6196 \[hep-th\]](#).
- [115] M. Botta-Cantcheff, P. J. Martínez, and G. A. Silva, “The gravity dual of real-time cft at finite temperature,” *Journal of High Energy Physics* **2018** no. 11, (2018) 129.
- [116] E. Witten, “Anti-de Sitter space and holography,” *Adv. Theor. Math. Phys.* **2** (1998) 253–291, [arXiv:hep-th/9802150](#).
- [117] B. C. van Rees, “Real-time gauge/gravity duality and ingoing boundary conditions,” *Nucl. Phys. Proc. Suppl.* **192-193** (2009) 193–196, [arXiv:0902.4010 \[hep-th\]](#).
- [118] X. Dong, A. Lewkowycz, and M. Rangamani, “Deriving covariant holographic entanglement,” *JHEP* **11** (2016) 028, [arXiv:1607.07506 \[hep-th\]](#).
- [119] J. de Boer, M. P. Heller, and N. Pinzani-Fokeeva, “Holographic Schwinger-Keldysh effective field theories,” *JHEP* **05** (2019) 188, [arXiv:1812.06093 \[hep-th\]](#).
- [120] B. Chakrabarty, J. Chakravarty, S. Chaudhuri, C. Jana, R. Loganayagam, and A. Sivakumar, “Nonlinear Langevin dynamics via holography,” [arXiv:1906.07762 \[hep-th\]](#).
- [121] J. de Boer, V. E. Hubeny, M. Rangamani, and M. Shigemori, “Brownian motion in AdS/CFT,” *JHEP* **07** (2009) 094, [arXiv:0812.5112 \[hep-th\]](#).
- [122] S. Chaudhuri and R. Loganayagam, “Probing Out-of-Time-Order Correlators,” *JHEP* **07** (2019) 006, [arXiv:1807.09731 \[hep-th\]](#).
- [123] B. Chakrabarty, S. Chaudhuri, and R. Loganayagam, “Out of Time Ordered Quantum Dissipation,” *JHEP* **07** (2019) 102, [arXiv:1811.01513 \[cond-mat.stat-mech\]](#).
- [124] G. Penington, “Entanglement Wedge Reconstruction and the Information Paradox,” [arXiv:1905.08255 \[hep-th\]](#).

- [125] A. Almheiri, N. Engelhardt, D. Marolf, and H. Maxfield, “The entropy of bulk quantum fields and the entanglement wedge of an evaporating black hole,” *JHEP* **12** (2019) 063, [arXiv:1905.08762 \[hep-th\]](#).
- [126] J. V. Rocha, “Evaporation of large black holes in AdS: Coupling to the evaporon,” *JHEP* **08** (2008) 075, [arXiv:0804.0055 \[hep-th\]](#).
- [127] G. Penington, S. H. Shenker, D. Stanford, and Z. Yang, “Replica wormholes and the black hole interior,” [arXiv:1911.11977 \[hep-th\]](#).
- [128] A. Almheiri, T. Hartman, J. Maldacena, E. Shaghoulian, and A. Tajdini, “Replica Wormholes and the Entropy of Hawking Radiation,” [arXiv:1911.12333 \[hep-th\]](#).
- [129] B. Chakrabarty and S. Chaudhuri, “Out of time ordered effective dynamics of a quartic oscillator,” *SciPost Phys.* **7** (2019) 013, [arXiv:1905.08307 \[hep-th\]](#).
- [130] P. Martin, E. Siggia, and H. Rose, “Statistical dynamics of classical systems,” *Phys.Rev.A* **8** (1973) 423–437.
- [131] S. S. Gubser, “Absorption of photons and fermions by black holes in four-dimensions,” *Phys. Rev.* **D56** (1997) 7854–7868, [arXiv:hep-th/9706100 \[hep-th\]](#).
- [132] D. Birmingham, I. Sachs, and S. N. Solodukhin, “Conformal field theory interpretation of black hole quasinormal modes,” *Phys.Rev.Lett.* **88** (2002) 151301, [arXiv:hep-th/0112055](#).
- [133] A. Bzowski, P. McFadden, and K. Skenderis, “Scalar 3-point functions in CFT: renormalisation, beta functions and anomalies,” *JHEP* **03** (2016) 066, [arXiv:1510.08442 \[hep-th\]](#).
- [134] M. Becker, Y. Cabrera, and N. Su, “Finite-temperature three-point function in 2D CFT,” *JHEP* **09** (2014) 157, [arXiv:1407.3415 \[hep-th\]](#).
- [135] I. Heemskerk and J. Polchinski, “Holographic and Wilsonian Renormalization Groups,” *JHEP* **06** (2011) 031, [arXiv:1010.1264 \[hep-th\]](#).
- [136] T. Faulkner, H. Liu, and M. Rangamani, “Integrating out geometry: Holographic Wilsonian RG and the membrane paradigm,” *JHEP* **08** (2011) 051, [arXiv:1010.4036 \[hep-th\]](#).

- [137] S. Chatterjee, C. Jana, R. Loganayagam, and A. Rudra, “Renormalisation in open quantum field theory III: Non-local divergences,” *to appear* (2020) .
- [138] T. Filk, “Divergencies in a field theory on quantum space,” *Phys. Lett.* **B376** (1996) 53–58.
- [139] S. Minwalla, M. Van Raamsdonk, and N. Seiberg, “Noncommutative perturbative dynamics,” *JHEP* **02** (2000) 020, [arXiv:hep-th/9912072](#) [[hep-th](#)].
- [140] M. Van Raamsdonk and N. Seiberg, “Comments on noncommutative perturbative dynamics,” *JHEP* **03** (2000) 035, [arXiv:hep-th/0002186](#) [[hep-th](#)].
- [141] R. Loganayagam, K. Ray, and A. Sivakumar, “Fermionic Open EFT from Holography,” *to appear* (2020) .
- [142] V. E. Hubeny, S. Minwalla, and M. Rangamani, “The fluid/gravity correspondence,” in *Black holes in higher dimensions*, pp. 348–383. 2012. [arXiv:1107.5780](#) [[hep-th](#)]. [[,817\(2011\)](#)].
- [143] A. Denner and S. Dittmaier, “Reduction of one loop tensor five point integrals,” *Nucl. Phys.* **B658** (2003) 175–202, [arXiv:hep-ph/0212259](#) [[hep-ph](#)].
- [144] A. Denner and S. Dittmaier, “Reduction schemes for one-loop tensor integrals,” *Nucl. Phys.* **B734** (2006) 62–115, [arXiv:hep-ph/0509141](#) [[hep-ph](#)].
- [145] “*NIST Digital Library of Mathematical Functions*.” [Http://dlmf.nist.gov/](http://dlmf.nist.gov/), release 1.0.26 of 2020-03-15. <http://dlmf.nist.gov/>. F. W. J. Olver, A. B. Olde Daalhuis, D. W. Lozier, B. I. Schneider, R. F. Boisvert, C. W. Clark, B. R. Miller, B. V. Saunders, H. S. Cohl, and M. A. McClain, eds.